AD-A166 377 HIGH RESOLUTION MEASUREMENTS OF OH INFRARED AIRGLOW STRUCTURE(U) AIR FORCE INST OF TECH WRIGHT-PATTERSON AFB OH P C NEAL 1985 AFIT/CI/NR-86-26D 1/3

UNCLASSIFIED F/G 4/1 NL

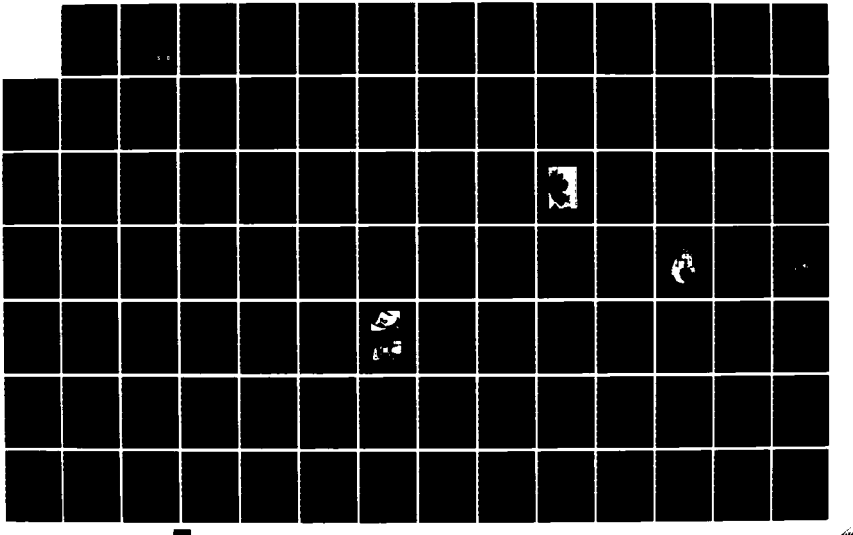

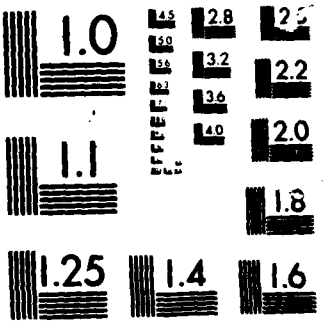

MICROCOPY RESOLUTION TEST CHART

SECURITY CLASSIFICATION OF THIS PAGE (When Data Entered)

REPORT DOCUMENTATION PAGE		READ INSTRUCTIONS BEFORE COMPLETING FORM
1. REPORT NUMBER AFIT/CI/NR 86- 26D	2. GOVT ACCESSION NO.	3. RECIPIENT'S CATALOG NUMBER
4. TITLE (and Subtitle) High Resolution Measurements of OH Infrared Airglow Structure		5. TYPE OF REPORT & PERIOD COVERED THESIS/DISSERTATION
		6. PERFORMING ORG. REPORT NUMBER
7. AUTHOR(s) Parris Cornel Neal		8. CONTRACT OR GRANT NUMBER(s)
9. PERFORMING ORGANIZATION NAME AND ADDRESS AFIT STUDENT AT: Utah State University		10. PROGRAM ELEMENT, PROJECT, TASK AREA & WORK UNIT NUMBERS
11. CONTROLLING OFFICE NAME AND ADDRESS AFIT/NR WPAFB OH 45433-6583		12. REPORT DATE 1985
		13. NUMBER OF PAGES 267
14. MONITORING AGENCY NAME & ADDRESS(if different from Controlling Office)		15. SECURITY CLASS. (of this report) UNCLASS
		15a. DECLASSIFICATION/DOWNGRADING SCHEDULE

16. DISTRIBUTION STATEMENT (of this Report)

APPROVED FOR PUBLIC RELEASE; DISTRIBUTION UNLIMITED

17. DISTRIBUTION STATEMENT (of the abstract entered in Block 20, if different from Report)

18. SUPPLEMENTARY NOTES

APPROVED FOR PUBLIC RELEASE: IAW AFR 190-1

LYNN E. WOLAVER 2 Apr 86
Dean for Research and
Professional Development
AFIT/NR, WPAFB OH 45433-6583

19. KEY WORDS (Continue on reverse side if necessary and identify by block number)

20. ABSTRACT (Continue on reverse side if necessary and identify by block number)

DD FORM 1 JAN 73 1473 EDITION OF 1 NOV 65 IS OBSOLETE

SECURITY CLASSIFICATION OF THIS PAGE (When Data Entered)

ABSTRACT

High Resolution Measurements

of OH Infrared Airglow Structure

by

Parris Cornel Neal, Doctor of Philosophy

Utah State University, 1985

Major Professors: Dr. Doran J. Baker and Dr. Kay D. Baker
Department: Electrical Engineering

Disturbances in the normally calm atmospheric airglow layer, which cause bright and dark bands or "stripes" to appear, have been observed. These disturbances are attributed to "gravity waves" propagating through the atmosphere. An instrument capable of resolving the temporal, spatial, and spectral attributes of OH infrared emissions was designed to gather quantitative data on airglow structure.

An optically-compensated interferometer-spectrometer was chosen as the basic instrument to measure this phenomenon. This high-throughput instrument (0.285 cm^2 sr) is an order of magnitude more sensitive than more conventional spectrometers having a noise equivalent spectral radiance of 16 R/cm^{-1} at 1.5 μm. A spectral resolution of 2 cm^{-1} was obtained. The high-throughput of the optically-compensated

interferometer makes possible temporal resolution as short as 30 seconds. Spatial data were obtained by matching the interferometer's high throughput to a unique optical system which includes a 50-cm diameter telescope. This ~~relatively large diameter~~ Dall-Kirkham telescope maintains the large throughput of the interferometer but narrows the instrument field of view to less than a degree. The spatial resolution of the system is 14 milliradians.

The interferometer was operated in conjunction with a low-light level infrared imaging isocon camera system provided by the University of Southampton, England. The camera was co-aligned with the telescope to provided an infrared video "eye" for the interferometer.

A bright OH Meinel airglow structure event was recorded on June 15, 1983 from an observation site located at Sacramento Peak, New Mexico. The structures were measured at elevation angles near the horizon. Apparent wavelengths, periods, and phase velocities, of 24±1 km, 14±1 minutes, and 28±2 meters/second respectively, were calculated for the recorded structure. The interferometer data show intensity modulations of 20-40% within the structure. Rotational temperatures were also calculated using the interferometer spectral data. A mean rotational temperature of 165 °K was calculated and temperature modulations of 5-10 °K were recorded in phase with the intensity modulations.

(267 pages)

AFIT RESEARCH ASSESSMENT

The purpose of this questionnaire is to ascertain the value and/or contribution of research accomplished by students or faculty of the Air Force Institute of Technology (AU). It would be greatly appreciated if you would complete the following questionnaire and return it to:

AFIT/NR
Wright-Patterson AFB OH 45433

RESEARCH TITLE: _____

_____

AUTHOR: _____

RESEARCH ASSESSMENT QUESTIONS:

1. Did this research contribute to a current Air Force project?

( ) a. YES ( ) b. NO

2. Do you believe this research topic is significant enough that it would have been researched (or contracted) by your organization or another agency if AFIT had not?

( ) a. YES ( ) b. NO

3. The benefits of AFIT research can often be expressed by the equivalent value that your agency achieved/received by virtue of AFIT performing the research. Can you estimate what this research would have cost if it had been accomplished under contract or if it had been done in-house in terms of manpower and/or dollars?

( ) a. MAN-YEARS _____ ( ) b. $_____

4. Often it is not possible to attach equivalent dollar values to research, although the results of the research may, in fact, be important. Whether or not you were able to establish an equivalent value for this research (3. above), what is your estimate of its significance?

( ) a. HIGHLY SIGNIFICANT ( ) b. SIGNIFICANT ( ) c. SLIGHTLY SIGNIFICANT ( ) d. OF NO SIGNIFICANCE

5. AFIT welcomes any further comments you may have on the above questions, or any additional details concerning the current application, future potential, or other value of this research. Please use the bottom part of this questionnaire for your statement(s).

NAME GRADE POSITION

ORGANIZATION LOCATION

STATEMENT(s):

HIGH RESOLUTION MEASUREMENTS OF OH INFRARED AIRGLOW STRUCTURE

by

Parris Cornel Neal

A dissertation submitted in partial fulfillment

of the requirements for the degree

of

DOCTOR OF PHILOSOPHY

in

Engineering

UTAH STATE UNIVERSITY
Logan, Utah
1985

HIGH RESOLUTION MEASUREMENTS OF OH INFRARED AIRGLOW STRUCTURE

by

Parris Cornel Neal

A dissertation submitted in partial fulfillment

of the requirements for the degree

of

DOCTOR OF PHILOSOPHY

in

Engineering

Approved:

Major Professor

Major Professor

Committee Member

Committee Member

Committee Member

Dean of Graduate Studies

UTAH STATE UNIVERSITY
Logan, Utah
1985

ACKNOWLEDGEMENTS

The author wishes to gratefully acknowledge those who have assisted and encouraged him in making possible this research. Appreciation is extended to the US Air Force Academy for sponsoring this educational experience. Special appreciation is expressed to Dr. Doran Baker for his excellent direction and guidance. Also appreciation is extended to Dr. Kay Baker, Dr. William Pendleton, Dr. Clair Wyatt, and Dr. Allan Steed for the time spent in assisting with the research and reviewing this dissertation. Thanks is extended to Dr. Gene Ware for his time and assistance in developing the algorithms and computer programs used herein. Also to Mr. Chuck Harris and Mr. Pat Espy for their assistance with the interferometer optical design and OH rotational model development. Appreciation is also given to Mr. Peter Mace for his invaluable assistance in gathering the data for this study. Appreciation is given to the University Southampton, especially Mr. Mike Taylor, for their willingness to gather the video data used in this study.

Especially to my wife, Dorothy, gratitude is expressed for her constant encouragement, confidence and understanding patience. Also to my children, for unselfishly becoming orphans during this trying period.

Parris Cornel Neal

TABLE OF CONTENTS

LIST OF TABLES

LIST OF FIGURES

CHAPTER I

INTRODUCTION

The mesosphere is the interface region between the earths' inner and outer atmospheres. Occurrences at the mesopause include: the temperature gradient makes a sign change, the atmospheric pressure, density, and mean molecular weight all have an inflection point in their respective curves [Banks and Kockarts 1973]. The atmosphere makes a transition from a fluid to free molecular flow in this region which accounts for these changes. The unique properties of the mesospheric region are of great interest in understanding the middle atmosphere and its influence on the energy budget of the earth.

The 80 to 100 km region (mesosphere) is a difficult region to study because the altitude is too low for direct satellite observations and too high for direct balloon or airplane measurements. Ground based studies are hampered by the intervening atmosphere. There are some relatively transparent atmospheric "windows" in the near infrared, however. Hydroxyl radicals (OH) reside in this mesospheric region in sufficient concentrations to radiate a large amount of energy at the red and near infrared wavelengths [Baker 1978].

The excitation of OH is caused by various solar and chemical processes. The excited OH radical is a complex vibrational-rotational system which emits radiation spectrally. The spectral radiation distribution is near Maxwell-Boltzmann in nature [Baker 1978]; therefore, the OH spectral radiation can be measured, the Boltzmann distribution determined, and a rotational temperature calculated [Ware 1980]. This temperature can then be used to help understand the chemistry and physics of the entire region. Banks and Kockarts [1973] show that mesospheric temperatures during the summer months at a mid-latitude site can be expected to be between 150 °K and 190 °K.

Recent studies have shown that mesospheric optical radiation called airglow has, at times, exhibited some "wavelike" structure [Taylor et al. 1980]. These waves have been studied using photographic and photometric methods. The object of this study was to develop and utilize an instrument to provide quantitative data of OH rotational temperature and intensity variations during these airglow structure events .

Airglow Structure Measurement Background

The atmospheric airglow layer has been observed and studied for many years using a variety of methods. The studies conducted during the decades from 1930 to 1970, however, failed to recognize the nature of the airglow structure phenomenon. Rayleigh [1931] was among the first

to recognize the difference between airglow and aurora. He referred to the enhanced airglow as "non-polar aurorae." Photographs of the airglow structure were presented in 1952 by Hoffmeister [1952]; but again, neither the identity nor the source of the airglow structure was understood. Chamberlain [1961] briefly outlines the historical efforts in airglow studies up until 1961. During the decade of the 60s the techniques of photometry were perfected and most optical atmospheric study efforts were centered around these methods.

Kieffaber [1973] presented photographic evidence in 1972 of apparent airglow "waves" and "cells'" in the 750-900 nm wavelength region using infrared film and a 35-mm camera. She proposed that the airglow stripes originated from a disturbance in the OH layer. Again in late 1972, Peterson and Kieffaber [1973] recorded more occurrences of structure at their mid-latitude site near Albuquerque, New Mexico. The photographically recorded events were also tracked with infrared photometers (1.65 and 2.2 μm) and shown to be moving between 20 and 40 meters/second.

In 1975, Crawford et al. [1975] flew an image intensified isocon television system on board NASA's CV990 aircraft. Peterson and Kieffaber [1975] observed on the same flight with their cameras and photometers. Both groups recorded "cloud-like" airglow structures. Again using 35-mm cameras, Moreels and Herse [1977] measured extensive OH airglow structure over Europe. Their findings were similar

to those of Peterson and Kieffaber. Waves on the order of 40-km spatial wavelength appeared to be traveling at horizontal speeds from 15 to 20 meters/second. Peterson [1979] was able to record numerous occurrences from 1975 through 1978 with some of the events being enhanced enough to see the structure with the naked eye. The University of Southampton Atmospheric Physics group [Taylor et al. 1980 and Taylor 1984] recorded many structure events with the image isocon television cameras from 1975 through 1983. Using radiometric techniques, Huppi and Baker [1976] also recorded OH intensity variations. Takeuchi and Misawa [1981] record some short-period waves of OH intensity and rotational temperature using a tilting filter photometer. This study used a narrow field of view, fast scan rate instrument. The spectral resolution was rather coarse, however, (unable to resolve the base line between adjacent band lines) and the measurements were taken without the aid of any photographic or video equipment making it difficult to identify what was being observed. Airglow structure was also recorded by Peterson and Adams [1983] during a total lunar eclipse in the summer of 1982. In this lunar eclipse study extensive use was made of photographic equipment as well as a vertical sounding radar.

During the decade of the 1970's, interferometric-spectroscopy applied to middle atmospheric research matured as a measurement science. Interferograms processed using computer-based fast Fourier transform (FFT) methods yielded

high-resolution OH airglow spectra from which intensity and rotational temperatures could be extracted. Baker [1978] presents an excellent summary of the studies conducted in this area. However, because the instruments used had wide fields of view (therefore integration over large areas), low throughput (therefore long integration times), or low spectral resolution the small spatial airglow variations were not able to be spectroscopically measured at high resolution.

The references cited and many others have recorded OH airglow structure events. However, none of the researchers were able to provide a measure of high-resolution spectral changes and therefore calculate the differences in OH rotational temperature of the dark and bright band "waves." This dissertation gives the design, development, and operation of a special high-throughput, narrow field of view, fast scan interferometer-spectrometer which can spectrally, spatially, and temporally resolve the OH airglow emission structure.

Airglow Structure and the Theory of Atmospheric Gravity Waves

In a landmark paper, Hines [1960] suggested that under certain conditions the atmosphere could be disturbed by a "gravity wave." Later, Hines [1965] hypothesized that the passage of internal gravity waves (IGW's) through the atmosphere would cause some reversible, adiabatic heating

(temperature fluctuations associated with waves) until the dissipation of the wave became excessive. Along with his gravity wave hypothesis, Hines [1965] gave a simple model to describe his suspected IGW temperature fluctuations. Using some constants from the high-altitude vapor-trail measurements of Kochanski [1964] in the Hines model, a calculated temperature change of ±6 °K could be expected in conjunction with the passage of an IGW through the atmosphere. Temperature and wind measurements by Rai and Fejer [1971] using rocket-grenade techniques support the IGW hypothesis put forth by Hines.

The atmospheric scientific community in the Soviet Union has done extensive work in the area of an adiabatic-oscillation IGW model similar to the work of Hines [1960]. Krassovsky et al. [1977] summarize much of the modeling and measurement efforts of this group. The basic instrument used is a three-axis diffraction spectrograph, supported by various photometers. The large data base of measurements presented, shows strong correlation between the magnitude of the temperature modulation and the period of the IGW. The observational data presented exhibit, for IGW periods of about 25 minutes, the calculated rotational temperature changes of about 6 °K with the passing of the wave [Krassovsky et al. 1977]. Additionally, the Soviet work indicates that a significant rotational temperature difference can be seen between high level and low level OH vibrational transitions. The observed differences range

from 5 to 25 °K with the high vibrational level transitions appearing hotter.

Interferometers and Fourier Transform Spectroscopy

The Michelson interferometer was invented in the 1880's by Albert Abraham Michelson [Shankland 1974]. In the Michelson-Morley experiment, the instrument was used in an attempt to measure the earth's movement through an "ether." Michelson also used his interferometer to determine the exact length of the standard meter and to measure the diameter of celestial bodies. He also discovered the spectral fine structure of hydrogen, mercury, and thallium [Shankland 1974]. This pointed out the potential for what would be later be called "Fourier spectroscopy."

Optically-sensitive detectors were subsequently used in conjunction with Michelson interferometers, in which one mirror was mechanically displaced at a constant rate, to produce an electrical interferogram. The interferogram was then inverted using Fourier transform techniques to yield direct spectral data. In 1910, Ruben and Woods [Connes 1963] obtained the first far infrared spectrum using this method. Fellgett [1949] and Jacquinot [1954] independently showed the inherent advantage that the interferometer has over grating and prism spectrometers. This advantage results from measuring all spectral components simultaneously. This improvement was referred to by

Fellgett as "multiplex spectroscopy." Jacquinot [Connes 1963] also showed that absence of slits in Michelson spectrometry also improved system throughput when compared with conventional grating methods.

The advent of large, fast computers and the development of the fast Fourier transform [Forman 1966], which together could calculate a large Fourier transform quickly, spread the use of Fourier transforms for power spectral density analysis into many fields. Notable contributions were made in the field in the 1950's, 1960's, and 1970's by Mertz [1959], Connes [1956], Gebbie and Vanasse [1956], Strong and Vanasse [1959], Forman [1966], Stair and Baker [1974], Haycock and Baker [1975], and Steed [1978]. Many of the improvements in the field were reported at the 1970 Aspen Conference on Fourier Spectroscopy [Vanasse et al. 1971].

Figure 1-1 shows the typical layout of the Michelson interferometer. The system is comprised of a beamsplitter that divides the incoming light beam into two equal parts, two mirrors (M_1 is stationary and M_2 is mobile), and a condenser lens to focus the light on to a detector.

The incoming light is divided into two portions by the beamsplitter with each portion directed to its respective mirror. The energy is then reflected by the mirrors and is recombined at the beamsplitter and passed onto the detector system. The recombined beam is modulated by differences in the path lengths between the beamsplitter and each of the mirrors. If the mobile mirror M_2 is in a position such

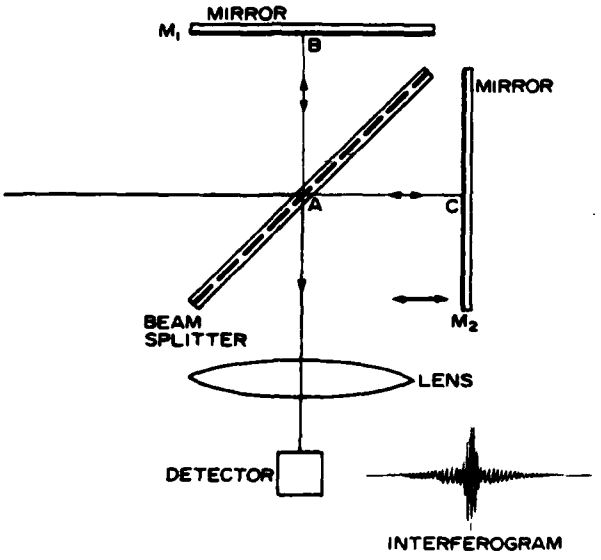

Figure 1-1. Layout of a conventional Michelson interferometer.

that the path length AC is the same as the path length AB, then the recombined signals are in phase and thus add constructively. The same constructive addition occurs when the path length difference BC-AC is any integral number of wavelengths of the incoming signal. On the other hand, if the path length difference is not an integral multiple of the wavelength, then the recombined signal will have varying amounts of destructive interference depending upon the phase difference. As the path length AC is changed in a uniform manner, by moving M_2 at a constant rate, the electrical signal from the detector is the interferogram of the incoming optical signal. The Fourier transformed interferogram yields the spectral content of the incoming light.

The simultaneous measurement of high-resolution spectral, temporal, and spatial characteristics of the OH airglow structure requires an instrument with both a narrow field of view and high throughput. The standard Michelson interferometer, when used for high-resolution measurements, has a narrow field of view but its low throughput would make it an order of magnitude less sensitive.

The narrow field of view limitation of a standard Michelson interferometer is illustrated in Figure 1-2. When incoming energy is allowed to enter the interferometer off-axis ($\theta \neq 0°$) the relationship between the displacement of mirror M_2 and the actual path difference between the two mirrors is altered. The path difference or retardation is no longer $2d$ as it is when light is coming straight into the instrument, but now is $2d\cos\theta$, where θ is the angle of the incoming light with respect to the entry normal. For an instrument with a given resolving power the maximum usable field of view for a standard Michelson interferometer is, according to Vanasse [1977]

$$\Omega_{max} = 2\pi / R \quad , \tag{1.1}$$

where

Ω_{max} = maximum field of view in steradians,

R = resolving power of instrument.

To increase the throughput (thus achieving a faster scan rate) an optically-compensated interferometer was chosen for use in this study. There have been many proposed methods

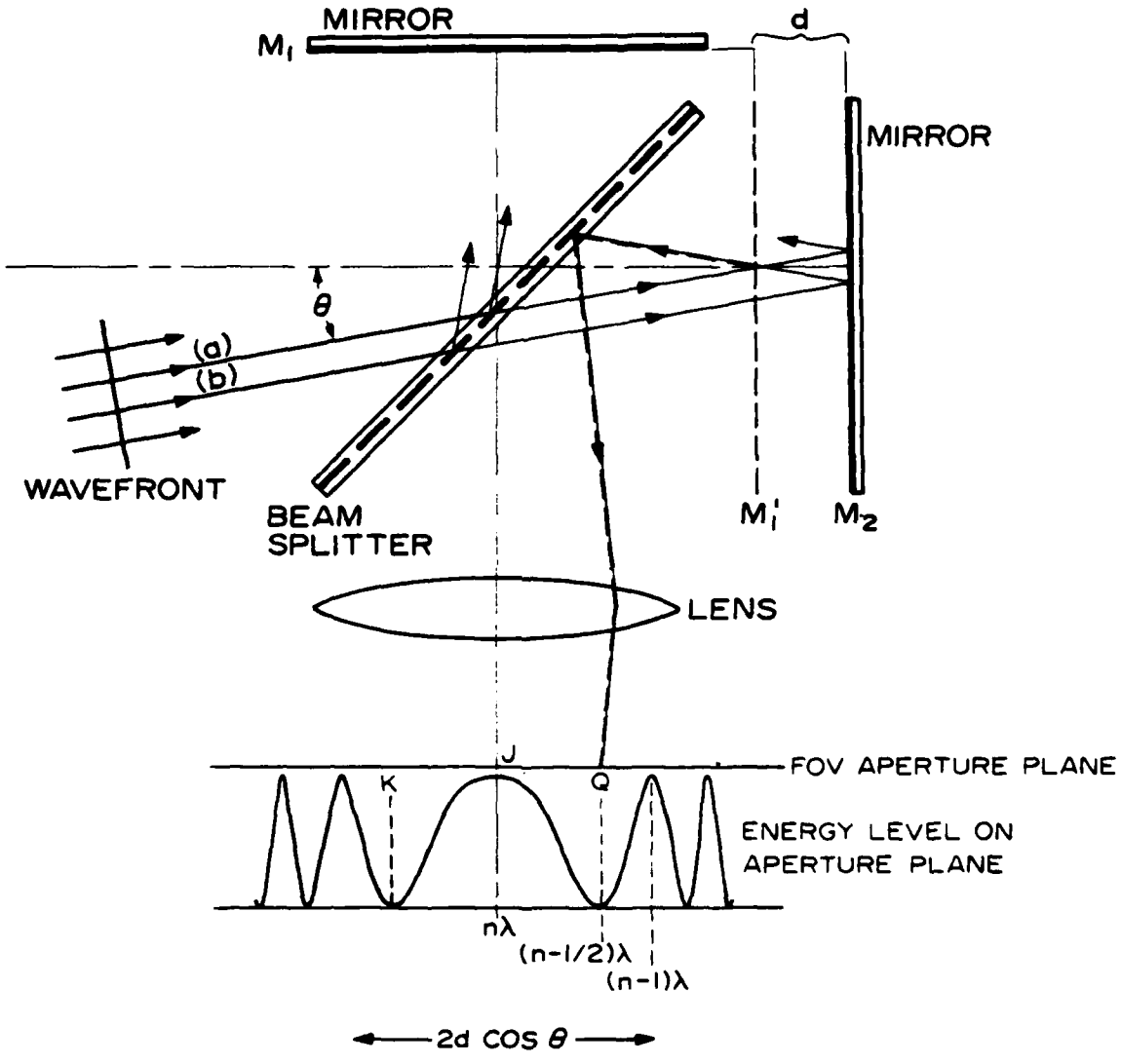

Figure 1-2. Interaction of off-axis rays in conventional Michelson interferometer [Steed 1978].

of field-widening or optical-compensation for increasing the throughput of an interferometer. These techniques are reviewed by Baker [Vanasse 1977]. The method used for the instrument in this study was first proposed by Connes [1956], and uses optical-compensation wedges or prisms in each leg of the interferometer (specific details are discussed in Chapter II). Optical compensation increases the throughput by increasing the usable field of view of the instrument. However, the measurement of OH airglow structure requires a small field of view. The high throughput of the compensated interferometer was matched (maintaining temporal resolution) to a special optical system which included a large-diameter telescope to obtain the desired narrow field of view while maintaining throughput.

The interferometer system was now able to simultaneously resolve the spectral, temporal, and spatial characteristics of the OH airglow structure. However, because the measured radiation was in the infrared it was necessary to locate and measure a structure occurrence and to characterize the total structure into which the interferometer was looking. The video viewing system used is described in the next section.

Isocon Television System

Taylor [1983-84] participated in this research by providing and operating a low light-level infrared television camera used in conjunction with the interferometer-spectrometer. This Southampton University infrared TV camera allowed any airglow structure to be quickly and efficiently identified and permanently recorded as video information. Taylor's system employed an image intensified isocon television system. This isocon television system is briefly described here for completeness.

The isocon tube is different than other scanning image tubes in that it uses a different portion of the scanning electron beam to create the signal. The low-energy electron beam scans a high-resistance target as in other tubes; however, the isocon signal comes from the electrons that are scattered off the target [Soule 1968] rather than the reflected electrons used by conventional equipment (orthicons use the reflected beam). The scattered signal, although small in magnitude, has a high signal-to-noise ratio, and is particularly well suited to the viewing of the low-contrast, faint OH airglow.

The TV system used to image the airglow structures was specially modified to enable clear images of the OH airglow patterns to be obtained in less than a second [Taylor 1984]. The television camera used was an English Electric Valve Miniature Isocon, Type P1477 fitted with a single-stage

image intensifier, optically coupled to a 55-mm image isocon tube. The camera has a signal-to-noise ratio of approximately 40 dB at 10 ft-candles (starlight conditions) and a dynamic range of about 2000:1.

To further enhance the capability of the camera to image very faint airglow structures, it was arranged for the electronic image to be integrated on the target of the TV tube for a period of up to a second (longer integration times allow the image charge on the target to migrate and thus smear the image) before being scanned and recorded onto video tape [Taylor 1984]. This technique is particularly useful as it improves the signal-to-noise ratio of the airglow signal by nearly an order of magnitude (7 times for a 1-second integration period) with no significant loss of temporal resolution.

The camera has an extended red spectral response (S25) with a peak sensitivity at about 500 nm and a long wavelength cut off at 900 nm. Images of the near-infrared OH structure were obtained by placing a Schott RG715 band stop filter in front of the camera lens. The combined response of this filter and the TV camera gave a bandwidth (half maximum) of 715 to 850 nm and a peak sensitivity around 750 nm. This bandwidth is illustrated in Figure 1-3. The location of all the OH emission bands within this spectral range are indicated. The intensity in the zenith of the OH emission within this bandpass is typically 5 to 15 kR; the principal emissions are the OH (9,4) and (5,1)

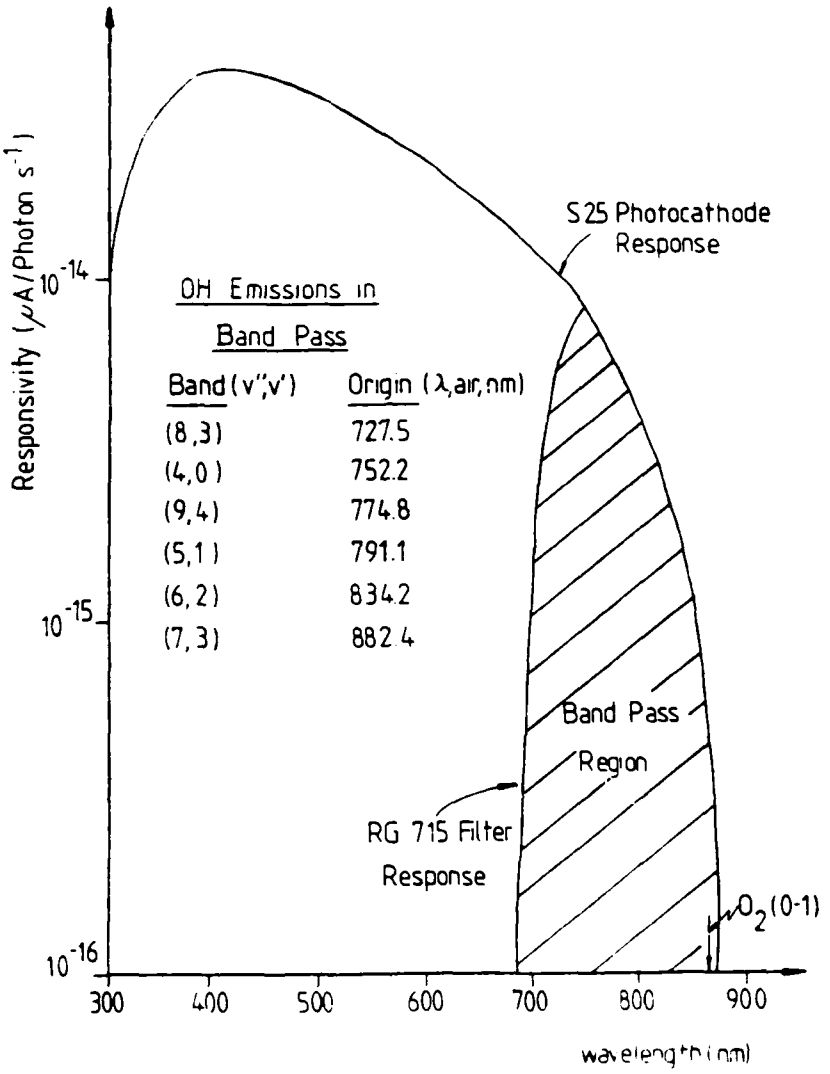

Figure 1-3. Isocon camera system spectral range including the OH emissions within that range [Taylor 1983-84].

Meinel bands [Taylor 1984]. The camera was fitted with a Nikon 85-mm, f/1.4 lens and was adjusted to give an almost square field of view of 15° horizontal by 13° vertical. The isocon camera used in this study is shown in Figure 2-9, mounted on the interferometer telescope.

The Southampton TV cameras have been used for many years to "photograph" the near-infrared OH airglow structure. An example of the quality of the video data gathered is shown in Figure 1-4. This video frame was taken in August of 1980 while observing over the Swiss Alps. The bright and dark bands each subtend about 1° of arc. These data were the basis upon which the interferometer's field of view was designed in order to resolve the spatial nature of the OH airglow structure.

Scope and Objectives

The specific goals and objectives are outlined as follows:

1. Design and develop an optical instrumentation system capable of quantifying the spatial, spectral, and temporal characteristics of OH near-infrared night airglow structure. The instrumental field of view must be one degree or less to resolve the structural characteristics of the airglow. The system must have spectral resolution of better than 3 cm^{-1} in order to provide spectra from which OH rotational temperatures can be calculated using appropriate algorithms and digital computer programs. The NESR must be sufficient to resolve the OH near-infrared airglow with scan times of less than 1 minute to resolve the temporal fluctuations of the airglow structure.

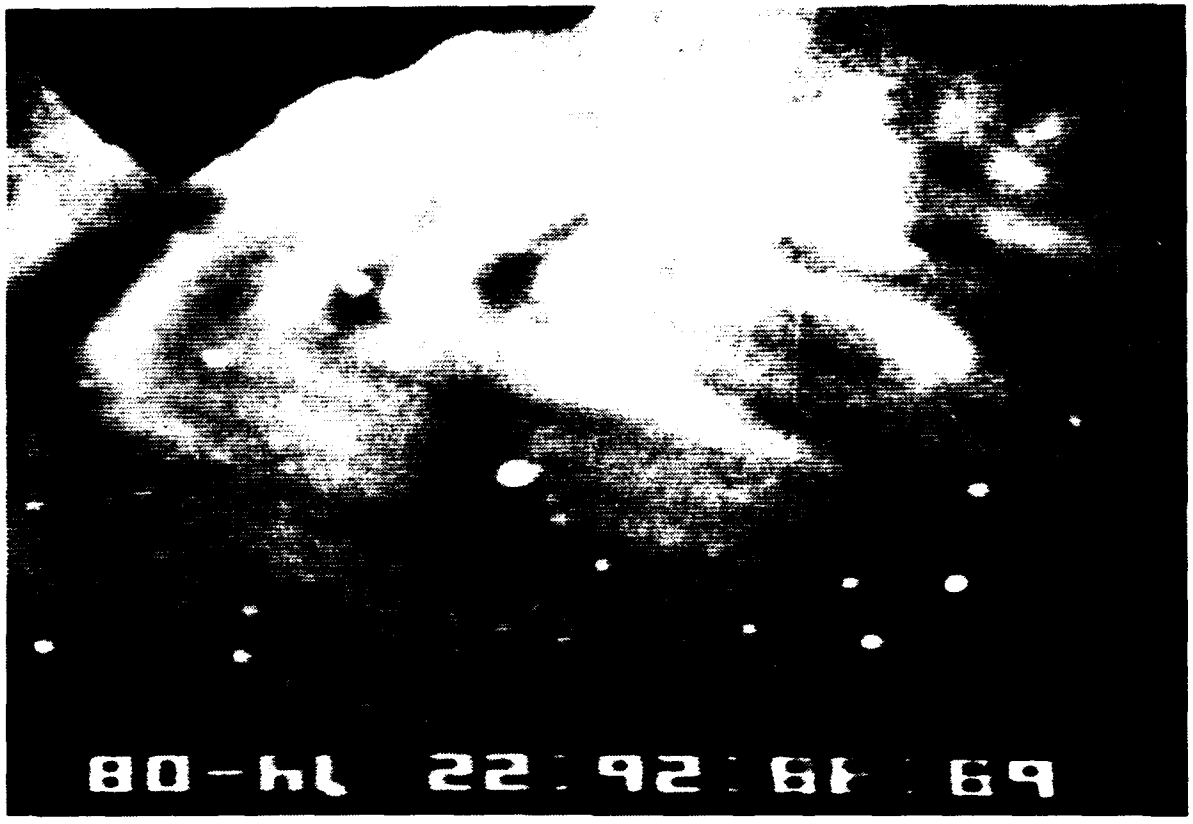

Figure 1-4. Image isocon photo of OH airglow structure taken by Taylor et al. [1980] in Switzerland in August of 1980.

2. Use the instrumentation system to measure the spectral, spatial, and temporal characteristics of OH near-infrared airglow structure from a mid-latitude observing site.
3. Develop and apply signal processing procedures extending the sampling and FFT work of Ware [1980] to extract both radiance and rotational temperature variations of OH airglow structure.
4. Derive error bounds on the measurement data, based upon system specifications such as field of view, scan speed, and spectral resolution, as well as instrument calibration, and signal processing techniques.
5. Present the observational results, correlate intensity variations, temperature fluctuations, and structure with simultaneous near-infrared video images, and compare the findings with expected OH airglow dynamics studies from other investigators.

CHAPTER II

OPTICAL INSTRUMENTATION SYSTEM DESIGN

Design Philosophy

The goal of this study was to develop a technique for simultaneously measuring the spatial, spectral, and temporal characteristics of OH near-infrared airglow structures. The basic instrumental approach chosen to provide the spectral resolving capability is a Michelson interferometer-spectrometer which is optically-compensated to achieve a very high throughput. The compensation technique used makes it possible for obliquely incident optical energy up to 5 degrees off axis to contribute to the detected signal without sacrificing spectral resolution. This resulting high throughput, within the interferometer, is matched at the input to a large diameter collecting telescope yielding a sub-degree field of view needed for spatial resolving power. The entire optical system is diagrammatically shown in Figure 2-1.

An optically-compensated interferometer has the high throughput needed to achieve a relatively high temporal resolving power, in other words, a scan time of less than a minute. Temporal variations are therefore identified while maintaining a spectral resolution of 2 cm^{-1} in the near-infrared. A spectral resolution nearly this high is

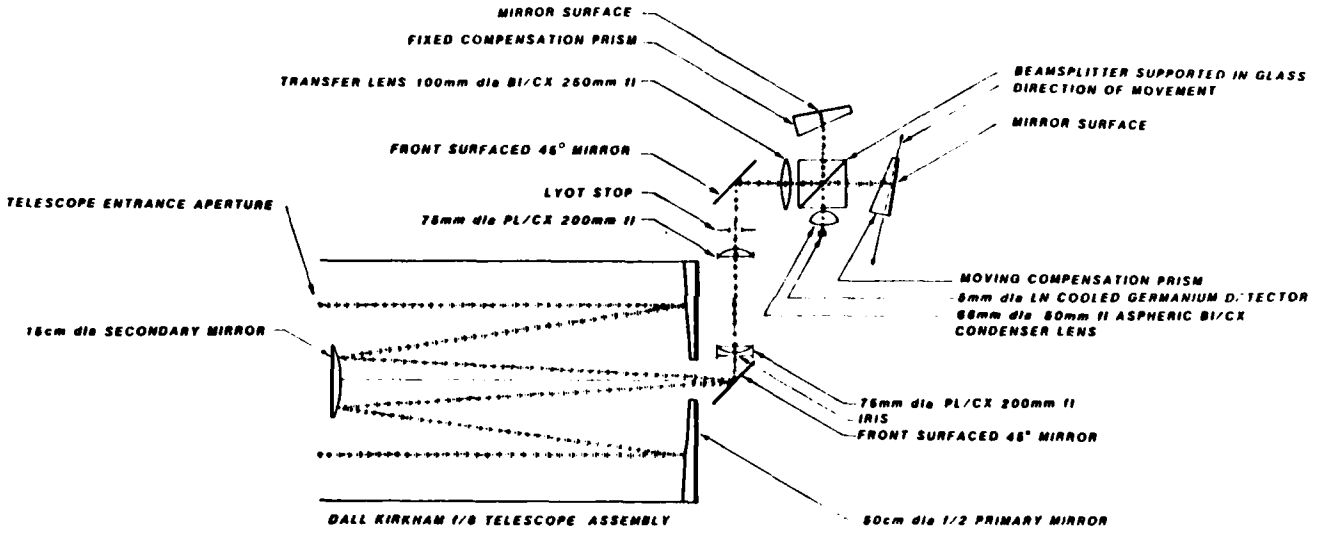

Figure 2-1. Optical layout of interferometer telescope system.

desirable in order to unambiguously compute OH rotational temperatures from the measured spectra. A free spectral range of 0.8 to 1.6 μm has been obtained using a cryogenically-cooled intrinsic germanium detector. The optical system was designed to maintain the high throughput capability (0.285 cm^2 sr) of the interferometer while operating at a narrow field of view (<1°) in order to be able to resolve the spatial nature of the airglow structure.

The design criteria and the resulting design for an optically-compensated interferometer are given in this chapter. Then an analysis is made of the resulting interferometer-spectrometer system.

High-Throughput Interferometer Design

The optical layout of a conventional Michelson interferometer was discussed in Chapter I. Referring to Figure 1-2, the retardation or path difference is a function of the entry angle of the incoming energy. The relationship is, $\Delta=2d\cos\theta$, where d is the on-axis ($\theta=0°$) drive distance and θ is the angle of the off-axis ray. The maximum field of view for a standard Michelson interferometer is, $\Omega_{max}=2\pi/R$ (Eq 1.1), where Ω_{max} is the maximum field of view of the instrument and R is the resolving power. When viewing faint airglow events this limitation on throughput is a severe one. The optical system is compensated to increase system throughput for temporal resolution. This high-throughput has been matched to a collector system to

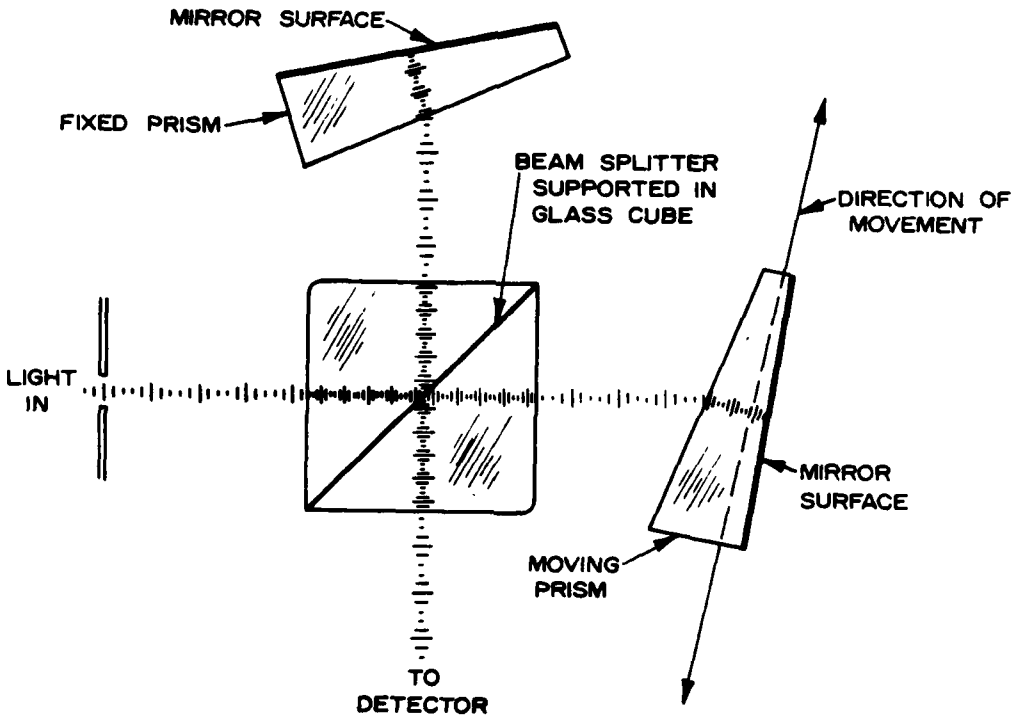

Figure 2-2. Optical compensation method conceived by Connes [1956].

maintain the throughput while narrowing the field of view (for spatial resolution).

The method used in this study to improve the throughput of the interferometer system is the one analyzed by Bouchareine and Connes [1963] and is depicted in Figure 2-2. The compensated-optics design used follows that developed by Despain et al. [1971], and the design limitations previously derived will be summarized here for completeness. Figure 2-3 shows the compensation analysis approach of Steed [1978]. With the optical compensation prisms inserted, the retardation is

$$\Delta_c = 2d \cos\theta + 2tn \cos\phi - 2t \cos\theta \quad , \quad (2.1)$$

where

Δ_c = retardation with compensation prisms inserted,

t = thickness of optical material,

n = index of refraction of optical material,

d = mirror drive distance, AC - AB,

θ = angle of off-axis ray,

ϕ = refraction angle of off-axis ray through optical material.

The retardation equation shown above can be expanded in a Taylor series and like terms collected to show the field of view dependency more directly; namely,

$$\Delta_c = 2\left[t(n-1) + d\right] + \left[t\,\frac{n-1}{n} - d\right]\theta^2 + \left[\frac{d}{12} + \frac{t(n^2-1)}{3n^3} + \frac{t}{12n^3} - \frac{t}{12}\right]\theta^4 \quad . \quad (2.2)$$

which is a quartic equation in θ.

Ideally, the retardation Δ_c should be independent of the entry angle θ. Equation 2.2 shows that this is not possible by varying only the drive distance d and the index of refraction n. However, a significant improvement can be realized by designing such that,

$$d = t\left[\frac{n-1}{n}\right] \quad , \quad (2.3)$$

which eliminates the θ^2 term in the retardation Equation 2.2 by forcing the θ^2 coefficient to zero. This leaves only

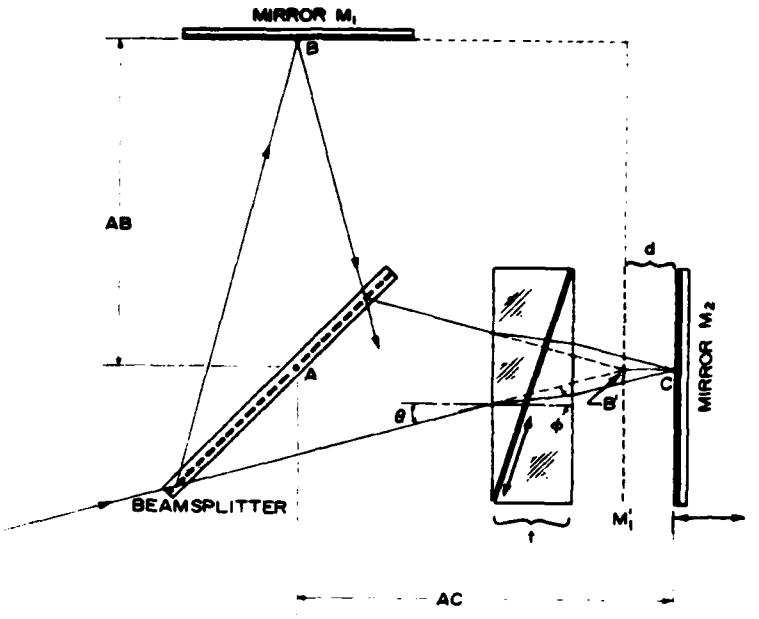

Figure 2-3. Optical compensation with an optical section inserted into one leg of a Michelson interferometer [Steed 1978].

the θ^4 term and since θ is small this term is relatively insignificant.

Designing the compensation wedges to satisfy Eq 2.3 and then solving Equation 2.2 for an on-axis ray ($\theta=0°$), the resulting retardation Δ_{co} is

$$\Delta_{co} = \frac{2t}{n}[n^2-1] \quad . \tag{2.4}$$

Assuming a monochromatic wave front and using the results of Eq 2.4, the general retardation for the compensated case is

$$\Delta_c = \Delta_{co} + \Delta_{co}\left[\frac{\theta^4}{8n^2}\right] \quad , \tag{2.5}$$

where

Δ_C = compensated retardation,

Δ_{CO} = retardation for an on-axis ray.

θ = entry angle for incoming ray in radians

n = index of refraction of compensation prisms.

The analysis for the Connes [1956] method shown in Figure 2-2, in which only one optical component is driven, is the same as for the system shown in Figure 2.3. The thickness of the optical material must, however, increase with the drive distance d in order to maintain optical compensation (see Equation 2.3). The increase in optical-material thickness needed to maintain compensation is obtained by driving one of the optical wedge/mirror assemblies in synchronism with the drive motor. Referring to Figure 2-2, it can be seen that the reflective elements or mirrors in this method are created by depositing the mirrored surface to the back side of each wedge.

Steed [1978] derived the limits on field of view as a function of resolving power based upon aberration limits. The results are categorized into several groups. The first is chromatic aberration, that is, differences in the compensation because the index of refraction of the optical material is a function of wavelength. The chromatic limit is

$$\Omega_C = \left[\frac{\Omega_M \, n(n^2 - 1) \, \lambda}{\delta n \;\; \Delta_{CO}}\right] R \quad , \qquad (2.6)$$

where

Ω_c = field of view at wavelength λ in steradians,

Ω_M = field of view for conventional Michelson interferometer,

n = index of refraction at wavelength λ,

δn = $n-n_c$ *where* n_c = index of refraction at compensated wavelength,

R = desired resolving power,

Δ_{co} = retardation for on-axis ray,

λ = wavelength expressed in same units as Δ_{co}.

The second limiting factor on field of view is that of spherical aberration. This limit is also derived by Steed [1978]. The maximum field of view assuming only spherical aberrations is

$$\Omega_s = \Omega_M \, n \sqrt{(2R)} \quad . \tag{2.7}$$

The third type of aberration is astigmatism. In the Connes method a wedge is placed in each leg of the interferometer; however, only one of the wedges is driven. This simplifies the mechanical design but because a wedge is in each optical path, astigmatism aberrations occur. The severity of the aberration increases as the angle (α) of the compensation wedges increases. Bouchareine and Connes [1963] quantify this aberration as

$$\Omega_A = 2\Omega_M / \tan^2 \alpha \quad , \tag{2.8}$$

where

α = prism angle of the compensation wedge.

The aberrations considered were each derived assuming the net effect of the distortion was a shift of one fringe in the interference pattern. These degradations prove to be the limiting factors upon the maximum usable field of view. Figure 2-4 is a plot of Equations 2.6, 2.7, and 2.8 and shows the relationship between these various limits. At least an order of magnitude improvement in throughput is obtainable using the wedge prism compensation technique.

The next step in the system design is to ascertain the optical retardation for the Connes [1956] method. Referring to Figure 2-5, Steed [1978] showed the drive plane is parallel with the apparent image plane of the optical wedges. The difference in optical path length or retardation between image points A1 and A2 separated by a drive distance X is

$$\Delta = 2X \sin(\beta-\gamma) \quad , \tag{2.9}$$

where

$\beta = \sin^{-1}(n \sin\alpha)$,

$\gamma = \alpha - \tan^{-1}\left[\left(\frac{n-1}{n}\right) \tan\alpha\right]$,

α = wedge angle,

X = drive distance.

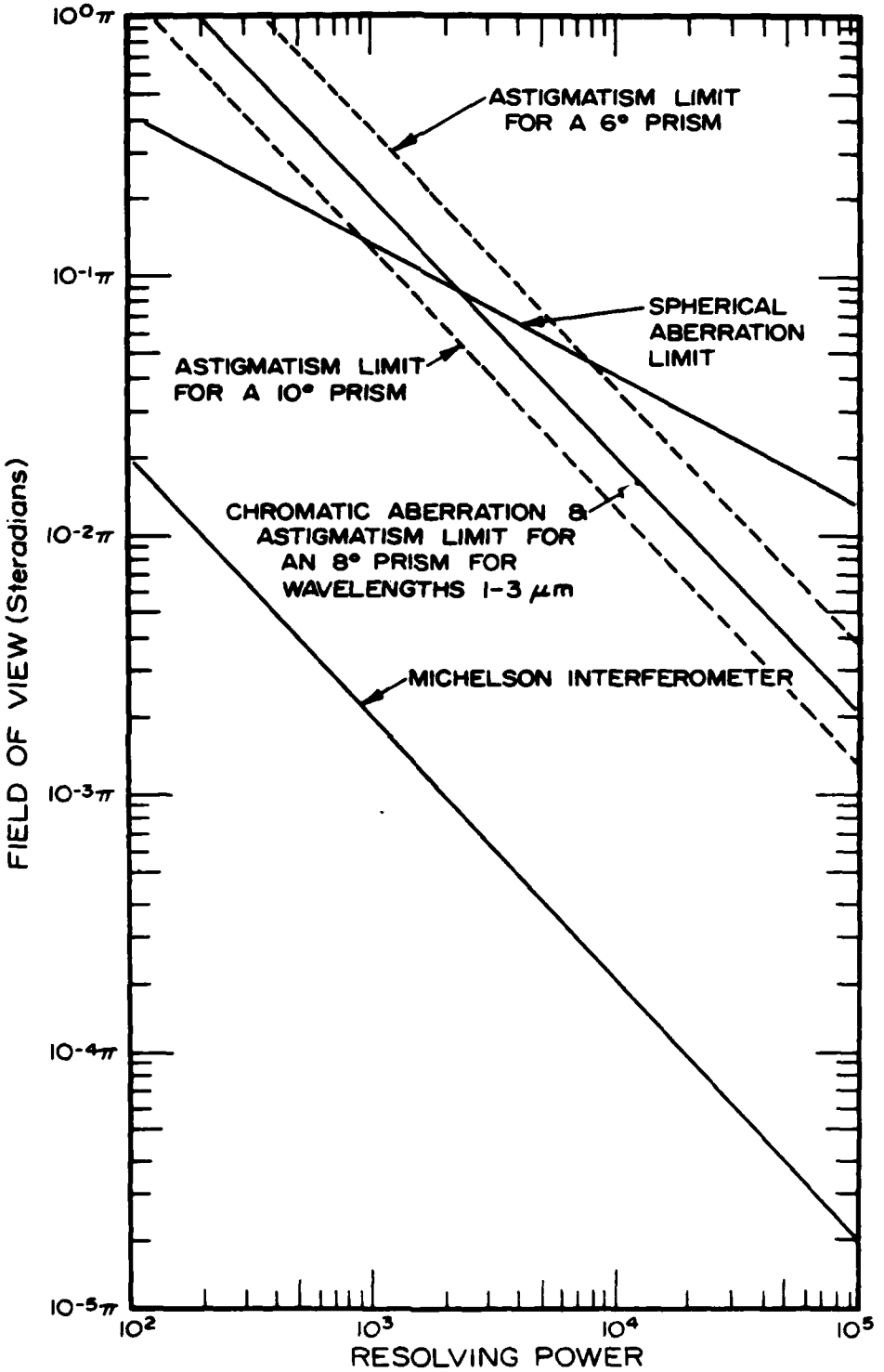

Figure 2-4. Plot of aberration limits for Connes [1956] method of optical compensation compared with conventional Michelson interferometer [Steed 1978].

Drive System

Examination of Equation 2.9 shows that the choice of a large wedge angle reduces the actual drive distance, thereby easing the mechanical drive requirements. However, the choice must be made in conjunction with the limits on distortion presented in Figure 2-4. The wedges and cube beamsplitter used in this instrument are made of a high quality quartz, namely, Infrasil I, manufactured by Amersil Corporation. The measured index of refraction for this material is 1.45. A compensation prism wedge angle of 8° was chosen. Solving Equation 2.9 for this wedge angle, then $\beta = 11.64°$, $\gamma = 5.50°$, and $\Delta = 0.21X$. The optical retardation for this compensation technique is only about 20% of the drive distance, where as in a conventional Michelson interferometer the retardation is equal to $2d$ where d is the drive distance. Thus, for a given spectral resolution the compensated interferometer requires a drive distance of 2/.21=9.5 times longer than the conventional Michelson approach.

An optically-compensated interferometer with a spectral resolution of 2 cm^{-1} requires a slide movement of 3.1 cm. This comparatively large drive distance is accomplished using a gas-lubricated platform, providing near-zero friction, developed by Haycock [1975]. The platform translates the optical wedge/mirror assembly and as such must maintain mechanical tolerances as close as possible to the wavelength dimensions of the infrared light being

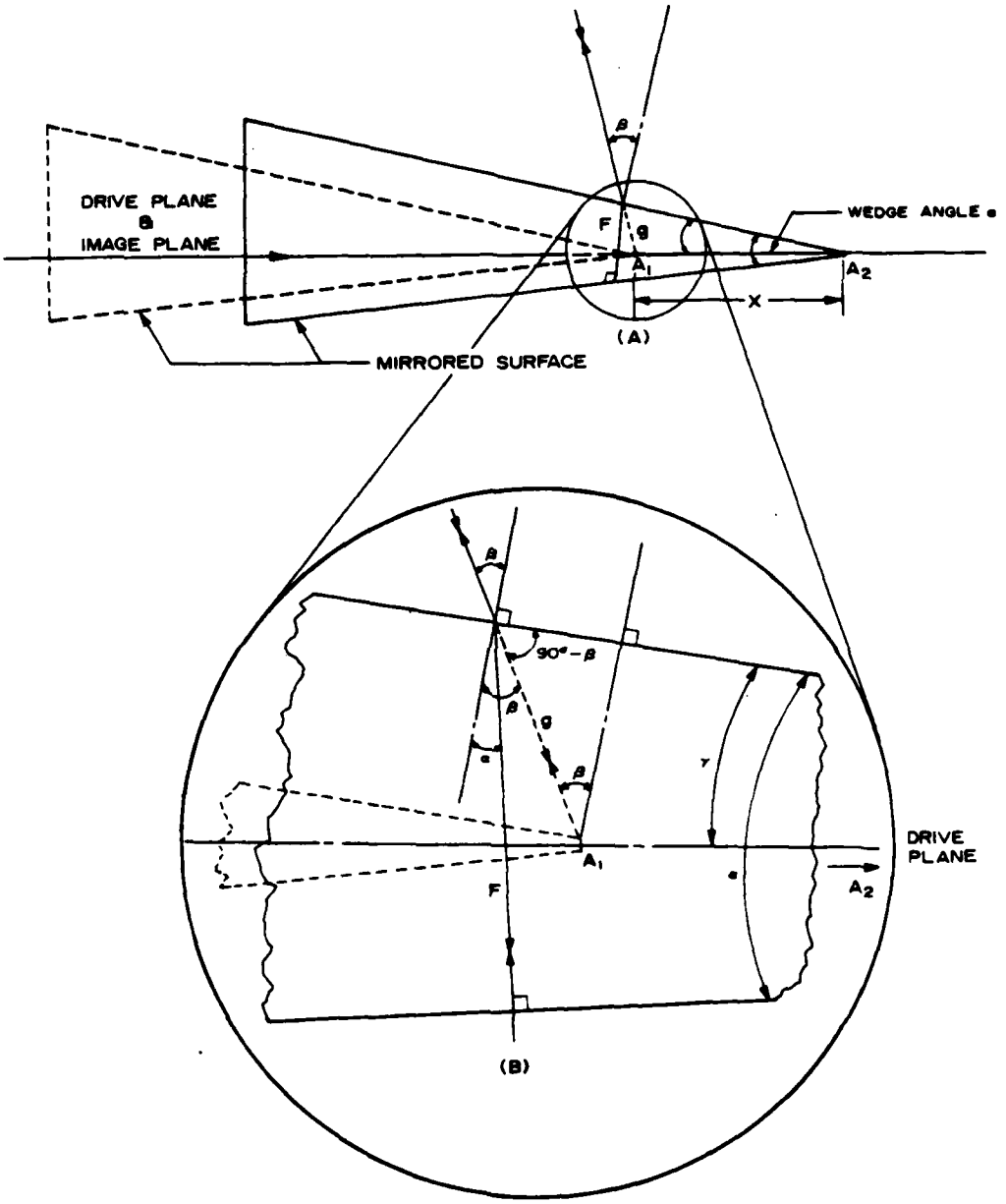

Figure 2-5. Cross section of optical wedge in two drive positions a distance *X* apart [Steed 1978].

measured. The gas bearing surfaces are lapped to a tolerance of about 1 wavelength of 5461 Å light and operate with a clearance of 2.5×10^{-4} cm. At an operating pressure of 6-12 psi the bearing will maintain an optical alignment of 1 arc second while translating 5 cm [Haycock 1975]. The optical components are then mounted on the bearing-supported optical platform. Adjustment for parallelism is accomplished on an optical bench using a laboratory He-Ne laser as a light source. The material used in the platform and bearing assembly is a specially formulated Invar alloy, chosen for its excellent temperature and stability characteristics and to match the thermal expansion characteristics of the optical material. This sophisticated platform provides the relatively long drive distances required (up to 5 cm) as well as the mechanical accuracy needed to translate the optical components properly.

The platform is driven by a "voice coil" motor and therefore makes no physical contact with the rest of the instrument. The motor is driven by a standard servo-amplifier with feedback from positional and velocity sensors located within the platform slide. The main signal driving the slide is generated by a digitally-controlled ramp which can be adjusted for slide velocity and drive distance. The slide controller can produce variable scan times of 5 seconds up to several minutes, and a drive distance of up to 5 cm. The completed interferometer uses a 10-cm cube beamsplitter and 11.4-cm diameter end wedges with a prism

angle of 8°. The interferometer with bearing system is shown in Figure 2-6.

For simplicity, a secondary HeNe laser-excited interferometer is used, with its independent moving mirror on the same optical platform as the primary optical signal channel, to monitor the slide position. The laser signal is counted down by 6 and used to digitize the main channel interferogram. This method provides sufficient sample points for a 16k fast Fourier transform.

The other specifications for accuracy of the optical and mechanical components are described in detail by Steed [1978]. The entire system was originally designed to be operated at liquid nitrogen temperature (77 °K) to reduce background radiation at longer wavelengths (>2 μm). The spectral range used in this study (0.8 to 1.6 μm) is not background limited and therefore does not require the added complexity of optical train cooling.

Detector System

The optically-compensated interferometer has a very large throughput ($A\Omega$ = 1 $cm^2 sr$). The desired goal of optical compensation was to improve the sensitivity of the interferometer system; however, to take advantage of the large throughput a large diameter detector is required. For example, assuming a throughput of 1 cm^2 sr and collector optics with a very fast f-number of 0.5, the detector diameter would have to be 0.650 cm. Large infrared

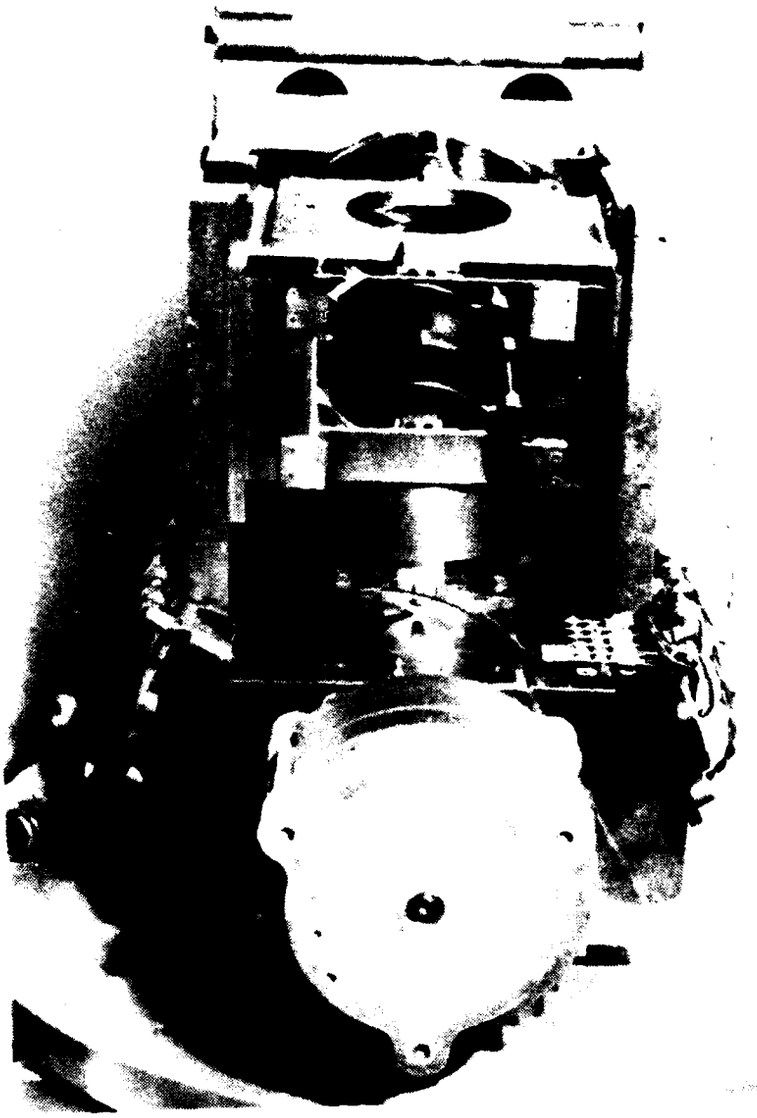

Figure 2-6. Optically-compensated interferometer showing beamsplitter, wedges, and bearing assemblies.

detectors with the necessary detectivity are very difficult to manufacture; therefore, some compromise was necessitated. The required detector diameter and the speed of the collecting optics shown in the example are both somewhat impractical.

A detector system was chosen which was readily available and had proven effective in the past. The detector selected was an RCA Ltd., solid state germanium device with a self-contained preamplifier and load resistor in a liquid-nitrogen dewar. Figure 2-7 is a picture of the detector dewar. The detector is 5 mm in diameter and has a noise equivalent power (NEP) of 1.12×10^{-14} W/√Hz at 1.27 µm and covers a spectral range of 0.8 to 1.6 µm.

It was decided that a scan rate of 30 seconds would be sufficient to resolve the temporal variations of first interest in the OH airglow structure. This decision was based upon video data gathered by Taylor et al. [1980]. A 30-second scan, a minimum wavelength of 0.8 µm, and a drive distance of 3.1 cm (spectral resolution of 2 cm^{-1}) set the detector electrical bandwidth at 150 Hz. The RCA detector has a bandwidth of 600 Hz. Appendix A contains the detailed specifications of the detector system.

Telescope Design

The spatial characteristics of the airglow structure, shown by Taylor [1983-84], dictated that the instrument field of view be less than 1° full angle. The goal of the

Figure 2-7. Picture of RCA Limited liquid-nitrogen cooled germanium detector system.

optical design was to maintain the inherent high throughput of the compensated interferometer throughout the entire system. All portions of the optical path were examined in order to ascertain where the system was throughput-limited. The choice of a detector, and practical limitations on the f-number of available condenser lenses proved to be the limiting factors. An optical system was designed, incorporating the interferometer, using a large diameter collector, which maintained the system throughput while narrowing the field of view to under 1°. The instrument system was now capable of measuring the temporal, spectral, and spatial variations of the airglow layer.

The design of the optical system began with the detector and choice of its condenser lens and proceeded back towards the telescope collector. The entire optical system is described diagrammatically in Figure 2-1. The diameter of the condenser lens must, however, allow the converging beam to pass through the beamsplitter and wedges without vignetting. A commercially available condenser lens with a diameter of 68 mm and an effective focal length of 50 mm was chosen. The condenser lens and detector diameter of 5 mm set the system throughput or $A\Omega$ at 0.28 cm^2sr. Referring to Figure 2-1, a throughput of 0.28 cm^2sr translates to a beam diameter entering the interferometer of 92 mm and converging in a 6° full field of view. The physical dimensions of the detector optics outlined here fit well within the size constraints of the basic interferometer. The field of view

is also within the aberration limits, shown in Figure 2-4, for an optically-compensated interferometer.

The calculated throughput can now be used to design the telescope needed to narrow the field of view to 1° or less. A throughput, dictated by the detector system, of 0.28 cm^2sr and a 1° field of view design goal, set the collector diameter at $D = A\Omega/2\pi(1-\cos\theta)=44$ cm. A 50.8-cm (20-inch) diameter system was chosen because of availability and to allow for some error in aligning the telescope optics. Taking advantage of the larger collector, the field of view was narrowed to 0.8° requiring a 48-cm diameter collector, within the 50.8-cm mirror size and still allowing for some error in optical system alignment. For portability, an f/2 primary was specified to minimize the telescope length. An overall system f number of 8 was selected to transfer the telescope image to the proper position.

In this application, the purpose of the telescope is to gather energy and transfer it to the detector, rather than to transfer a spatial image. Therefore, the quality of the optical image within the field of view is not of as great a concern as it would be in an imaging system. Many types of folded telescope systems were considered. In order to simplify the optics Driscoll and Vaughan [1973] suggests a Dall-Kirkham type because of the spherical secondary, if the resulting image distortion is acceptable. The distortion for a Dall-Kirkham system of this size was calculated using the formula in Driscoll and Vaughan [1973], and found to be

less than 0.4% of the area (coma and astigmatism distortion were calculated in terms of primary mirror area that will be degraded) of the primary mirror. Therefore, a Dall-Kirkham type of telescope, being more than adequate, was chosen for its simplicity and relatively low cost. This type of telescope has a spherical secondary mirror and an elliptical primary mirror. The telescope-equipped interferometer system with the isocon camera mounted on the telescope is pictured in Figure 2-9.

The last step in the optical design was to provide an optical interface between the telescope and the detector sub-systems. Two primary considerations were given emphasis in this interface design: (1) imaging the detector on the primary mirror, and (2) imaging the condenser lens on the telescope focal plane. The detector may have an uneven response across its area, therefore imaging the detector on the primary mirror minimizes the effects of off-axis rays by illuminating the entire detector by light entering within the field of view of the instrument. An image of the detector condenser lens at the telescope focal plane allows for independent control of the system field of view.

An adjustable iris was then placed at the focal plane for adjusting the field of view while still allowing the entire detector to be illuminated by energy within the field of view. Careful choice of physical dimensions and optics allow the transfer of each image independent of the other.

The goal of placing a detector image on the primary mirror was accomplished by the use of two lenses. Referring to Figure 2-1, a transfer lens, which has a diameter of 100 mm and a focal length of 250 mm, is placed near the interferometer beamsplitter. This lens produces an image of the detector at a focal point near the physical entrance to the interferometer housing. The magnification ratio of this transfer lens focal length to the focal length (50 mm) of the condenser lens determines the detector image size at this point; therefore, the detector image is 25 mm in diameter. A field stop is placed at this point to limit the detector image size throughout the rest of the system. Another transfer lens, which has a 75-mm diameter and a focal length of 200 mm, is placed at the focal plane of the telescope. This lens transfers the detector image at the field stop onto the primary mirror. As can be seen from Figure 2-1, two angled mirrors were required to meet the physical constraints of the design.

The second design objective of the optical transfer system was to place an image of the detector condenser lens on the telescope focal plane. A collimated image of the condenser lens is generated by the 100-mm diameter transfer lens that is placed near the interferometer beamsplitter. The addition of a 75-mm diameter, 200-mm focal length lens placed at the field stop focuses this image at the telescope focal plane. The placement of this lens at a detector image point does not affect that image. An adjustable iris was

then placed at the telescope focal plane for control of the field of view. The field stop and the iris provide the limiting apertures for the entire system. The optical system described here was verified by Harris [1984] using a computer-aided optical ray-tracing program.

The optical lenses used in the design are made of commercial-grade optical glass and have no coatings. The beamsplitter and wedges are constructed of quartz and are not coated. The primary and secondary telescope mirrors are aluminized reflection surfaces with a SiO_2 coating.

Instrument Housing

The interferometer-spectrometer with its associated optical and telescope systems was placed in a 30-inch diameter, 45-inch tall, round container. The interferometer placed in the instrument housing is shown in Figure 2-8. The telescope attached to the container is shown in Figure 2-9. The large container size was chosen to support the telescope in a stable manner. The base of the package was mounted upon a rotating stand which provides the ability to move the telescope in azimuth. The rotating base has attached three large pneumatic tires for system mobility and three leveling screws to stabilize the interferometer for operation. The telescope is mounted to the side of the container with a 10-inch diameter ball-bearing allowing the telescope to be rotated in elevation. The two rotating joints provide the telescopy with complete pointing freedom.

The specifications of the instrument with the telescope are given in Table 2-1.

TABLE 2-1. Summary of interferometer-spectrometer specifications.

Throughput	0.28 $cm^2 sr$
Scan period (minimum)	1 scan/ 30 seconds
Collector diameter	50.8 cm
Field of view (full angle)	0.8 degrees
Spectral range	0.8 to 1.6 μm
Spectral resolution	2 cm^{-1}
Detector type	Intrinsic germanium
Detector NEP	1.1×10^{-14} watts/√hz at 1.5 μm
Dynamic range	80 dB
System sensitivity	16 R/cm^{-1} at 1.5 μm

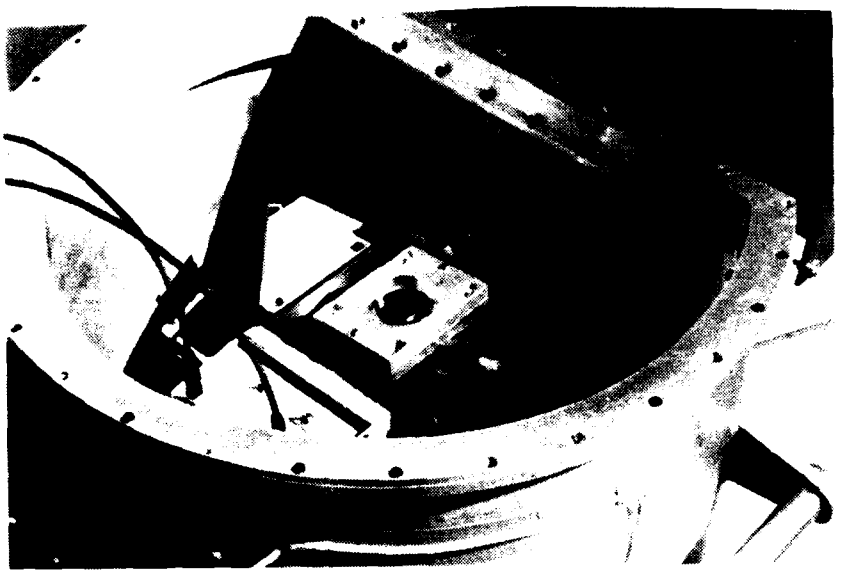

Figure 2-8. Interferometer placed inside housing.

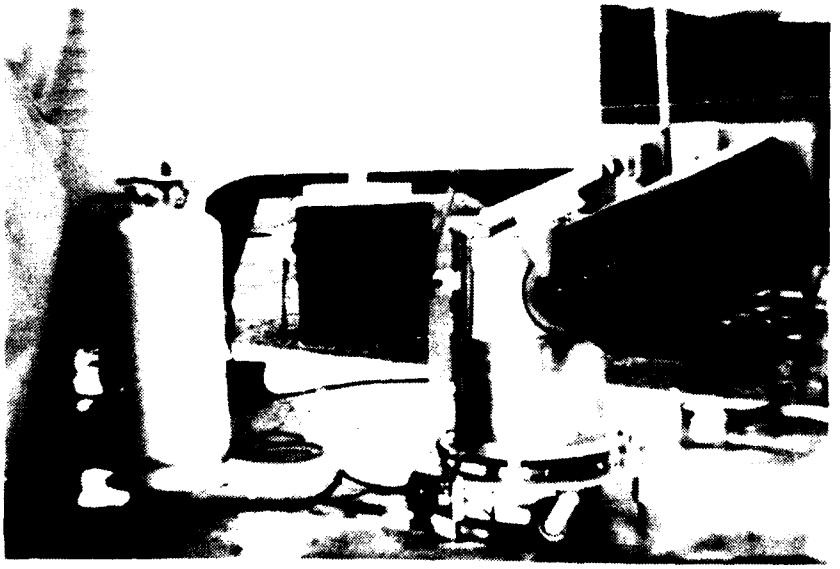

Figure 2-9. Interferometer system equipped with 20-inch diameter telescope. The isocon camera is also mounted on the telescope.

CHAPTER III

MEASUREMENT THEORY

The Interferogram

The electronic signal from the interferometer detector is a low-frequency time-continuous signal called an interferogram. The interferogram is a scaled analog of the incoming light frequency. Using the approach of Loewenstein [1971], and referring to the layout of a Michelson interferometer in Figure 1-1, the interferogram signal is of the form

$$f_s = v\sigma \quad , \tag{3.1}$$

where

σ = input light wavenumber in cm^{-1},

v = rate of change of effective path difference in cm/second,

f_s = scaled frequency output of interferometer (the interferogram) in Hz.

The detector used in this study is sensitive in the region from 12500 to 6250 cm^{-1} (λ = 0.8 to 1.6 μm). The scan rate for the interferometer was set at 30 seconds; therefore, the input light frequency was scaled to audio frequencies of less than 200 Hz.

The light power reaching the detector in an ideal interferometer is [Loewenstein 1971]

$$P_{det} = 2A^2(1+\cos 2\pi\sigma x) \quad , \qquad (3.2)$$

where

A = amplitude of on-axis monochromatic point source,

x = effective path difference in cm.

In the Loewenstein model, the single line of Equation 3.2 is replaced by an input power density spectrum of the form $A^2=B(\sigma)$. Making this substitution in Equation 3.2, neglecting the constant (dc) part, and integrating over σ produces

$$I(x) = 2\int_0^\infty B(\sigma)\cos(2\pi\sigma x)\,d\sigma \quad , \qquad (3.3)$$

where $I(x)$ is defined as the interferogram. The desired information $B(\sigma)$ (the input spectrum) is obtained by taking the inverse Fourier transform of $I(x)$. The signal produced by the interferometer is referred to as a "double-sided" or "symmetric" interferogram. An example of a double-sided interferogram is shown in Figure 3-1; note that the same information is available on both sides of the large center which occurs at zero path difference. The interferometer slide is moved an equal distance on each side of the optical zero path difference to create a symmetrical signal.

Since the interferogram $I(x)$ in Equation 3.3 is symmetric, the spectrum $B(\sigma)$ may be obtained using a simple

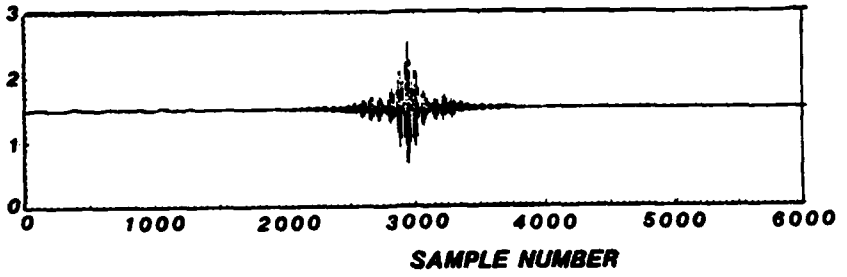

Figure 3-1 Typical "double sided" interferogram.

cosine transform of the form

$$B(\sigma) = \int_0^{\infty} I(x) \cos(2\pi\sigma x)\, dx \quad . \qquad (3.4)$$

The power spectral density is computed with a digital computer using a Fast Fourier Transform (FFT). The FFT used to process the data for this study was developed by Ware [1980]. The digitized interferogram was produced using a 12 bit analog to digital converter on the detector amplifier output and enough samples were taken to perform a 16,384-point transform. The implementation of the FFT is beyond the scope of this paper but that used in Fourier transform spectroscopy was adapted by Forman [1966] from the radar signal processing work of Thomas Stockham, then at MIT Lincoln Laboratory. The FFT is explained extensively by Brigham [1974].

The computation of the FFT requires that the interferogram be sampled at uniform increments of path difference. Ideally, the laser reference channel should be a short wavelength laser beam which passes through the

interferometer optical train as does the signal. Otherwise, the reference beam may experience different motion stability than the signal beam, due to nonidentical geometry. However, for simplicity, a separate laser (λ = 6328 Å) interferometer channel was used and provides the uniform sampling function signal. The laser channel signal is divided to obtain a sample rate of 650 Hz. The interferogram is digitized at a free running rate of 50 kHz. The values taken between laser channel zero crossings are then averaged and stored as the data point for the slide position corresponding halfway between adjacent laser crossings. This over-sampling method will, according to Ware [1980], minimize the system noise gain as well as minimize the effects of slide velocity variations in the sampled data.

Calibration Source

The determination of relative OH spectral line strengths is sufficient to compute rotational temperatures. Since this is a major interest in this study, a calibration technique to produce a relative instrument response was developed. The absolute calibration of an interferometer-spectrometer is an intricate process; details of the approach are outlined by Wyatt [1978]. Ware [1980] performed an interferometer wavenumber response calibration as a function of optical alignment. He found that the relative response must be reestablished each time the

instrument is realigned at the time of data collection because the instrument would only remain in acceptable alignment for about 2 hours..

A relative instrument response was obtained by causing the interferometer to view a calibration source composed of a tungsten bulb illuminating a pair of ground glass diffusion screens (see Figure 3-2). The intensity of the illumination was controlled by placing a plate with a small 3-mm aperture between the bulb and the diffusion screens. The second screen was then imaged by a projector lens onto a 24-inch diameter ground glass viewing screen placed ten feet away. The net brightness of the source was adjusted so the calibration source intensity as viewed by the interferometer was approximately that of the night sky. The calibration source assembly was mounted inside of a 24-inch diameter, 10-foot long tube. The viewing screen was sufficiently large to completely fill the interferometer field of view, thus providing a diffuse source.

The long length (3.0 meters) of the calibration source was chosen to ensure that the illumination on the viewing screen was uniform across the entire surface viewed by the interferometer. The quality of the calibration source was calculated using the geometry described above and assuming the tungsten bulb was a blackbody source with correction for the emissivity of tungsten.

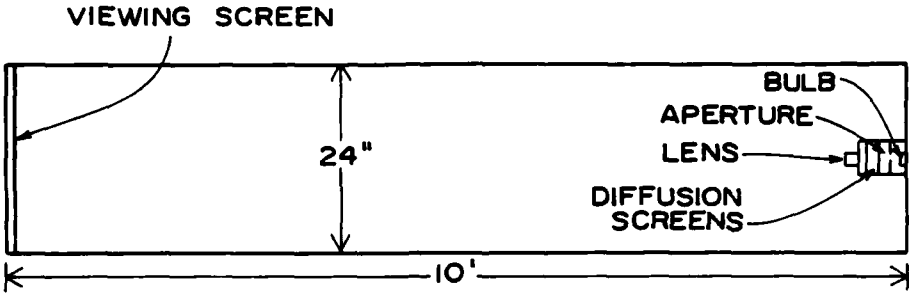

Figure 3-2. Interferometer Calibration Source.

Instrument Response

A relative instrument response was obtained each time the instrument was realigned during the data taking process. The calibration alignment process was repeated about every 2 hours. The interferograms obtained from the instrument when observing the calibration source were transformed using the same FFT and apodization (discussed later in this chapter) routines as were used for the airglow data signal processing described above. The calibration source spectral or "blackbody" curves were then averaged together (from 5 to 10 frames) to minimize noise and irregularities.

The tungsten bulb in the calibration source has a blackbody equivalent temperature of 2370 °K when operated at the specified current (750 mA), according to Gilway Technical Lamp [1982], its manufacturer. The Plank equation can be used to calculate the spectral sterance $L_B(\lambda)$ in watts/meter, for the assumed blackbody radiation source as, shown by Wyatt [1978]

$$L_B(\lambda) = \left[\frac{2hc^2}{\lambda^5 \left[\left(\exp \frac{hc}{\lambda k T} \right) - 1 \right]} \right] , \qquad (3.5)$$

where

h = 6.6262×10^{-34} (Js) (Plank's constant) [Wyatt 1978],

c = 2.9979×10^{8} (m/s) (speed of light) [Wyatt 1978],

λ = wavelength (m),

k = 1.3806×10^{-23} (J/°K) (Boltzmann's constant) [Wyatt 1978],

T = absolute temperature (°K).

The interferometer detector measures energy coming from the interference of two light rays of the same optical frequency; and the germanium detector operates in a photon sensitive mode. As a consequence, in the analysis it is desirable to manipulate Plank's equation into terms of wavenumber and quanta (photons). The relationship between sterance and photon sterance is

$$L_p = L_B \lambda / (hc) \quad . \qquad (3.6)$$

Noting the relationship between wavenumber and wavelength and that Equation 3.5 is a density function

$$\sigma = 1/\lambda \quad , \qquad (3.7)$$

$$d\sigma = - 1/\lambda^2 \, d\lambda \quad . \qquad (3.8)$$

Using Equations 3.7 and 3.8 and converting from meters to centimeters, Plank's equation can now be shown in terms of photons cm^{-2} sr^{-1} sec^{-1} cm^{-1} or

$$L_p(\sigma) = \left[\frac{2c\sigma^2}{(\exp \frac{hc\sigma}{kT}) - 1} \right] \quad . \qquad (3.9)$$

The photon sterance for the 2370°K tungsten bulb calibration source was calculated using Equation 3.9 and corrected for the emissivity of tungsten using data from Weast [1977]. The averaged blackbody spectrum taken by viewing the calibration source, was then divided by the photon sterance. The resulting curve was normalized to its peak value and constitutes the relative instrument response used in the rotational temperature calculation model developed in Chapter IV. The values for the instrument response curve are shown as part of Tables 4-1, 4-2, 4-3, and 4-4.

Phase Correction

The spectrum computed from an interferogram using the selected FFT is algebraically complex (contains both real and imaginary parts) [Ware 1980]. The incoming signal contains no inherent phase information; therefore, any phase angle computed during the FFT process is an artifact of the system. A nonzero phase relationship is caused by two main factors. First, phase shifts occur in optically-compensated interferometers because the optical beamsplitter, wedges, and lenses are not strictly uniform as a function of wavenumber. Second, a linear phase shift occurs during the sampling of the interferogram for FFT processing, when the

zero path difference point is not centered in the signal time window.

The amplitude of the measured spectrum could be obtained by the magnitude operation (square root of the sum of the squares of the real and imaginary parts). However, this operation always yields positive noise components, increasing the noise by $\sqrt{2}$. This increase in noise is especially harmful when several frames of data are signal averaged (coadded) to help identify low weak features in the airglow emission spectrum. The sampling phase shift error may also vary from frame to frame. Consequently, a method of phase correction based upon the data within each frame must be used.

The phase characteristics of each data frame could be obtained by Fourier transforming a small data set around the "center" of the interferogram. This process would yield a very low resolution spectrum from which the slowly varying phase information could be easily extracted. However, this truncation and transform process is the same as convolving the original spectrum with the Fourier transform of the truncating function. As described by Ware [1980], this convolution is merely a digital filter operating in the frequency/phase domain. Hamming [1977] showed that for a given filter width the minimum noise gain is obtained when the convolving function is rectangular in shape. The phase characteristics are not related to the incoming signal in any way so the rectangular filtering process may be

repeated as many times as necessary to identify and remove the phase anomalies from the computed spectrum. When the filtering process is complete, the remaining "real" part of the transform is used as the measured spectrum (power spectral density function).

The spectral frames were phase corrected with convolving filter windows of 3, 5, 9, 17, and 65 sample point widths in a repetitive manner. Figure 3-3 shows an instrument uncorrected blackbody curve both before and after phase correction, and Figure 3-4 shows the same information for a spectral frame. Examination of Figures 3-3 and 3-4 show that the imaginary portion of the power spectral density (caused by chromatic variations within the instrument optics) has been eliminated by the phase correction algorithm.

Apodization and Interpolation

The calculation of OH airglow rotational temperatures was a major goal of this study. The calculation of temperature requires the extraction of relative spectral line intensities from the transform of the interferogram. The relative instrument response and phase correction steps described above are modifiers in signal processing the line intensities.

The shape of an individual spectral line is of interest because the shape will affect how the a best estimate of the line emission intensity is extracted from the data. Due to

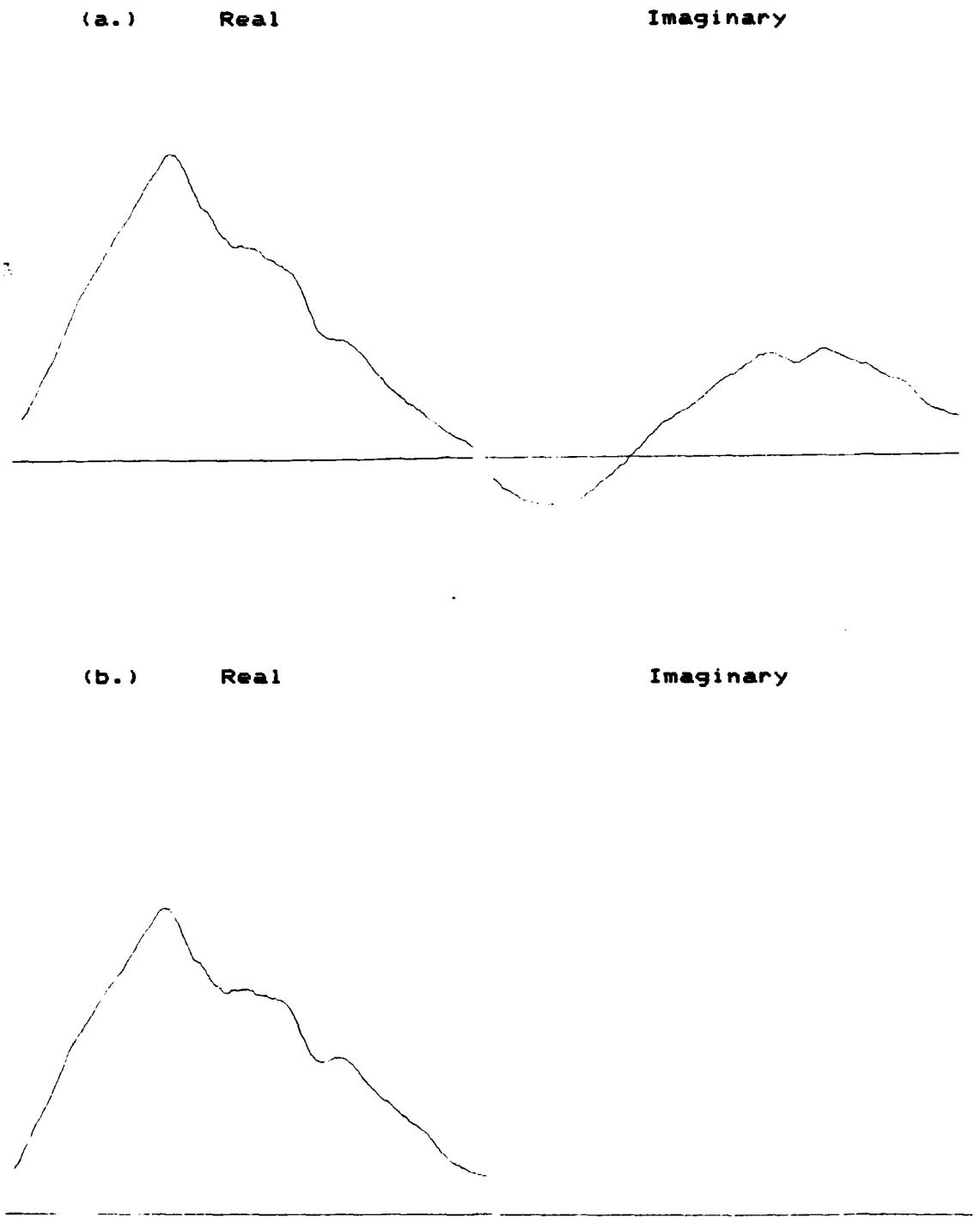

Figure 3-3. Real and imaginary parts of a blackbody curve (a.) before and (b.) after phase correction.

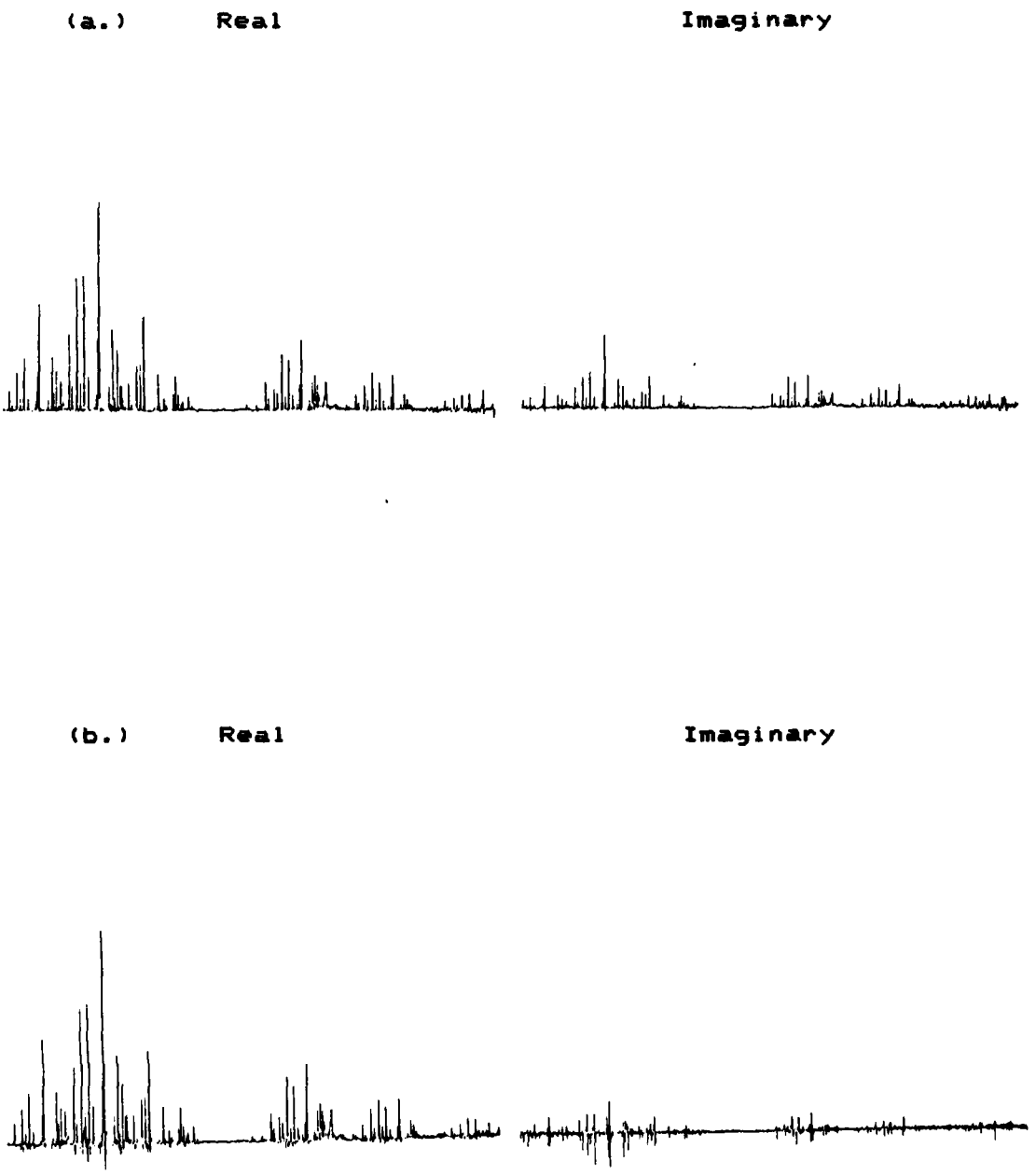

Figure 3-4. Real and imaginary parts of a spectral curve (a.) before and (b.) after phase correction.

the discrete nature of the transitions of the excited OH molecule, the spectral lines entering the interferometer are discrete in shape except for a small finite width due to Doppler and collisional broadening plus "time windowing" of each photon source. The numerical computation of an FFT requires that the sampling be limited in length. The truncation or multiplication of the interferogram by a rectangular "window" in the time domain is the same as frequency domain convolution of the discrete spectral frequencies with the Fourier transform of the rectangular window function. The Fourier transform of the rectangular window is a (sin x)/x or "sinc" function. This characteristic spectral line shape is referred to as an "instrument function." The high side lobe behavior of the sinc function (largest side lobe -13 dB down in amplitude) causes the various lines in the spectrum to interact or mesh together. Therefore, it is desirable to establish a technique to suppress the sinc function behavior and force the signal component into as much of a discrete line shape as possible.

The process of suppressing the sinc function side lobes is called apodization. The apodization of the spectral information can be accomplished either in the interferogram domain by multiplying the interferogram with another window then performing the FFT, or by convolving the transform of the window with the transformed interferogram. The

convolution of the spectral data with the transform of the chosen window is the method used for this study.

Numerous apodization functions have been tried for use with Fourier transform spectroscopy. In choosing an apodizing function the trade-off is among instrument function width (resolution), side lobe attenuation, and computational efficiency. Norton and Beer [1976] computed over 1100 different apodization windows and plotted each as a function of central peak width versus height of maximum side lobe. Their study indicated an optimal boundary existed between the two plotted parameters. Figure 3-5 shows the Norton and Beers limit with some specific functions also shown. Vagin [1980] independently computed over 3000 functions and also showed that this boundary exists. However, he went on to analytically show that for a chosen characteristic (either side lobe suppression or resolution) an optimal apodization function can be computed. Harris [1978] presents an excellent analysis of many of these apodization functions and shows the trade-offs associated with each. Nuttall [1981] shows some corrections to Harris's work and presents additional functions for consideration.

The present interferometer's full-width half-maximum (FWHM) instrument function is 1.8 cm^{-1}. The OH spectrum in the 1-μm wavelength region has line separations on the order of 10 cm^{-1}. This occurrence renders the prime consideration in the choice of an apodization function as one of side lobe

attenuation and ease of computation, rather than maximum resolution.

As can be seen from Figure 3-5 the Hamming window (sometimes referred to as the "minimum 2-point" window) is located on the optimal boundary. This function is comparatively simple to compute because it contains only two terms and provides side lobe attenuation of -43 dB (a 20 dB improvement over that provided by the sinc function). The additional side lobe attenuation is sufficient because the data collected for this study have signal-to-noise ratios of about 100, thus placing the side lobe behavior below the noise level. The Hamming window yields good spectral resolution by providing a FWHM central lobe of 2.7 cm^{-1} which is sufficient to identify the OH spectral characteristics. This window also has an asymptotic side lobe roll-off of 6 dB per octave [Harris 1978].

The Hamming convolution function takes the form

$$I_{\sigma_0} = \sum_{k=-6}^{k=+6} I_{\sigma}\left[0.53836\ \mathrm{sinc}[\pi c(k\Delta\sigma_0)] + 0.46164\ \left[\frac{\mathrm{sinc}(\pi[c(k\Delta\sigma_0)+1])+\mathrm{sinc}(\pi[c(k\Delta\sigma_0)-1])}{2}\right]\right] , \quad (3.10)$$

where

$\Delta\sigma = \sigma-\sigma_0$,

k = counter for integer sample numbers centered at transform point nearest σ_0,

σ = wavenumber at integer sample in cm^{-1},

σ_s = wavenumber at point where intensity is being computed in cm^{-1},

I_σ = intensity of transformed data at integer transform wavenumber σ,

I_{σ_s} = intensity of apodized data at wavenumnber σ_s,

c = number of sample points per wavenumber.

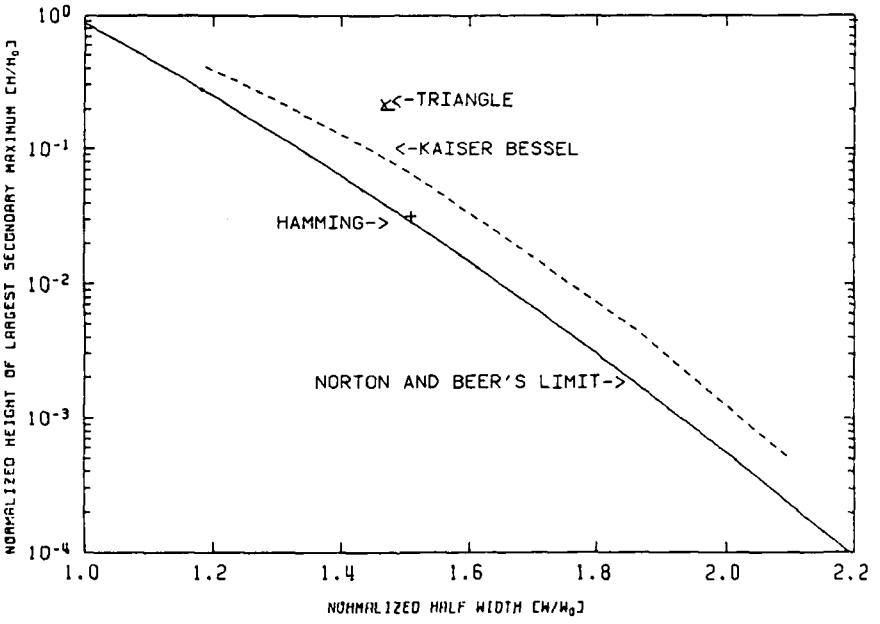

Figure 3-5. Optimal apodization functions, showing resolution vs. side lobe attenuation [Espy 1984].

The discrete spectral data points computed by the FFT occurred at 1.5-cm^{-1} intervals; therefore, as can be seen from Equation 3.10, the convolution computation was summed over ± 4 sample numbers. Examination of Equation 3.10 shows that this equation, in addition to suppressing side lobes, can be used to interpolate spectral values between the

discrete computed points of the FFT. Figure 3-6 shows the Hamming instrument function compared with the "square window" sinc function and also the common "triangle window" $sinc^2$ function. All three functions have been normalized to their respective peak values at 1000 for comparison.

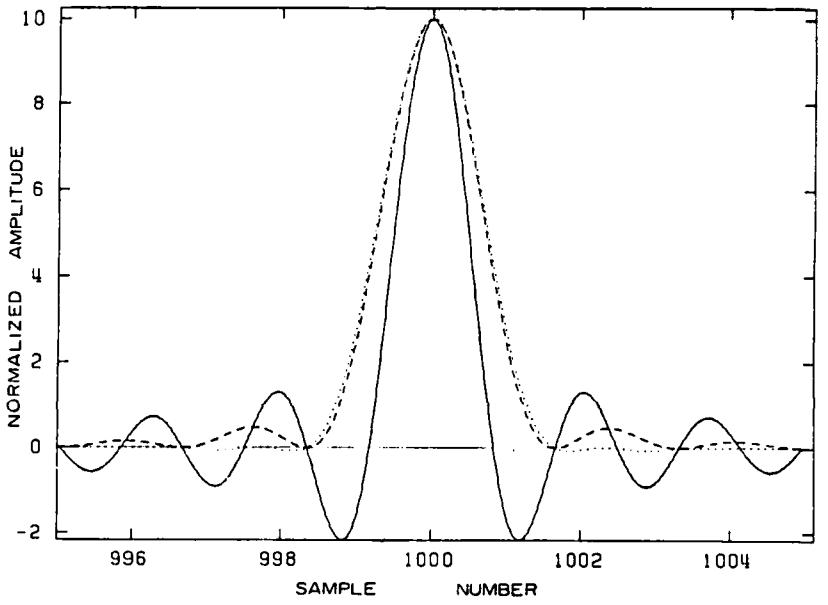

Figure 3-6. Comparison of normalized instrument functions; sinc(——), $sinc^2$(- -), and Hamming(···) [Espy 1984].

Line Amplitude Extraction

The interferograms were recorded in "raw" form on analog tape during the measurement campaigns. The analog tapes were later played back, digitized, formatted by computer and stored on digital tape. The digitized interferograms were then submitted to the FFT signal processing routine. The power spectral density information generated by the FFT for

each interferogram was also stored on digital tape for later processing.

The information of interest within each spectral frame, needed for rotational temperature calculations, was the intensity of a few specific OH spectral lines (the temperature model is explained in Chapter IV). In order to identify the spectral features of interest, each of the transformed frames of data was plotted on paper using an x-y recorder and a simple computer routine which performed a straight line connect between each of the discrete points computed by the FFT. Each of the plotted frames was examined manually, and the lines of interest were identified by FFT sample number. The lines selected were bright lines within each OH band which were far enough apart as to not be contaminated by other features and situated at wavelengths of minimal atmospheric absorption by H_2O and CO_2. Examination of the plots showed that the position of each line never varied from frame to frame more than ±1 FFT sample number. The selected FFT sample point was then recorded as the initial position of each of the spectral lines of interest.

The extraction of spectral line intensities was accomplished using the Hamming apodization function to interpolate between the discrete FFT data points. Allowing for additional error in the chosen position of each line, the interpolation routine was operated in a sample number window ±3 data points around that manually chosen line

position. The line intensity was then computed at 0.01 sample number increments (0.015 cm^{-1} increments) over the data point window using the Hamming function. The routine saved the maximum value found within the sample window as the line amplitude for that spectral feature.

The instrument calibration function and the correct spectral line amplitudes could now be used in the temperature model for extraction of OH rotational temperatures as a function of each interferometer scan.

CHAPTER IV

OH ROTATIONAL TEMPERATURE MODELING

Introduction

Hydroxyl is a minor atmospheric constituent, residing in a thin layer (about 7 km thick) at an altitude near 87 km [Baker et al. 1985]. Although minor in concentration (between 10^4 and 10^6 molecules/cm^3 at night, Baker [1978]) it is the major atmospheric near-infrared airglow radiator at night. The radiation generated by OH occurs in spectral bands known as the Meinel bands, since their discovery and identification by Meinel [1950]. After their discovery, the measurement of these bands has been of great interest to the atmospheric science community. OH airglow emission band measurements contain information about mesospheric populations and temperatures, and as such provide insight into the dynamics of the entire middle atmospheric region. A rotational-temperature model is developed in this chapter similar to the technique used by Hill et al. [1979]. The field measurements are then fit to the model in a least-squares sense. The quality of the fit will also determine error bounds on both relative band intensity and absolute rotational temperature.

The Excited OH Radical

The hydroxyl radical is a diatomic heteronuclear molecule and has a nonzero electric dipole moment. The molecule, therefore, has the ability to be easily excited and radiate electromagnetic radiation. The OH Meinel radiation bands in the infrared are caused by vibration-rotation transitions within the ground electronic state of the OH molecule. (The electronic absorption and emission spectra of OH occur in the ultraviolet.)

Hydration of ozone and perhydroxyl reduction are the primary processes for the creation of vibrationally-excited OH in the earth's upper atmosphere [Baker 1978]. The vibrationally-excited states of OH are quantized and are populated according to certain dipole selection rules described by Hertzberg [1971]. The quantum numbers associated with the vibrationally-excited states take on values $v = 0,1,2,3,\ldots,9$ and the allowed transitional changes during emission are

$$v'-v'' = \Delta v = 1,2,3, \ldots,9 \quad , \qquad (4.1)$$

where v' is the upper-state energy level and v'' is the lower-state energy level. The Meinel radiation bands are known by the value of Δv associated with the transition. The band sequences measured in this study are $\Delta v=2$ (4,2 and 3,1) and $\Delta v=3$ (8,5 and 7,4) transitions since they have energy differences in the near-infrared region. A typical measured spectrum is shown in Figure 4-1.

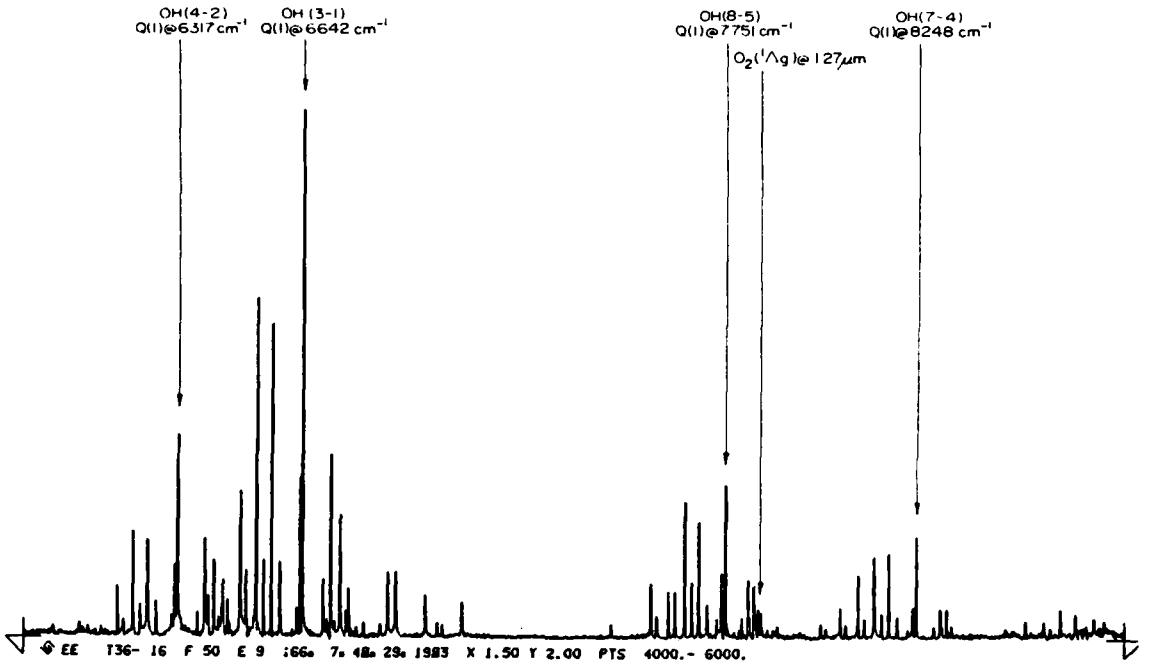

Figure 4-1. Measured OH spectra showing (4,2), (3,1), (8,5), and (7,4) Meinel bands.

Each band sequence shown in Figure 4-1 is a complex group of spectral lines. The complexity is due to transitions in molecular rotational energy in addition to the changes in vibrational levels. These angular momentum changes modulate the vibrational transitions causing the intricate spectral structure. Appendix A includes additional information on OH radical transition theory.

Rotational Temperature Model

In extracting temperatures from OH spectral data it is assumed that the OH molecular population is in rotational-state thermal equilibrium. The population distribution over the different quantum numbers can then be described by the

Maxwell-Boltzmann distribution law [Baker 1978],

$$N_{v'J'} = C_{v'} w_{J'} \exp(-E_{v'J'}/kT) \quad , \qquad (4.2)$$

where

$N_{v'J'}$ = number of molecules in vibrational level v' and rotational level J' at temperature T,

$w_{J'}$ = 2J'+1 or the statistical weight of state J' with its (2J'+1)-fold degeneracy,.

$C_{v'}$ = a constant, equal to $N_{v'}/Q_r$ where Q_r is the partition function for rotational level v,

$E_{v'J'}$ = energy of the rotational state, and equal to $F_{v'}(J')hc$, where $F_{v'}(J')$ is the term value for the upper-rotational state,

k = Boltzmann's constant.

The volume emission rate in photons sec^{-1} cm^{-3} of a central line is given by Mies [1974] as

$$I_{v'J',v''J''} = N_{v'J'} A_{v'J',v''J''} \quad , \qquad (4.3)$$

where

$I_{v'J',v''J''}$ = intensity of emission from upper-state v'J' to lower-state v''J'',

$A_{v'J',v''J''}$ = Einstein transition probability of spontaneous emission from state v'J' to state v''J''.

Inserting Equation 4.2 into Equation 4.3 gives the volume emission rate of each rotational line arising from a transition from an upper-state v'J' to a lower-state v''J''.

$$I_{v'J',v''J''} = C_{v'}\, w_{v'}\, A_{v'J',v''J''} \exp(-E_{v'J'}/kT) \quad . \quad (4.4)$$

The computation of a rotational temperature from Equation 4.4 requires a value for the absolute line intensity $I_{v'J',v''J''}$; however, the ratio of two relative line intensities can be taken and a temperature computed [Ware 1980] without the need for precise absolute spectral radiance values. However, the ratio technique proves to be a nonlinear (logarithmic) process and when several line pair temperatures within a band are calculated, the averaging of the pair temperatures to obtain a true band temperature is difficult. The line intensities are extracted from data whose noise characteristics are spectrally flat (white noise) and gaussian distributed [Ware 1980]. The difficulty comes about in the nonlinear temperature computation because the uncertainty of the calculation is not simply a linear extension of the input data uncertainty. The combining of the line pair temperatures, therefore, cannot be computed using traditional averaging techniques.

A model of the Boltzmann distributed data was developed to eliminate the problems described above. The model would describe all the lines that could occur within a band and then be fitted to the measured data using a least-squares technique. The mathematical model is

$$M_i(A_0,B_0) = \frac{A_0 R_i I_i \exp(-F_i B_0)}{\sum_j [I_j \exp(-F_j B_0)]} \quad , \quad (4.5)$$

where

M_i = the value of the model at wavenumber i,

A_0 = relative total integrated band intensity,

$f_i \propto A(2J'+1) = \sigma^3 S$, which is the Einstein coefficient times the J' state degeneracy or the wavenumber cubed times the line strength,

$B_0 = hc/kT$, where T is rotational temperature in °K,

F_i = term value for upper-state transition,

R_i = relative instrument response at wavenumber i,

Σ = summation over all lines within the band, is a scaling factor to ensure the entire band intensity is contained within the A_0 term.

The model shown above is similar to the intensity calculation shown in Equation 4.5. The difference is that the model pertains to an entire band of transitions and is modified by R_i to appear like the measured data. All quantities within the model are now known except the band intensity A_0, and the temperature term B_0. Within each OH band, the measured data points can be subtracted from the model at the same wavenumber and any differences will be contained within small changes of A_0 and B_0 times the derivative of the model at points A_0 and B_0.

$$D_i - M_i = \Delta A_0 \left[\frac{\partial M_i(A_0, B_0)}{\partial A_0} \right] + \Delta B_0 \left[\frac{\partial M_i(A_0, B_0)}{\partial B_0} \right] , \quad (4.6)$$

where D_i is the measured data point. Equation 4.6 can be shown for (j) data points within a band in matrix form as

$$\begin{bmatrix} (D_i - M_i) \\ \cdot \\ \cdot \\ \cdot \\ (D_j - M_j) \end{bmatrix} = \begin{bmatrix} \left(\frac{\partial M_i}{\partial A_0}\right) & \left(\frac{\partial M_i}{\partial B_0}\right) \\ \cdot & \cdot \\ \cdot & \cdot \\ \cdot & \cdot \\ \left(\frac{\partial M_j}{\partial A_0}\right) & \left(\frac{\partial M_j}{\partial B_0}\right) \end{bmatrix} \begin{bmatrix} \Delta A_0 \\ \Delta B_0 \end{bmatrix} , \qquad (4.7)$$

where the left matrix is the difference between each measured line intensity within a band and the line intensity as predicted by the model. The right hand side of Equation 4.7 must be equal to the preceding difference.

The computation of Equation 4.7 requires the solution for each of the derivatives

$$\frac{\partial M_i}{\partial A_0} = \frac{R_i \, \ell_i \, \exp(-F_i \, B_0)}{N} , \qquad (4.8)$$

and,

$$\frac{\partial M_i}{\partial B_0} = \frac{A_i \, R_i \, \ell_i \, \exp(-F_i B_0)}{N^2} \left[\left[\sum_j (\ell_j F_j \exp(-F_j B_0)) \right] - N \, F_i \right] , \qquad (4.9)$$

where $N = \sum_j \ell_j \exp(-F_j B_0)$ or the normalization factor. All the terms in Equation 4.7 are computed and submitted to a least-squares fitting routine, developed by Lawson and Hanson [1974] which returns the values of ΔA_0 and ΔB_0. The least-squares routine is used to solve problems of the form

$$Ax = B , \qquad (4.10)$$

where

A = the derivative matrix of Equation 4.7,

x = the unknown or Δ matrix,

B = the difference matrix.

To begin the process a starting temperature was chosen and all terms computed. The result of this first fit is to determine an appropriate initial value for A_0 (A_0 is merely a relative intensity term). Once the initial values for B_0 and A_0 were ascertained, the least-square fitting routine was operated in a loop, the derivative matrix vectors were each scaled to unity value before submission to insure convergence of the fit, and each time the routine would return values for ΔA_0 and ΔB_0. The Δ values were added to the previous values for A_0 and B_0, the model values recomputed and resubmitted to the routine. The value of ΔB_0 was tested after each iteration until the temperature change (temperature is part of B_0) from the previous fit was less than 0.5° K. When the least-squares routine converged to the 0.5 °K limit the values for A_0 (relative band intensity) and T (the temperature part of B_0) were stored along with the time and date of the frame.

The constant terms used in the model were computed by Espy [1984] using the molecular constants measured by Coxon and Foster [1982] and OH dipole moments derived by Werner et al. [1983]. The values of these terms are given in Tables 4-1 through 4-4. The tables show the wavenumber, a typical relative instrument response, the term value for the upper-

TABLE 4-1. Molecular data for OH Δv=2, (4,2) band.

Line	Wavenumber (cm^{-1})	Relative Response	Term Value (cm^{-1})	Line Strength
$P_1(4)$*	6159.634	0.147	13421.921	0.23415100E+13
$P_2(4)$*	6174.994	0.166	13514.125	0.19663726E+13
$P_1(3)$*	6200.353	0.199	13320.758	0.16226162E+13
$P_2(3)$*	6219.070	0.224	13428.966	0.13226441E+13
$P_1(2)$*	6238.114	0.247	13248.923	0.88080260E+12
$P_2(2)$*	6260.766	0.275	13377.615	0.70291000E+12
$Q_1(3)$	6301.517	0.326	13421.922	0.25067365E+12
$Q_1(2)$	6309.948	0.336	13320.758	0.71495030E+12
$Q_1(1)$	6315.828	0.344	13248.923	0.11681950E+13
$R_2(1)$	6368.381	0.411	13428.966	0.60586570E+12
$R_1(1)$	6387.661	0.440	13320.758	0.74062960E+12
$R_1(2)$	6411.112	0.473	13421.921	0.12600000E+13

(* lines used in fit).

TABLE 4-2. Molecular data for OH Δv=2, (3,1) band.

Line	Wavenumber (cm^{-1})	Relative Response	Term Value (cm^{-1})	Line Strength
$P_1(4)$*	6480.230	0.572	10352.446	0.27218330E+13
$P_2(4)$*	6495.579	0.593	10443.293	0.22819520E+13
$P_1(3)$*	6522.332	0.626	10247.071	0.18861154E+13
$P_2(3)$*	6541.239	0.650	10354.206	0.15350037E+13
$P_1(2)$*	6561.409	0.679	10172.300	0.10240617E+13
$P_2(2)$*	6584.562	0.712	10300.410	0.81566820E+12
$Q_1(3)$	6627.706	0.770	10352.446	0.57940270E+12
$Q_1(2)$	6636.171	0.782	10247.071	0.82784900E+12
$Q_1(1)$	6642.081	0.789	10172.300	0.13556844E+13
$R_2(1)$	6697.063	0.867	10354.206	0.35196955E+12
$R_1(1)$	6716.853	0.892	10247.071	0.86348040E+12
$R_1(2)$	6741.555	0.931	10352.446	0.14703511E+13

(* lines used in fit)

TABLE 4-3. Molecular data for OH Δv=3, (8,5) band.

Line	Wavenumber (cm^{-1})	Relative Response	Term Value (cm^{-1})	Line Strength
P_1 (5)	7555.155	1.000	24163.096	0.54607000E+13
P_2 (5)	7569.641	0.997	24248.912	0.47194710E+13
P_1 (4)	7600.862	0.992	24055.028	0.41913920E+13
P_2 (4)	7617.468	0.990	24152.797	0.35340550E+13
P_1 (3)*	7642.345	0.984	23971.237	0.29201550E+13
P_2 (3)*	7661.252	0.985	24083.736	0.23944700E+13
P_1 (2)*	7679.631	0.978	23911.582	0.15952644E+13
P_2 (2)*	7700.808	0.972	24042.113	0.12846050E+13
Q_1 (3)	7726.136	0.960	24055.028	0.95265240E+12
Q_1 (2)	7739.286	0.952	23971.237	0.13444194E+13
Q_1 (1)	7748.511	0.945	23911.582	0.21738030E+13
R_2 (1)	7791.408	0.900	24803.736	0.11463823E+13
R_1 (1)	7808.166	0.874	23971.237	0.13900488E+13
R_1 (2)	7823.076	0.857	24055.028	0.23899920E+13

(* lines used in fit)

TABLE 4-4. Molecular data for Δv=3, (7,4) band.

Line	Wavenumber (cm^{-1})	Relative Response	Term Value (cm^{-1})	Line Strength
P_1 (5)*	8049.708	0.786	21763.099	0.66072740E+13
P_2 (5)*	8064.112	0.779	21847.340	0.56979800E+13
P_1 (4)*	8096.397	0.765	21649.131	0.40669700E+13
P_2 (4)*	8113.112	0.754	21745.519	0.42663300E+13
P_1 (3)*	8138.903	0.740	21560.824	0.35302450E+13
P_2 (3)*	8158.204	0.725	21672.328	0.28898620E+13
P_1 (2)*	8177.237	0.711	21497.994	0.19277462E+13
P_2 (2)*	8199.208	0.696	21628.204	0.15491604E+13
Q_1 (3)	8227.210	0.680	21649.131	0.11407934E+13
Q_1 (2)*	8240.067	0.672	21560.824	0.16141494E+13
Q_1 (1)*	8249.071	0.668	21497.994	0.26171900E+13
R_2 (1)*	8294.714	0.646	21672.328	0.13787860E+13
R_1 (1)*	8311.901	0.642	21560.824	0.16761780E+13
R_1 (2)*	8328.374	0.635	21649.131	0.28788900E+13

(* lines used in fit)

state transition, and the theoretical line strength for each line. The wavenumber shown is the average of the two Λ-doubled lines; the term value is also the average of the two lines, and the line strength given is the sum of the two line strengths. The sum of the line strengths was used because the measured line is actually the sum of the Λ-doubled pair. Data for all the strong lines are listed for use in the normalization factor of the model but only those with "*" were used in the fit. The reason all were not used in the fit was that many were determined to have been contaminated by water vapor absorption or by other emission lines [Roychourdhury 1983].

Error Analysis and Testing of Model

The model used here is over-determined with only two unknowns and at least four equations (in (8,5) band fit, more in other bands) and as such, the additional information can be used to estimate the accuracy of the least-squares fit. Examination of Equations 4.7 and 4.10 show that when the fitting routine is complete, the derivative matrix A is left as a 2X2 upper-triangulated matrix. The rest of the terms in the A matrix are of little significance because the least-squares routine has manipulated the data into the upper-triangulated portion in order to solve the equations. The upper-triangulated matrix now takes on the form

$$R = \begin{bmatrix} r_{1,1} & r_{1,2} \\ 0 & r_{2,2} \end{bmatrix} \quad , \tag{4.11}$$

where

R = upper-triangulated coefficients returned in the derivative matrix A.

Upon completion of the fitting routine, the values left in the matrix x must be equal to zero, except for noise in the fit, and the upper two values in the vector B must also be equal to zero, also except for noise, because the system of equations has been solved. But because noise does exist in the fit then some residual remains. Therefore, the equation system is left in the form

$$R\ x = n \quad , \tag{4.12}$$

where n is the noise vector.

In order to calculate the accuracy of the models' fit to the two system unknowns (temperature and band intensity) it is necessary to obtain the covariance matrix which contains the variance of each parameter in the least-squares fit. It can now be shown by manipulation of Equation 4.12 that the covariance matrix is [Lawson and Hanson 1974]

$$\langle x\ x^T \rangle = \bar{R}\ \langle n\ n^T \rangle\ \bar{R}^T \quad , \tag{4.13}$$

where

$\langle x\ x^T \rangle$ = covariance matrix,

$\overline{R}$ = inverse of R,

T indicates the transpose operation,

$\langle n\ n^T \rangle$ = the variance of white uncorrelated noise.

The noise in the system fit is assumed to be white and uncorrelated because all the mathematical manipulations performed were linear in nature.

A measure of the noise in the system is returned by the least-squares fitting routine. The returned parameter is the Euclidean norm of the residual vector and is called R_{norm}. The variance of the system fit can be computed from R_{norm} as

$$\sigma^2 = (R_{norm}{}^2)/(M-K) \quad , \qquad (4.14)$$

where

σ^2 = variance of fit,

M = number of equations in the fit,

K = number of unknowns in the fit.

The covariance matrix can be solved in terms of the variance of the model's fit

$$\langle x\ x^T \rangle = \sigma^2\ I\ (\overline{R^T\ R}) \quad , \qquad (4.15)$$

where I is the identity matrix.

The standard deviation for each of the fit variables can be computed from Equation 4.15 in terms of the original variables of the residual matrix R and the variance σ^2.

$$\sigma_A = \left[\frac{(r_{2,2}^2 + r_{1,2}^2)}{(r_{1,1}\, r_{2,2})^2} (\sigma^2) \right]^{\frac{1}{2}} , \qquad (4.16)$$

where σ_A is the standard deviation of the intensity function.

The standard deviation on the variable B (temperature is part of B) is

$$\sigma_B = \left[\frac{\sigma^2}{r_{2,2}^2} \right]^{\frac{1}{2}} . \qquad (4.17)$$

Referring to Equation 4.5 for the relationship between temperature T and the variable B, the standard deviation of the temperature can be calculated

$$\sigma_T = (\sigma_B hck)/(B_0^2) , \qquad (4.18)$$

where σ_T is the standard deviation of the temperature as calculated by the model.

The model presented herein provides a method for calculating relative band intensity, rotational temperature, and the standard deviation on both parameters. Appendix D presents the computer programs which implement the data processing algorithms developed.

As verification of the quality of the model, the process outlined was used to compute the intensity and temperature of synthetic spectra generated by Espy [1984]. The signal-to-noise ratio of the synthetic spectra was varied from a low of 2 to a high of 20 and then each was submitted to the

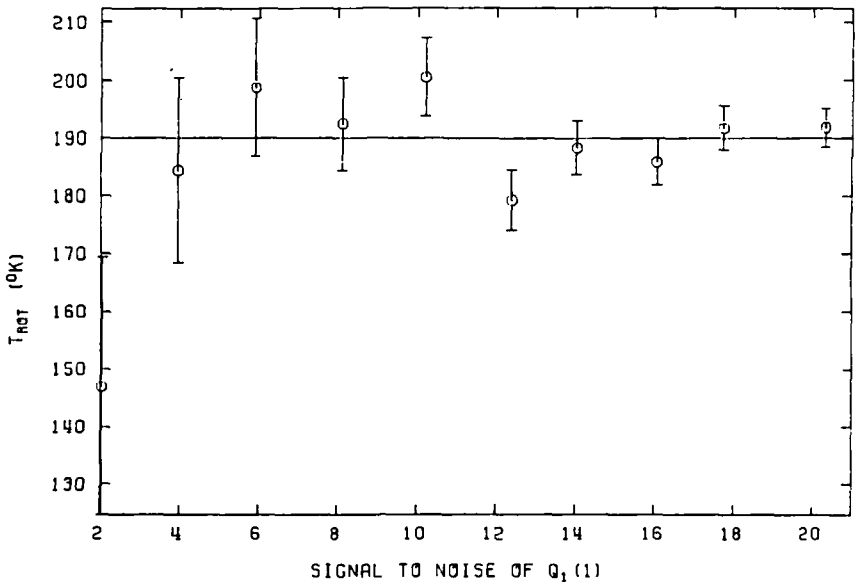

Figure 4-2. Model temperature test results on synthetic spectra vs. signal-to-noise ratio with standard deviation shown as bars [Espy 1984].

model for processing. Figures 4-2 and 4-3 show the results of the test. As can be seen, the mean intensity and temperature of the model closely track the actual parameters even in very high-noise environments. The error bars shown on both figures indicate a 1 sigma uncertainty associated with the calculation, and as the noise increased, the uncertainty of the calculation increased as expected. The tests were conducted on a single frame of data; therefore, an improvement could be made by averaging frames at the cost of temporal resolution degradation. The signal-to-noise ratio of the measured data was usually about 100, which is

much higher than the signal-to-noise ratio of the test frames; therefore, the uncertainty should continue to decrease so the confidence in the model is very high.

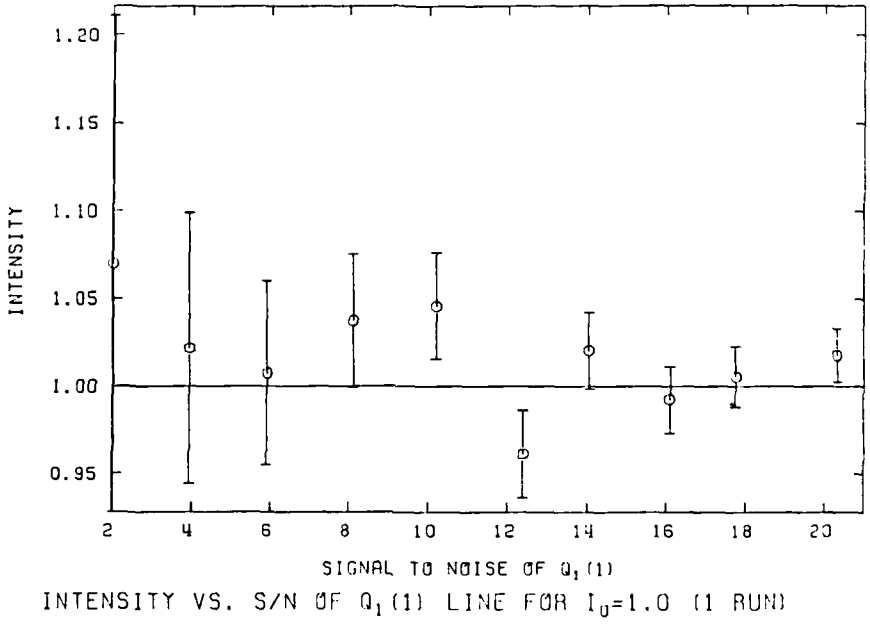

Figure 4-3. Model intensity test results on synthetic spectra vs. signal-to-noise ratio with standard deviation shown as bars [Espy 1984].

AD-A166 377 HIGH RESOLUTION MEASUREMENTS OF OH INFRARED AIRGLOW STRUCTURE(U) AIR FORCE INST OF TECH WRIGHT-PATTERSON AFB OH P C NEAL 1985 AFIT/CI/NR-86-26D 2/3

UNCLASSIFIED F/G 4/1 NL

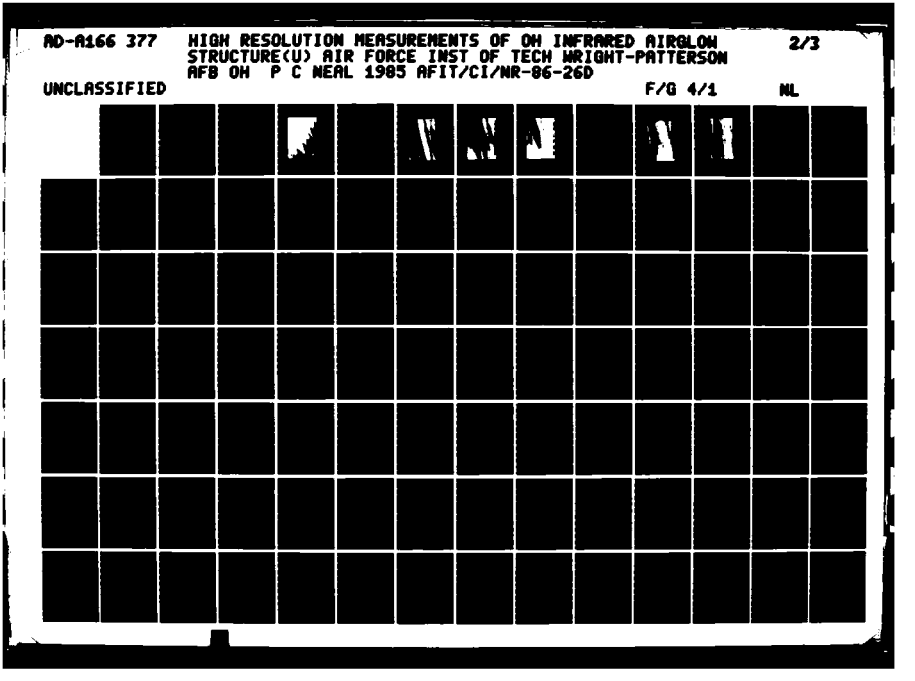

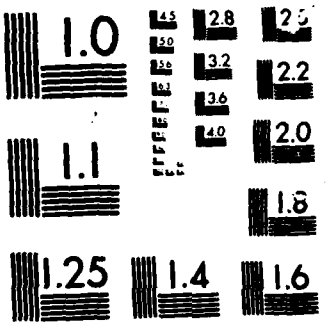

MICROCOPY RESOLUTION TEST CHART

CHAPTER V

RESULTS

Introduction

The high-throughput, narrow field of view interferometer-spectrometer was taken to several airglow observation sites in the western United States in the spring of 1983. Over several months of observation, one of the brightest airglow structure events was seen and recorded on June 15, 1983, thus fulfilling the primary goal of this study. The observation was made from Sacramento Peak, New Mexico. The site is located at 105°48'16" west longitude, 32°47'57" north latitude at an elevation of 9570 feet. The results presented in this chapter were taken from this site between June 13 and June 15, 1983. A complete catalog of the results computed from the interferometer data is presented in Appendix C.

Background

The interferometer with an image-intensified infrared isocon camera mounted on and coaligned with the interferometer telescope (see Figure 2-9) was used to collect data at the observation sites. A second Isocon camera was mounted on its own tripod and was used to search the skies for indication of structure prior to moving the

more bulky interferometer. The infrared cameras were supplied by the University of Southampton, England. Taylor [1983-84] operated the camera equipment and provided experience and expertise in the search for airglow structure events. The cameras were the "eyes" for the interferometer in determining if any OH airglow structure was present. Once an area of OH airglow structure was located in the sky the camera-interferometer system was positioned to view that area. The data from the two coaligned systems were used to correlate the viewed and calculated intensities and temperatures.

An infrared radiometer [Huppi 1976] was also used to gather trend and absolute intensity data of the OH activity. The radiometer looked in the zenith and has a field of view of 9°. The radiometer spectral bandpass was centered at 1.53 μm wavelength.

Infrared Isocon Camera Results

The Isocon camera systems' response is in the near-infrared from about 700 to 850 nm. The response curve and the OH transitions which occur within this bandpass are shown in Figure 1-3.

Figure 5-1 shows a video frame taken with the large, independently-mounted isocon camera at 8:15 hrs. UT on June 15, 1983. The field of view for the photo is 28° vertical and 37° horizontal at an azimuth of about 320° and the bottom of the picture beginning at 10° elevation.

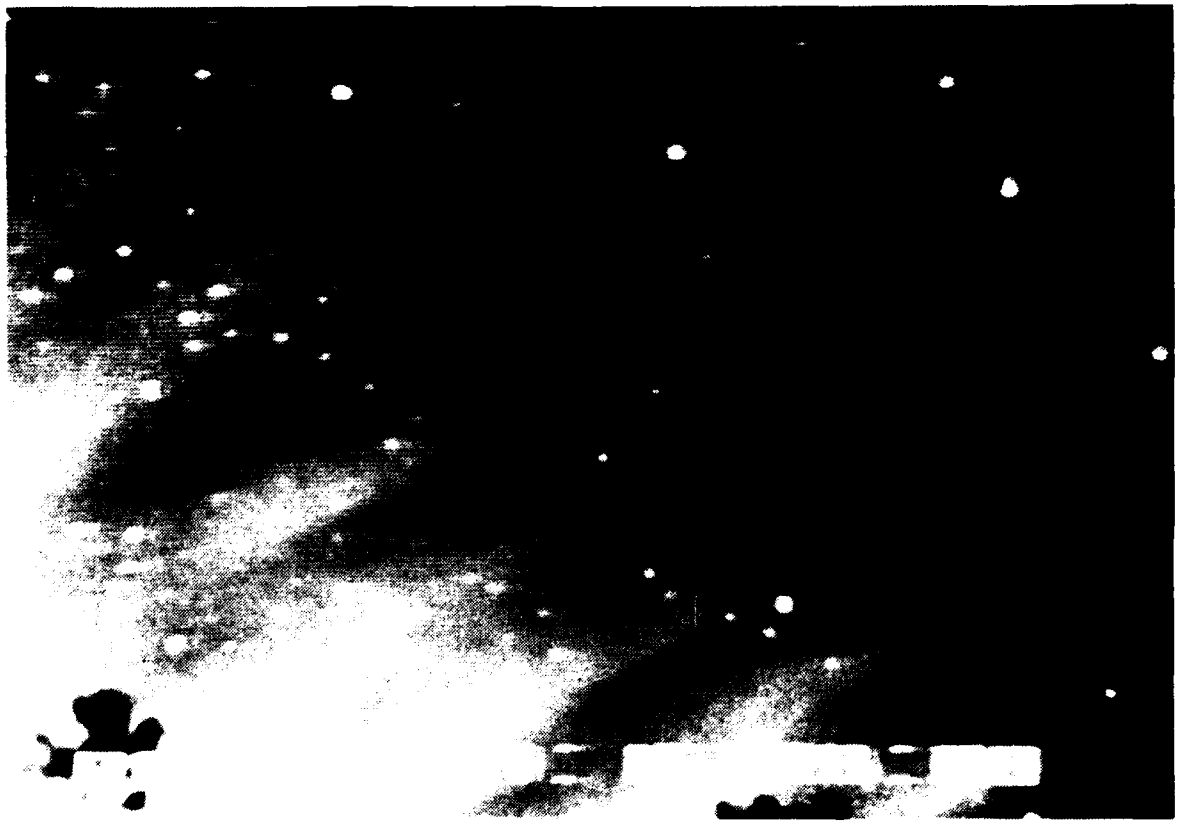

Figure 5-1. Large isocon IR camera photo, day 166, 8:15 hrs. UT, camera field of view 28° vertical, 37° horizontal, at an elevation of about 10°.

Examination of this frame shows 7 distinct bright OH emission bands. The bands are moving northward in a direction normal to the bands (moving towards lower right hand corner of frame). These structural bands extended across the entire northern half of the sky. The structure depicted in Figure 5-1 was observed and recorded beginning at 7:30 hrs. UT continuing until 10:15 hrs. UT on this date.

Using the video record, Taylor [1983-84] calculated the apparent wavelength and velocity of the band structure, with techniques described by Hapgood and Taylor [1982]. Using the location and altitude of the observation site, radius of the earth, viewing angles of the camera, and assuming that the band structure resided on a spherical shell at an constant altitude of 87 km, the apparent temporal wavelength derived was 24±1 km, and the apparent period was 14±1 minutes. Based on these two values the apparent velocity is 28±2 meters/second which agrees closely with other similar observations [Taylor et al. 1980].

The small isocon camera which was mounted on and coaligned with the interferometer, was operated during the same time frame as the large camera. The field of view of the small camera is nearly square being 13° vertical by 15° horizontal.

Figures 5-2 through 5-4 show a sequence of video frames beginning at 7:32 hrs. UT and taken at 8 minute intervals with the small camera. Each frame again shows, in more detail, the OH emission structure. The "X" in each frame

Figure 5-2. Isocon IR camera photo, day 166, 7:32 hrs. UT, field of view = 13° vertical 15° horizontal, interferometer looking at "X" on a bright band.

Figure 5-3. Isocon IR camera photo, day 166, 7:40 hrs. UT, field of view = 13° vertical 15° horizontal, interferometer looking at "X" on a dark band.

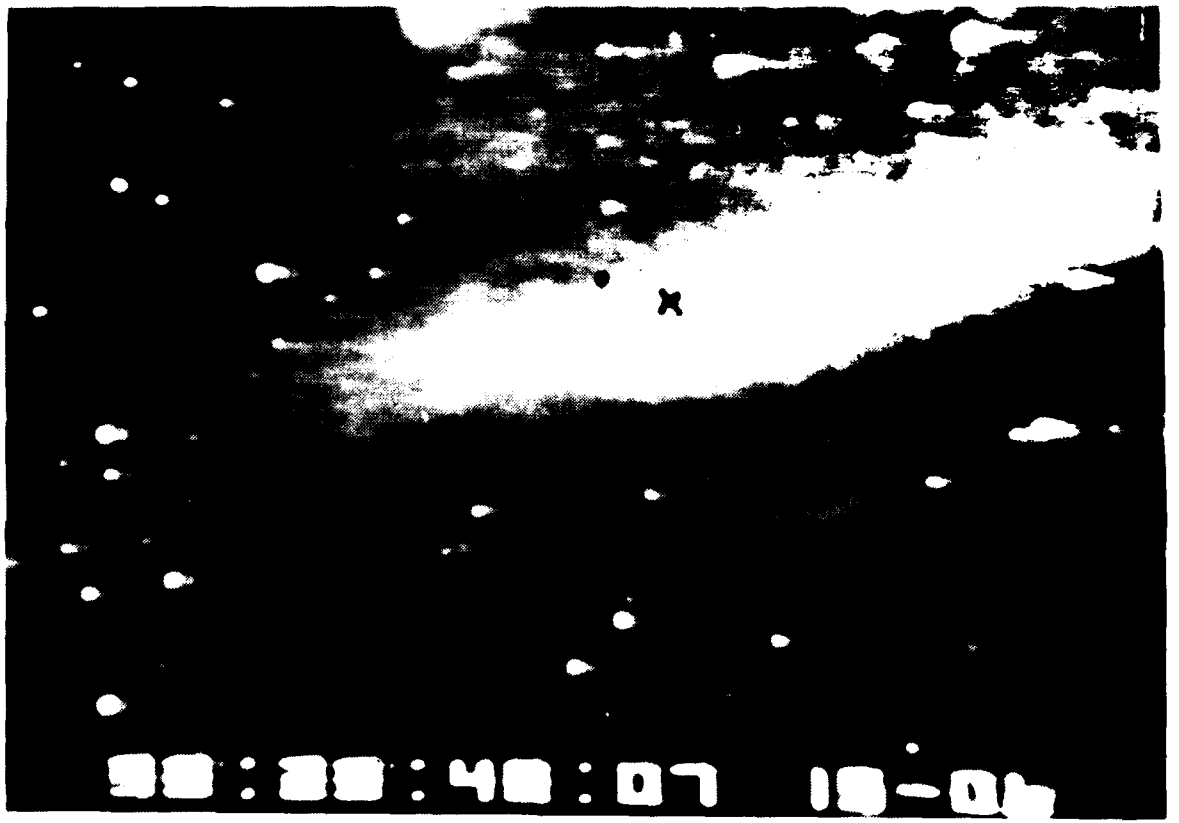

Figure 5-4. Isocon IR camera photo, day 166, 7:48 hrs. UT, field of view = 13° vertical 15° horizontal, interferometer looking at "X" on a bright band.

marks the center of the interferometer's field of view within the video frame. The interferometer's field of view is 0.8° full field and, therefore, is about 0.4 inches in diameter on each frame. This small field of view permits the interferometer to resolve the bright and dark portions of the structure. The interferometer is viewing at an elevation angle of 17° and an azimuth angle of 328° in the sequence. The three photos show one of the periods where the interferometer was able to view a bright, a dark, and a bright band in sequence as the structure moved through the field of view.

Figures 5-5 and 5-6 show another similar sequence of video frames observed later in the night beginning at 8:31 hrs. UT at an interval of 11 minutes. This later series of frames again shows the interferometer viewing a dark then a bright emission band as the structure moves. The interferometer was viewing at an elevation angle of 15.5° and an azimuth angle of 340° in these last two figures.

Taylor [1983-84] compared the bright and dark bands recorded by the small isocon camera with the OH (3,1) band intensity plots computed using the interferometer data (shown later in Chapter V and in Appendix C). In the time period from 7:30 to 10:15 hrs. UT the two independent records show that for each bright or dark band depicted in the video data a corresponding increase or decrease in intensity is also shown in the interferometer data. This

Figure 5-5. Isocon IR camera photo, day 166, 8:31 hrs. UT, field of view = 13° vertical 15° horizontal, interferometer looking at "X" on a dark band.

Figure 5-6. Isocon IR camera photo, day 166, 8:42 hrs. UT, field of view = 13° vertical 15° horizontal, interferometer looking at "X" on a bright band.

comparison showed 16 distinct points of correlation between the video frames and the interferometer intensity plots.

Infrared Radiometer Data

The radiometer was used to show trend and absolute radiance values for the OH infrared activity as viewed within a 9° field of view in the zenith. Radiometer data are included to show for the night before (June 14, 1983) and the night of (June 15, 1983) the recorded structure, OH airglow emission intensity exhibited some unusual trends and modulations. Figure 5-7 shows the radiometer data for three specific days and is calibrated in kilo-Rayleighs (kR) of intensity of OH (3,1) band emission. The scale has been shifted to show the three days all on one chart.

Day 162 is a typical curve of near-infrared OH activity and was taken from White Sands Missile Range (4300 feet elevation) and located about 30 miles from the Sacramento Peak site. As can be seen from the Day 162 curve, the intensity of the 1.53 μm radiation steadily decreases after local sunset (sunset occurred about 3:30 hrs. UT) and throughout the night.

The Day 165 radiometer curve, however, shows a markedly different trend in the OH activity. The post-sunset decrease starts, but at about two hours before local midnight (or 5:00 hrs. UT) the OH activity dramatically increased. After the peak, the OH activity remains high but also shows some modulation that could be interpreted as

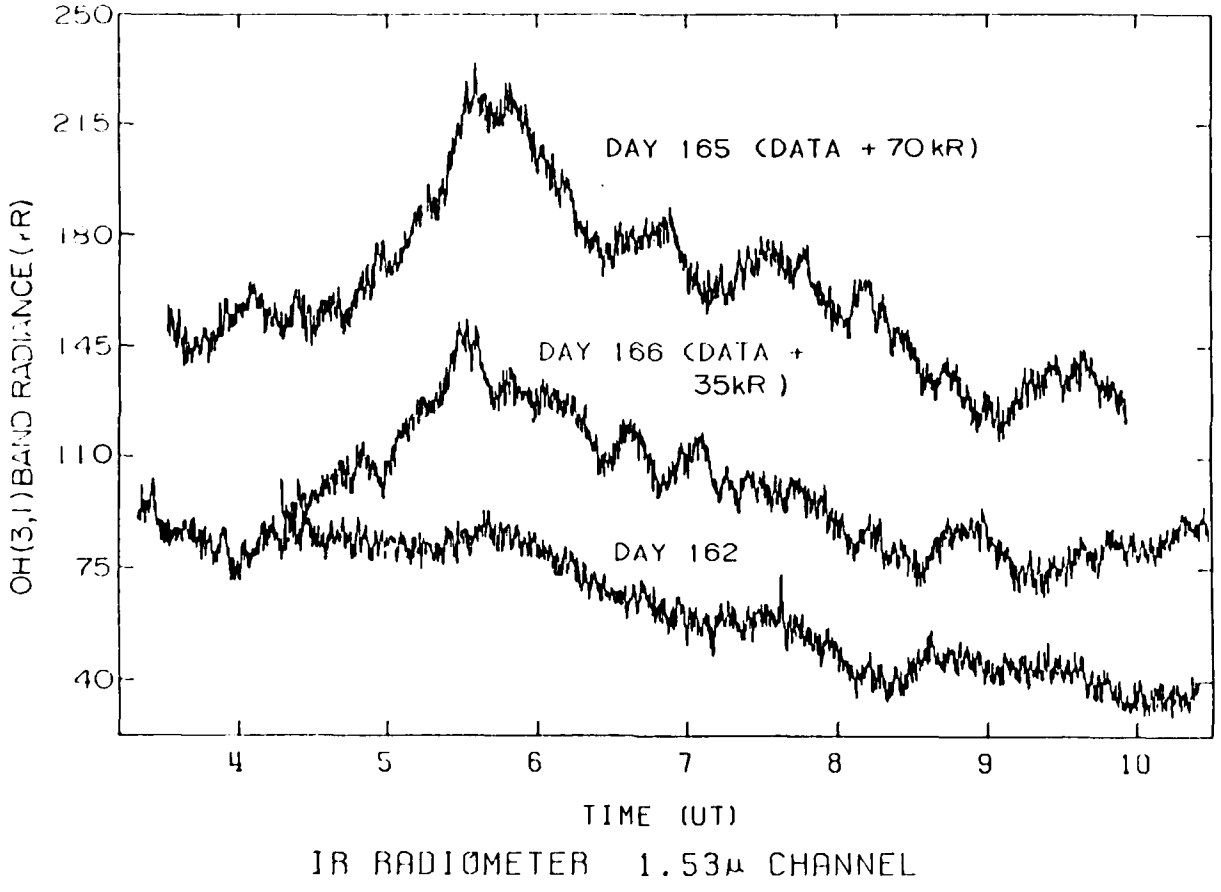

Figure 5-7. Radiometer readings for UT days 162, 165, and 166 during 1983. The data is for the 1.53 μm channel.

distinct large-scale wave structure passing overhead. The period of these intensity waves ranges from 30 to 60 minutes with a modulation (or contrast ratio) of from 5 to 10 percent. The waves were not distinguishable in the zenith with the infrared camera equipment because the zenith emission intensity is too faint and their large size exceeded the camera's field of view. A camera was lowered in elevation in an attempt to view the waves (lower elevations view the structure obliquely thus the waves appear compressed together and brighter due to the van Rhijn effect) but no structures were distinguishable by the camera throughout the entire night.

The radiometer curve in Figure 5-7 for day 166 also shows enhanced OH activity. Although not as intense as the previous night, a similar pre-midnight maximum is observed. After the pre-midnight maximum, the decrease is slower than normal and again some distinct wave structure is observed. The structure has periods of about 25 minutes and modulations in intensity of about 5 percent. Shortly after local midnight (7:00 hrs. UT), the moon had set far enough to lower the sensitive camera to the horizon to search for observable structure. The measurements gathered throughout the remainder of the night with the cameras and interferometer also exhibit high-contrast OH emission structure.

Direct Comparison of Interferometer and Radiometer Intensities

Prior to moonset on UT days 165 and 166 the interferometer was pointed to the zenith and was viewing the sky coincident with the radiometer. Therefore a direct comparison is made between the two records. Figure 5-8 shows the OH (3,1) band intensity from 3:30 to 7:15 hrs. UT on day 165. The radiometer data were used to provide the absolute calibration for the interferometer, but as the figure shows the trends in the interferometer intensity curve track the radiometer curve closely. The intensity peak appears at about 5:40 hrs. UT on this day. The standard deviation of the interferometer intensity calculation is about 2% (the standard deviation curve is included in Appendix C). The interferometer was realigned at 6:30 hrs. UT. Just prior to realignment, the standard deviation of the intensity increased. After alignment the intensity appeared to have increased. These observations make the rapid intensity decline at 6:00 hrs. UT suspect, as an instrument alignment drift problem.

Figure 5-9 presents the interferometer OH (3,1) band intensity for UT day 166. Again it compares favorably with the radiometer curve for the same day in Figure 5-7. The intensity peak occurs on this day at 5:30 hrs. UT. The same reservations about alignment drift occurred on this day at 6:00 UT as happened on the previous day.

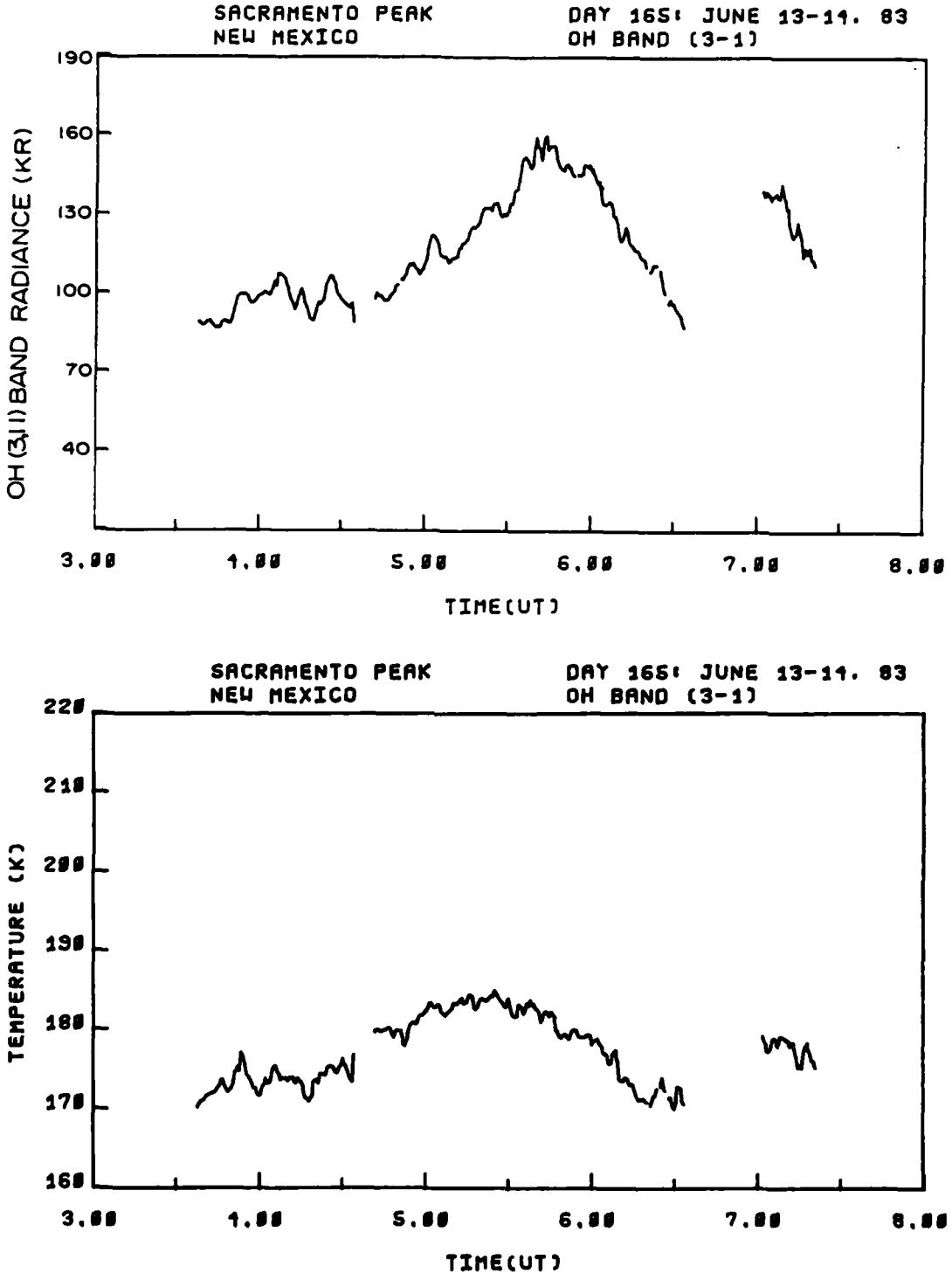

Figure 5-8. OH (3,1) band radiance and rotational temperature, viewing angle = zenith, day 165, 3:30-7:30 hrs. UT.

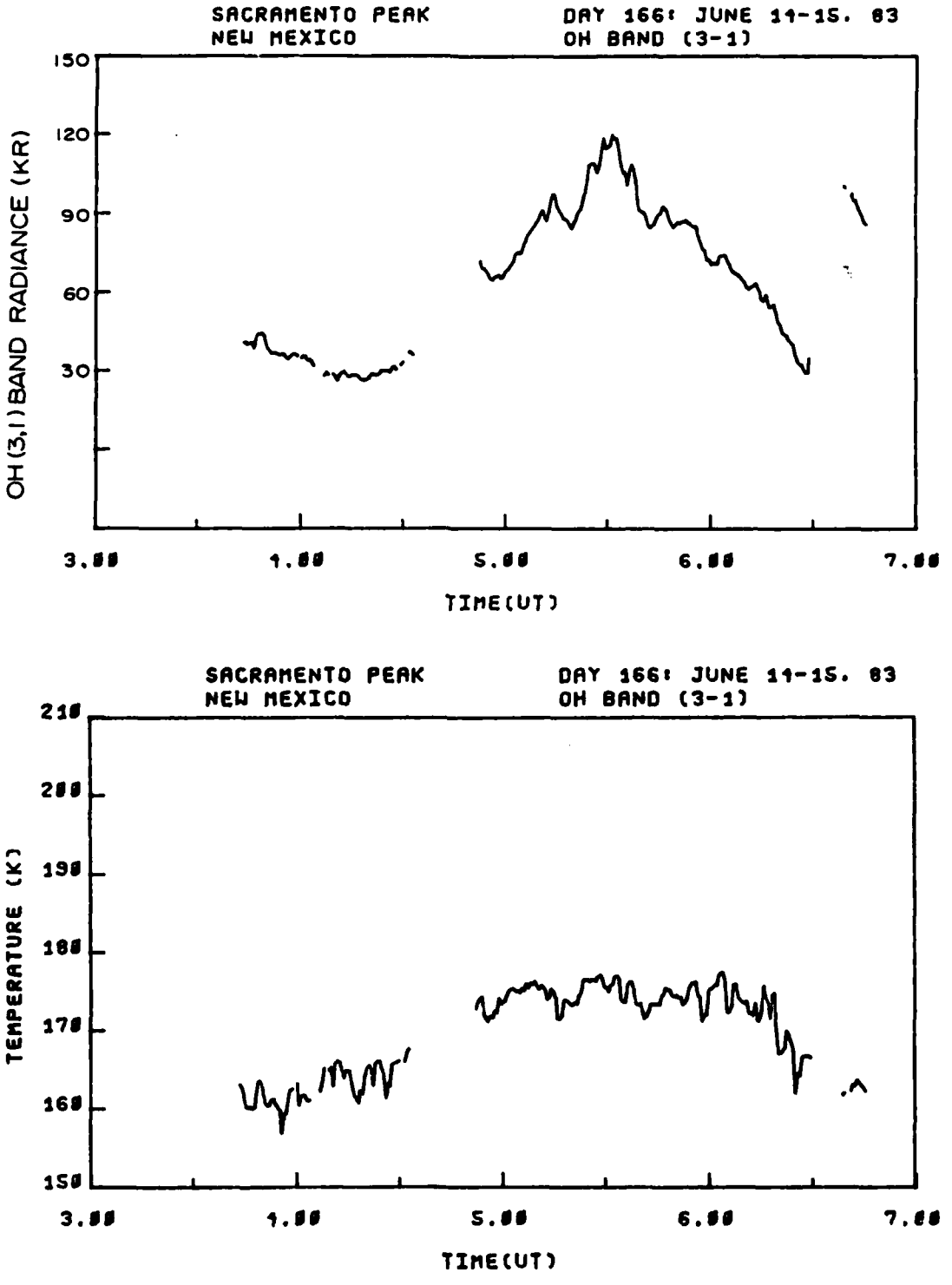

Figure 5-9. OH (3,1) band radiance and rotational temperature, viewing angle = zenith, day 166, 3:30-6:45 hrs. UT.

The calculated interferometer OH radiance and temperature curves for the other OH Meinel bands measured in this study are included in Appendix C. The absolute scales of radiance for the other OH bands were based on the (3,1) band (the radiometer was calibrated in terms of the (3,1) band) and using the band intensity ratios developed by Turnbull and Lowe [1983] ($I(4,2)=I(3,1)\times1.03$, $I(8,5)=I(3,1)\times0.14$, $I(7,4)=I(3,1)\times0.09$). Only when the interferometer is viewing in the zenith are the intensity curves plotted in absolute terms. The geometry of looking at low elevation angles for the other data precluded inclusion of absolute scales. Also shown in the Appendix are the standard deviations for all the calculations.

Rotational Temperatures for Interferometer Zenith Data

Included in Figures 5-8 and 5-9 are the calculated rotational temperatures for days 165 and 166 when the interferometer is viewing in the zenith. The temperature for day 165 indicates a rise in temperature and intensity, beginning at about 4:00 hrs. UT, with a mean temperature of about 175 °K. The total rise in temperature is 15 °K with the peak occurring at 5:20 hrs. UT. The temperature curve for day 166 shows the same increasing trend as on the previous day. The mean is about 170 °K with a total rise in temperature of 15 °K. The temperature peaks on day 166 at 5:10 hrs. UT. On both days as the interferometer views the

zenith, the peak of the temperature curve precedes the peak of the intensity curve by about 20 minutes (discussed more in Chapter VI).

Rotational Temperature

Smoothing Algorithm

The curve of calculated rotational temperatures appeared quite noisy at times. Consequently, smoothing algorithms were employed. The smoothing technique used is a 3 frame wide sliding window where the averaging is a weighted one. Only 3 data points were used so as to not degrade the temporal resolution of the data (this is about a 2 minute time window) and still provide sufficient smoothing. The weighting is accomplished using the reciprocal of the standard deviation squared (or reciprocal of variance) for each data point as its weighting factor in the running sum; therefore, if a particular data point has a large uncertainty it is weighted less in the average. This algorithm was chosen because in data sets with large differences from data point to data point, with significant differences in the variance of each point, this weighting technique best identifies the mean curve through all data points [Bevington 1969].

The specific algorithm used for the rotational temperature smoothing is

$$\bar{T}_i = \left[\sum_{i=1}^{3} (T_i/(\sigma_{T_i})^2) / \sum_{i=1}^{3} (1/(\sigma_{T_i})^2) \right] \quad , \qquad (5.1)$$

where

$\bar{T}_i$ = weighted average temperature at time i,

T_i = temperature at time i,

σ_{Ti} = standard deviation of temperature T_i.

The standard deviation on the smoothed curve is also changed due to the weighting and is recalculated using

$$\bar{\sigma}_{T_i} = \left[\sum_{i=1}^{3} (1/(\sigma_{T_i})^2) \right]^{-\frac{1}{2}} \quad , \qquad (5.2)$$

where

$\bar{\sigma}_{Ti}$ = averaged standard deviation at time i.

Figure 5-10 shows temperature and standard deviation curves before smoothing and Figure 5-11 shows the same curves after smoothing. All the temperature curves in Appendix C show a set of temperature curves for both before and after smoothing.

Interferometer Recorded Structure

This research project was undertaken in an attempt to quantify the intensity modulations and anticipated OH rotational temperature modulations associated with airglow structure events typified in Figure 1-4. The presentation in this section is the result of the processed interferometer OH (3,1) band records, which were observed during the airglow structure event of June 15, 1983. The

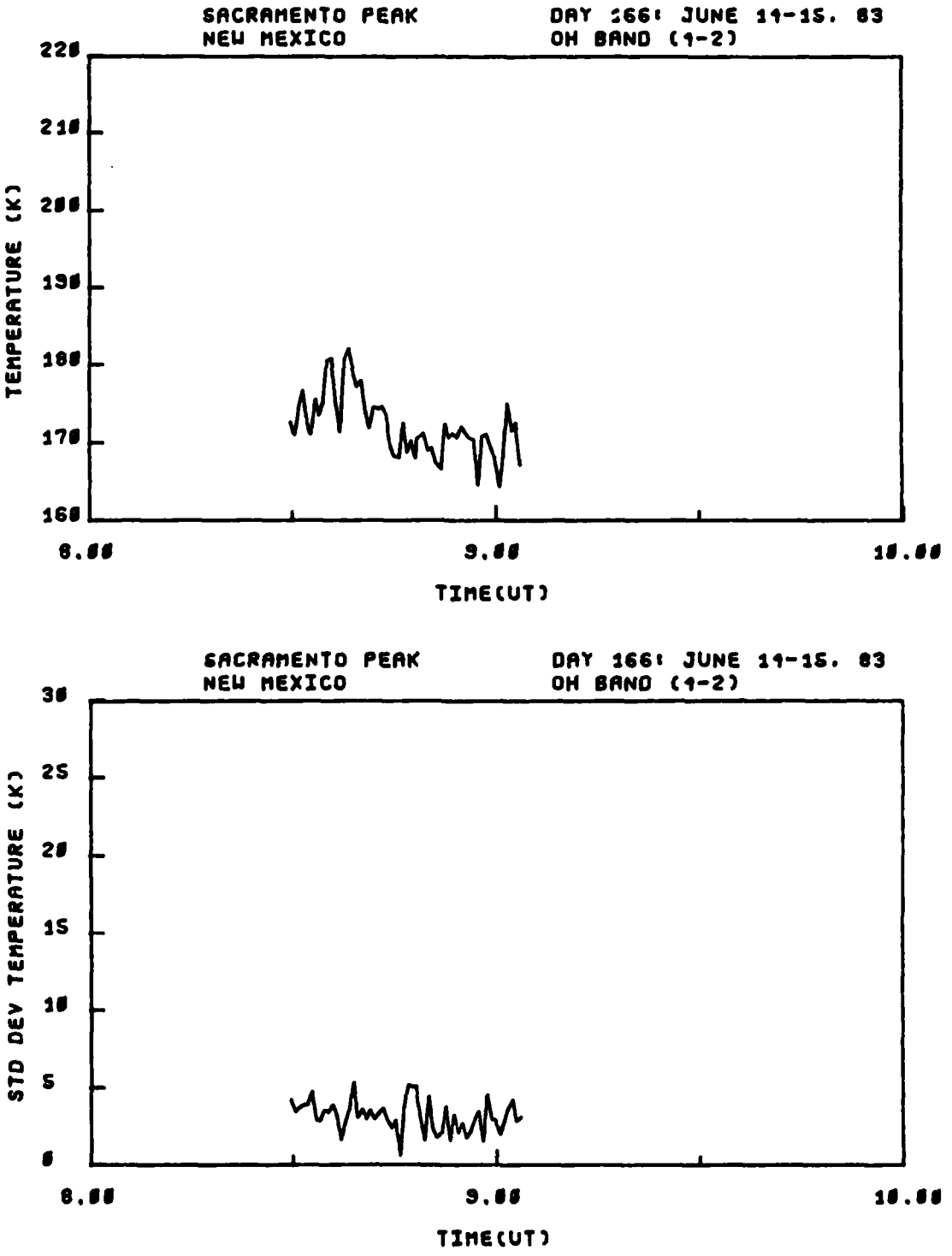

Figure 5-10. OH (4,2) band rotational temperature and standard deviation before smoothing.

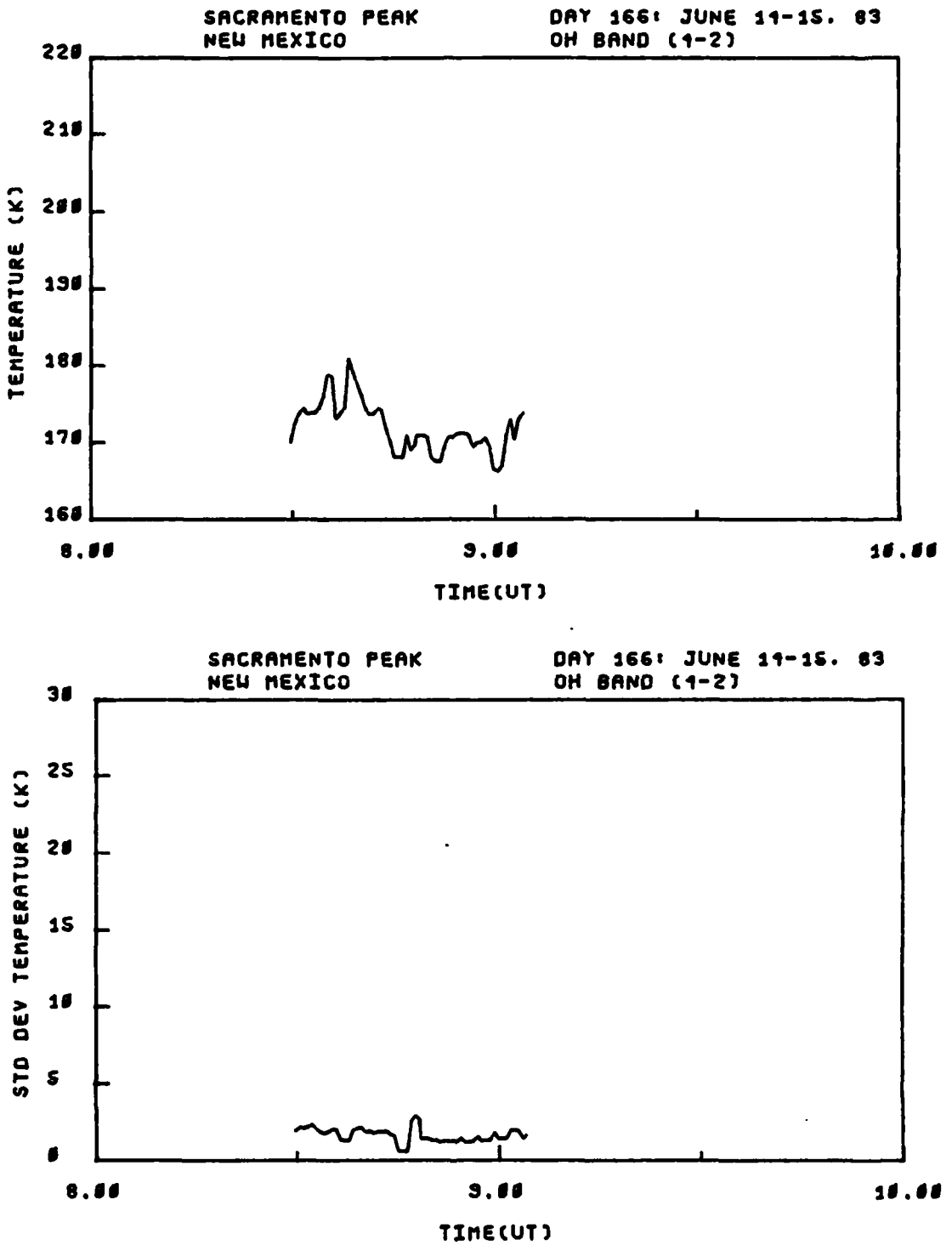

Figure 5-11. OH (4,2) band rotational temperature and standard deviation after smoothing.

OH (3,1) band data have the highest signal-to-noise ratio and, therefore, are felt to be the most reliable. The presentation is given in three segments corresponding to when the instrument was moved in viewing elevation or azimuth. A complete catalog of all the observed OH band intensities and rotational temperatures is contained in Appendix C.

The interferometer-isocon camera system was lowered to a viewing elevation angle of 17° and an azimuth angle of 328° at about 7:30 hrs. UT (after moonset) on this date. Figure 5-12 show the intensity modulations (and standard deviation) as seen by the interferometer until about 8:30 hrs. UT. The bright band, dark band, bright band sequence show a modulation in intensity of about 20%. This same sequence is also shown in the isocon video frames in Figures 5-2 through 5-4. Following the last bright band, the intensity falls off by 40%, indicating a relatively dark band. The simultaneous plot of the OH rotational temperature shown in Figure 5-13 has a mean temperature of about 165 °K. The modulations seen are in phase and correspond to the increases and decreases in intensity in Figure 5-12. The magnitude of the temperature modulations are from 5 to 8 °K. The standard deviation on the temperature calculation is about ±3 °K.

The interferometer was moved to a different viewing location at about 8:30 hrs. UT and remained there until about 9:15 hrs. UT. The new viewing angles were 15.5°

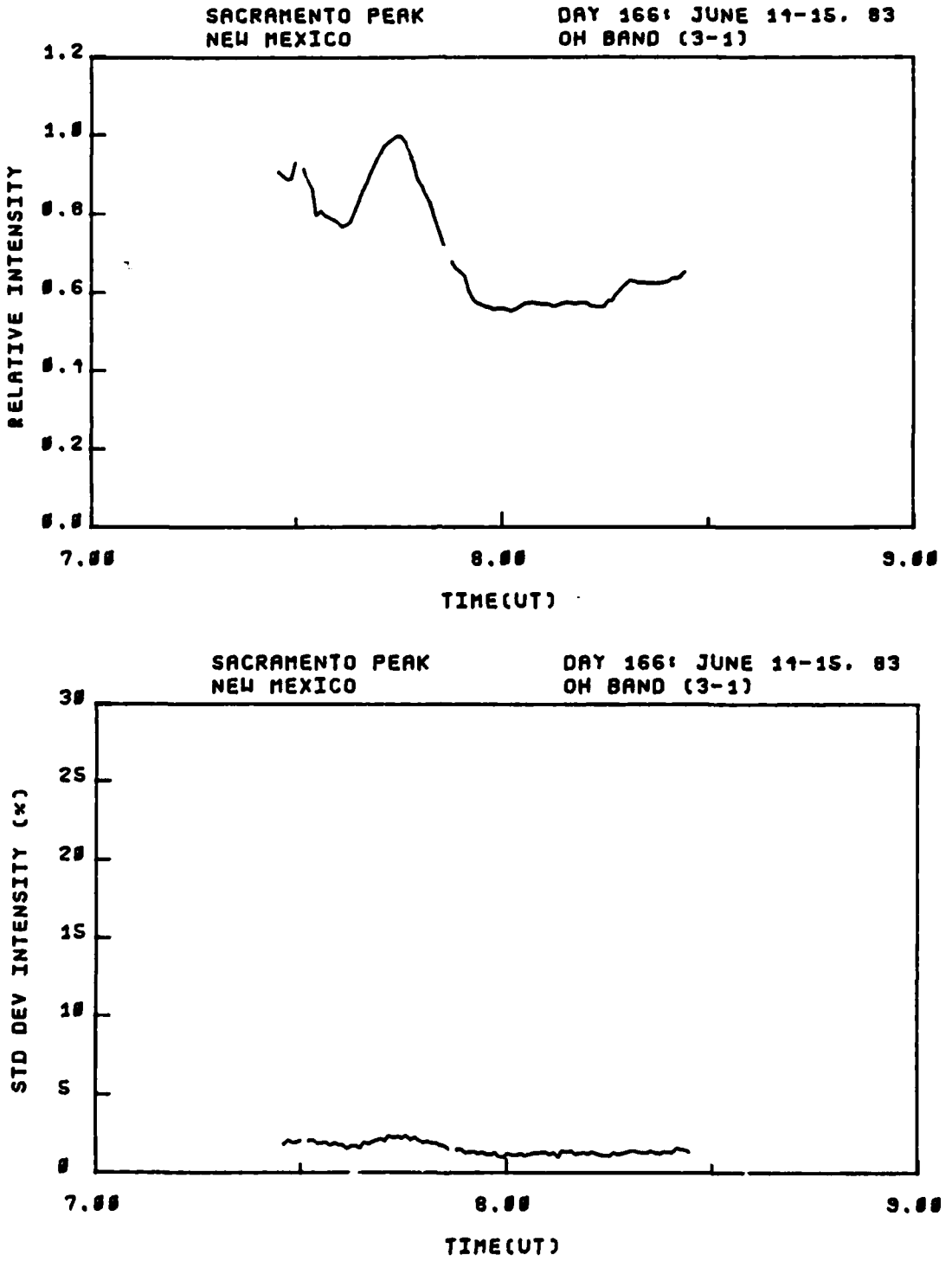

Figure 5-12. OH (3,1) band relative intensity and standard deviation, viewing angle = 17° El. 328°Az., day 166, 7:30-8:30 hrs. UT.

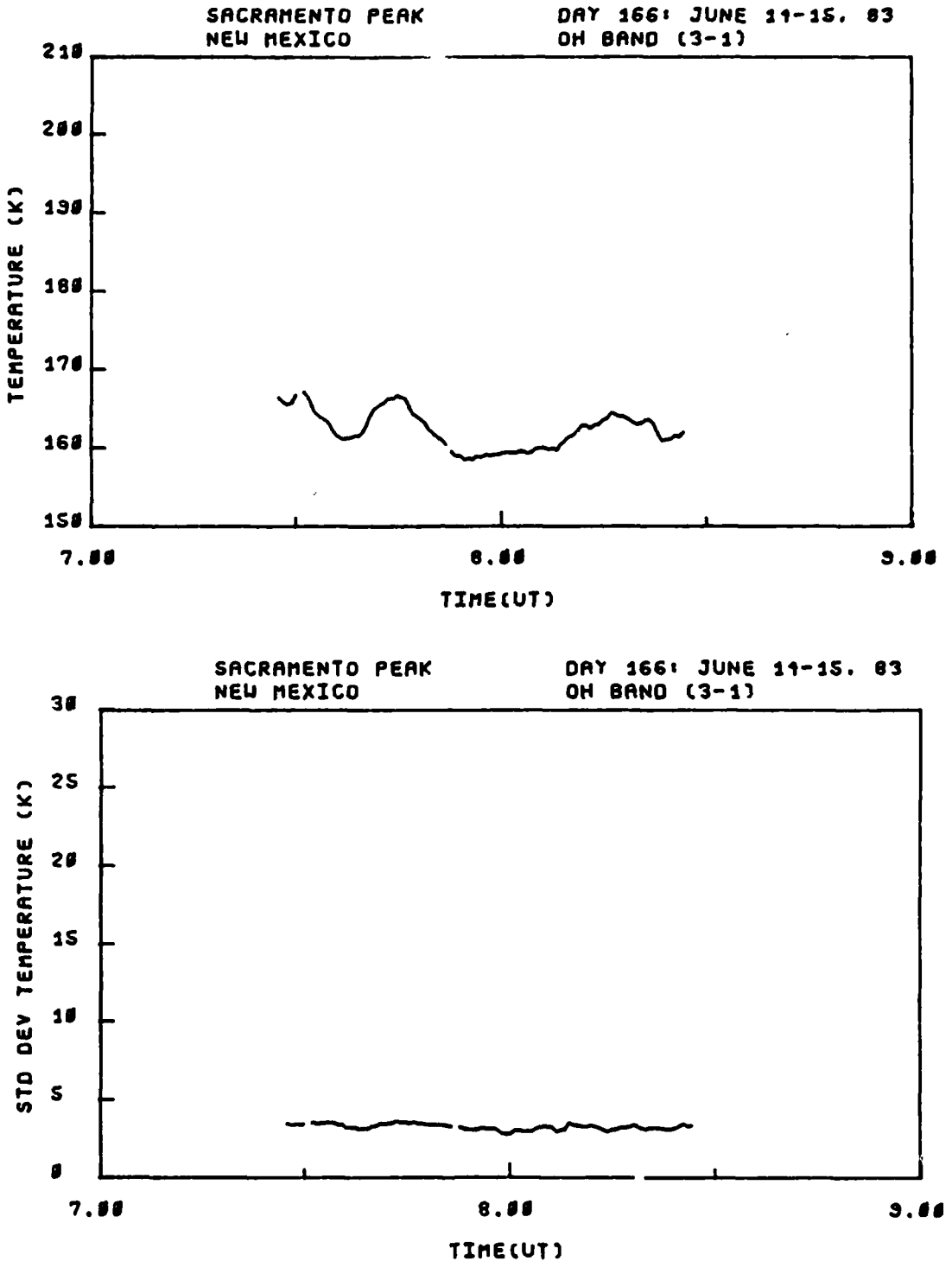

Figure 5-13. OH (3,1) band smoothed rotation temperature and standard deviation, viewing angle = 17° El. 328° Az., day 166, 7:30-8:30 hrs. UT.

elevation and 340° azimuth. The intensity modulations at this viewing position are shown in Figure 5-14. The first dark band, bright band, dark band sequence in this figure show a modulation of 40%. The intensity modulations shown after the first bright band are much smaller, being on the order of 10%. The video frames in Figures 5-5 and 5-6 correspond to the first dark band and occur just after the peak of the very bright band of Figure 5-14. The rotational temperature plot for this same time period is shown in Figure 5-15. The mean temperature is about 165 °K. with a maximum modulation of 10 °K. The uncertainty on the temperature calculations is about ±4 °K during this time frame. The temperature and intensity modulations, at the beginning of this measurement period, are again in phase with each other. The 10% intensity modulations shown in Figure 5-14 occurring after 8:50 hrs. UT, however, do not show any discernible modulations in the temperature.

The last observations of the night began at about 9:15 and lasted until 10:15 hrs. UT. The viewing position of the interferometer was again changed to 15.5° elevation and 309° azimuth. Figure 5-16 presents the intensity modulation record for this period. The curve shows the first sequence of structure exhibiting a modulat on of 40% and three more bright and associated dark bands with modulations of about 20%. The corresponding rotational temperature plot, Figure 5-17, once again has a mean temperature of 165 °K. The temperature modulations are from 5 to 8 °K with each rise

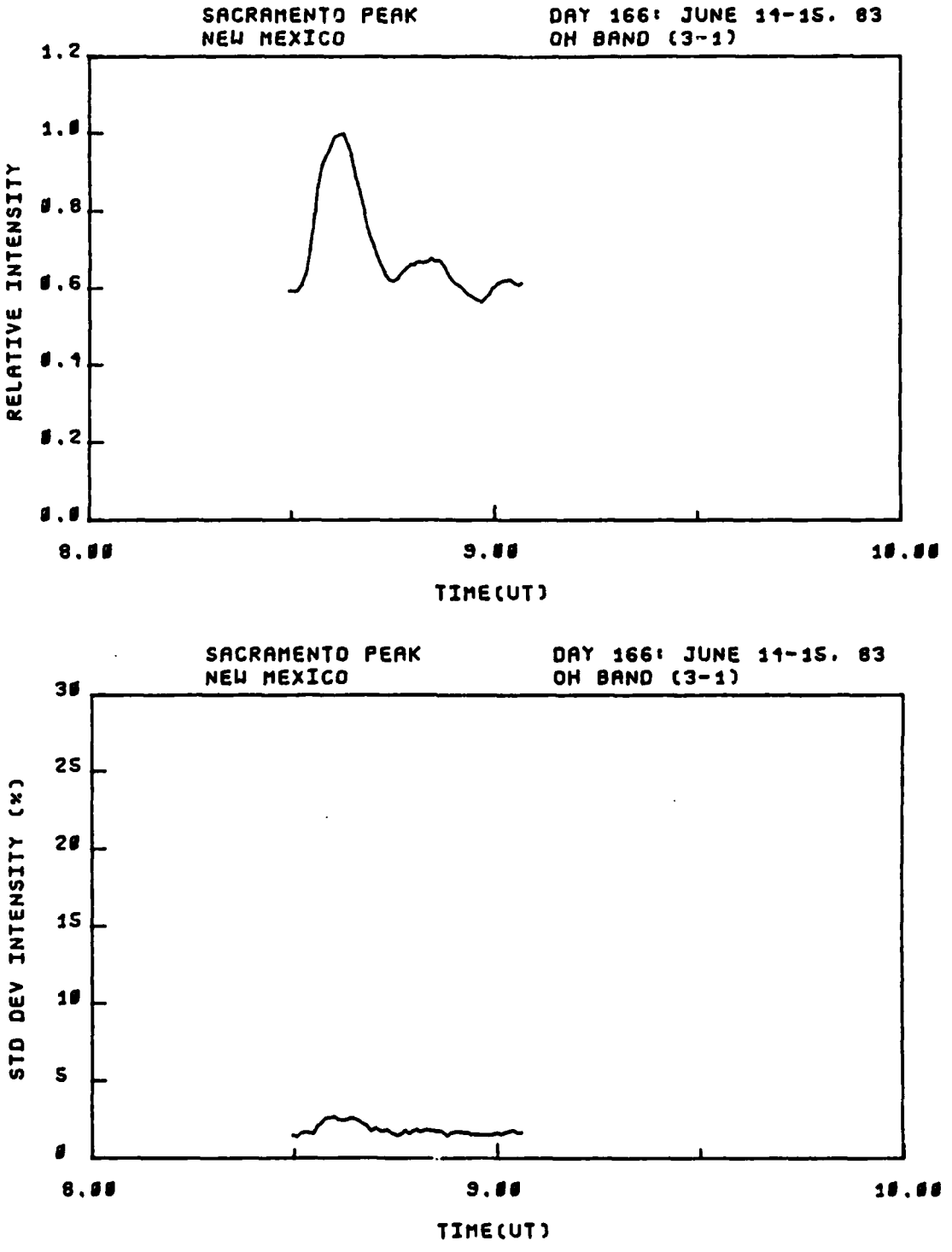

Figure 5-14. OH (3,1) band relative intensity and standard deviation, viewing angle = 15.5° El. 340°Az., day 166, 8:30-9:15 hrs. UT.

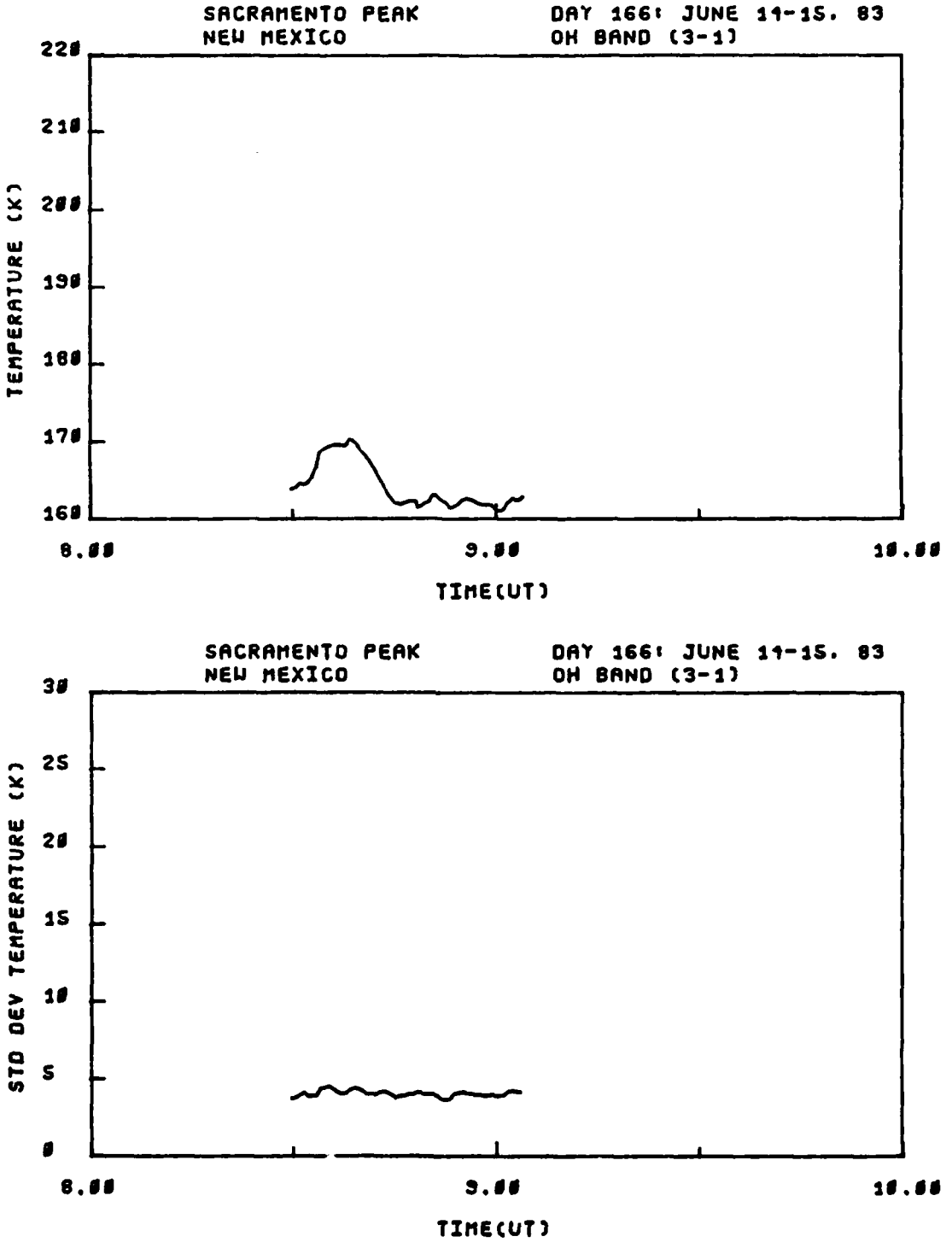

Figure 5-15. OH (3,1) band smoothed rotation temperature and standard deviation, viewing angle = 15.5° El. 340° Az., day 166, 8:30-9:15 hrs. UT.

in temperature having a corresponding rise in intensity of at least 20%. The uncertainty on the temperature calculations is again about ±4 °K.

The presentation in this chapter of the interferometer-recorded structure for June 15, 1983 is focused on the information extracted from the OH (3,1) band. Examination of the Appendix C records for the other OH bands, presents an additional observation. The two $\Delta v=2$ band temperatures track each other within the standard deviation of the calculations. The two $\Delta v=3$ band temperatures track each other within the standard deviation of the calculations. The $\Delta v=3$ band temperatures, however, are consistently from 15 to 32 °K hotter than the $\Delta v=2$ band temperatures (discussed more in Chapter VI). *Figure* 5-18 is an example with additional data available in Appendix C. Table 5-1 outlines a summary of the results presented in this chapter.

TABLE 5-1. Summary of OH airglow structure measurement results for June 15, 1983.

1.	Apparent structure period	14±1 minutes
2.	Apparent structure temporal wavelength	24±1 km
3.	Apparent structure phase velocity . . .	28±2 meters/sec
4.	Intensity modulations measured	10 to 40 %
5.	Rotational temperature modulations measured	5 to 10 °K
6.	Phase relationship of recorded rotational temperature and intensity measurements	In phase
7.	Mean zenith OH (3,1) band intensity	75 kR

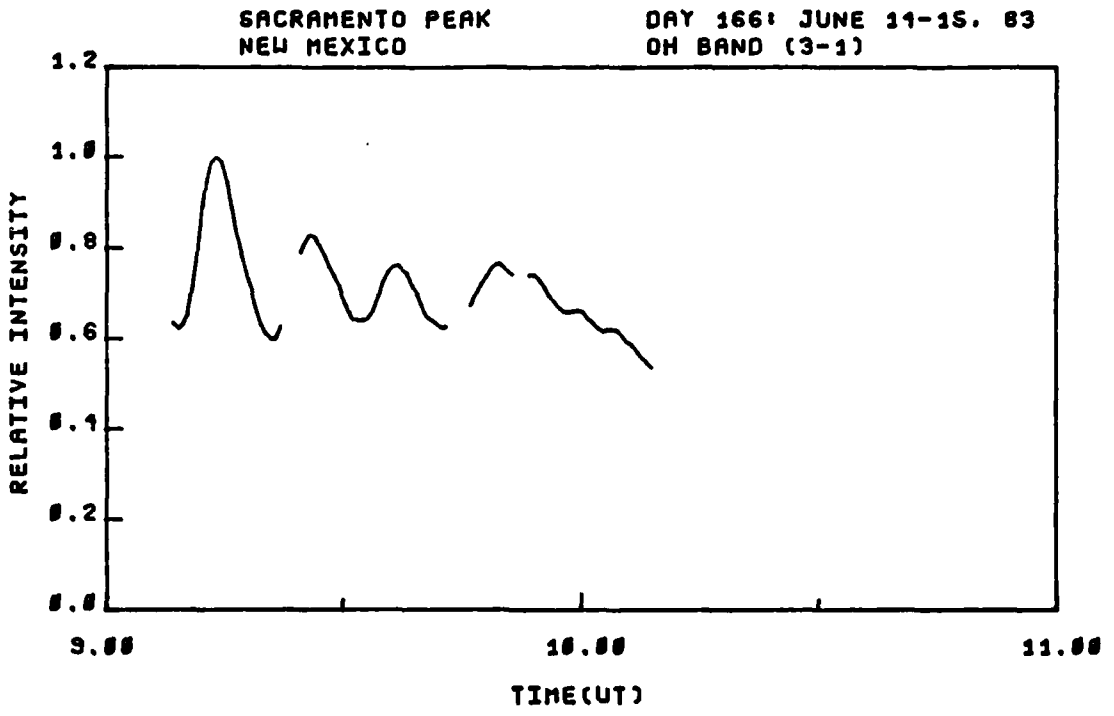

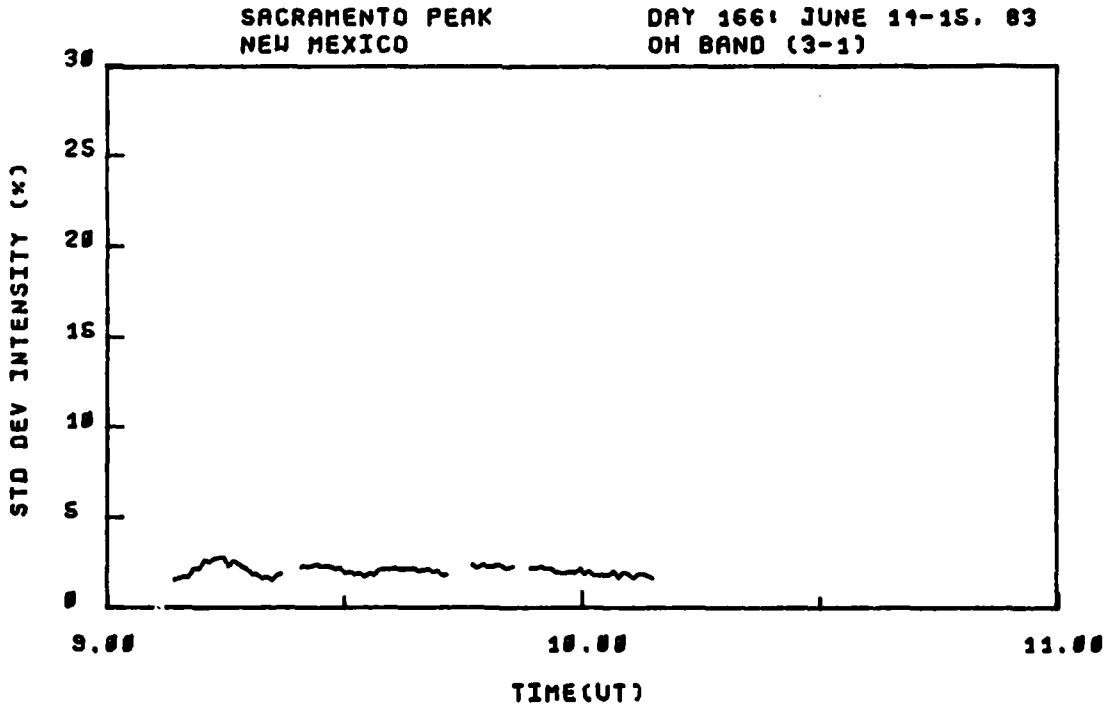

Figure 5-16. OH (3,1) band relative intensity and standard deviation, viewing angle = 15.5° El. 309°Az., day 166, 9:15-10:15 hrs. UT.

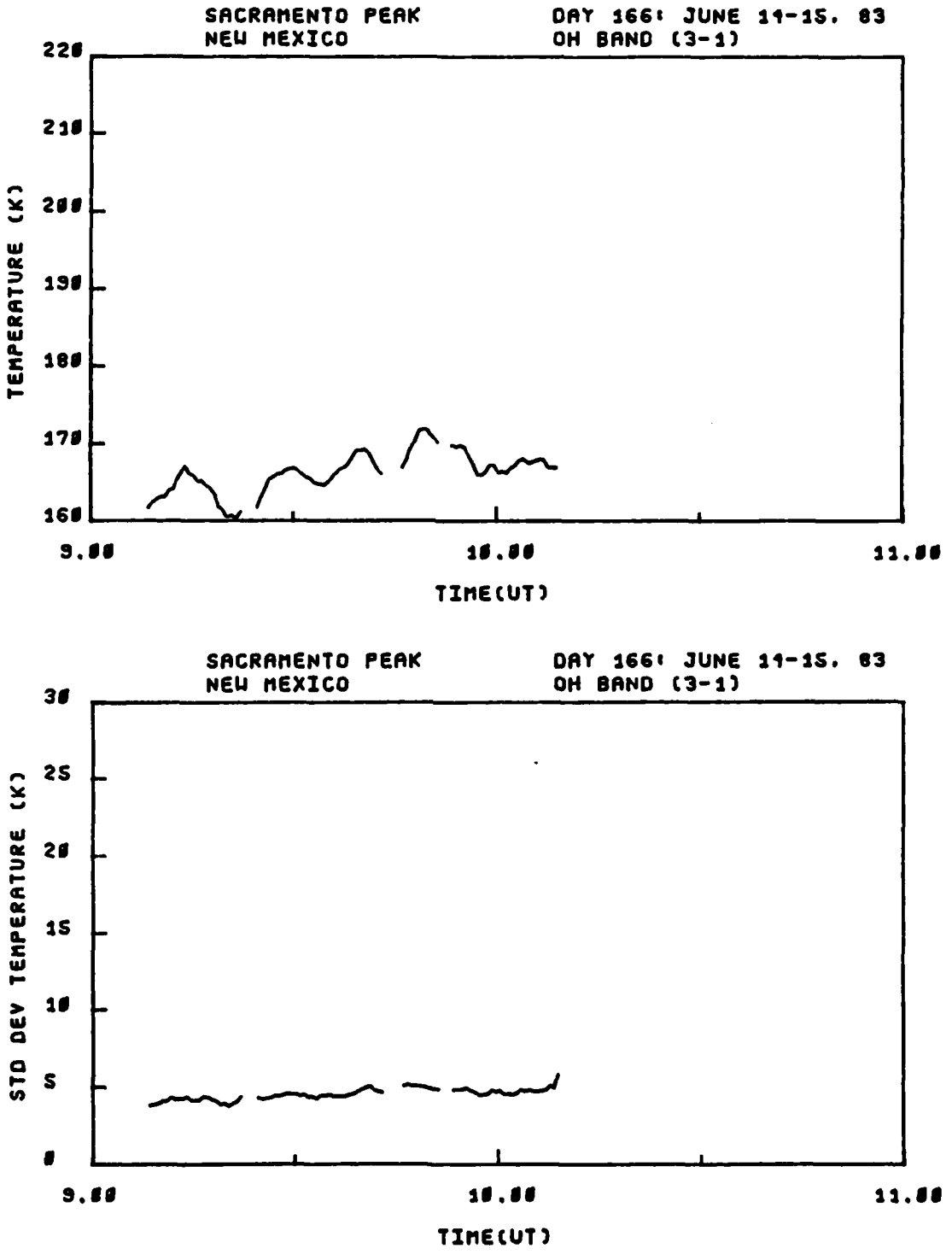

Figure 5-17. OH (3,1) band smoothed rotation temperature and standard deviation, viewing angle = 15.5° El. 309° Az., day 166, 9:15-10:15 hrs. UT.

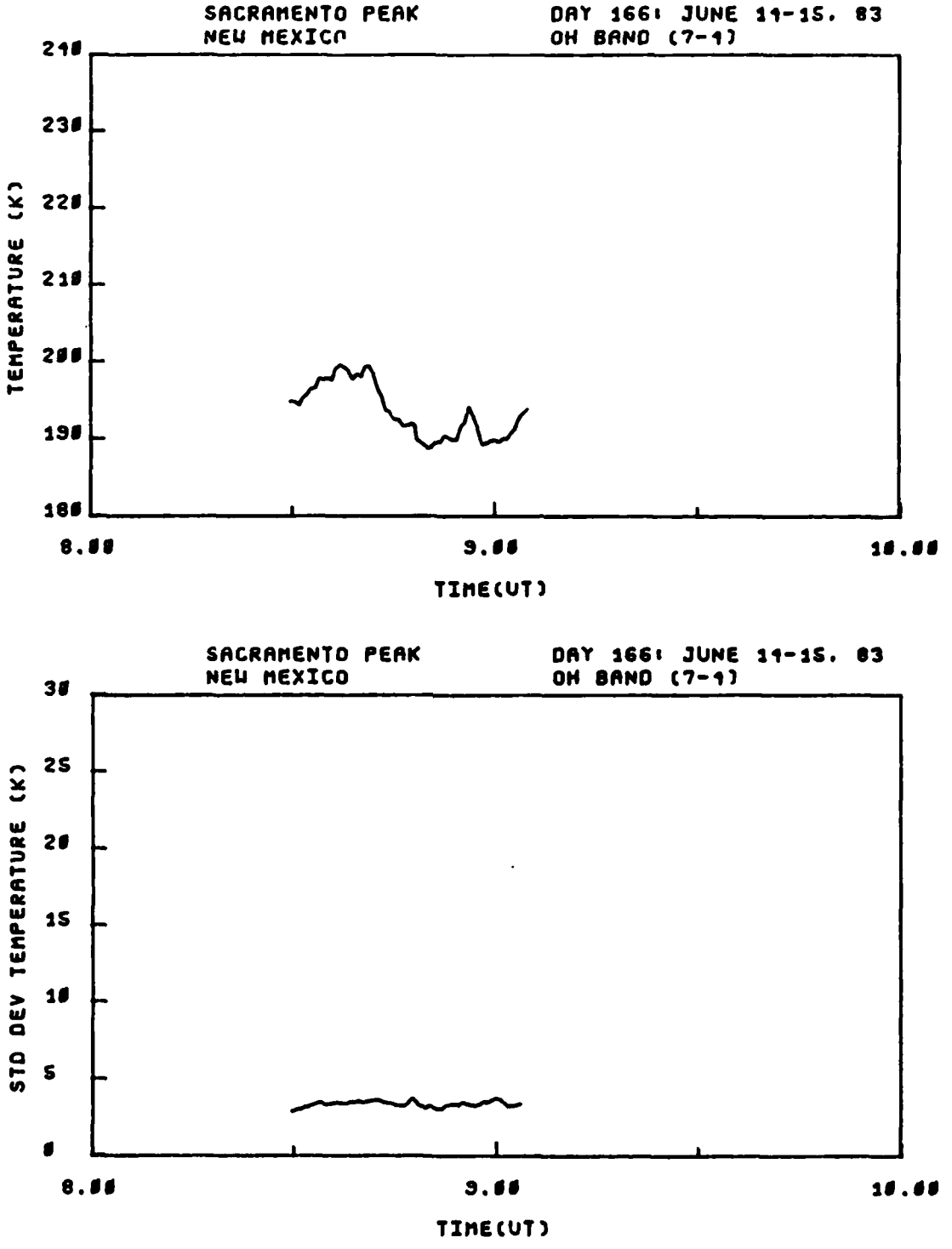

Figure 5-18. OH (7,4) band smoothed rotation temperature and standard deviation, viewing angle = 15.5° El. 340° Az., day 166, 8:30-9:15 hrs. UT.

CHAPTER VI

DISCUSSION OF RESULTS

Rotational Temperatures

The mean mesopause temperature for the month of June at a mid-latitude site is expected to be about 170 °K with variations of ±20 °K possible during the month [NOAA 1976 and references therein]. Noxon [1978] also recorded OH Meinel rotational temperatures at Fritz Peak, Colorado (≈40° N) during May 1977. During the last few days of May, he recorded nightly mean temperatures of about 160 °K.

The mean OH rotation temperatures presented in Chapter V are for an observing site at ≈32° N and are between 165 °K and 175 °K. The references cited above suggest that these rotational temperatures are typical of the mesopause temperatures expected at mid-latitudes during the summer season.

Examination of the standard deviation plots on temperature (Chapter V and Appendix C) reveals typical values in the range 3-7 °K. This uncertainty is nearly as large as many of the temperature changes obtained from the structure measurements. It is felt, however, that much of the computed standard deviation may be systematic rather than statistical. The model used for the determination of rotational temperature is based on the assumption that OH

rotational populations are in true thermal equilibrium and are thus strictly Boltzmann distributed. A slight deviation from this assumption would cause a systematic error. Another possible source of error results from the assumption that all OH airglow radiation is emitted from a thin uniform layer; whereas in reality, the layer is about 7 km in thickness. In addition, at low viewing elevation angles ≤10° the layer geometry is much more complicated. At these low elevation angles atmospheric extinction, van Rhijn effect, and curved spherical geometry potentially have a significant impact on the interpretation of the measurements.

The interferometer spectral response calibration is very sensitive to alignment. The instrument typically remained in alignment for about 2 hours. As can be seen from the increase in the standard deviation as a function of time (7:30 to 10:15 hrs. UT, day 166), the alignment changed significantly and this change could account for a portion of the uncertainty. Therefore, the temperature modulations obtained from the spectral data are felt to be more accurately defined than is suggested by the standard deviation.

The assumption that the low observation elevation angles associated with the structure measurements did not unduly impact the computed temperature is supported by the fact that the temperature at 6:45 hrs. UT on day 166 was 163 °K (see Figure 5-9) and the temperature at 7:30 hrs. on the

same day was 166 °K (see Figure 5-13). These temperatures represent the values computed just before and just after the interferometer "look direction" was changed from the zenith to near the horizon.

Rotational Temperature and Intensity Modulations

The ranges of temperature and intensity modulations observed in the OH Meinel airglow structures are given in Chapter V. The "adiabatic oscillation" and "IGW" modeling of the OH Meinel airglow variations mentioned in Chapter I utilize a parameter which is readily calculated from the intensity and temperature modulations. This parameter is the ratio of the change in emission intensity normalized by the mean emission intensity, divided by the change in temperature normalized by the mean temperature and is deemed useful in studies of the OH airglow structure phenomena. The parameter is usually represented by the Greek letter eta (η) and is defined as follows:

$$\eta = [(\Delta I/\bar{I})/(\Delta T/\bar{T})] \quad , \qquad (6.1)$$

where

ΔI = change or modulation in emission intensity,

$\bar{I}$ = mean value of the emission intensity,

ΔT = change or modulation in rotational temperature,

$\bar{T}$ = mean value of the rotational temperature.

The value of η is potentially useful in distinguishing between chemical processes which give rise to the OH airglow emission and temperature structure. The physics of this parameter is discussed by Krassovsky [1972] and Weinstock [1978]. Pendleton [1985] has summarized the essential features of this parameter in Figure 6-1. In this figure, the η value is plotted versus the ratio (H/H_x), where H is the appropriate atmospheric scale height, and H_x is the scale height (near 85 km) of minor species "x". Here the letter "x" represents either oxygen (O) or hydrogen (H). The simple adiabatic-oscillation model of Krassovsky [1972] yields η values which are independent of (H/H_x), whereas the gravity-wave model of Weinstock [1978] yields (H/H_x) dependent values. The range of η values expected on the basis of values of (H/H_x) inferred from several measured atomic oxygen profiles is also shown in the figure. The information in Figure 6-1 indicates that values of η in the range from 3 to 6 might be expected based on current gravity-wave modeling and the ozone hydration process.

Using the numbers for the intensity and temperature modulations and means, presented in Chapter V, the range of calculated values for η are from 8 to 12. These values are about a factor of 2 greater than those shown in Figure 6-1. In view of the relatively large standard deviations on the temperature determinations, the nominal factor of two disparity between predicted and measured η values is not deemed significant.

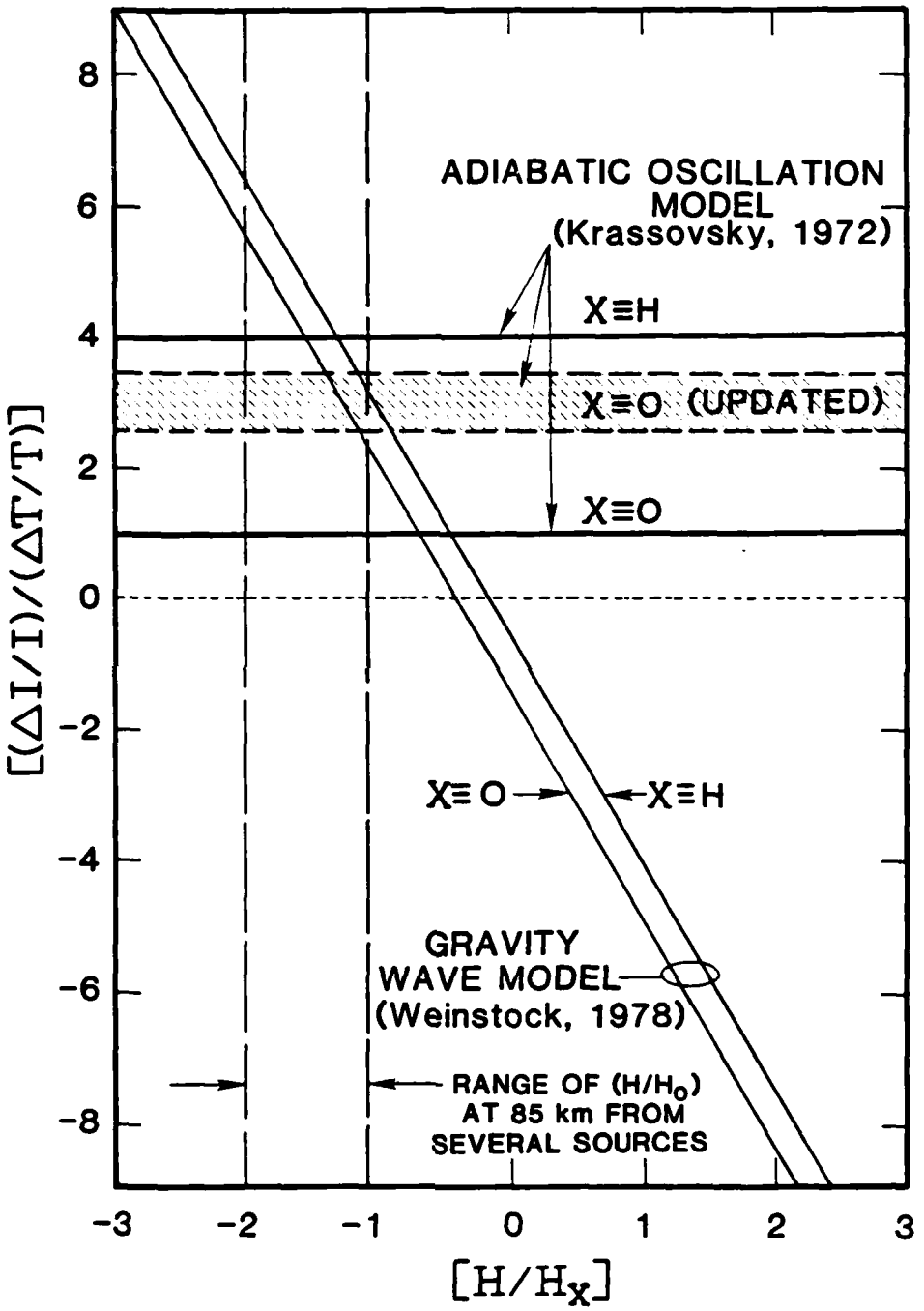

Figure 6-1. Expected values for η (vertical axis) based on gravity-wave models and oxygen measurements [Pendleton 1985].

The η values calculated for the time periods when the interferometer was viewing in the zenith were obtained by assuming the pre-midnight increase in both temperature and intensity reflected a wave-like disturbance. The zenith-viewing η values associated with the major pre-midnight (I,T) fluctuations on UT days 165 and 166 were found to be consistent with η values deduced from the low-elevation-angle data. The consistency of these two sets of calculations lends credence to the idea, once again, that viewing near the horizon had little impact on the η determinations although the modulation in both intensity and temperature may have been impacted by the geometry of the measurements.

The field of view (FOV) of the interferometer is 0.8° full field. Consideration of the OH structures in the nominally 13° by 15° video frames suggests that the 0.8° FOV of the interferometer results in a horizontal spatial integration over about one half cycle in the quasi-period structures. This integration will degrade the horizontal spatial resolution of the interferometer measurements. If the wave is assumed to be sinusoidal in nature and restricted to a very thin spherical shell, a simple integration over 1/2 cycle indicates that the rotational temperature modulations could be degraded by a factor of about 1.5. The horizontal intensity structure is expected to be more complex than the temperature structure [Weinstock 1978]. However, if a similar "degradation factor" were

applicable to the intensity measurements, then the satisfactory agreement of the η values deduced from the zenith-viewing and near-horizon-viewing measurements could be explained.

Temperature Differences Observed Between Bands

Rotational temperature differences between the high-v' and low-v' levels characterized both the zenith-viewing and near-horizon-viewing measurements. The high-v' rotational temperatures were consistently higher than those obtained from low-v' bands. The bands used for detailed comparison are the high-v' (7,4) band and the low-v' (3,1) band. These bands were chosen because of favorable instrument response and alignment stability in the spectral regions of occurrence. The temperature differences observed ranged between 15 and 32 °K. The smaller difference applied when looking in the zenith, and the difference gradually increased throughout the night as the telescope was physically moved, affecting the alignment. The increase in the temperature difference is largely attributed to instrument alignment drift because the standard deviations on the temperature calculations (which also reflect misalignment) increase simultaneously with (and at about the same rate) the increase in temperature difference.

Explanations were sought for this difference. It was discovered that an error in the line strength constant for

the OH (7,4), $P_1(4)$ line had been entered into the processing system. The constant was about 20% low in value. In order to assess the impact of this error, a synthetic OH spectrum was generated assuming a typical temperature with the associated error entered, and a Boltzmann plot was made. A line was fit to the points in a least-squares sense and an associated temperature extracted. The OH (7,4) band model used 12 lines in the fit; therefore, because the model fit is least-squares in nature the error from this incorrect constant was found to be less than 1%.

Another possible explanation of the high-v', low-v' temperature difference is slightly different (≈ 1-3 km) emitting altitudes. The ratio of ΔT to the mean temperature $\bar{T}$, if different for the high-v' low-v' measurements, would support such a difference in mean emitting heights [Pendleton 1985]. The $\Delta T/\bar{T}$ ratio within each observational time frame was calculated and the difference in the ratio, between the high and low rotational levels, was found to be less than 10%, with less than 30% difference among all frames. These differences in the $\Delta T/\bar{T}$ ratio between high-v' and low-v' bands when viewed in terms of the calculated standard deviations does not provide evidence for differences in mean emitting altitudes.

Within the standard deviation of the calculations, the rotational temperature differences between the high-v' and low-v' levels appears to be real. The magnitude for this

difference, as was mentioned in Chapter I, is within the range reported by Krassovsky and Shagaev [1977].

Temperature and Intensity Phase Relationship

The modeling of IGW's mentioned earlier predicts that the changes in the OH Meinel rotational temperature should be in phase with the IGW [Hines 1960]. The change in intensity, however, should be related to the IGW temporal structure in a potentially more complicated manner. This situation arises partly because of the finite chemical time constant associated with mesospheric ozone. The appropriate time constant for the cool (T ≈ 160 °K) summer-mesopause conditions is about 25 minutes [Pendleton 1985]. For IGW periods somewhat in excess of this value, chemical conversion of O_3 is expected to be a significant factor in the phenomenology, whereas for much smaller IGW periods chemical conversion should be unimportant. Examination of Figures 5-8 and 5-9 shows that the temperature maxima lead the intensity maxima by about 20 minutes. This apparent phase difference may relate to the aforementioned O_3 time constant, but it would be premature to draw this conclusion. It is suggested that additional attention be given to this interesting possibility.

The small-scale structures observed near the horizon on UT day 166 exhibit an in-phase relationship between intensity and temperature. The only exception to this is

when the measured intensity modulation was less than about 20%. Under these conditions, no direct correlation between intensity and temperature could be drawn. Since the measured period of the small-scale OH Meinel structures was significantly less than the nominal 85-km O_3 time constant, it does not appear that the in-phase behavior of the larger-amplitude fluctuations is necessarily inconsistent with the zenith measurements.

CHAPTER VII

CONCLUSIONS AND RECOMMENDATIONS

Overview

The goal of this study was to design, develop, and operate an instrument system capable of performing simultaneous spatial, spectral, and temporal high-resolution OH airglow measurements. The design herein, and the resulting data demonstrate the effectiveness of the technique. An airglow structure event which occurred on June 15, 1983 was measured with the interferometer-spectrometer system. OH Meinel intensities and rotational temperatures were obtained for the peaks and troughs of this wavelike structure.

Conclusions

The following are the specific accomplishments of this study. The areas addressed pertain both to the instrument designed for airglow structure measurements and to the data processing techniques used.

1. An optically-compensated interferometer for high throughput ($A\Omega$=0.285 cm^2 sr), was matched to a large area collector (50-cm diameter) to narrow the field of view (0.8°). A noise equivalent spectral radiance (NESR) (sensitivity) of 16 R/cm^{-1} at 1.5 μm was

achieved. In comparison, a conventional Michelson interferometer-spectrometer with the same detector, collector area, resolution, and scan time would have a NESR of 128 R/cm^{-1}, a factor of 8 less sensitive than the one developed for this study. When compared with a conventional Ebert spectrometer, using the same detector and operated at the same resolution, a sensitivity of 208 R/cm^{-1} could be achieved, a factor of 13 less sensitive.

2. A spectral resolution of 2 cm^{-1} was sufficient to resolve the OH emission line structure for the extraction of OH rotational temperatures. Based upon a rotational line separation of 10 cm^{-1} and the Hamming apodization function used, the spectral resolution of the instrument could be lowered to no more than 4 cm^{-1}.
3. Based upon the video records, the bright or dark bands of OH structure subtend about 1° of arc at these low elevation angles (≈ 15°). The apparent temporal wavelength was 24±1 km, with a period of 14±1 minutes, and an apparent phase velocity of 28±2 meters/second.
4. The interferometer system field of view was measured at 0.8°. The interferometer FOV is sufficiently narrow to independently view a "bright" or a "dark" structure band. Based on this limited data set and simple wave geometry, the field of view could be as large as 7° if these structures were viewed in the zenith.

5. The measured intensity modulations (contrast ratios) for the OH airglow structures ranged between 20 and 40% with interferometer recorded periods of 14 minutes The calculated standard deviation was typically 3%.

6. The mean calculated OH Meinel rotational temperature for the aforementioned event was 165 °K. The measured modulations in rotational temperatures associated with the changes in intensity ranged from 5-10 °K and are in phase with the intensity modulations. Typical standard deviations on the rotational temperature calculations ranged from 2-7 °K. The mean temperature and magnitude of the temperature fluctuations are consistent with both IGW theory and previous mesospheric temperature measurements.

7. The least-squares model used to extract band intensity and rotational temperature provides a computational efficient way (convergence to final values occurred within 4 iterations of the fitting routine) to simultaneously derive these values. The model also provides a measure (standard deviation) of how well the data fit a Boltzmann distribution.

8. The insight needed to identify what is being observed from the airglow layer can only be provided by the camera (or similar) video system. The measurement of OH airglow structure events with the interferometer system would not be possible without the simultaneous use of

the isocon camera, because with the interferometer alone, exactly what was being viewed would be unknown.

Recommendations for Future Research

The interferometer worked as designed and proved to be an excellent tool for this type of study. The model developed for the extraction of rotational temperatures and intensities is an accurate technique and provides computational flexibility. However, several suggestions are made for consideration for future work.

1. The optical path within the interferometer is very complex. There are 20 optical surfaces through which the incoming energy must pass before reaching the detector. Assuming a typical loss of 4% per surface, 80% of the incoming signal is lost before reaching the detector. This complex optical path should be redesigned to minimize the number of optical elements and optically coat the remaining elements to minimize reflection loss.
2. The physical size of the instrument should be reduced to facilitate portability to remote sites.
3. The instrument is very sensitive to optical alignment. The optical components need to be mounted in a more stable manner to hold their location better.
4. The alignment is very sensitive to temperature. It is necessary therefore to temperature control the

interferometer environment to preclude instrument changes as the outside temperature fluctuates.

5. The telescope pointing system needs to be automated. The sensitivity of alignment to physical motion as well as the need to point the instrument to an area of interest demand that the positioning of the system be automated.

6. An infrared camera system, like the one provided by the University of Southampton, needs to be permanently incorporated as part of the interferometer system. The interferometer cannot effectively gather data on airglow structure if the location of the structure is not known and the camera provides this input.

7. The instrument must be provided a better means of calibration. The blackbody sources used in this study give a reasonable indication of alignment and instrument response but as the system alignment drifts the calibration is less meaningful. Perhaps a technique utilizing OH spectral line pair ratios which are independent of rotational temperature but sensitive to alignment could be used as a dynamic measure of instrument alignment.

8. A recommendation is made to investigate other detectors, in order to extend the ability of the interferometer, with a wider spectral bandwidth and higher sensitivity. The RCA detector used in this study is an excellent detector where it is sensitive but is somewhat limited

in spectral bandwidth. A larger detector could also be used to increase the throughput, although the throughput is now almost limited by the size of the interferometer optics.

9. A new data system should be developed to record the interferometer data allowing for at least the digitization of the data during recording. The analog tapes are bulky and expensive but more importantly, playing back the tapes for data reduction is too time consuming.

10. The calibration curves provided to the model derived from occasional alignment processes with a tungsten blackbody could be improved. As was mentioned earlier, a dynamic calibration using information inherent in the spectrum could be used to better adjust the model to the instrument response.

11. Examination of Figures 3-3 and 3-4 shows that the phase correction used to eliminate the chromatic effects of the instrument on the data works well on the slowly varying blackbody curve but the negative information on the spectrum makes the technique suspect when applied to the rapidly changing data. A phase correction technique which operates in the interferogram "domain" where the shaping could be done with simple multiplication could prove to be more accurate.

12. The extraction of line amplitudes from the interferometer could be improved in two areas. First, the approximate locations of the spectral lines of interest are found in a manual manner. A template using a synthetic spectrum could be designed for each OH band and a correlation routine could be used to automatically search the raw data for the location of the lines. Secondly, the apodization routine used to extract the actual line amplitude from the data should be modified to calculate a line area rather than amplitude. The area routine would provide for the averaging out of noise whereas the amplitude routine always searches for the most positive peak.
13. The model should be modified to to use the "Q" branches of the OH bands. To do this the molecular constants for both Q_1 and Q_2 would need to be averaged as one because the interferometer does not resolve the two groups. This addition should add more accuracy to the model because the Q branches are the largest lines within each band.
14. The model could be modified to include a third variable, water column content, based on the several lines within the OH bands which are severely affected by water absorption. The model then could provide additional information about the atmosphere.

REFERENCES

Baker, D.J. 1978. Studies of Atmospheric Infrared Emissions. Final Report, AFGL-TR-78-0251. Air Force Geophysics Laboratory. Hanscom AFB, Mass. 79 p.

Baker, D.J., A.J. Steed, G.A. Ware, D. Offermann, G. Lange, and H. Lauche. 1985. Ground-Based Atmospheric Infrared and Visible Emission Measurements. Journal of Atmospheric and Terrestrial Physics 47(1-3):133-145.

Banks, P.M., and G. Kockarts. 1973. Aeronomy, Part A. Academic Press, New York and London. 430 p.

Bevington, P.R. 1969. Data Reduction and Analysis for the Physical Sciences. McGraw-Hill Book Company, New York. 336 p.

Bouchareine, P., and P. Connes. 1963. Interferometer with a Compensated Field of Spectroscopy by the Fourier Transform. Le Journal De Physique Et Le Radium 24:134-138.

Brigham, E.O. 1974. The Fast Fourier Transform. Prentice-Hall, Inc., Englewood Cliffs, New Jersey. 252 p.

Chamberlain, J.W. 1961. Physics of the Aurora and Airglow. Academic Press, New York and London. 704 p.

Connes, P. 1956. Augumentation du Produit Luminosite x Resolution des Interferometres Par l'emploi d une Difference de Marche Independante de l'incidence. Revue Opt. Theor. Instrum. 35:37-42.

Connes, J. 1963. Spectroscopic Studies Using Fourier Transformations. NAVWEPS Report 8099. U.S. Navel Ordinance Test Station, China Lake, California. AD 409 869. 127 p.

Coxon, J.A., and S.C. Foster. 1982. Rotational Analysis of Hydroxyl Vibration-Rotation Emission Bands: Molecular Constants for OH $X^2\Pi$, $6 \leq v \geq 10$. Canadian Journal of Physics 60:41-48.

Crawford, J., P. Rothwell, and N. Wells. 1975. Airborne Television Observations of Airglow Clouds in the Near Infrared. Nature 257:650-651.

Despain, A.M., F.R. Brown Jr., A.J. Steed, and D.J. Baker. 1971. A Large Aperture Field-Widened Interferometer-Spectrometer for Airglow Studies, p. 293-300. *In* G.A. Vanasse, D.J. Baker and A.T. Stair, Jr. (Eds.). Aspen International Conference on Fourier Spectroscopy, 1970. Air Force Cambridge Research Laboratories, AFCRL-71-0019, Special Reports No. 114, Hanscom AFB, Mass. 477 p.

Driscoll, W.G. (Ed.), and W. Vaughan (Associate Ed.). 1973. The Handbook of Optics. Sponsored by Optical Society of America. McGraw Hill, New York. Chapter 2:62-63.

Espy, P. 1984. Private communication with Mr. Espy, Physics Department, Utah State University, Logan, Utah. March.

Fellgett, P. 1949. Private communication to M.J.E. Golay. Multi-slit Spectrometry. Journal of the Optical Society of America 39:437-439.

Forman, M.L. 1966. Fast Fourier-Transform Technique and Its Application to Fourier Spectroscopy. Journal of the Optical Society of America 56:978-985.

Gebbie, H.A., and G.A. Vanasse. 1956. Interferometric Spectroscopy in the Far Infrared. Nature 178:432-436.

Gilway Technical Lamp Catalog. 1982. Part No. 8010. 272 New Boston Park, Woburn, MA.

Hamming, R.W. 1977. Digital Filters. Prentice Hall, Englewood Cliffs, New Jersey. 226 p.

Hapgood, M.A., and M.J. Taylor. 1982. Analysis of Airglow Data. Annales de Geophysique t. 38 fasc. 6:805-813.

Harris, C.R. 1984. Private communication with Mr. Harris, Data Reduction Specialist, Space Dynamics Laboratory, Utah State University, Logan, Utah. April.

Harris, F.J. 1978. On the Use of Windows for Harmonic Analysis with the Discrete Fourier Transform. Proceedings of the IEEE 66(1):51-83.

Haycock, R.H. 1975. A Gas Lubricated Precision Platform for Interferometric Measurements. PhD dissertation. Utah State University Library, Logan, Utah. 178 p.

Haycock, R.H., and D.J. Baker. 1975. Infrared Prism Interferometer-Spectrometer using a Gas-Lubricated Drive Bearing. Infrared Physics 14:259-265.

Hertzberg, G. 1971. The Spectra and the Structures of Simple Free Radicals. Cornell University Press Ithaca, New York. 195 p.

Hill, R.A., A.J. Mulac, D.P. Afschliman, and W.L. Flower. 1979. Temperatures From Rotational-Vibrational Raman Q-branches. Journal of Quantum Spectroscopy Radiation Transfer. Pergamon Press Ltd., Great Britian, 21:213-230.

Hines, C.O. 1960. Internal Atmospheric Gravity Waves at Ionospheric Heights. Canadian Journal of Physics 38:1441-1481.

Hines, C.O. 1965. Dynamical Heating of the Upper Atmosphere. Journal of Geophysical Research 70(1):177-183.

Hoffmeister, C. 1952. Investigations on Bright Night Sky and Luminous Bands. Journal of the British Astronomical Association 62(8):288-292.

Huppi, R.J. 1976. Radiometric Instrumentation and Techniques of Measuring Infrared Emissions from the Atmosphere and Targets. AFGL-TR-76-0253, Air Force Geophysics Laboratory, Hanscom AFB, Mass. 65 p.

Huppi, R.J., and D.J. Baker. 1976. Intensity Variations of Atmospheric Hydroxyl Emissions. Scientific Report No. 1, AFCRL-TR-76-0032, Contract No. F19628-74-C-0190, Utah State University, Logan, Utah. Air Force Geophysics Laboratory, Hanscom AFB, Mass. 77 p.

Jacquinot, P. 1954. The Luninosity of Spectrometers with Prisms, Gratings, or Fabry-Perot Etalons. Journal of the Optical Society of America, 44:761-764.

Kieffaber, L.M. 1973. Structure and Fluctuations of the OH Airglow at 1.65 and 2.15 μ. PhD Dissertation. University of New Mexico Library, Albuquerque, New Mexico. 127 p.

Kochanski, A. 1964. Atmospheric Motions from Sodium Cloud Drifts. Journal of Geophysical Research 69:3651-3656.

Krassovsky, V.I. 1972. Infrasonic Variations of OH Emission in the Upper Atmosphere. Annales de Geophysique 28:739-747.

Krassovsky, V.I., and M.V. Shagaev. 1977. Research Note, On the Nature of Hydroxyl Airglow. Planetary and Space Science 25:509-510.

Krassovsky, V.I., B.P. Potapov, A.I. Semenov, M.V. Shagaev, N.N. Shefov, V.G. Sobolev, and T.I. Toroshelidze. 1977. Internal Gravity Waves Near the Mesopause and the Hydroxyl Emission. Annales de Geophysique t. 33 fasc. 3:347-356.

Lawson, C.L., and R.J. Hanson. 1974. Solving Least Squares Problems. Prentice-Hall, Inc., Englewood Cliffs, New Jersey. 340 p.

Loewenstein, E.V. 1971. Fourier Spectroscopy; An Introduction, p. 3-18. *In* G.A. Vanasse, D.J. Baker and A.T. Stair, Jr. (Eds.). Aspen International Conference on Fourier Spectroscopy, 1970. Air Force Cambridge Research Laboratories, AFCRL-71-0019, Special Reports No. 114, Hanscom AFB, Mass. 477 p.

Meinel, A.B. 1950. OH Emission Bands in the Spectrum of the Night Sky. Astrophysics Journal 111:555-561.

Mertz, L. 1959. Paper presented at Congres de Stockholm, Heterodyne Interference Spectroscopy.

Mies, F.H. 1974. Calculated Vibrational Transitional Probabilities ($X^2\pi$). Journal of Molecular Spectroscopy 53:150-188.

Moreels, G., and M. Herse. 1977. Photographic Evidence of Waves Around the 85 km Level. Planetary and Space Science 25:265-273.

National Oceanic and Atmospheric Administration (NOAA). 1976. U.S. Standard Atmosphere. Washington D.C. 227 p.

Norton, R.H., and R. Beer. 1976. New Apodizing Functions for Fourier Spectrometry. Journal of the Optical Society of America 66:259-264.

Noxon, J.F. 1978. Effect of Internal Gravity Waves Upon Night Airglow Temperatures. Geophysical Research Letters 5(1):25-27.

Nuttall, A.H. 1981. Some Windows with Very Good Sidelobe Behavior. IEEE Transactions on Acoustics, Speech, and Signal Processing ASSP-29(1):84-91.

Pendleton, W.I. Jr. 1985. Private communication with Dr. Pendleton, Dept. of Physics and Space Dynamics Laboratories, Utah State University, Logan, Utah. July.

Peterson, A.W. 1979. Airglow Events Visible to the Naked Eye. Applied Optics 18(20):3390-3393.

Peterson, A.W., and G.W. Adams. 1983. OH Airglow Phenomena During the 5-6 July 1982 Total Lunar Eclipse. Applied Optics 22(17):2682-2685.

Peterson, A.W., and L.M. Kieffaber. 1973. Infrared Photography of OH Airglow Structures. Nature 242:321-322.

Peterson, A.W., and L.M. Kieffaber. 1975. Photography and Photometry of the Near Infrared OH Airglow. Nature 257:649-650.

Rai, D.B., and B.G. Fejer. 1971. Evidence of Internal Gravity Waves in the Lower Ionosphere. Planetary and Space Science 19:561-566.

Rayleigh, Lord (Strutt, R.J.). 1931. On a Night Sky of Exceptional Brightness, and on the Distinction between the Polar Aurora and the Night Sky. Proceeding of the Royal Society, London, A131:376-381.

Roychourdhury, D.K. 1983. Airglow Technique to Compute Mesospheric Temperature and Integrated Water Vapor Concentration of the Atmosphere. Masters Thesis. Utah State University Library, Logan, Utah. 135 p.

Shankland, R.S. 1974. Michelson and His Interferometer. Physics Today 4:37-48.

Soule, H.V. 1968. Electro-Optical Photography at Low Illumination Levels. John Wiley and Sons, Inc., New York. 392 p.

Stair, A.T., and D.J. Baker. 1974. Midlatitude Hydroxyl IR Airglow Spectra. AFCRL-TR-74, Air Force Geophysics Laboratory. Hanscom AFB. Mass. 172 p.

Steed, A.J. 1978. The Design, Evaluation, Optimization and Calibration of a Field-Widened Interferometer-Spectrometer used for Near Infrared Atmospheric Measurements. PhD dissertation. Utah State University Library, Logan, Utah. 145 p.

Strong, J.D., and G.A. Vanasse. 1959. Interferometric Spectroscopy in the Far Infrared. Journal of the Optical Society of America 49:844-851.

Takeuchi, I., and K. Misawa. 1981. Short-Period Oscillations of Intensity and Rotational Temperature of the OH(6-2) Band. Annales de Geophysique t. 37 fasc. 2:315-319.

Taylor, M.J. 1983-84. Private communication with Mr. Taylor, Department of Physics, University Southampton, England.

Taylor, M.J. 1984. Paper presented at The International Workshop on Noctilucent Clouds. TV Observations of Mesospheric Wave Structures. Tallinn, Estonian SSR, USSR, August.

Taylor, M.J., M. Hapgood, and P. Rothwell. 1980. Upper Atmosphere Wave Structure Imaged in Oxygen Green Line, Sodium and the Near Infrared Hydroxyl Airglow Emissions, p. 95-105. *In* Proc. of the Eight Annual Meeting on Upper Atmosphere Studies by Optical Methods, Dublin, Ireland, E. O'Mongain (Ed.), University College, Dublin, Sept.

Turnbull, D.N., and R.P. Lowe. 1983. Vibrational Population Distribution in Hydroxyl Night Airglow. Canadian Journal of Physics 61:244-250.

Vagin, V.A. 1980. Optimal Apodization in Fourier Spectrometry. Optical Spectrometry (USSR) 48(2):190-193.

Vanasse, G.A. (Ed). 1977. Spectrometric Techniques, Vol. 1. Academic Press, New York. 355 p.

Vanasse, G.A., D.J. Baker, and A.T. Stair Jr. (Eds.). 1971. Aspen International Conference on Fourier Spectroscopy, 1970. Air Force Cambridge Research Laboratories, AFCRL-71-0019, Special Reports No. 114, Hanscom AFB, Mass. 477 p.

Ware, G.A. 1980. OH Rotational Temperatures Using Optimal Interferometric Techniques. PhD dissertation. Utah State University Library, Logan, Utah. 271 p.

Weast, R.C., (Ed.). 1977. CRC Handbook of Chemistry and Physics. CRC Press, Cleveland, Ohio. p. E-204.

Weinstock, J. 1978. Theory of Interaction of Gravity Waves with $O_2(^1\Sigma)$ Airglow. Journal of Geophysical Research 13(A11):5175-5185.

Werner, H., P. Rosmus, and E. Reinsch. 1983. Molecular Properties from MCSCF-SCEP Wave Functions. I. Accurate Dipole Moment Functions of OH, OH-, and OH+. Journal of Chemical Physics, July 15, 79(2):905-916.

Wyatt, C.L. 1978. Radiometric Calibration: Theory and Methods. Academic Press, New York. 200 p.

APPENDICES

Appendix A

OH Transitions

This appendix briefly describes why the radiation from the OH molecule is so complex. The many spectral lines generated by the excited radical are depicted in Figure 4-1. The molecule rotates and vibrates simultaneously, and each of the motions are quantified and interactive.

The total molecular angular momentum without electronic spin $\vec{K}$ is also quantized and is identified by the quantum number K. The quantity $\vec{K}$ is comprised of two parts

$$\vec{K} = \vec{N} + \vec{\Lambda} \quad . \tag{A.1}$$

The vector $\vec{N}$ is the nuclear angular momentum and the vector $\vec{\Lambda}$ is the angular momentum of the orbiting electron cloud projected onto the internuclear axis. The quantum number Λ associated with the electronic orbital momentum can take on a value of +1 or -1 depending upon which way the electron cloud is orbiting with respect to the nuclear rotation. The double degeneracy of Λ leads to the so-called Λ splitting of each state; however, the split is less than 1 cm^{-1} at low rotational speeds [Baker 1978], which is less than the instrument resolution used for this study, therefore the Λ-split lines will be considered as one.

The quantum number K can take on values K = 1,2,3,... . The selection rule; however, is

$$\Delta K = 0, \pm 1 \quad . \tag{A.2}$$

The collection of lines within each band, grouped according to their respective ΔK, are called branches. The branch with $\Delta K = 0$ is called the Q branch, that for $\Delta K = +1$ is the R branch, and that for $\Delta K = -1$ is called the P branch.

The OH molecule has an odd number of electrons. This imbalance results in a net electronic spin angular momentum $\vec{S}$ and is represented by quantum number S. The odd electron gives rise to an even multiplicity 2S+1. Since the total number of electrons is odd, S is half integral ($S = \pm 1/2$), each transition state is a doublet. It is sometimes convenient to consider the total electron angular momentum $\vec{\Omega}$ as a separate entity. The total electron angular momentum is

$$\vec{\Omega} = \vec{\Lambda} + \vec{S} \quad . \tag{A.3}$$

Therefore, each vibration-rotation transition will split into two separate spectral lines according to whether $\Omega=3/2$ or $\Omega=1/2$.

The OH molecule is very light and as a consequence the odd electron spin $\vec{S}$ is only weakly coupled to the internuclear axis. The molecule is therefore, modeled as Hund's case (b) [Hertzberg 1971]. The total molecular angular momentum $\vec{J}$ can now be formed

$$\vec{J} = \vec{K} + \vec{S} \quad . \tag{A.4}$$

As can be seen from Equation A.4, for each value of K there are two values for J. Each branch of the OH spectra must also take on two values. If Ω=3/2, then

$$J = K + 1/2 = 1.5, 2.5, 3.5, \ldots \quad . \qquad (A.5)$$

These values for J lead to a set of spectral lines known as P_1, Q_1, and R_1 branches. If Ω=1/2, then

$$J = K - 1/2 = 0.5, 1.5, 2.5, \ldots \quad . \qquad (A.6)$$

These values for J give rise to a set of spectral lines known as P_2, Q_2, and R_2 branches. Additional information on the physics of OH molecule is readily available in the literature, among them are Baker [1978], Hertzberg [1971], and Mies [1974].

Appendix B

RCA Limited Germanium Detector Specifications

Series TE-71
TM 71

GERMANIUM PHOTODIODE PREAMPLIFIER SYSTEMS
For Detection of Radiation at Wavelengths from 0.8 — 1.7 Micrometers

TE−71
−NEP (1.42, 10, 1) = 10 [illegible] WHz [illegible]

TM−71
− NEP (1.42, 500, 1) = 10 [illegible] WHz$^{-1/2}$
− Area 0.20 cm[illegible]
− Cooled to 77 K
− Responsivity 10 [illegible] − 10 [illegible] VW[illegible]

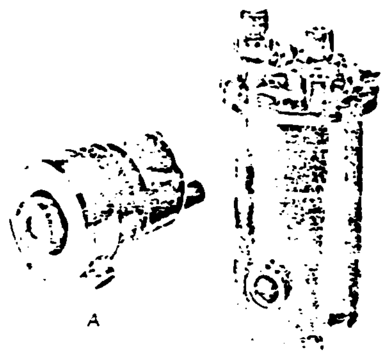

A

B

In order to achieve the good noise performance, it is necessary to cool both the detector and the preamplifier. Dewar A is for liquid nitrogen coolant; the hold time is about 10 hours, the weight is approximately 3 pounds and the overall size is roughly 9 cm diameter by 16 cm long. Dewar B is for liquid nitrogen, freon, CO_2, or any other convenient coolant; the hold time for liquid nitrogen is about 7 hours, weight is about 7 pounds, and the overall size is roughly 11 cm diameter by 21 cm long. Either Dewar allows thruput from the side or bottom if specified.

Special optics. *The standard window is quartz; different window material*, special filters, or condensing optics can be fitted provided no substantial mechanical redesign is necessary. The normal field of view for the detector is close to 90°.

If the customer desires to operate the TM-71 system at very high frequencies, it is possible to trade NEP for frequency response. Other special features may be added to these developmental systems. The necessary changes can be made for a small additional cost.

RCA Limited — Research Laboratories
Ste-Anne-de-Bellevue, Que.
Telephone (514) 453-9000

The responsivity varies according to the spectral curve. Some variation in this curve is possible according to the customer requirements.

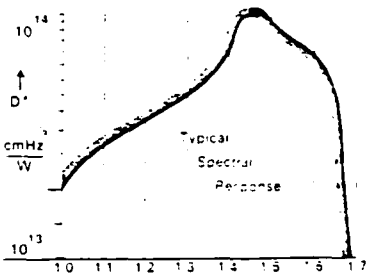

Figure B-1. Typical detector spectral response.

TABLE B-1. Germanium detector technical data.

	TE Series 71	TM Series 71
Operating Temperature	77 K	77 K
Noise equivalent power (guaranteed) WHz	NEP (1.42,10.1) = 1x10	NEP(1.42,500.1) = 1x10
Best noise equivalent power (achieved in the past) WHz	NEP (1.42,23.1) = 1x10	NEP(1.42,4000.1) = 3x10
Noise level (at output)	~1 V	~10 V
Impedance level (at output)	~500Ω	~50Ω
Responsivity v w	~ 5 x 10	~ 5 x 10
Linear range for power w	10 - 10	10 - 10
Useable limit (power) w	~ 6 x 10	~ 2 x 10
Frequency characteristic	f	flat, 3dB at 500 Hz
Detector area (circular) cm	0.2	0.2
Operating volts (typical) v	−10	− 10, + 10

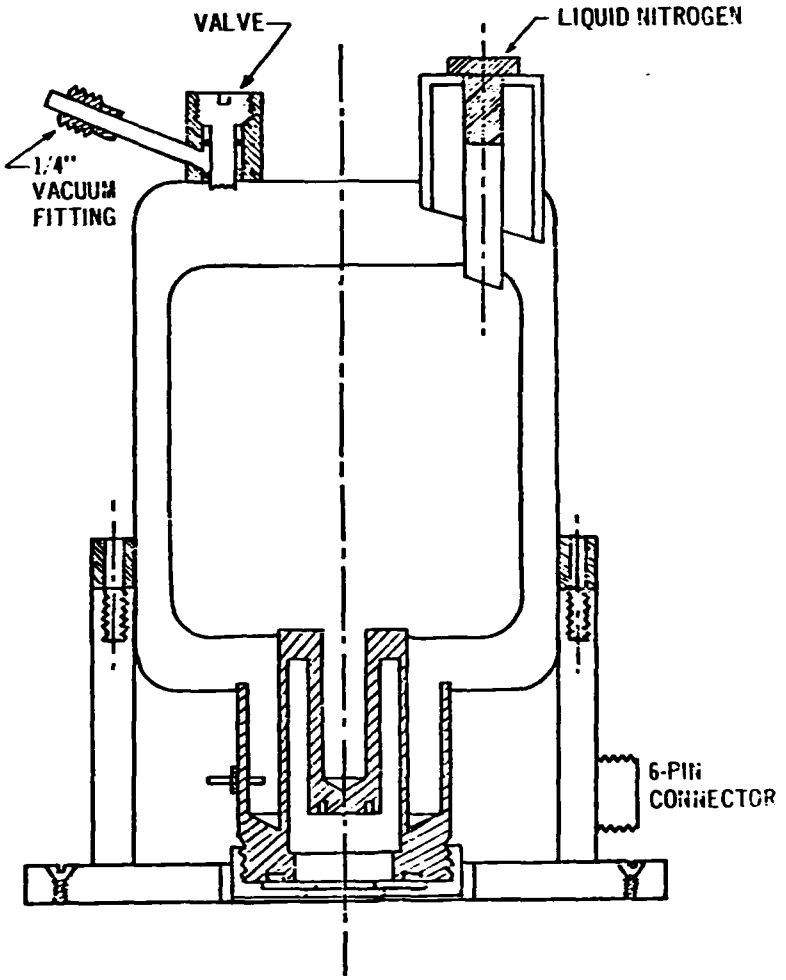

Figure B-2. RCA germanium detector liquid-nitrogen dewar outline.

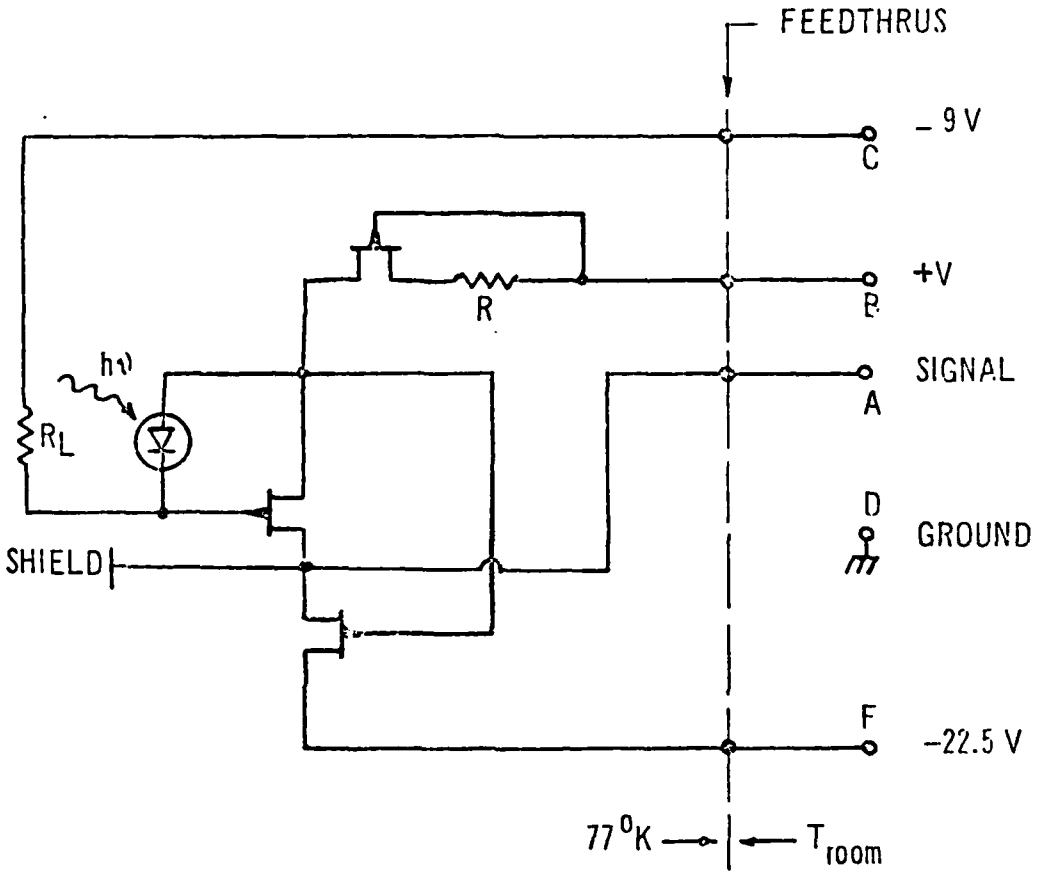

Figure B-3. Detector preamplifier circuit.

TABLE B-2. Detailed specifications on RCA detector.

WAVELENGTH (MICROMETER)	NEP (WATT)	MEASURED QUANTUM EFFICIENCY	CALCULATED QUANTUM EFFICIENCY	ABSORPTION COEFFICIENT	NEUTRAL DENSITY FILTER	DIODE SIGNAL (MVOLT)	THERMOPILE SIGNAL GAIN 1000X (MVOLT)	DRUM POSITION (MDEGS)	POWER ON DIODE (WATT)	RESPONSIVITY (VOLT/WATT)
1.0000	2.57E-14	2.87E-01	3.11E-01	12000.000	770.0	42.90	23.00	0.50	1.707E-09	2.490E 07
1.0500	2.37E-14	2.97E-01	3.47E-01	10000.000	735.0	54.00	25.70	2.00	1.998E-09	2.703E 07
1.1000	1.90E-14	3.54E-01	3.66E-01	9000.000	785.0	70.00	28.50	3.80	2.075E-09	3.374E 07
1.1500	1.50E-14	4.11E-01	3.81E-01	8300.000	795.0	89.90	30.50	5.50	2.192E-09	4.101E 07
1.2000	1.37E-14	4.51E-01	3.98E-01	7500.000	755.0	110.00	31.00	7.20	2.346E-09	4.688E 07
1.2500	1.19E-14	4.94E-01	4.15E-01	6700.000	765.0	125.00	31.00	9.00	2.316E-09	5.394E 07
1.3000	1.02E-14	5.55E-01	4.56E-01	5000.000	780.0	142.00	31.00	10.60	2.271E-09	6.253E 07
1.3500	1.04E-14	5.28E-01	4.92E-01	4000.000	750.0	130.00	27.60	12.30	2.103E-09	6.182E 07
1.4000	9.97E-15	5.29E-01	5.03E-01	3200.000	700.0	77.00	14.70	14.00	1.200E-09	6.417E 07
1.4500	8.47E-15	6.09E-01	5.54E-01	60.000	725.0	148.00	24.90	15.80	1.963E-09	7.541E 07
1.5000	1.10E-14	4.47E-01	4.82E-01	15.000	745.0	120.00	26.90	17.50	2.063E-09	5.818E 07
1.5500	1.65E-14	2.89E-01	4.03E-01	6.000	745.0	76.00	25.50	19.10	1.956E-09	3.886E 07
1.6000	2.79E-14	1.65E-01	2.66E-01	2.000	720.0	44.00	24.20	20.90	1.921E-09	2.291E 07
1.6500	5.47E-14	8.18E-02	9.18E-02	0.350	725.0	21.20	23.00	22.50	1.813E-09	1.169E 07
1.7000	1.66E-13	2.62E-02	1.92E-02	0.060	750.0	6.20	21.10	24.20	1.608E-09	3.857E 06

Appendix C

Interferometer Data Catalog

The interferometer data for observations taken on June 13-15, 1983 are contained within this appendix in their entirety. All data presented were recorded at Sacramento Peak, New Mexico. The figures are all organized chronologically beginning on day 165 at 3:30 hrs. UT and proceeding through day 166, 10:15 hrs. UT.

Both of the observation days' records begin with the interferometer viewing in the zenith. At moonset on day 166 the interferometer and camera systems were lowered to view near the horizon. The low elevation viewing period during day 166 is divided into three time frames, corresponding to when the interferometer was adjusted in viewing location. The time period and viewing position are identified in each figure caption.

Within each time segment of the data presentation, the figures are organized according to the OH Meinel band from which the data were calculated. First is the OH (4,2) band, second the OH (3,1), third the OH (8,5) band, and fourth the OH (7,4) band. Each of the band groups shows curves for first the intensity, second the rotational temperature, and third the smoothed rotational temperature calculation with the associated standard deviation for each.

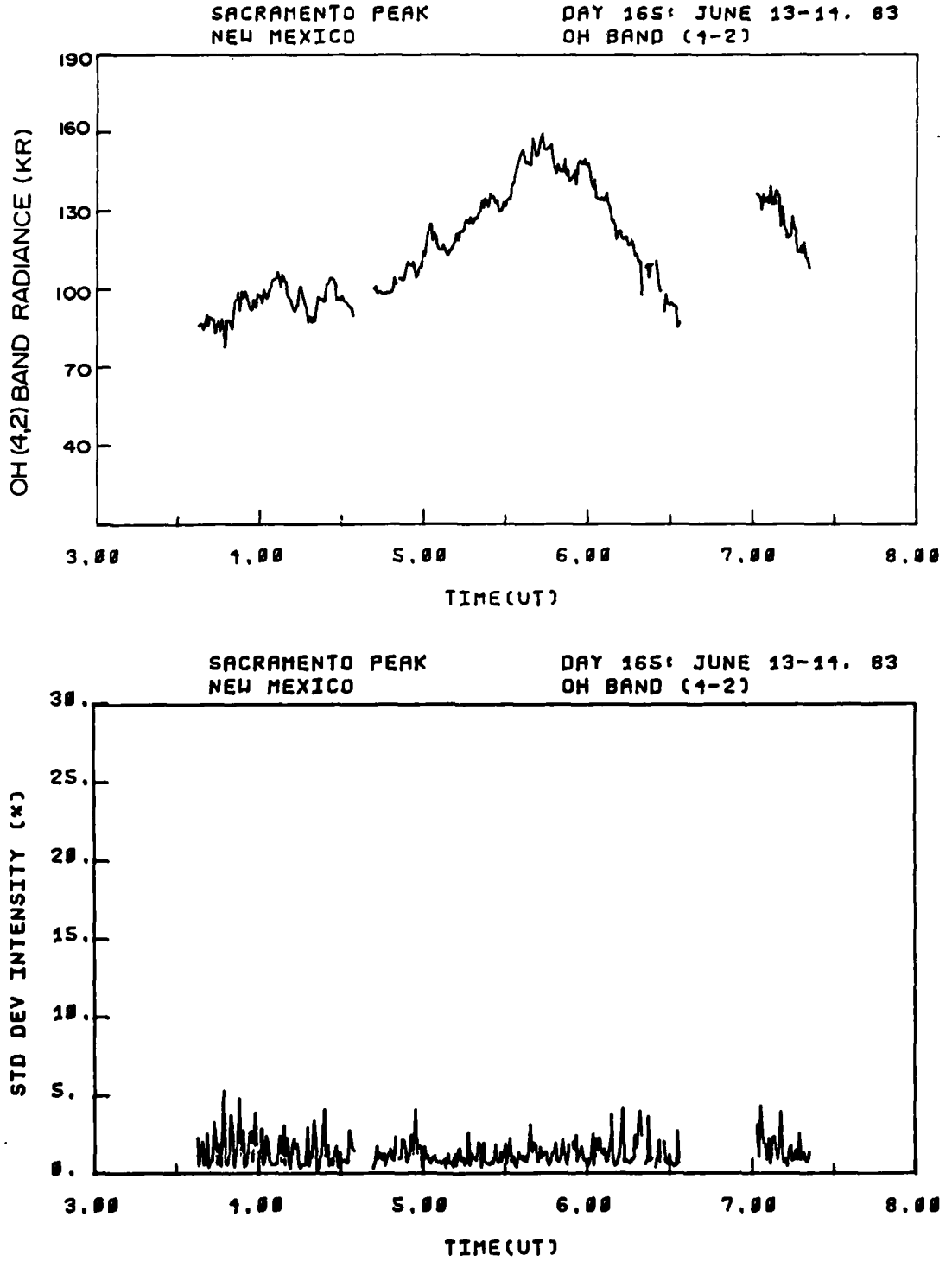

Figure C-1. OH (4,2) band radiance and standard deviation, viewing angle = zenith, day 165, 3:30-7:30 hrs. UT.

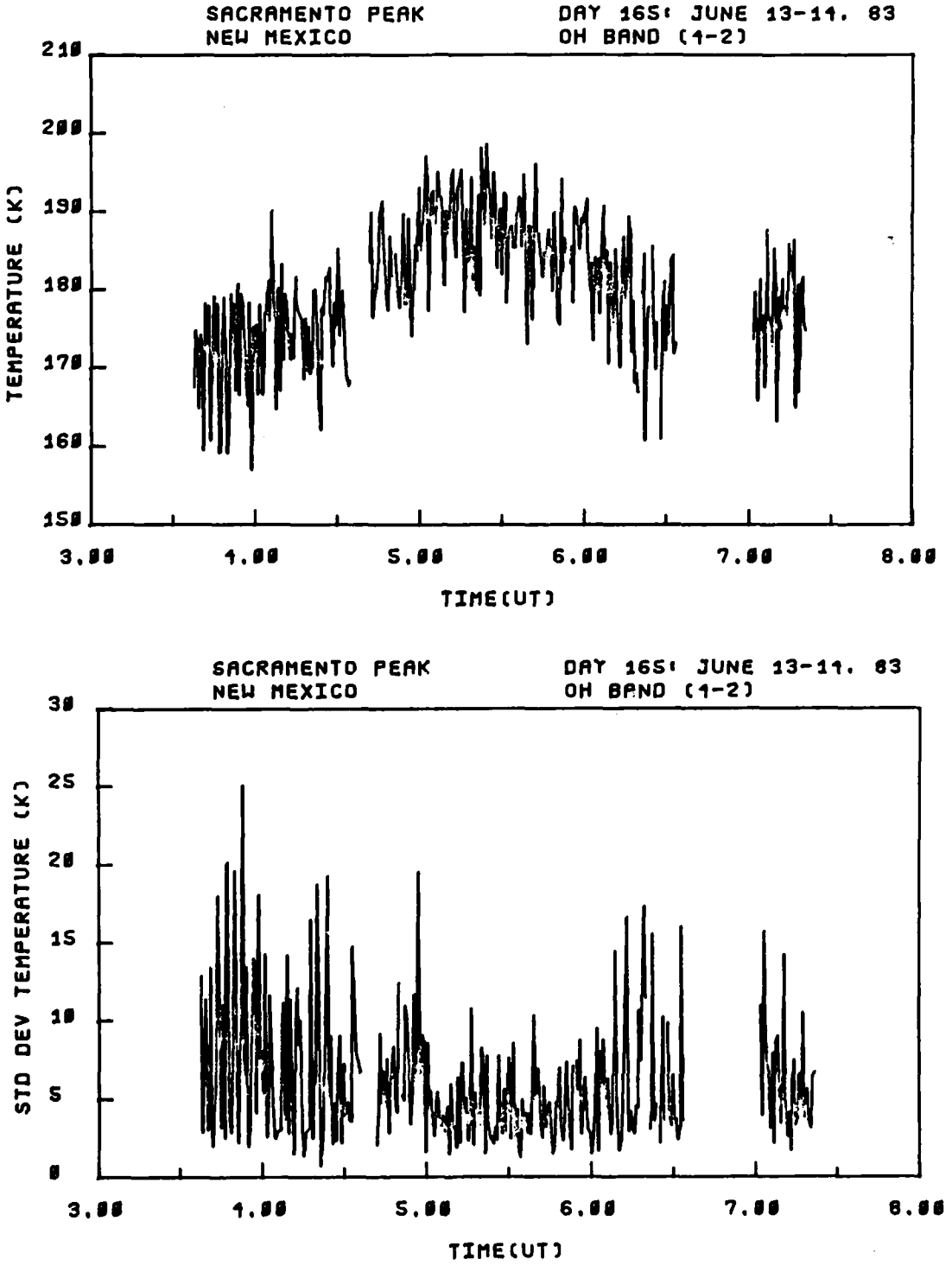

Figure C-2. OH (4,2) band rotational temperature and standard deviation, viewing angle = zenith, day 165, 3:30-7:30 hrs. UT.

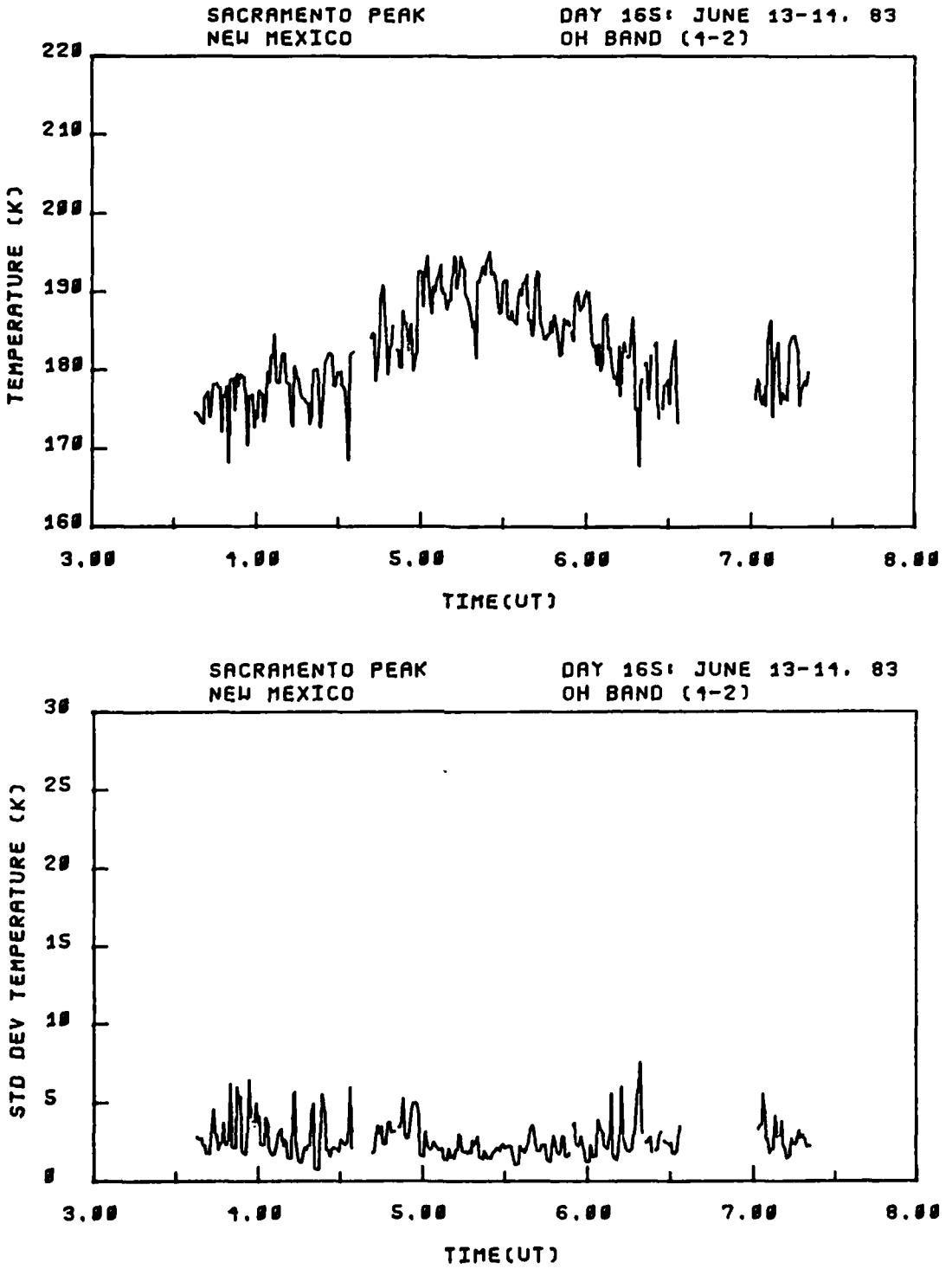

Figure C-3. OH (4,2) band smoothed rotational temperature and standard deviation, viewing angle = zenith, day 165, 3:30-7:30 hrs. UT.

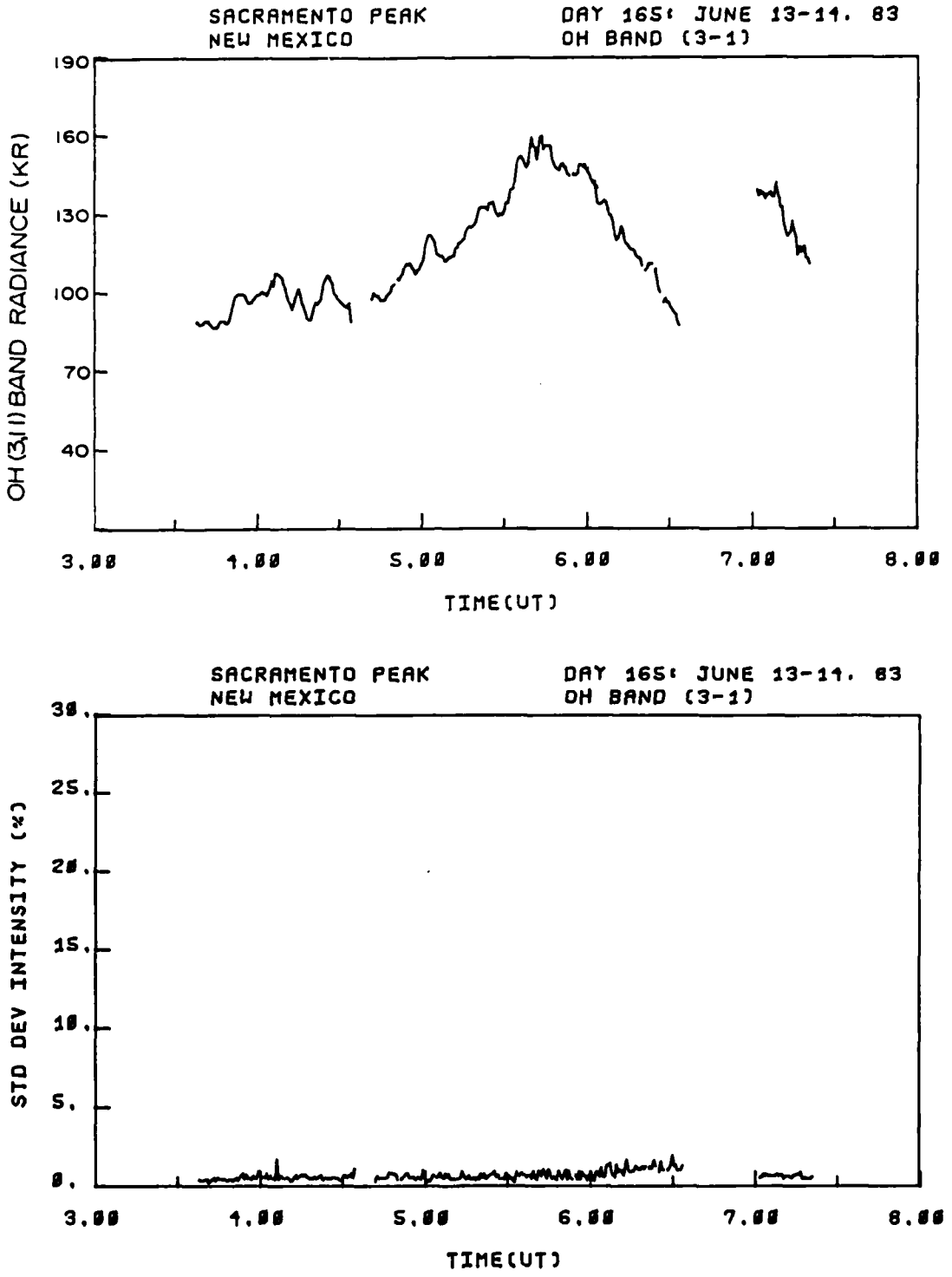

Figure C-4. OH (3,1) band radiance and standard deviation, viewing angle = zenith, day 165, 3:30-7:30 hrs. UT.

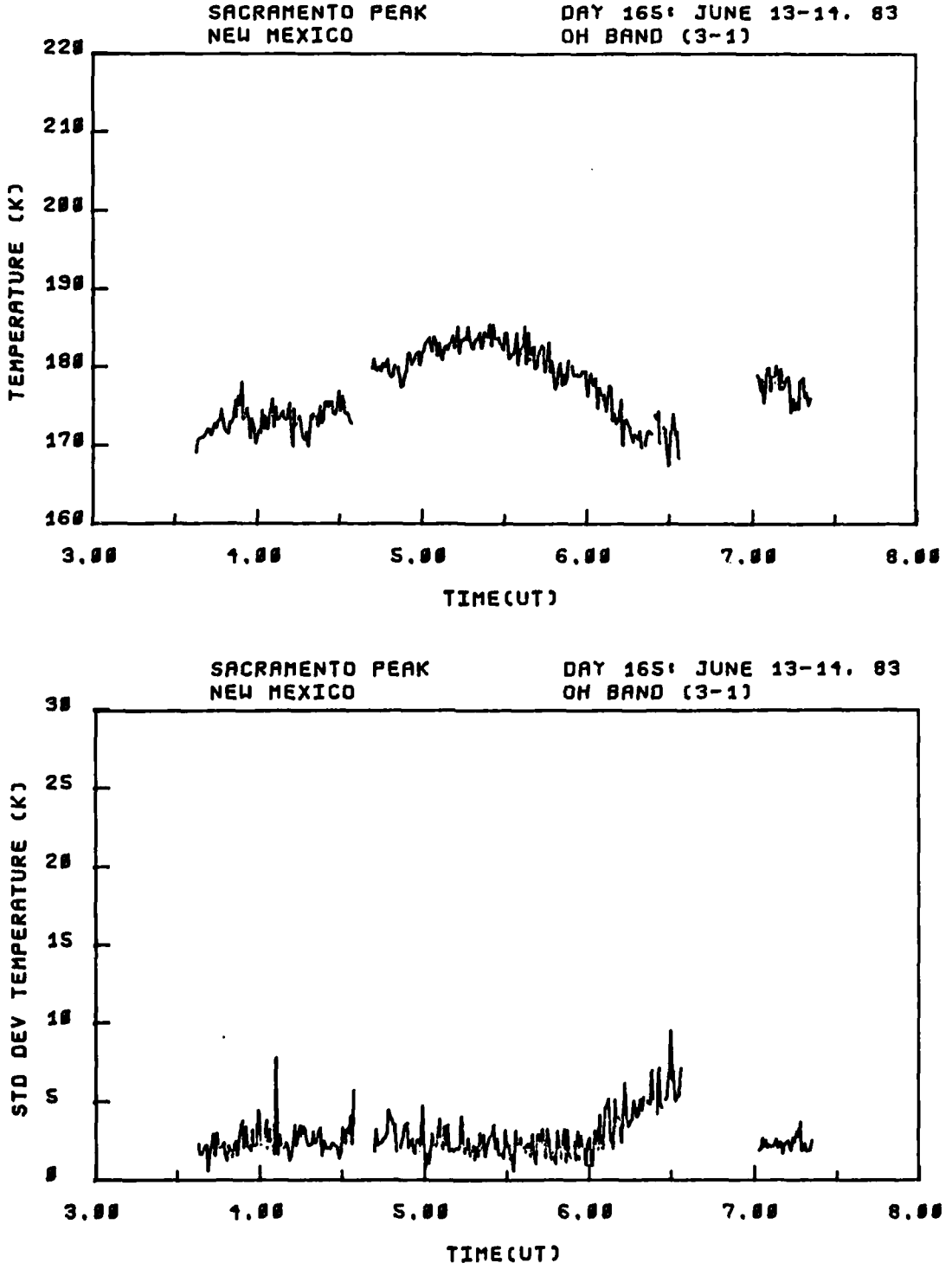

Figure C-5. OH (3,1) band rotational temperature and standard deviation, viewing angle = zenith, day 165, 3:30-7:30 hrs. UT.

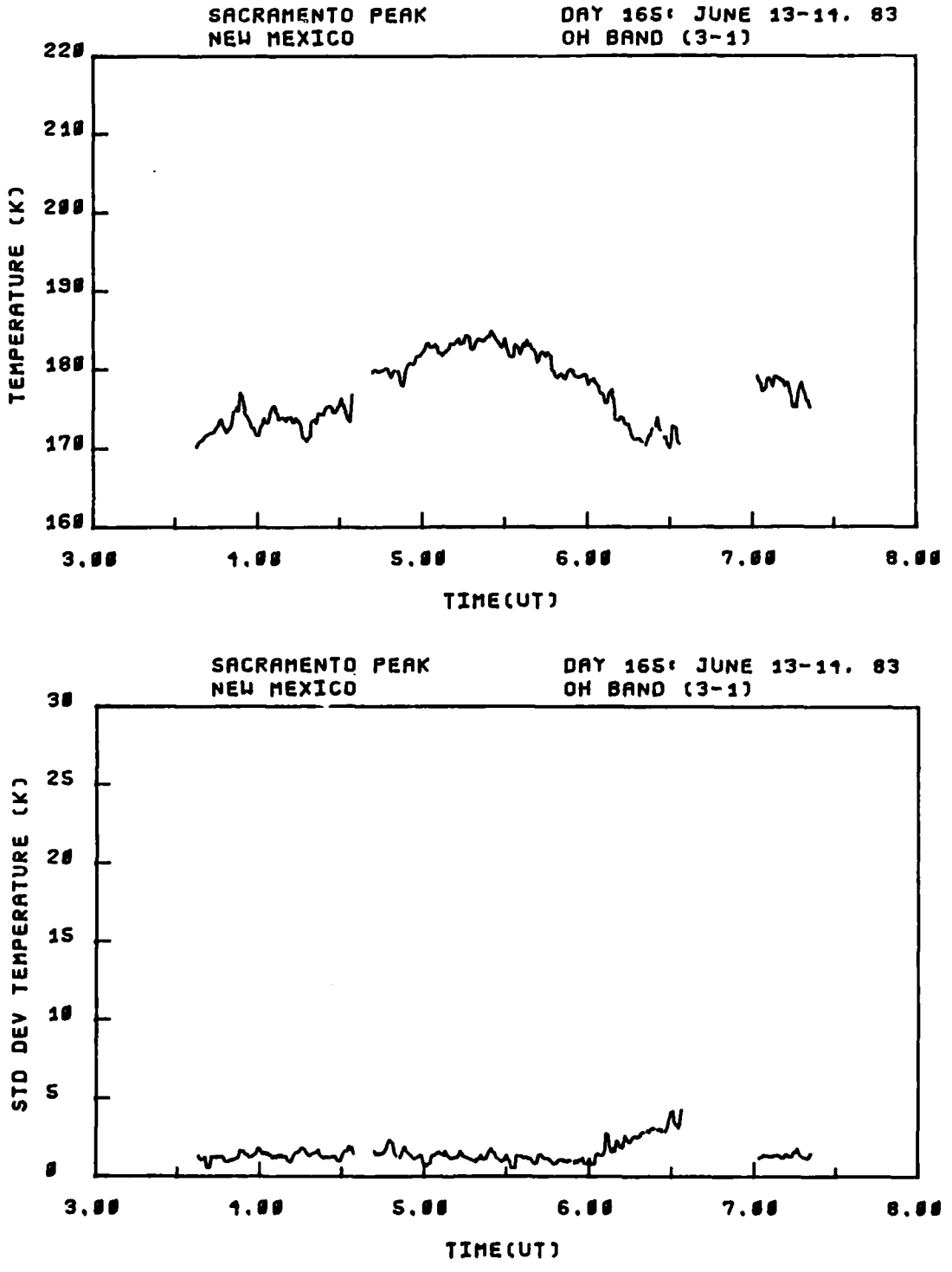

Figure C-6. OH (3,1) band smoothed rotational temperature and standard deviation, viewing angle = zenith, day 165, 3:30-7:30 hrs. UT.

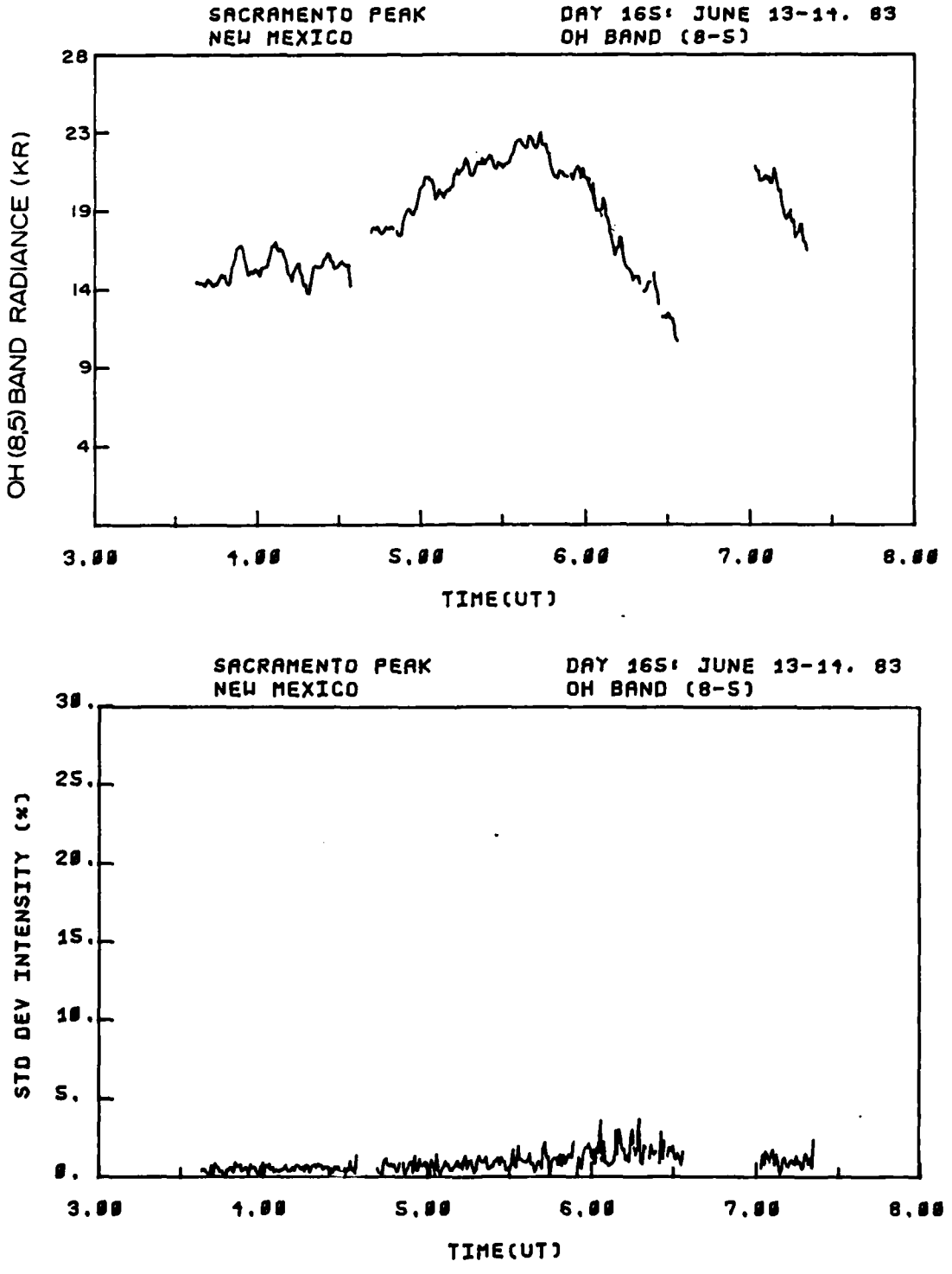

Figure C-7. OH (8,5) band radiance and standard deviation, viewing angle = zenith, day 165, 3:30-7:30 hrs. UT.

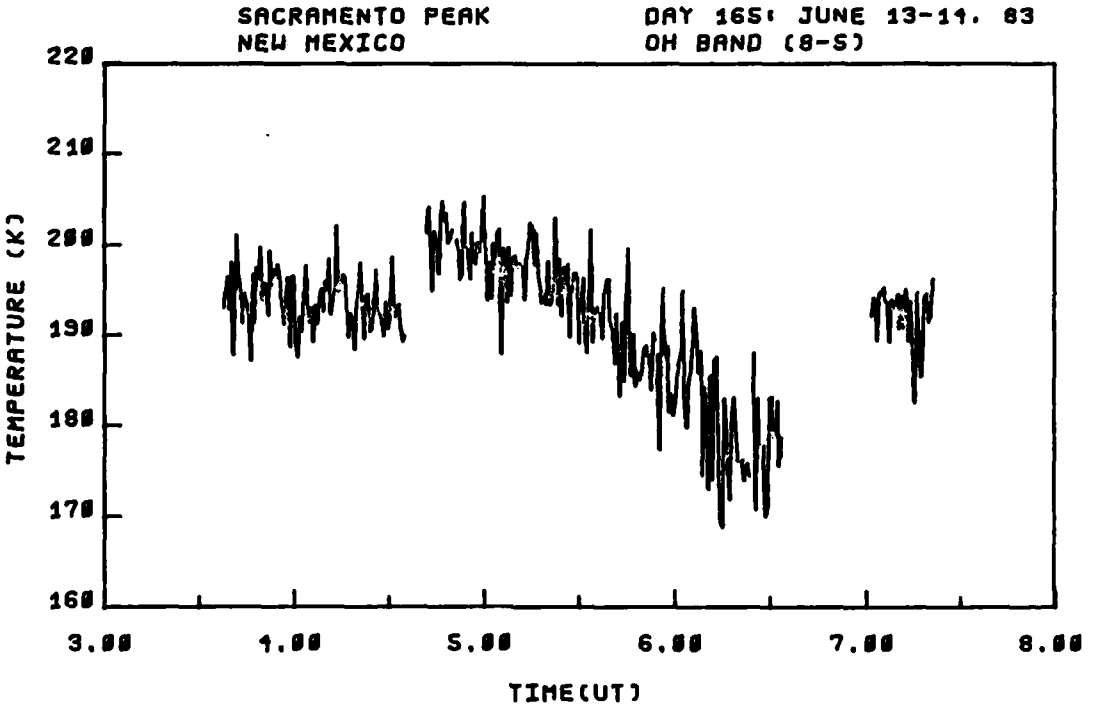

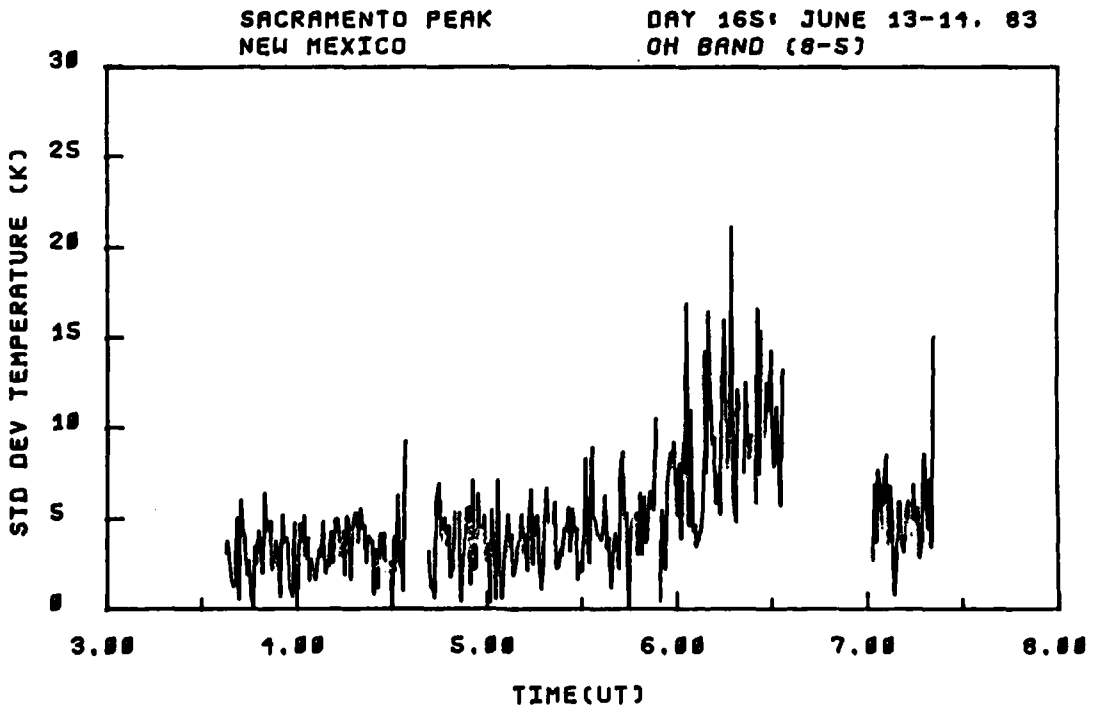

Figure C-8. OH (8,5) band rotational temperature and standard deviation, viewing angle = zenith, day 165, 3:30-7:30 hrs. UT.

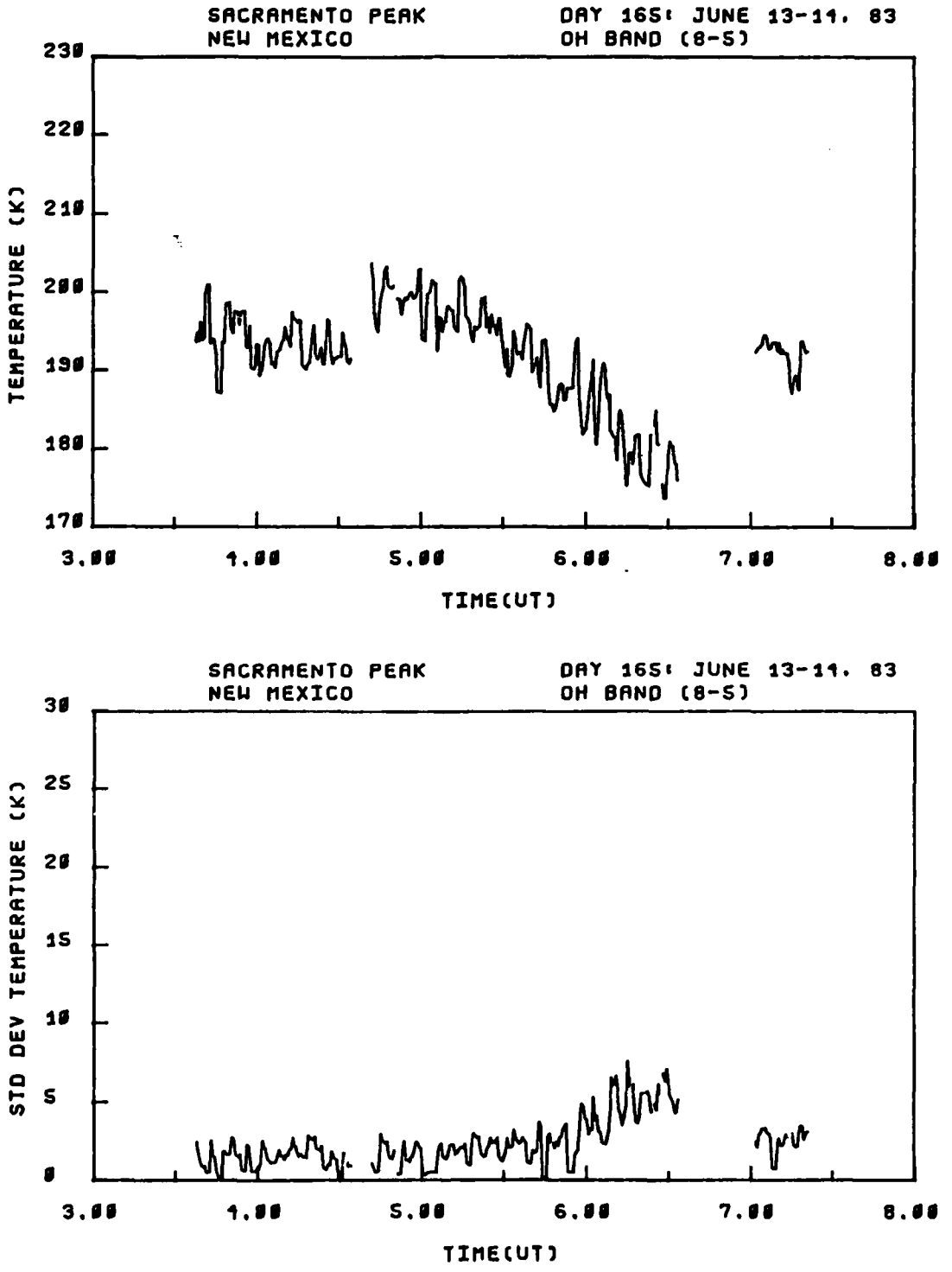

Figure C-9. OH (8,5) band smoothed rotational temperature and standard deviation, viewing angle = zenith, day 165, 3:30-7:30 hrs. UT.

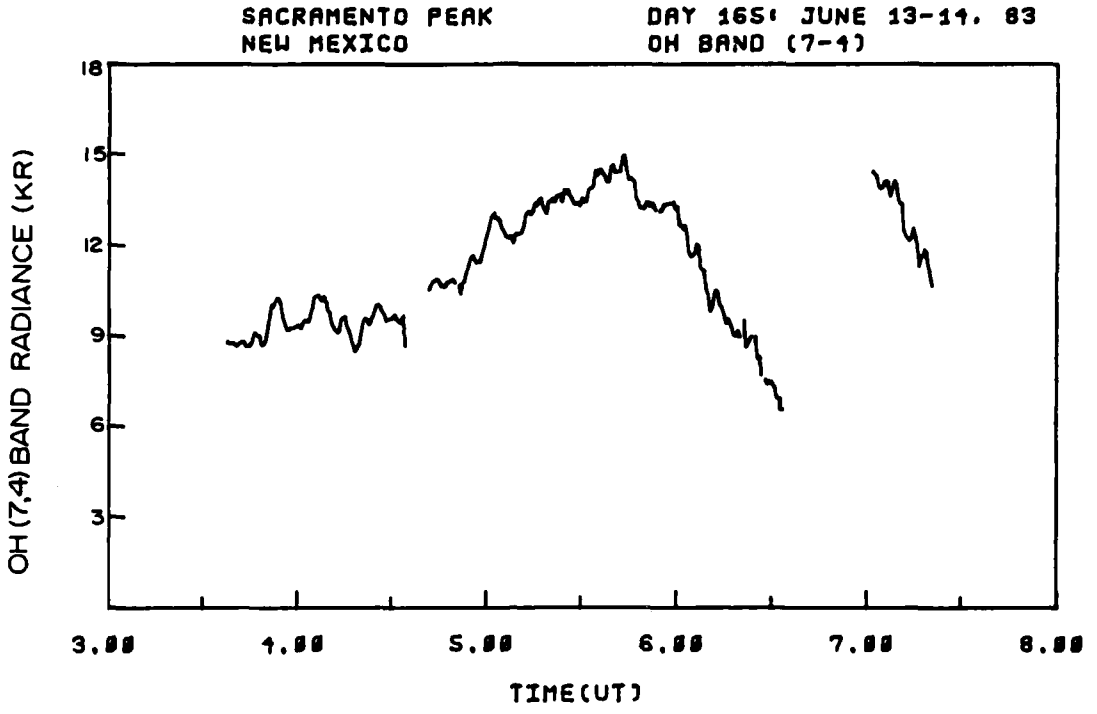

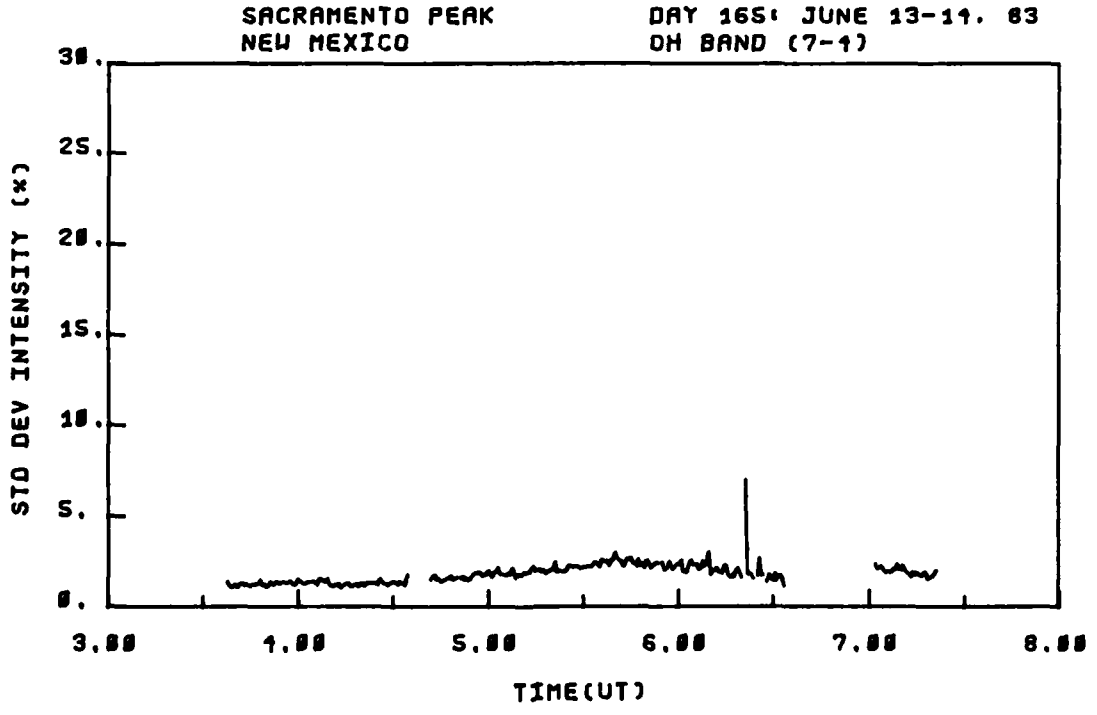

Figure C-10. OH (7,4) band radiance and standard deviation, viewing angle = zenith, day 165, 3:30-7:30 hrs. UT.

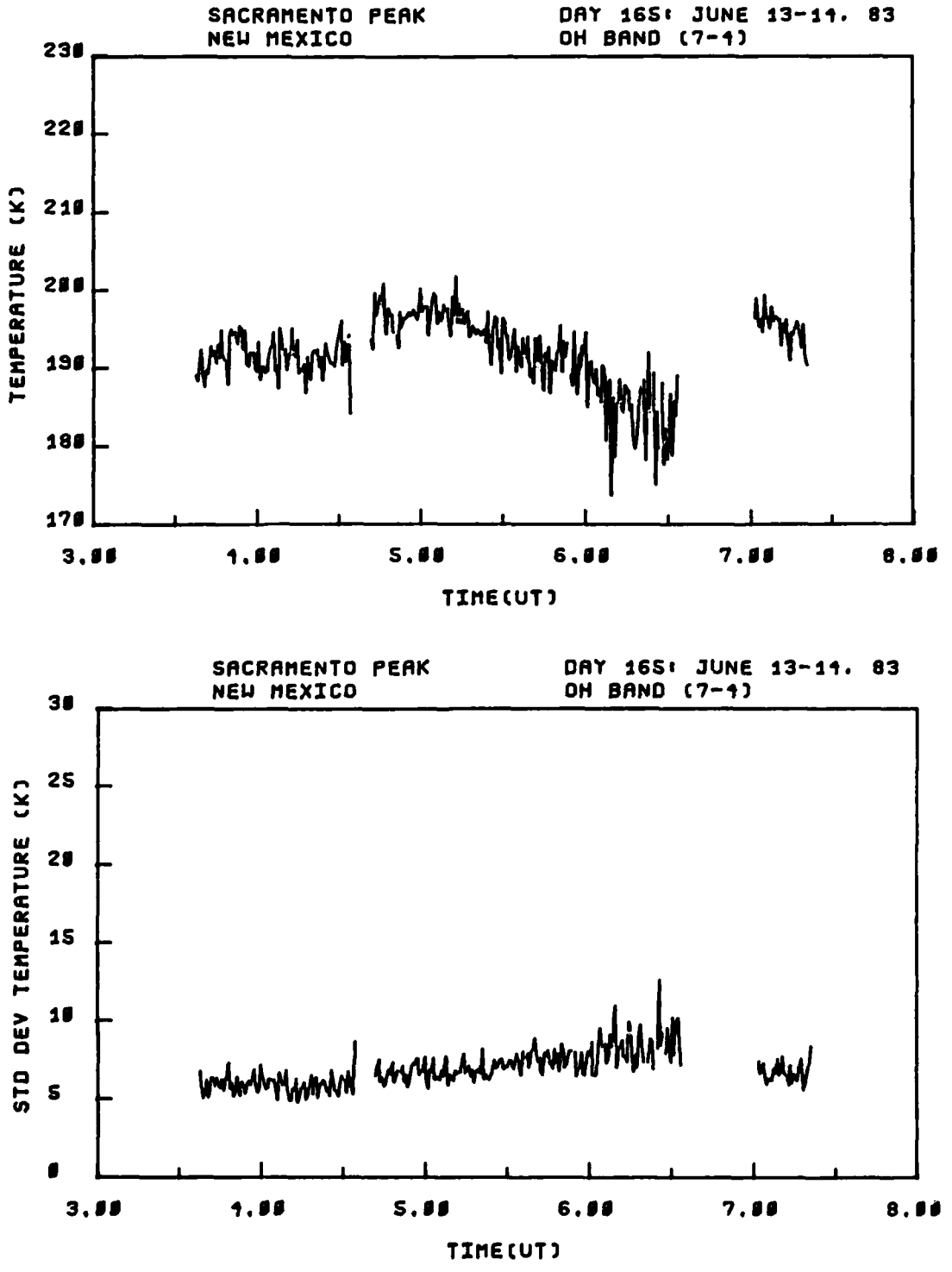

Figure C-11. OH (7,4) band rotational temperature and standard deviation, viewing angle = zenith, day 165, 3:30-7:30 hrs. UT.

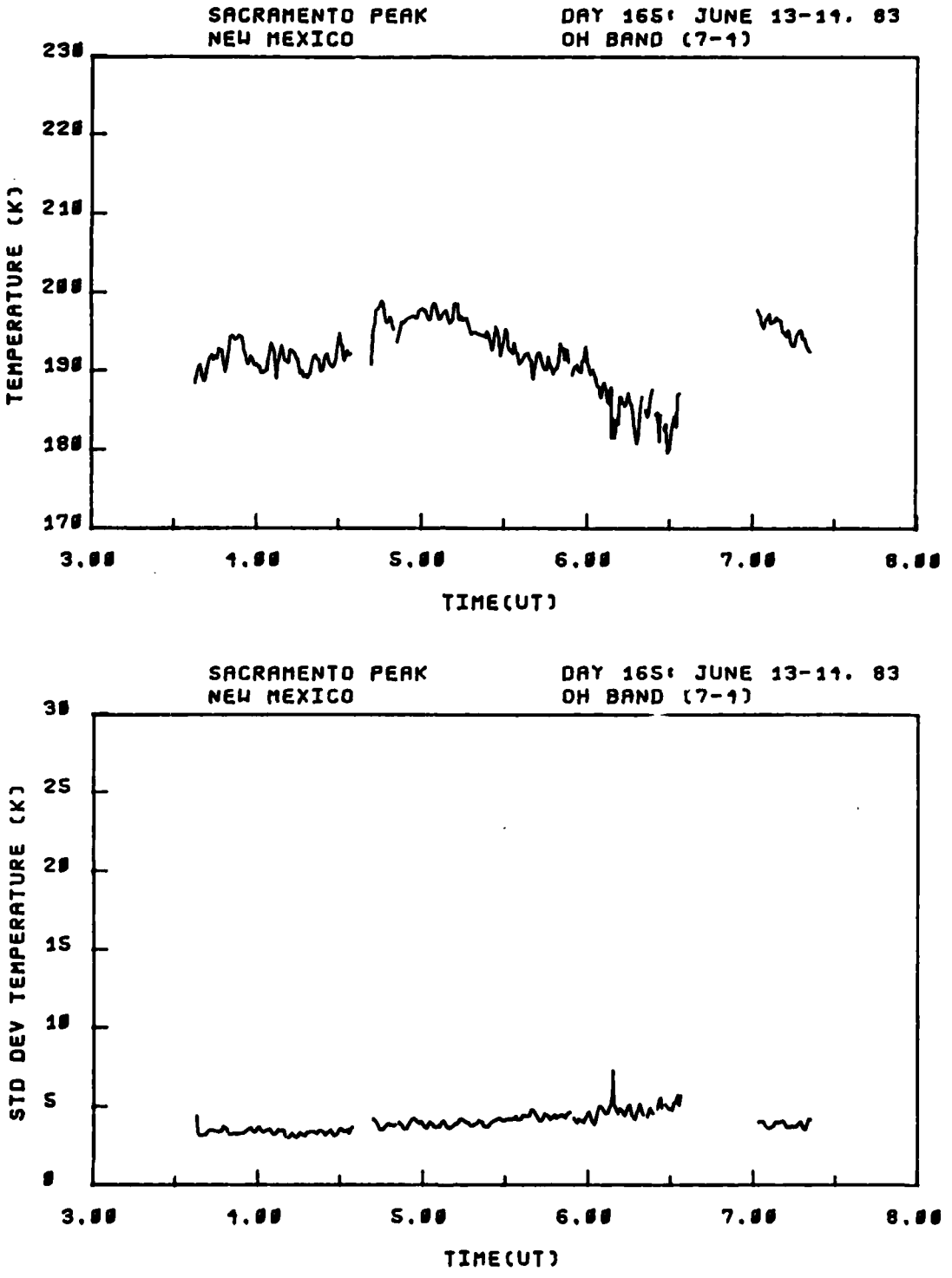

Figure C-12. OH (7,4) band smoothed rotational temperature and standard deviation, viewing angle = zenith, day 165, 3:30-7:30 hrs. UT.

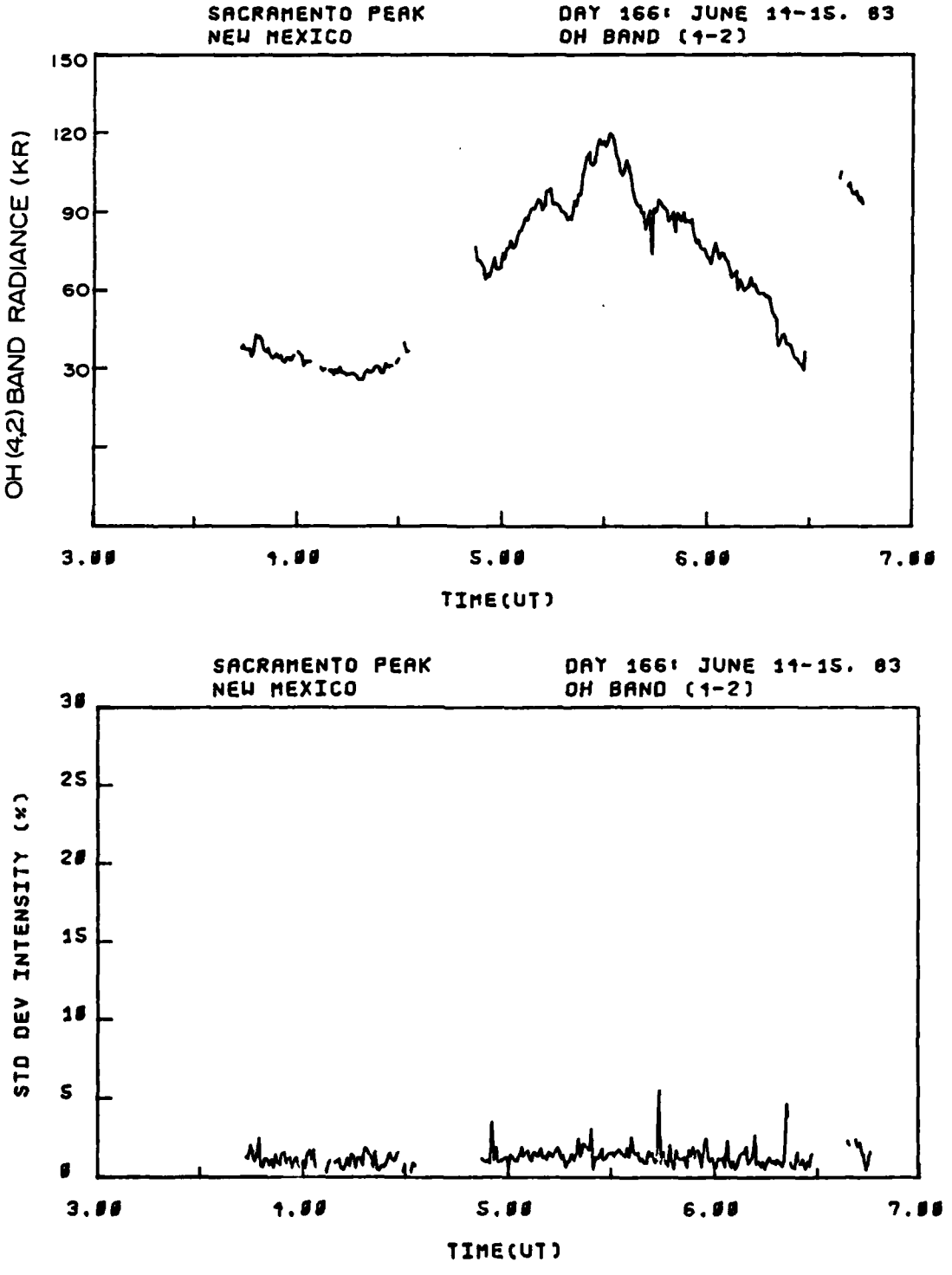

Figure C-13. OH (4,2) band radiance and standard deviation, viewing angle = zenith, day 166, 3:30-6:45 hrs. UT.

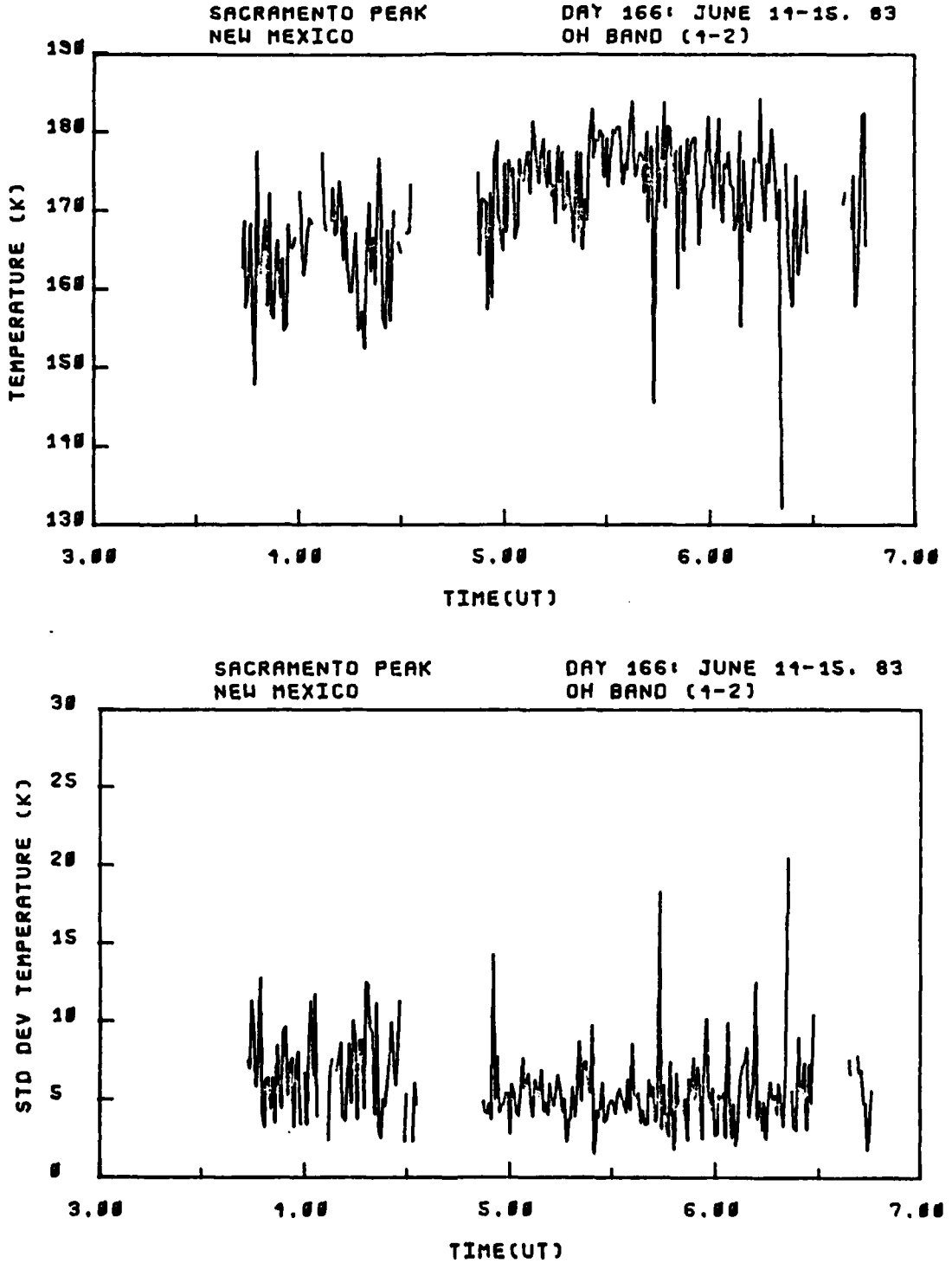

Figure C-14. OH (4,2) band rotational temperature and standard deviation, viewing angle = zenith, day 166, 3:30-6:45 hrs. UT.

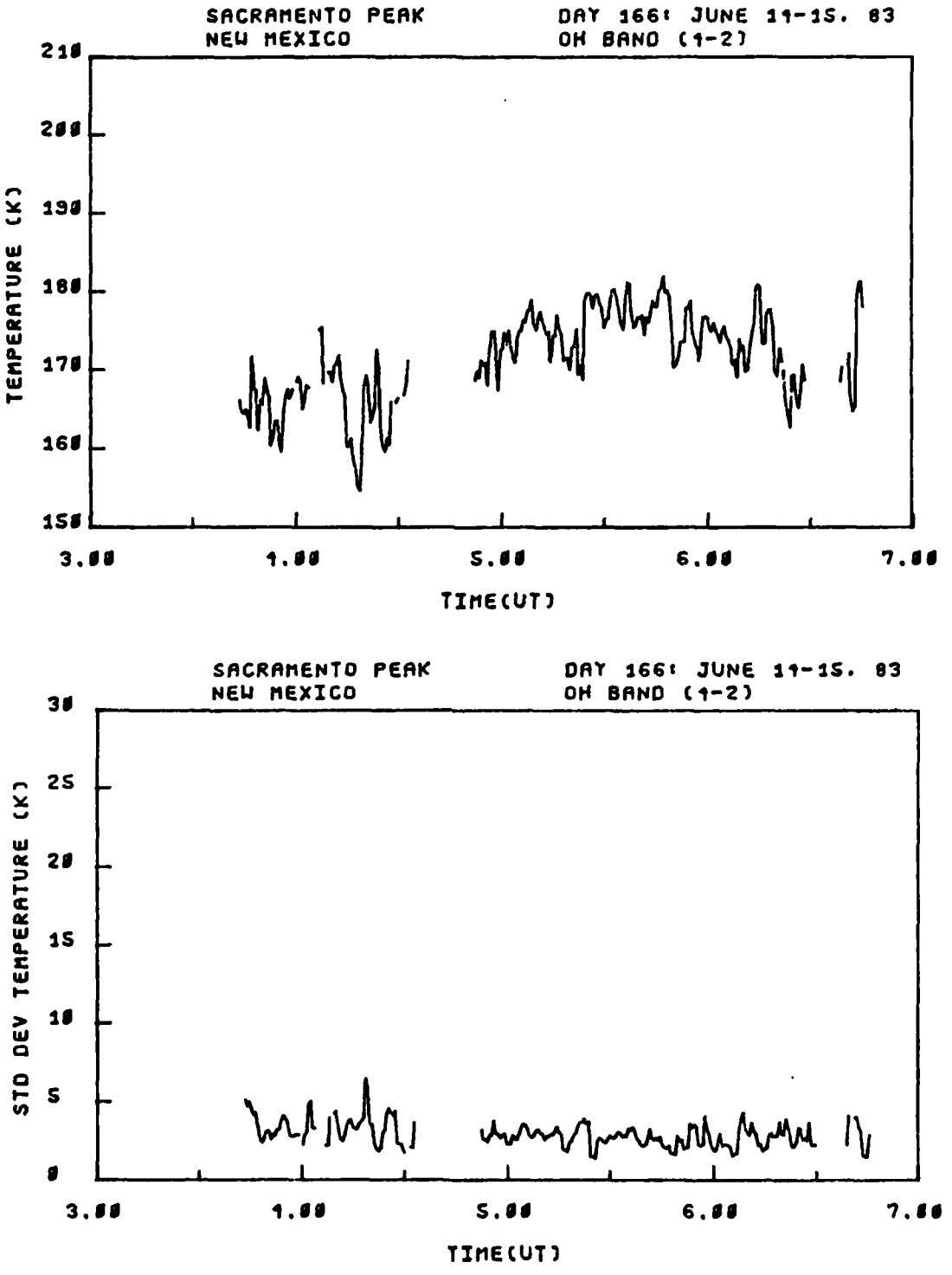

Figure C-15. OH (4,2) band smoothed rotational temperature and standard deviation, viewing angle = zenith, day 166, 3:30-6:45 hrs. UT.

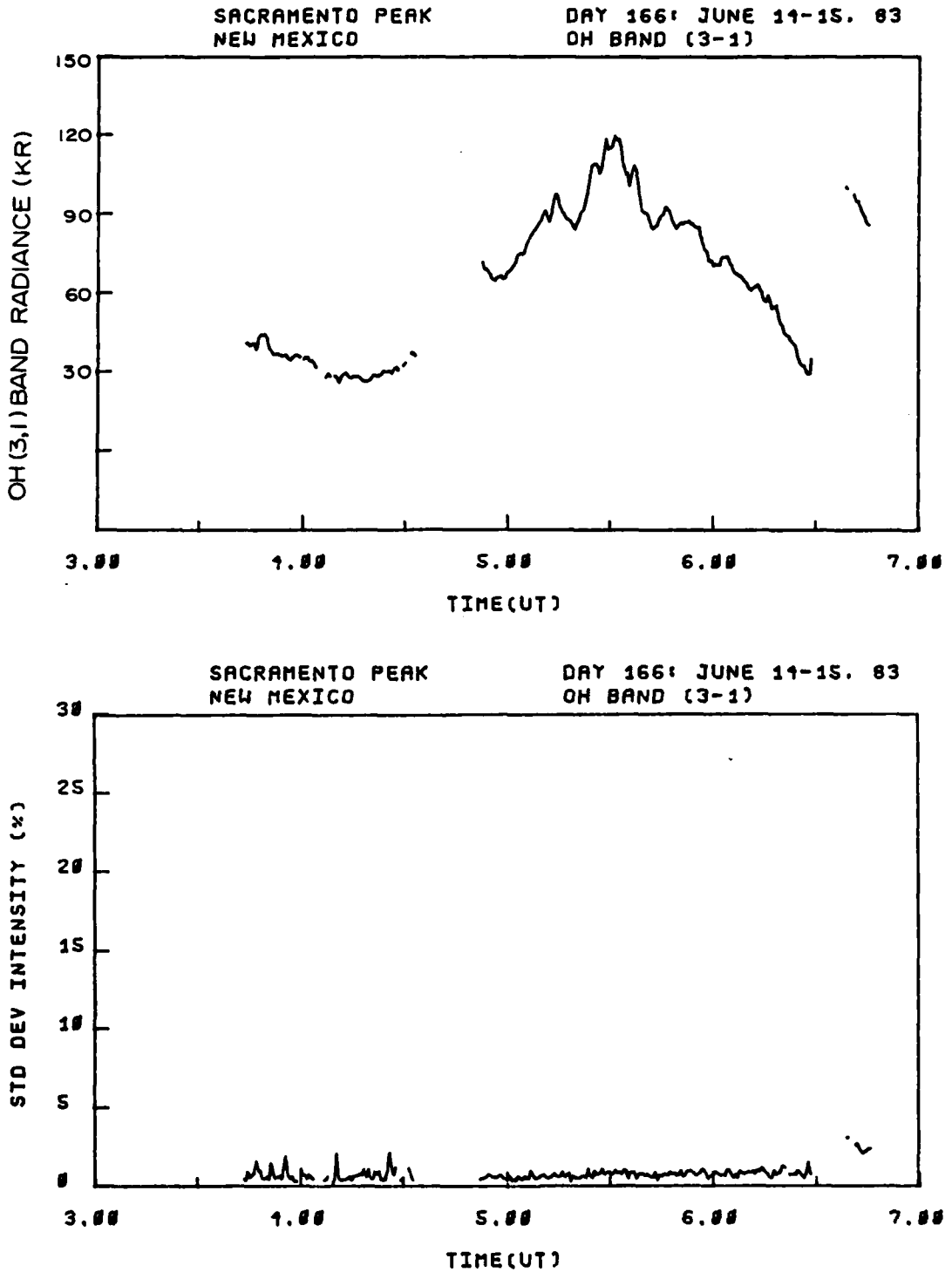

Figure C-16. OH (3,1) band radiance and standard deviation, viewing angle = zenith, day 166, 3:30-6:45 hrs. UT.

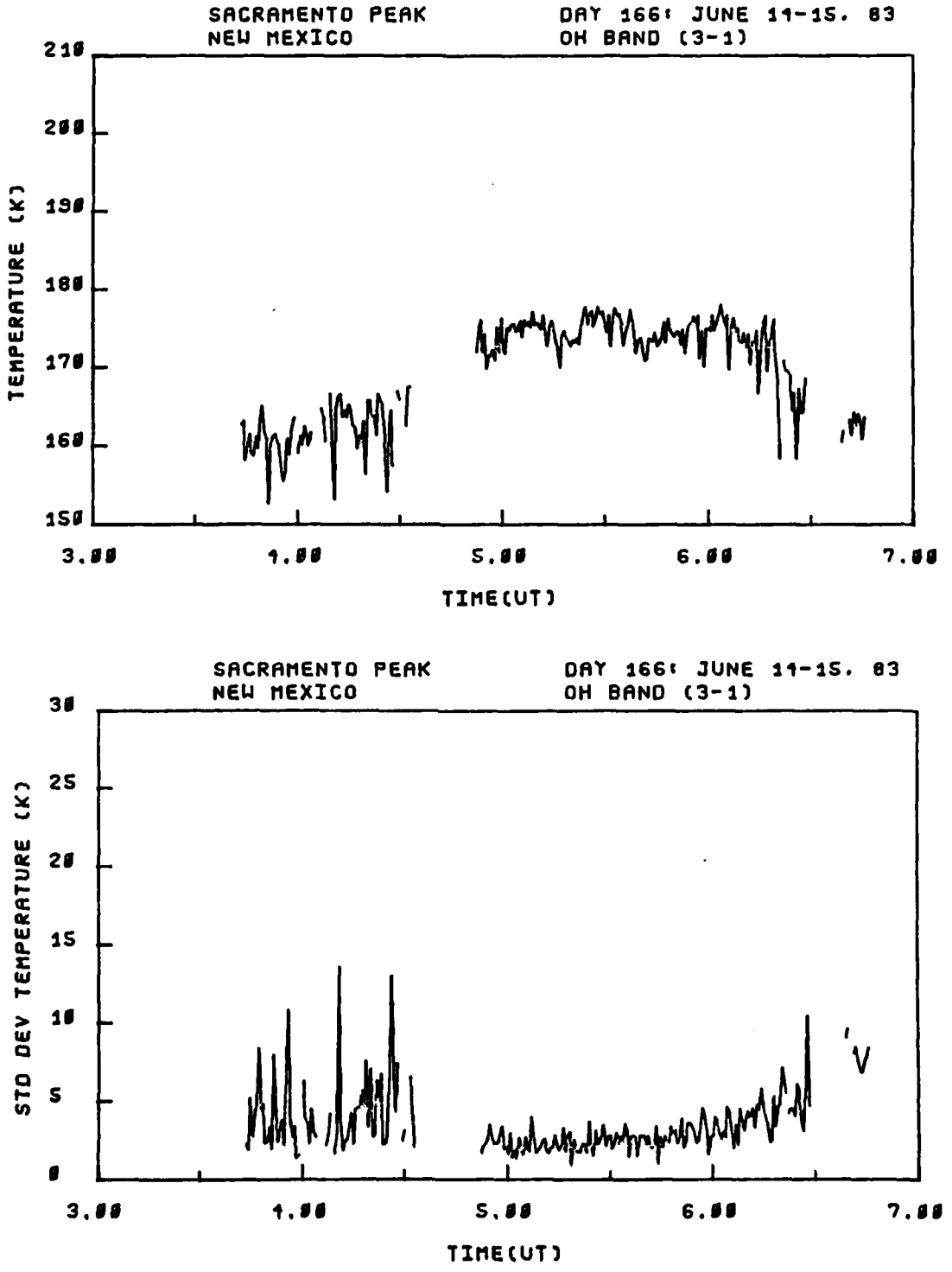

Figure C-17. OH (3,1) band rotational temperature and standard deviation, viewing angle = zenith, day 166, 3:30-6:45 hrs. UT.

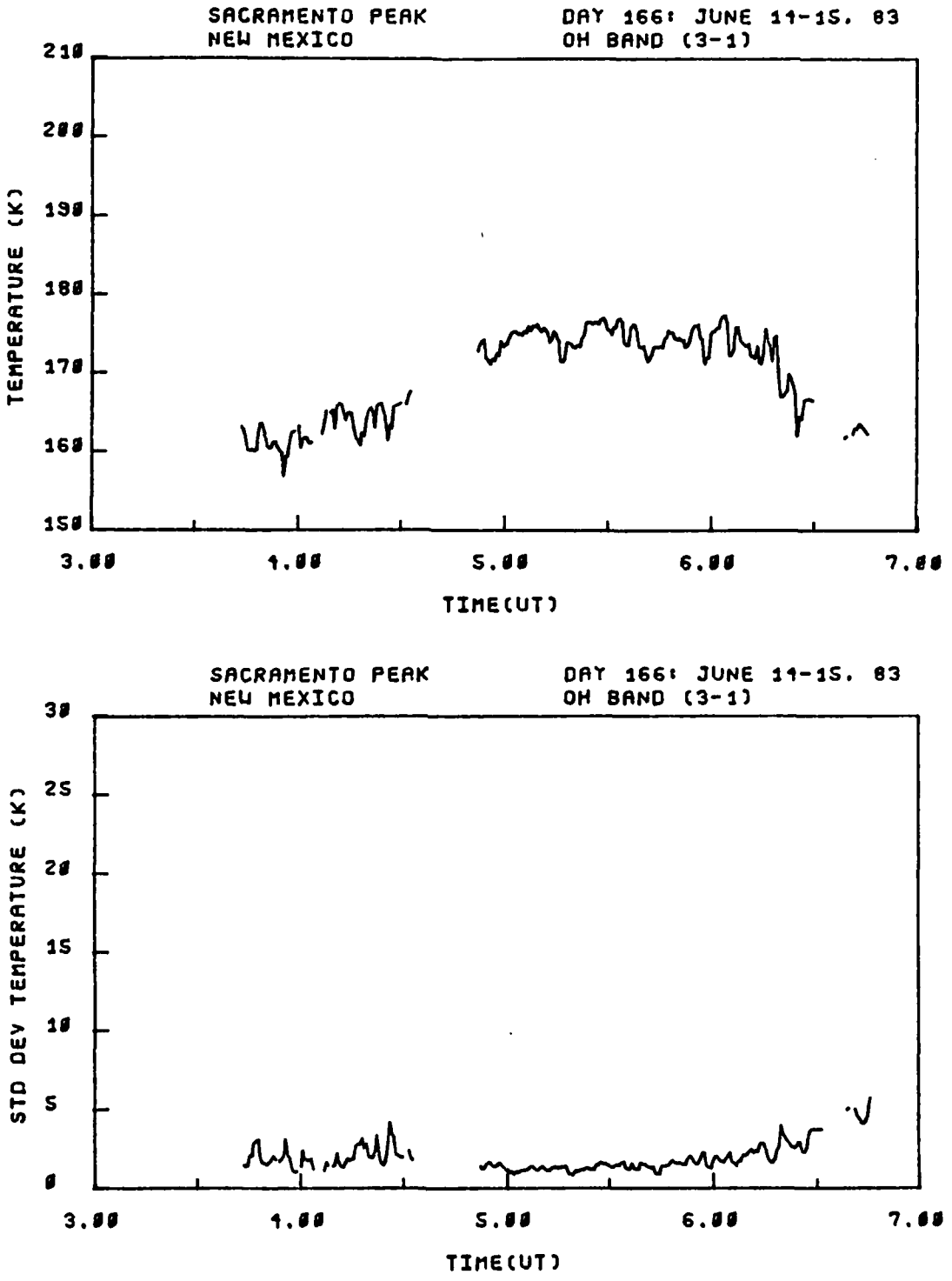

Figure C-18. OH (3,1) band smoothed rotational temperature and standard deviation, viewing angle = zenith, day 166, 3:30-6:45 hrs. UT.

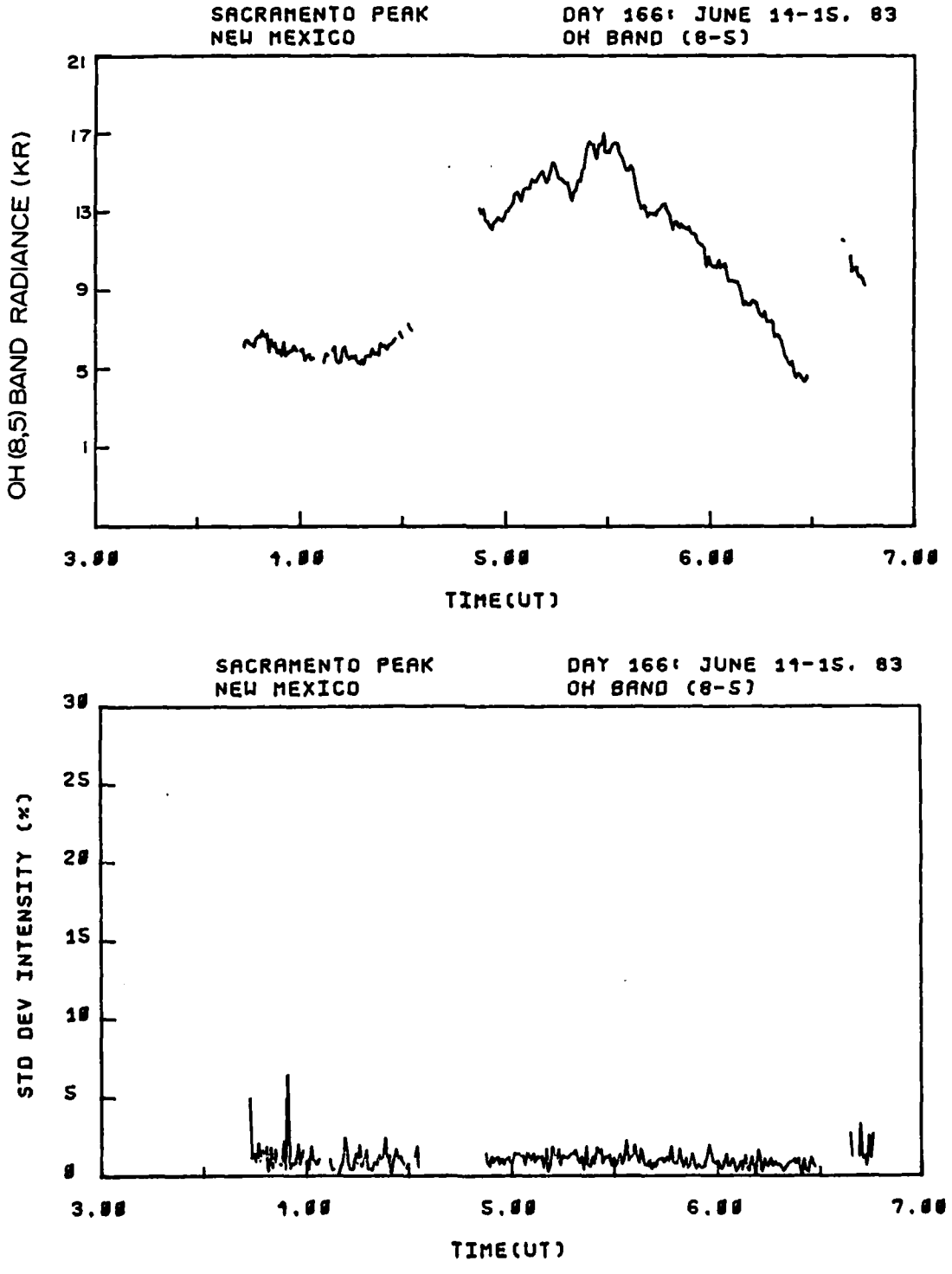

Figure C-19. OH (8,5) band radiance and standard deviation, viewing angle = zenith, day 166, 3:30-6:45 hrs. UT.

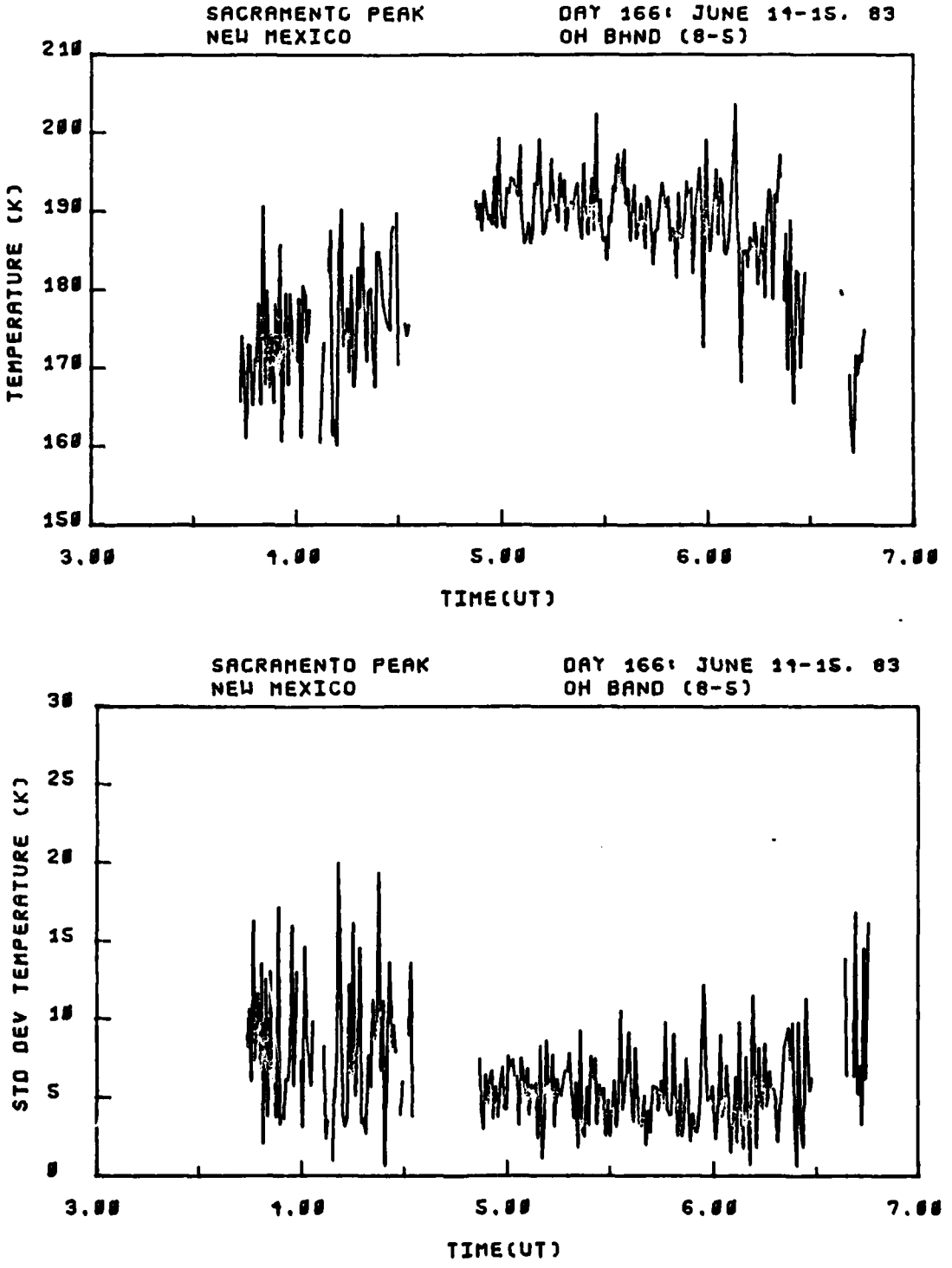

Figure C-20. OH (8,5) band rotational temperature and standard deviation, viewing angle = zenith, day 166, 3:30-6:45 hrs. UT.

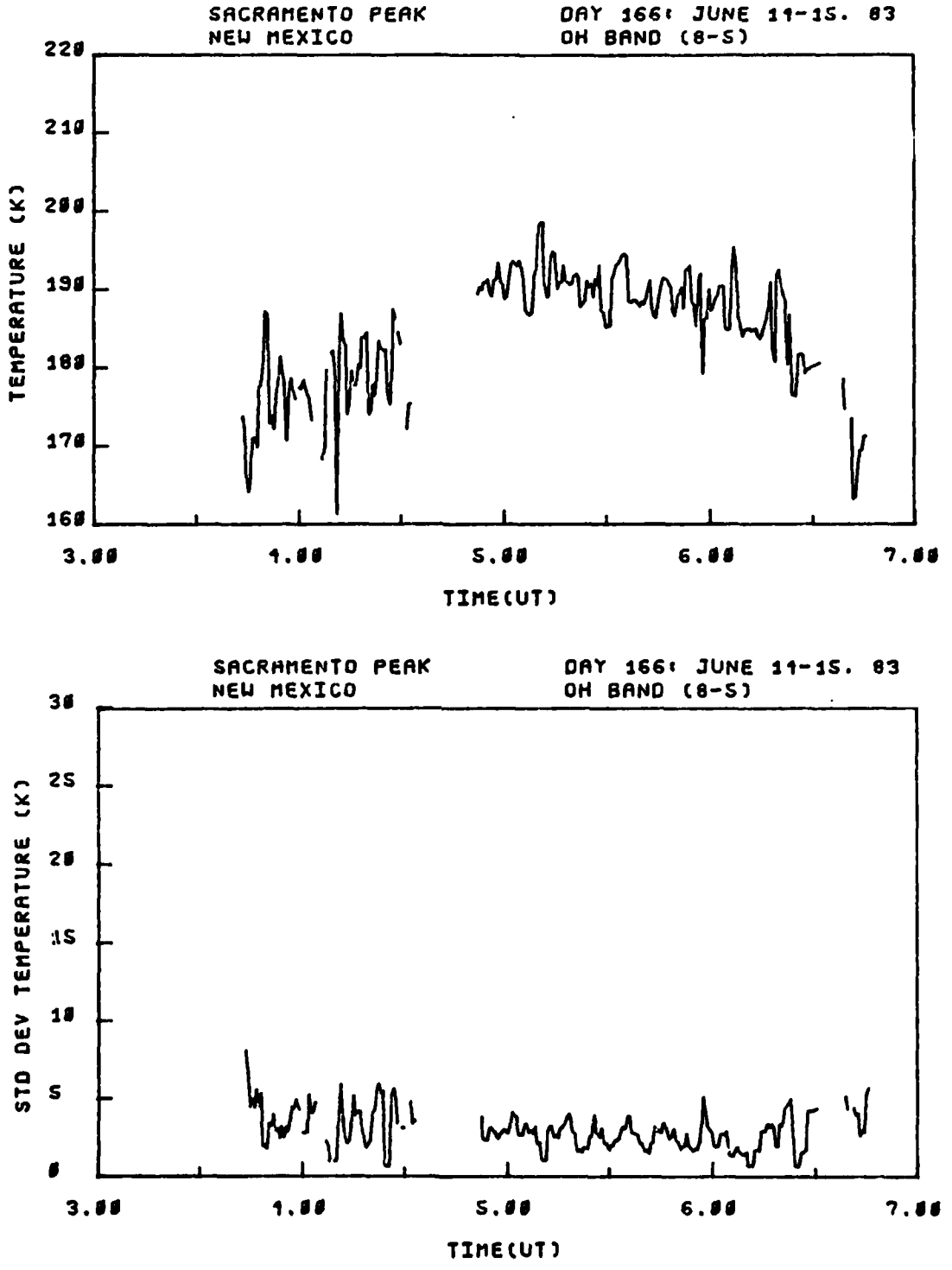

Figure C-21. OH (8,5) band smoothed rotational temperature and standard deviation, viewing angle = zenith, day 166, 3:30-6:45 hrs. UT.

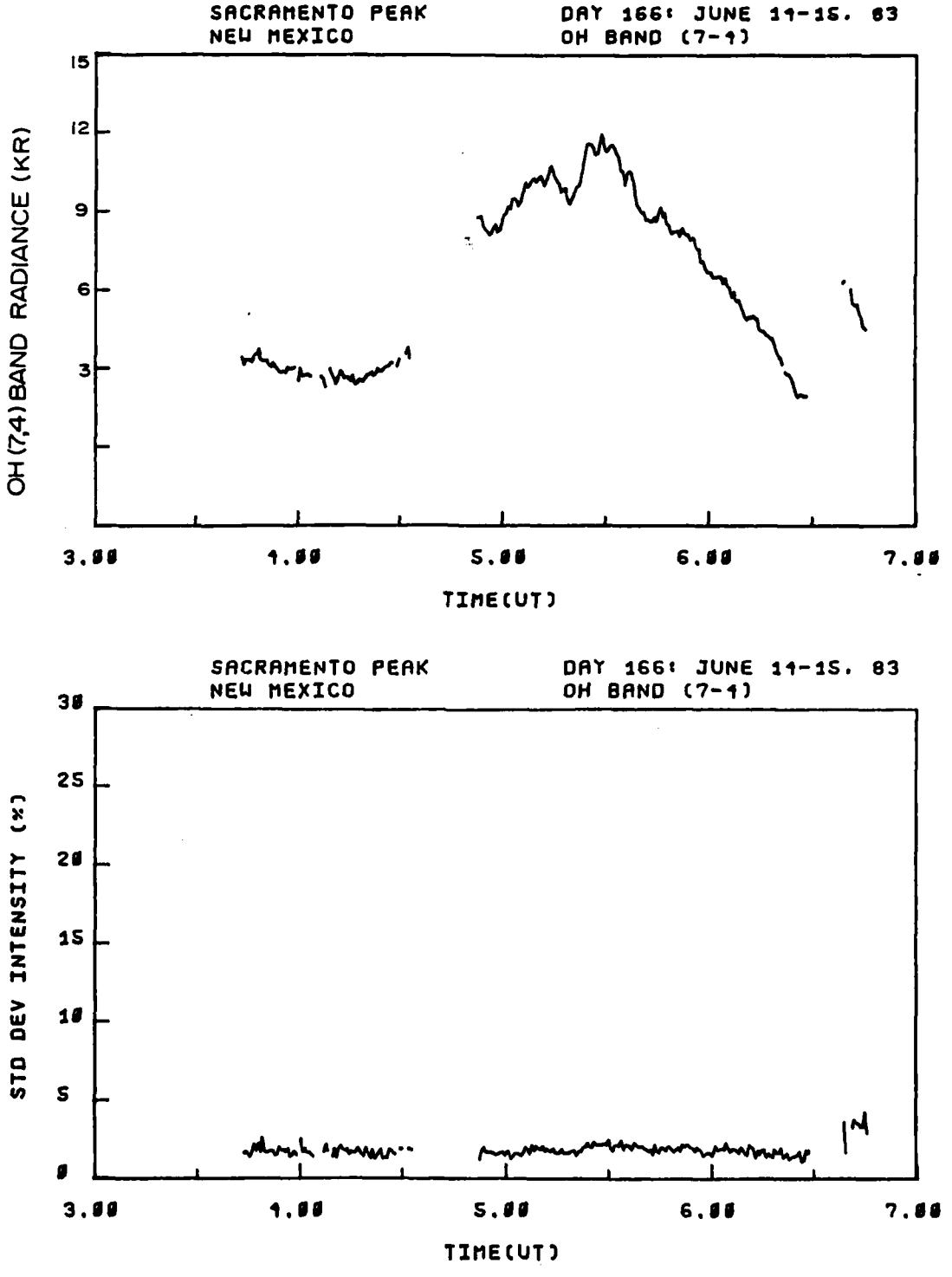

Figure C-22. OH (7,4) band radiance and standard deviation, viewing angle = zenith, day 166, 3:30-6:45 hrs. UT.

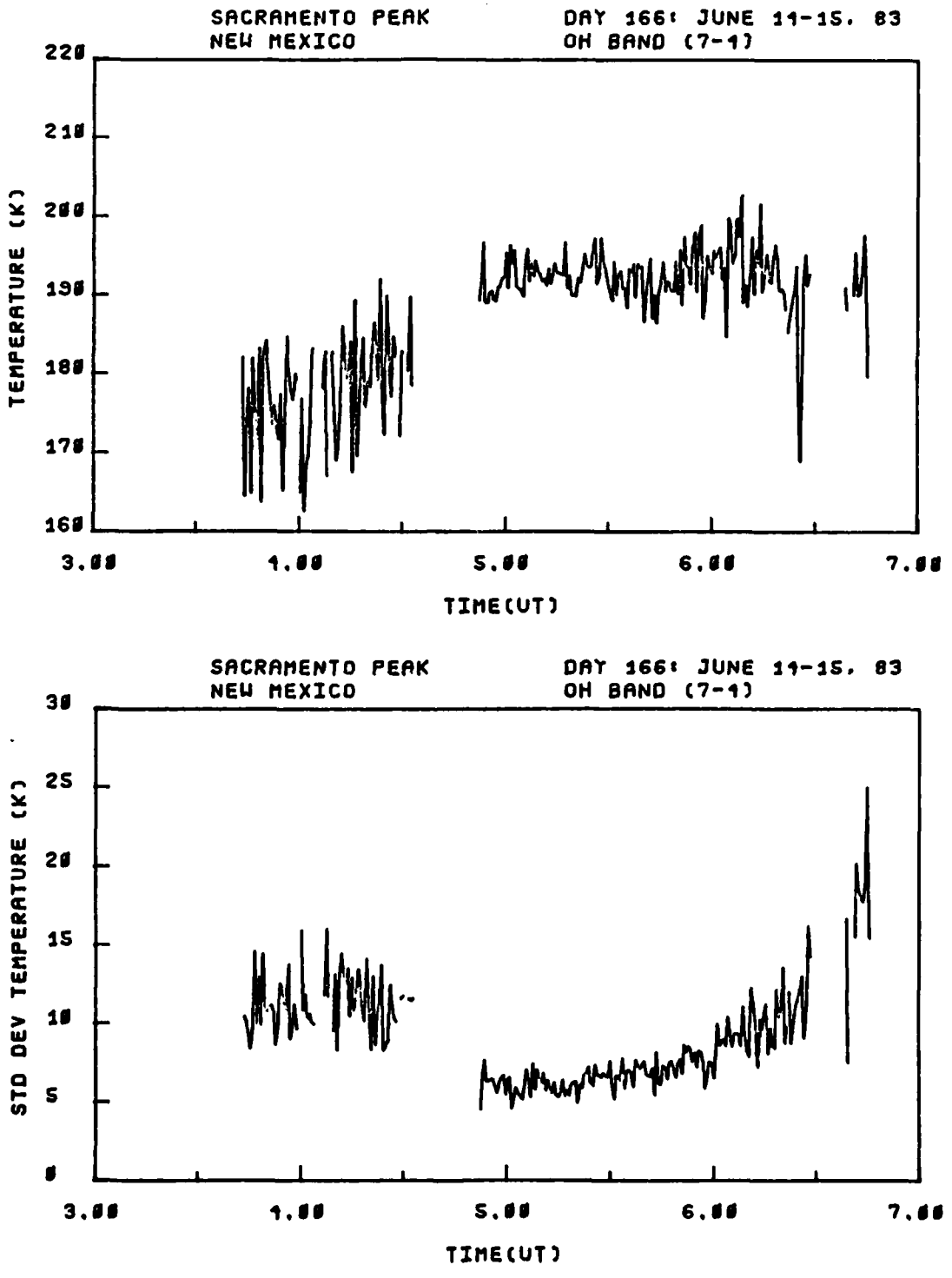

Figure C-23. OH (7,4) band rotational temperature and standard deviation, viewing angle = zenith, day 166, 3:30-6:45 hrs. UT.

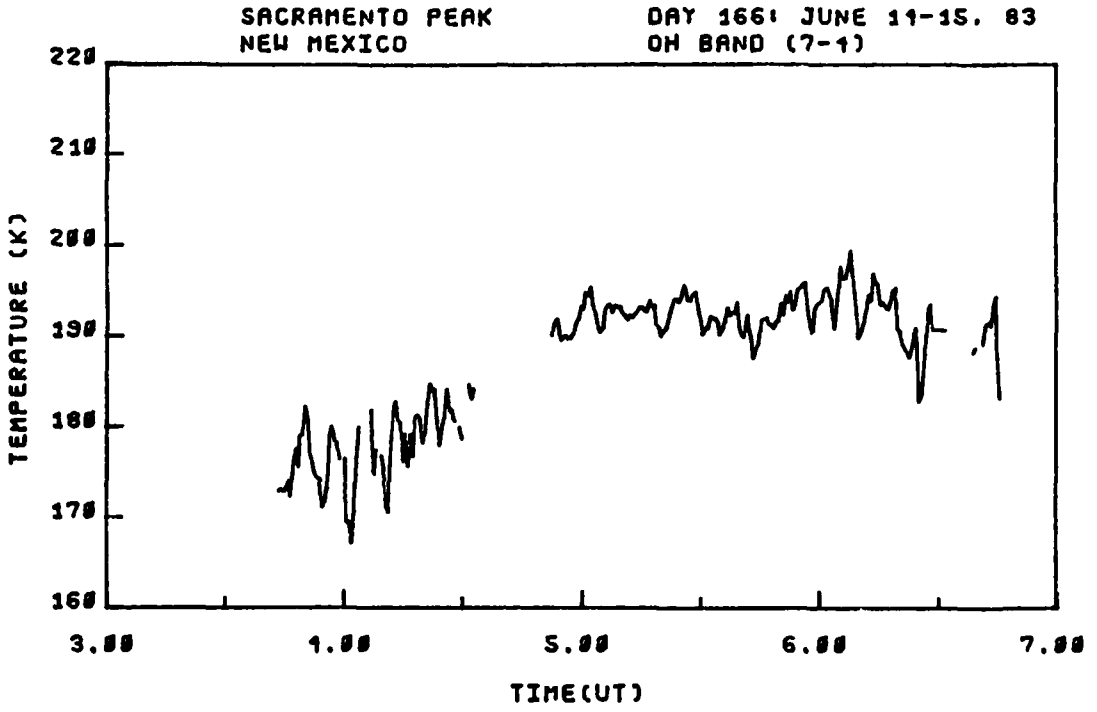

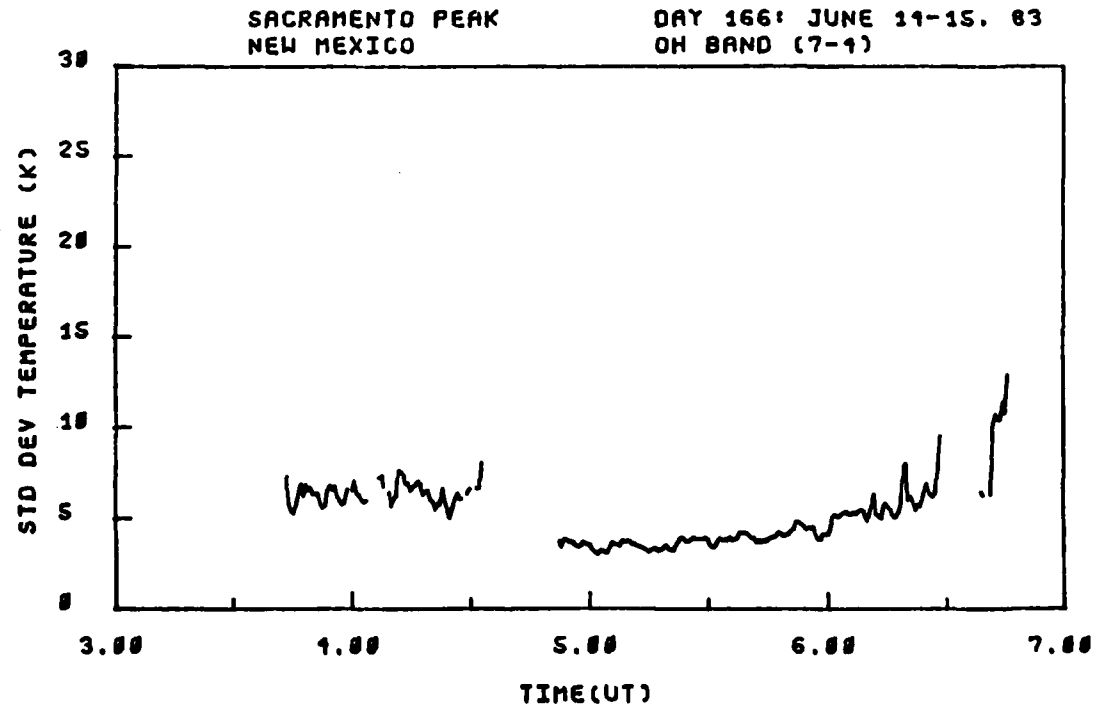

Figure C-24. OH (7,4) band smoothed rotational temperature and standard deviation, viewing angle = zenith, day 166, 3:30-6:45 hrs. UT.

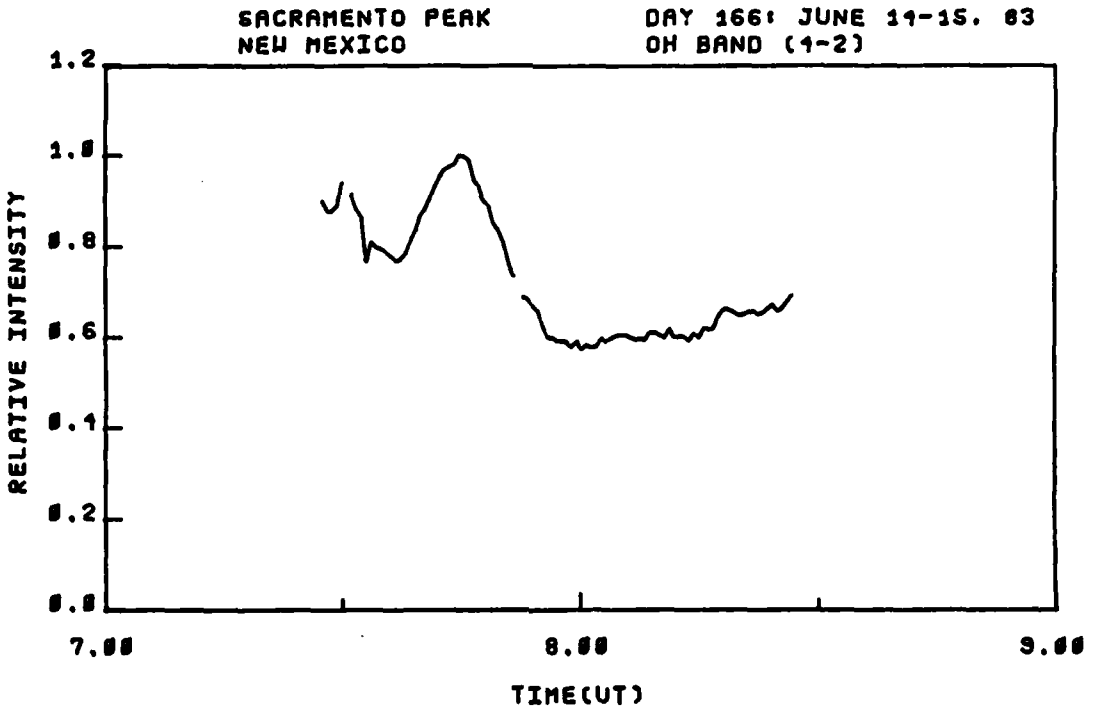

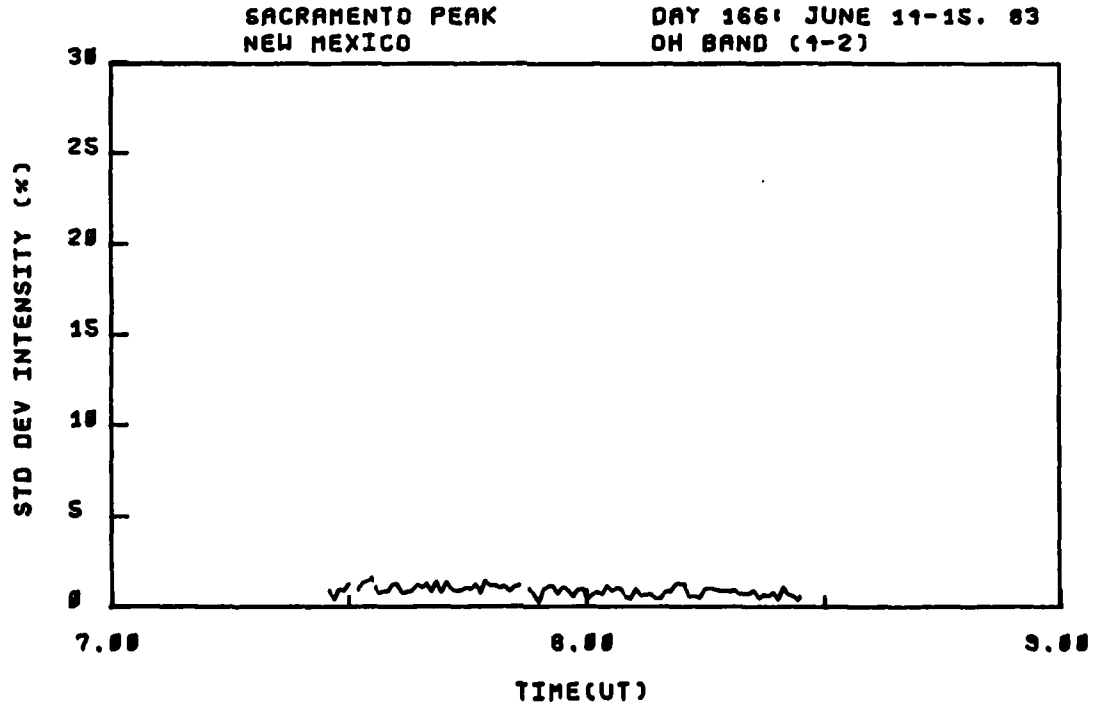

Figure C-25. OH (4,2) band relative intensity and standard deviation, viewing angle = 17° El. 328° Az., day 166, 7:30-8:30 hrs. UT.

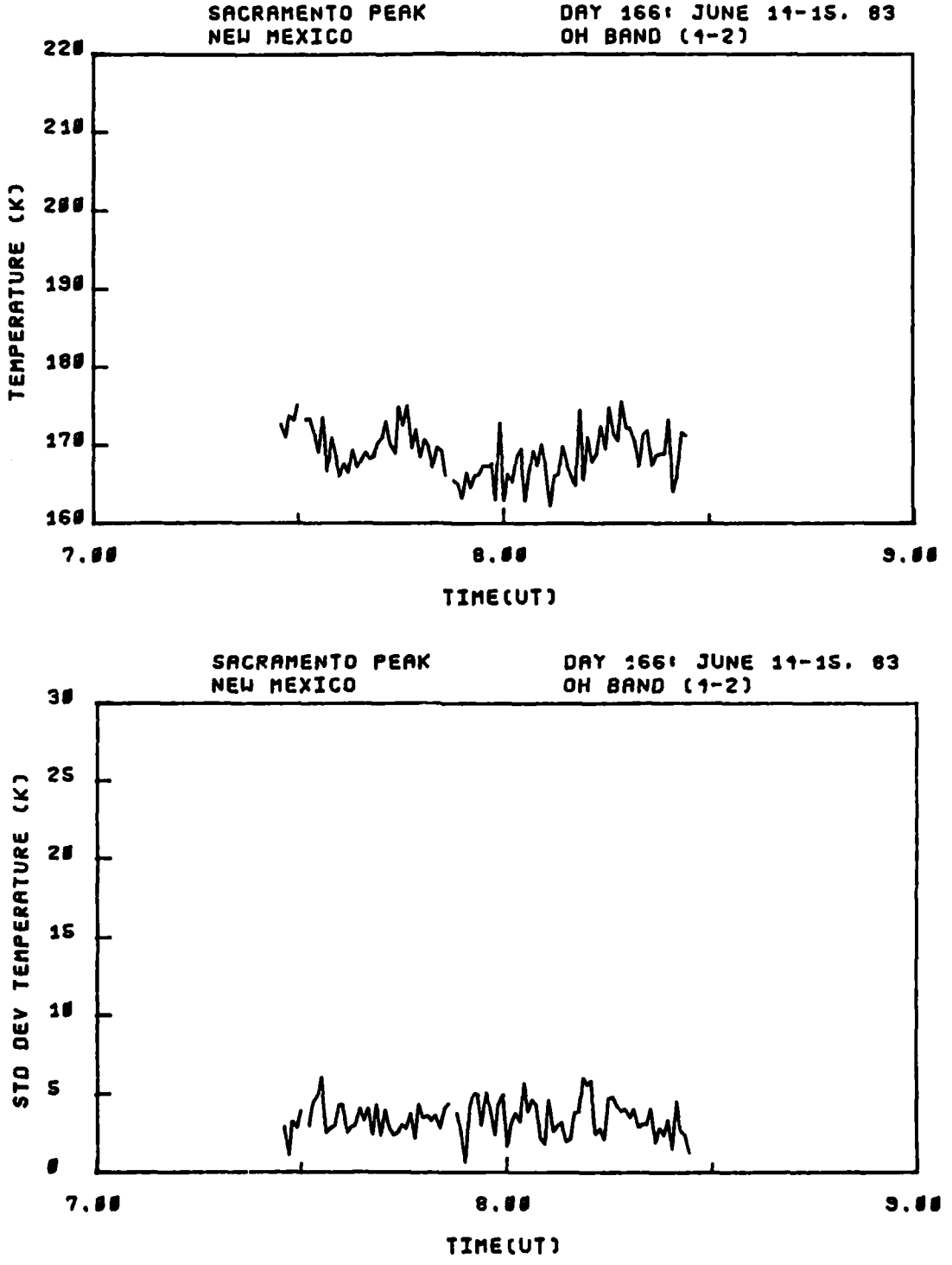

Figure C-26. OH (4,2) band rotational temperature and standard deviation, viewing angle = 17° El. 328° Az., day 166, 7:30-8:30 hrs. UT.

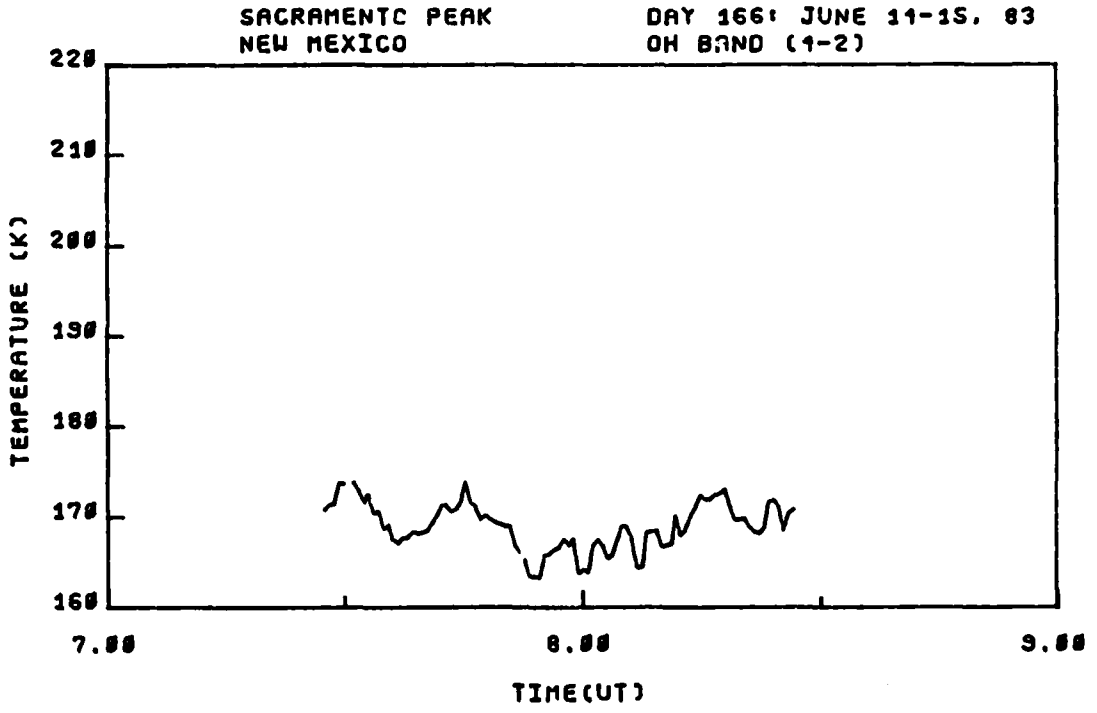

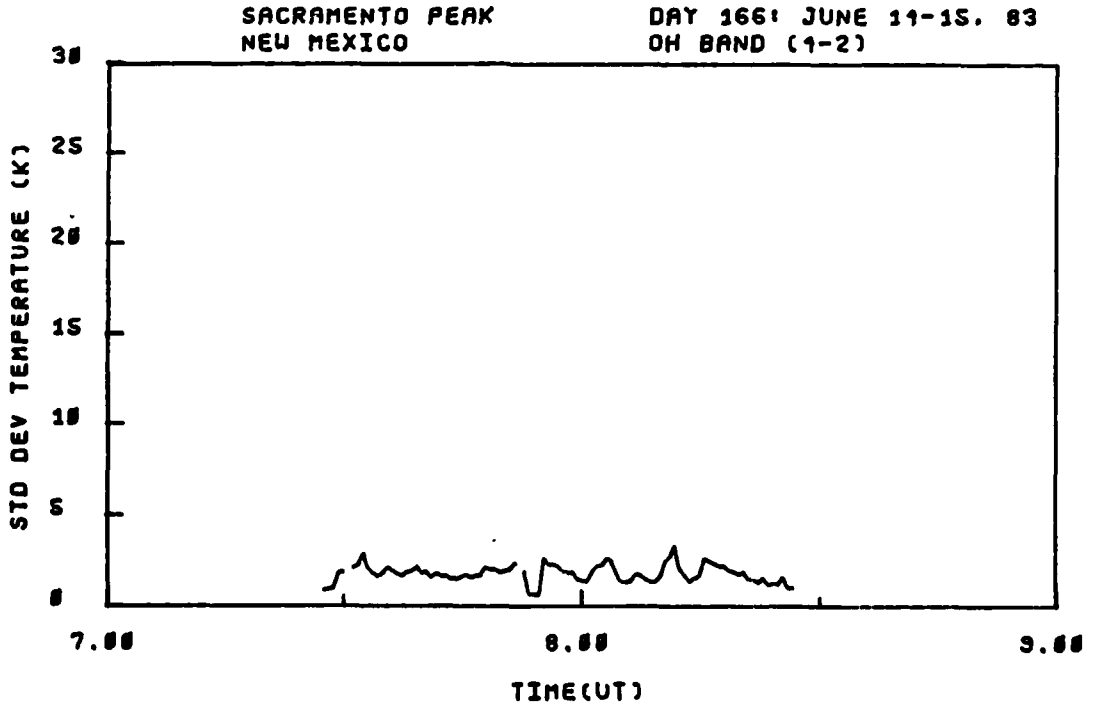

Figure C-27. OH (4,2) band smoothed rotational temperature and standard deviation, viewing angle = 17° El. 328° Az., day 166, 7:30-8:30 hrs. UT.

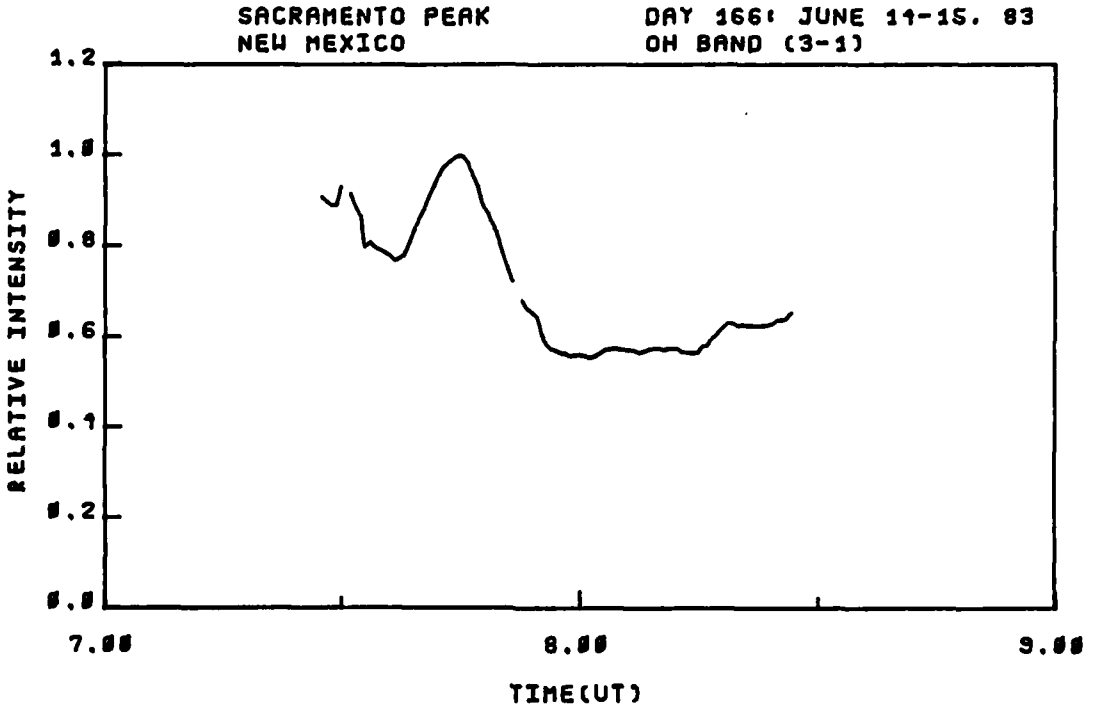

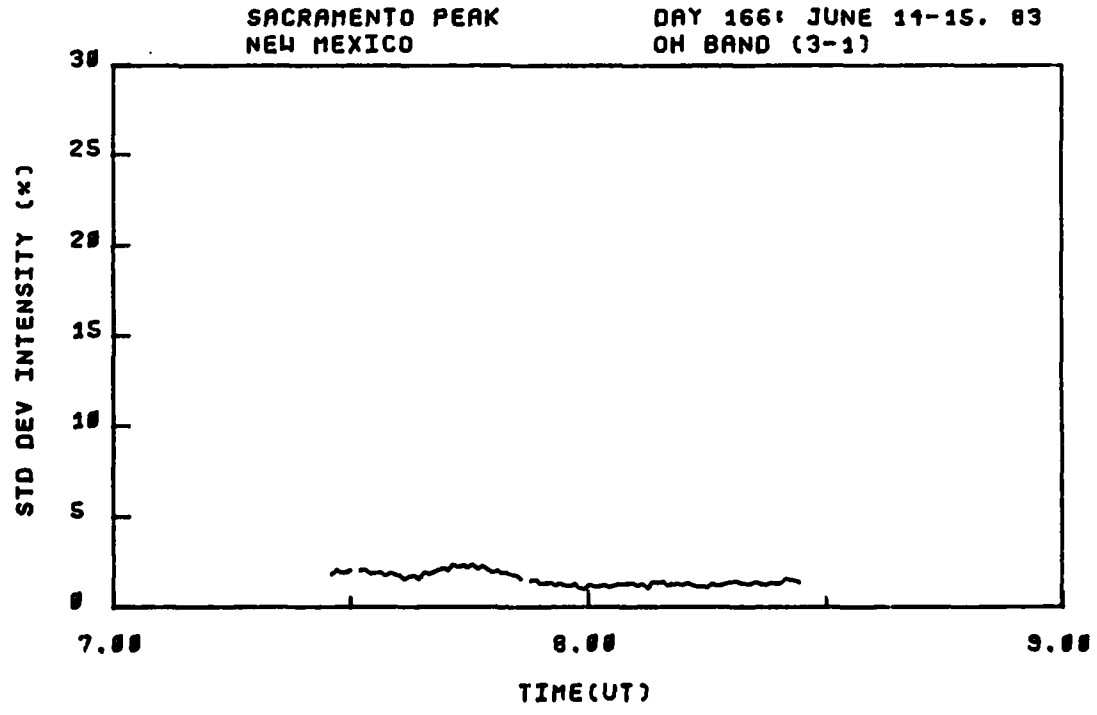

Figure C-28. OH (3,1) band relative intensity and standard deviation, viewing angle = 17° El. 328° Az., day 166, 7:30-8:30 hrs. UT.

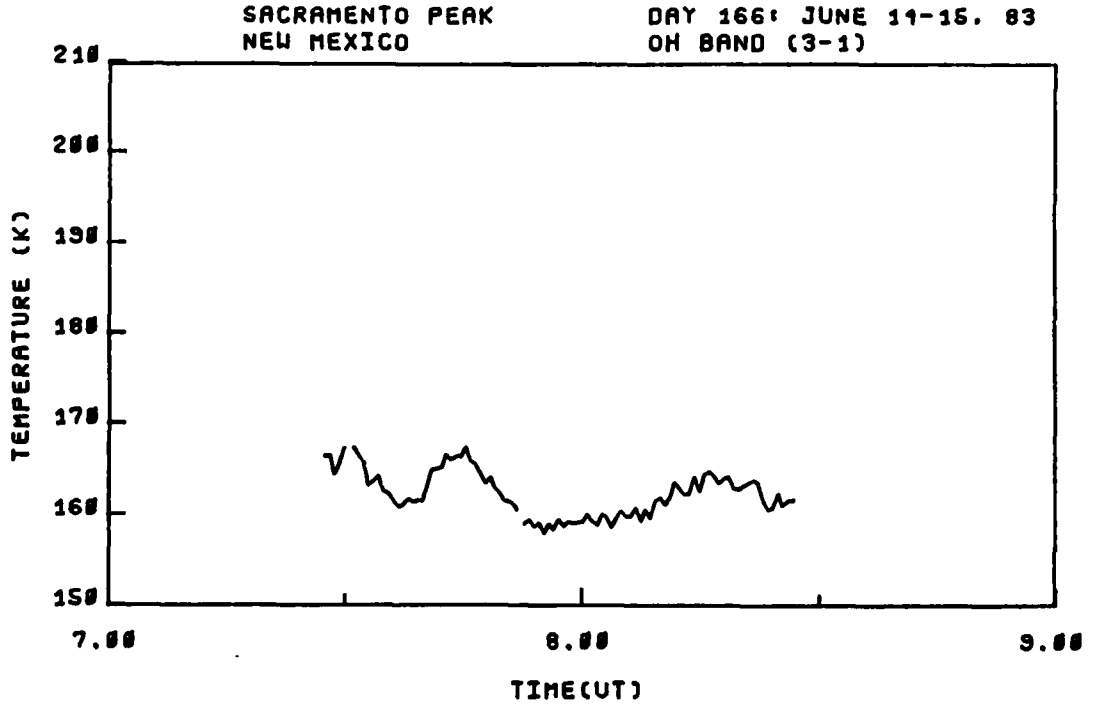

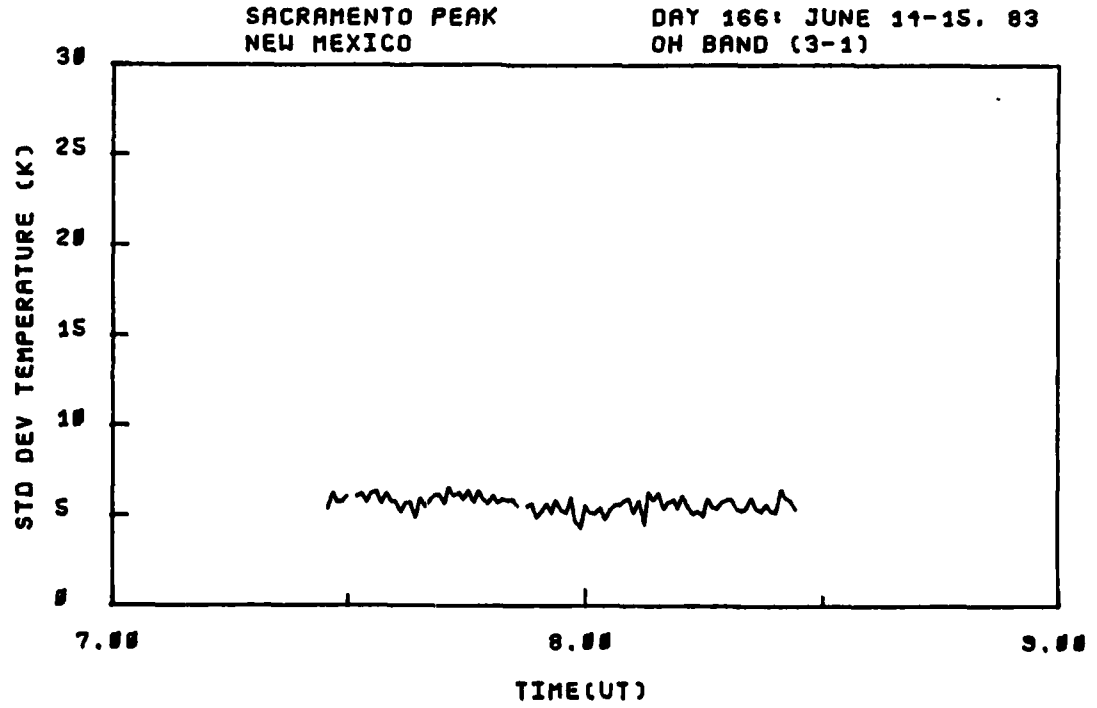

Figure C-29. OH (3,1) band rotational temperature and standard deviation, viewing angle = 17° El. 328° Az., day 166, 7:30-8:30 hrs. UT.

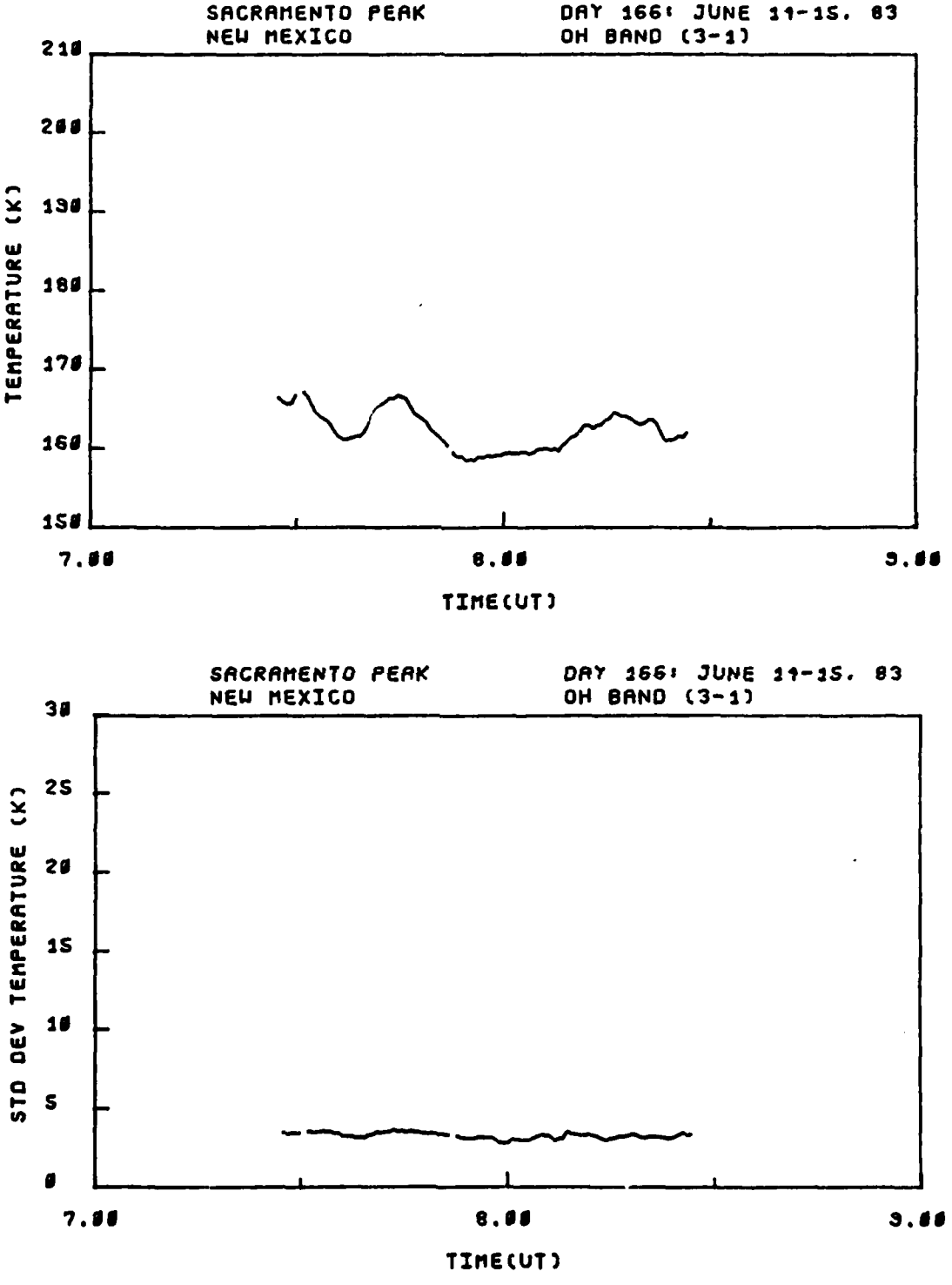

Figure C-30. OH (3,1) band smoothed rotational temperature and standard deviation, viewing angle = 17° El. 328° Az., day 166, 7:30-8:30 hrs. UT.

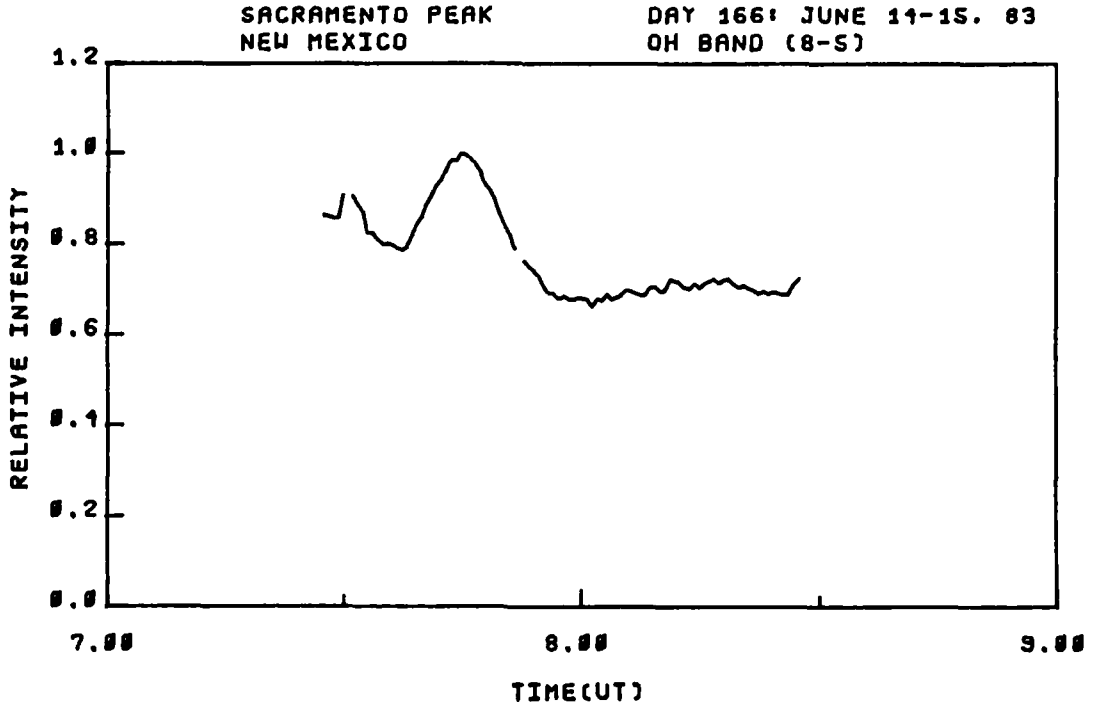

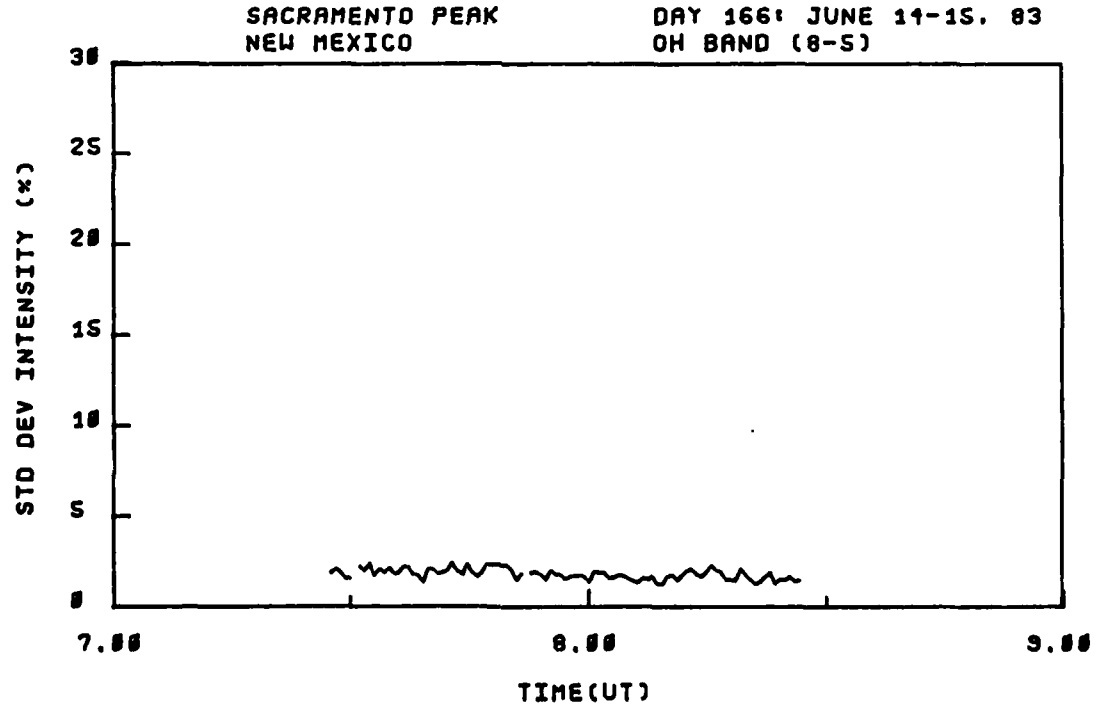

Figure C-31. OH (8,5) band relative intensity and standard deviation, viewing angle = 17° El. 328° Az., day 166, 7:30-8:30 hrs. UT.

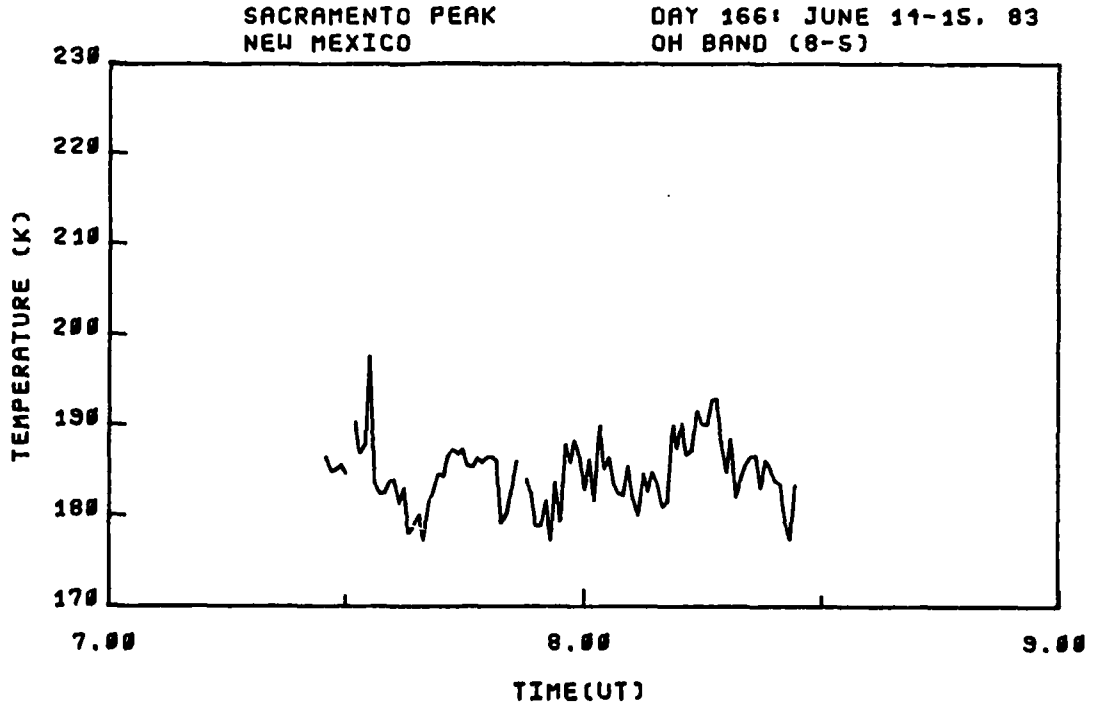

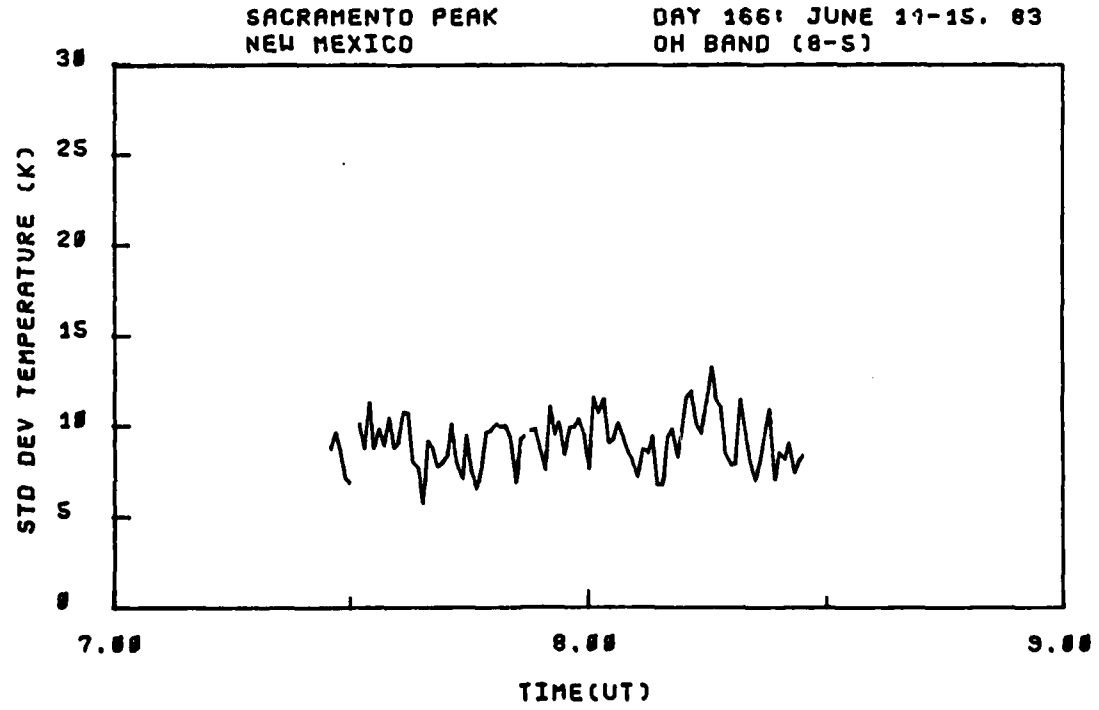

Figure C-32. OH (8,5) band rotational temperature and standard deviation, viewing angle = 17° El. 328° Az., day 166, 7:30-8:30 hrs. UT.

AD-A166 377 HIGH RESOLUTION MEASUREMENTS OF OH INFRARED AIRGLOW STRUCTURE(U) AIR FORCE INST OF TECH WRIGHT-PATTERSON AFB OH P C NEAL 1985 AFIT/CI/NR-86-26D 3/3

UNCLASSIFIED F/G 4/1 NL

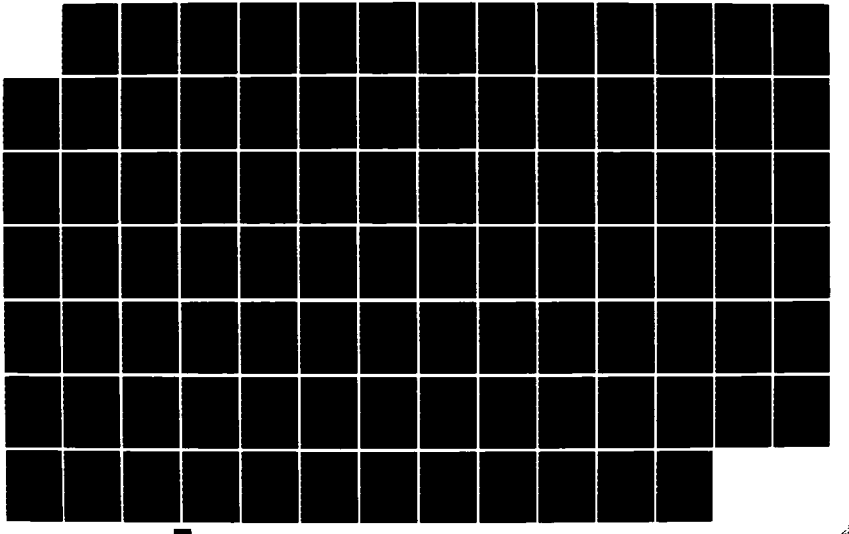

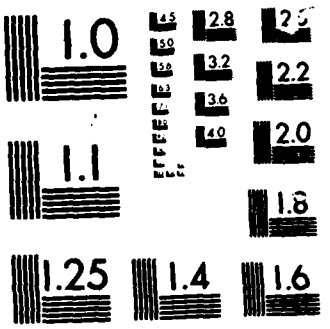

MICROCOPY RESOLUTION TEST CHART

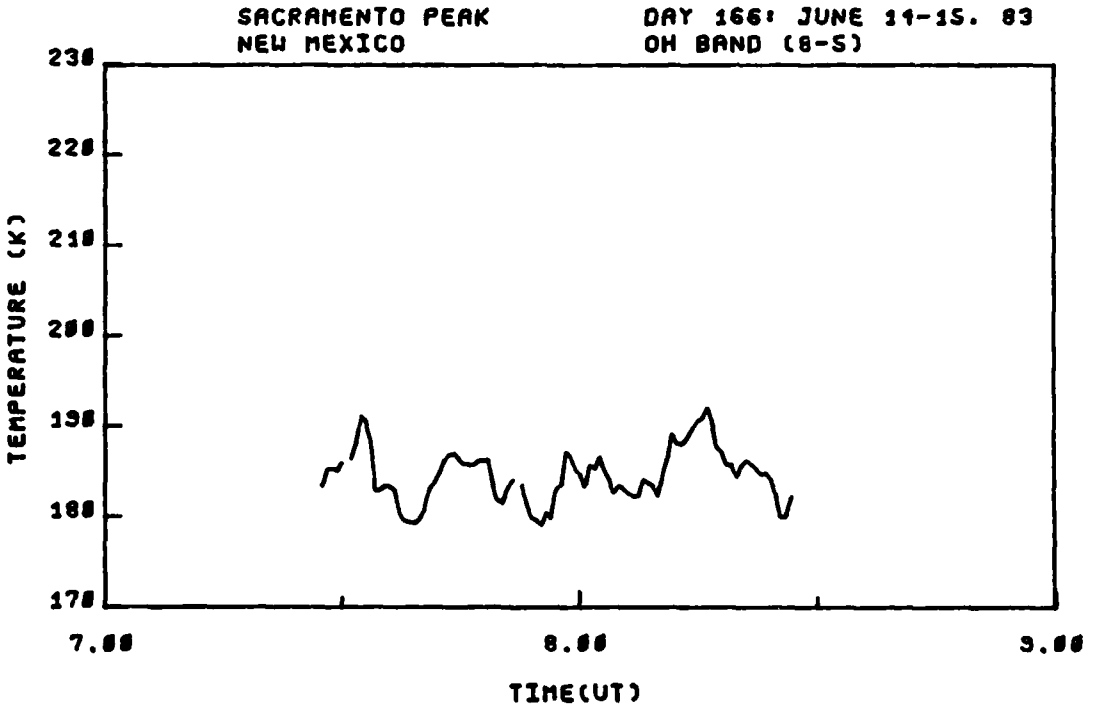

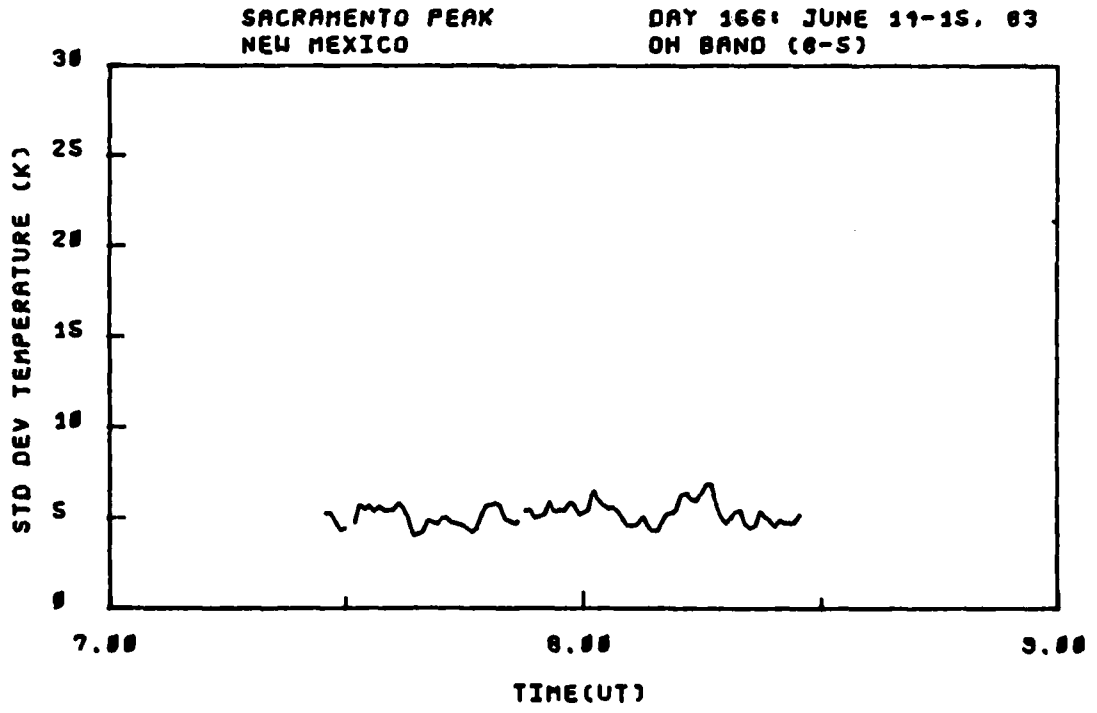

Figure C-33. OH (8,5) band smoothed rotational temperature and standard deviation, viewing angle = 17° El. 328° Az., day 166, 7:30-8:30 hrs. UT.

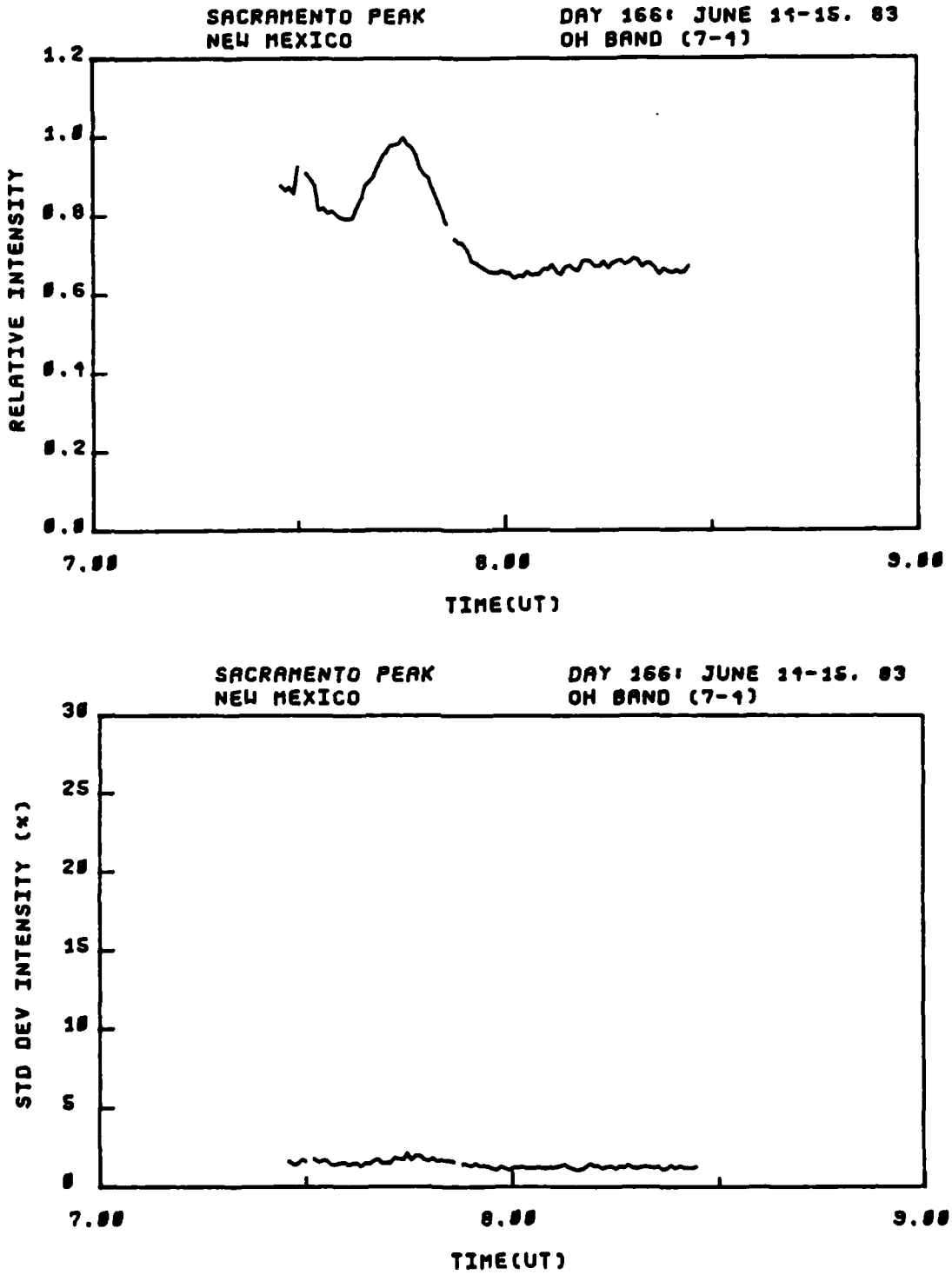

Figure C-34. OH (7,4) band relative intensity and standard deviation, viewing angle = 17° El. 328° Az., day 166, 7:30-9:30 hrs. UT.

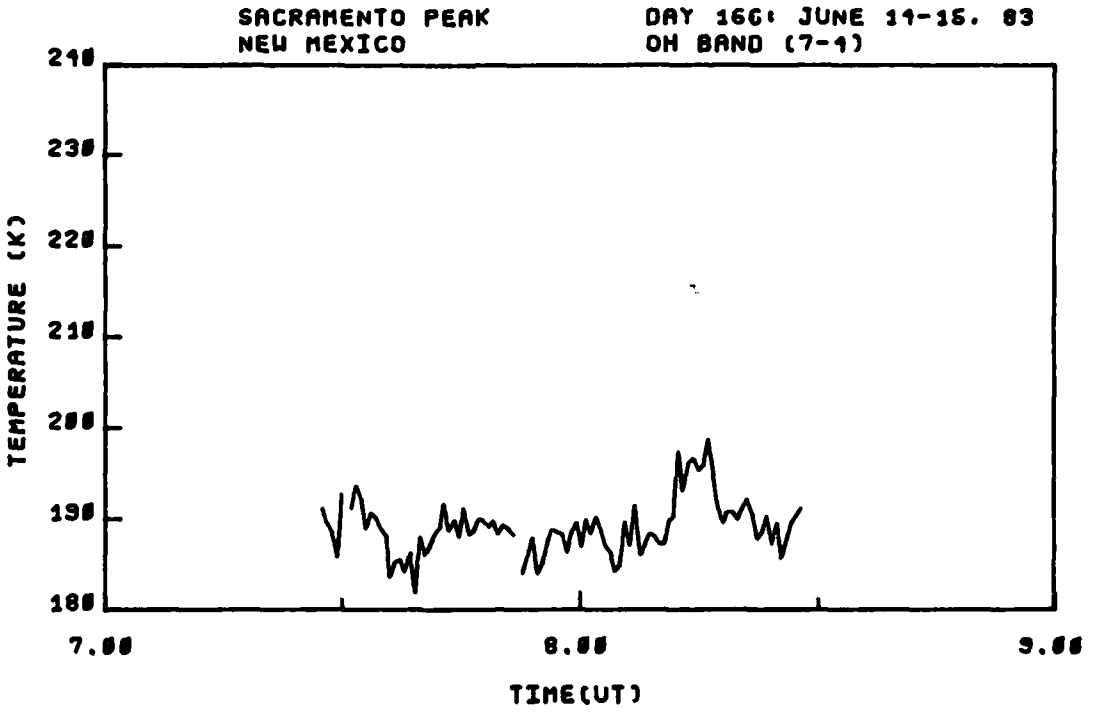

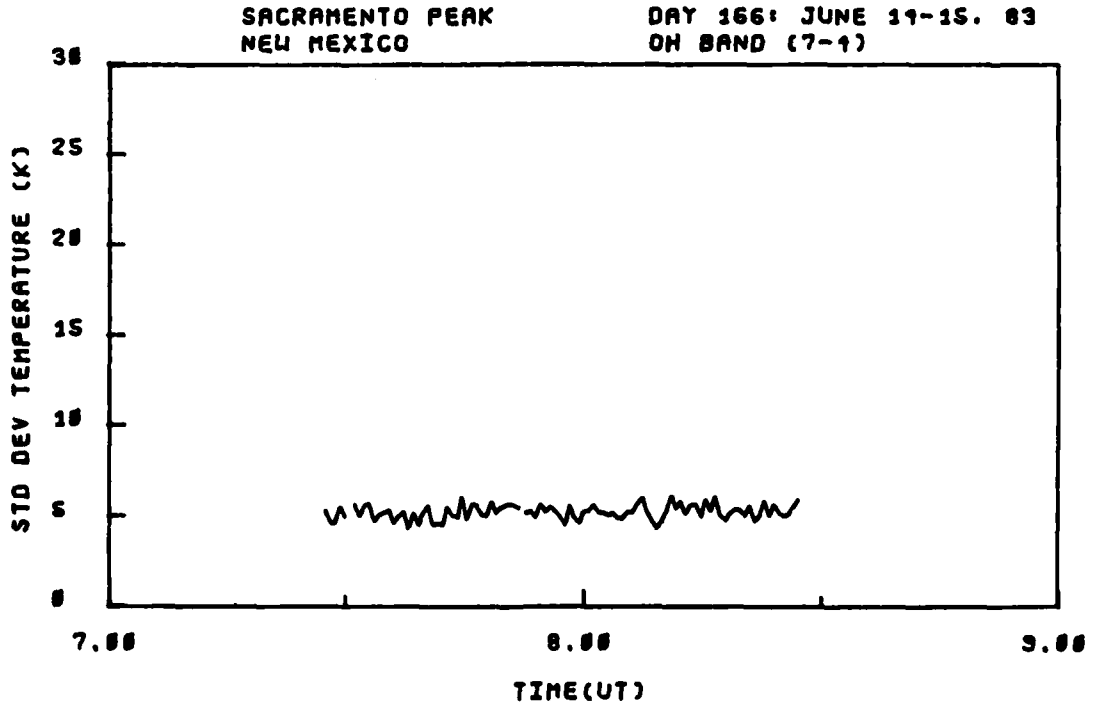

Figure C-35. OH (7,4) band rotational temperature and standard deviation, viewing angle = 17° El. 328° Az., day 166, 7:30-8:30 hrs. UT.

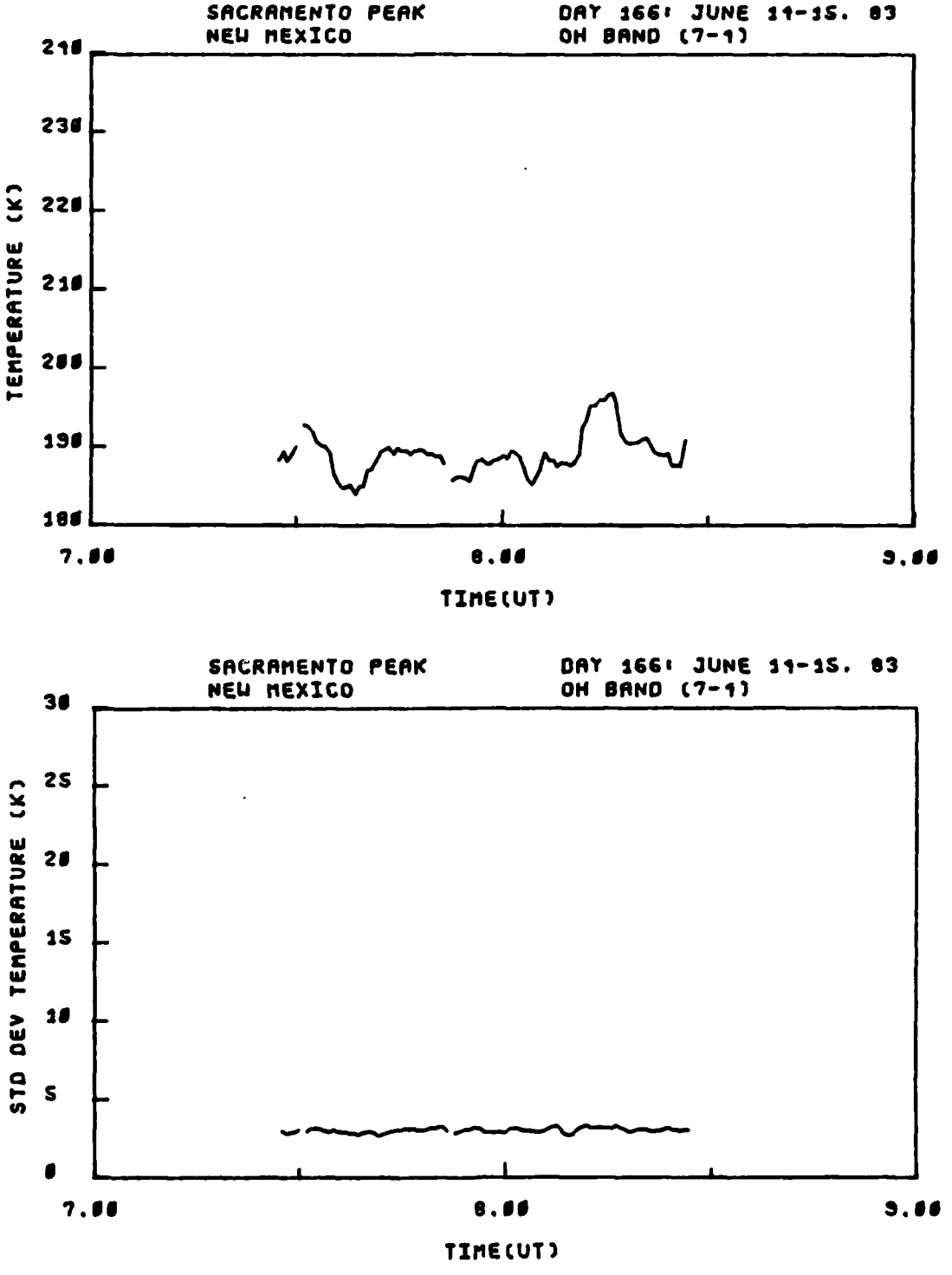

Figure C-36. OH (7,4) band smoothed rotational temperature and standard deviation, viewing angle = 17° El. 328° Az., day 166, 7:30-8:30 hrs. UT.

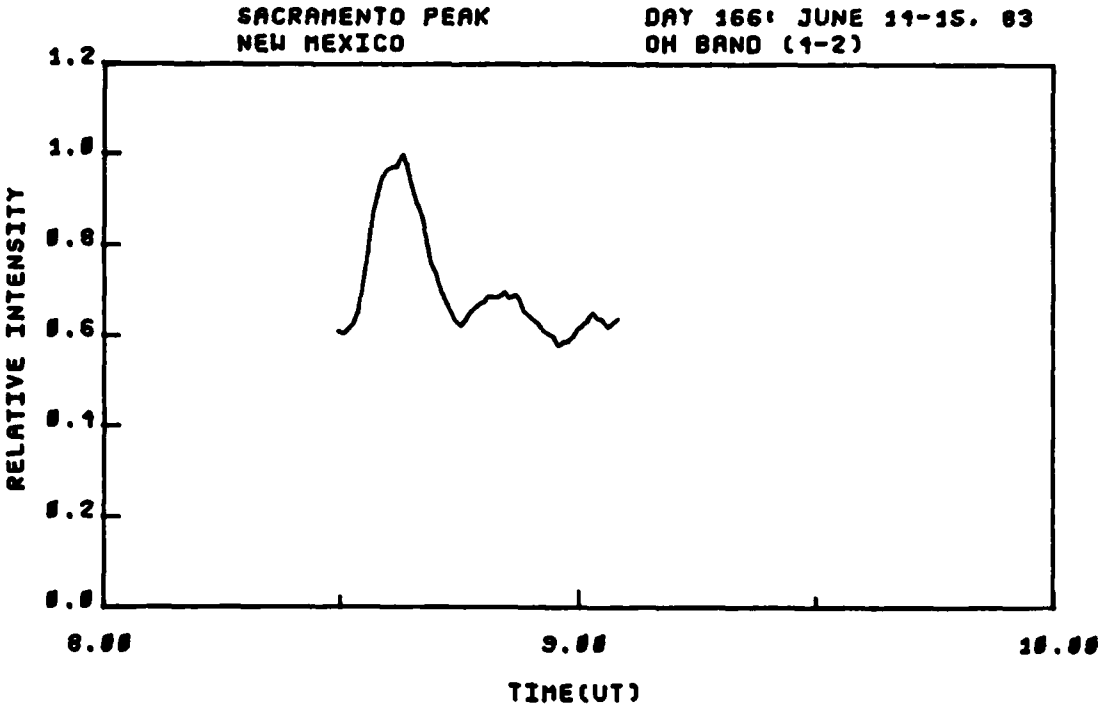

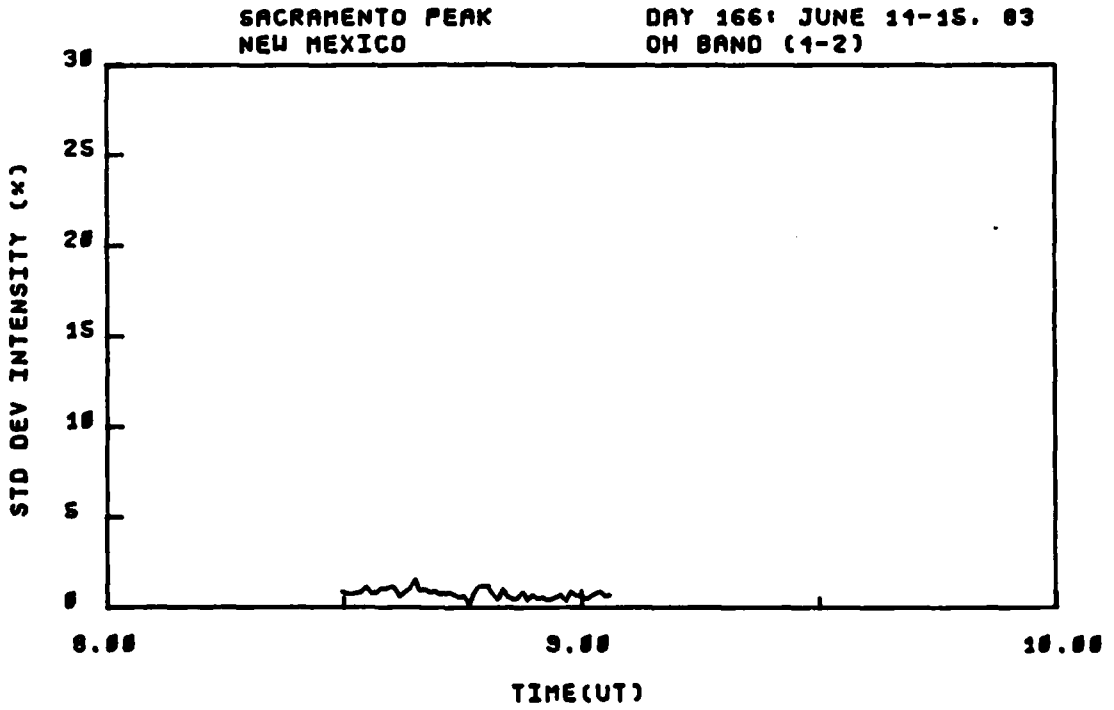

Figure C-37. OH (4,2) band relative intensity and standard deviation, viewing angle = 15.5° El. 340° Az., day 166, 8:30-9:15 hrs. UT.

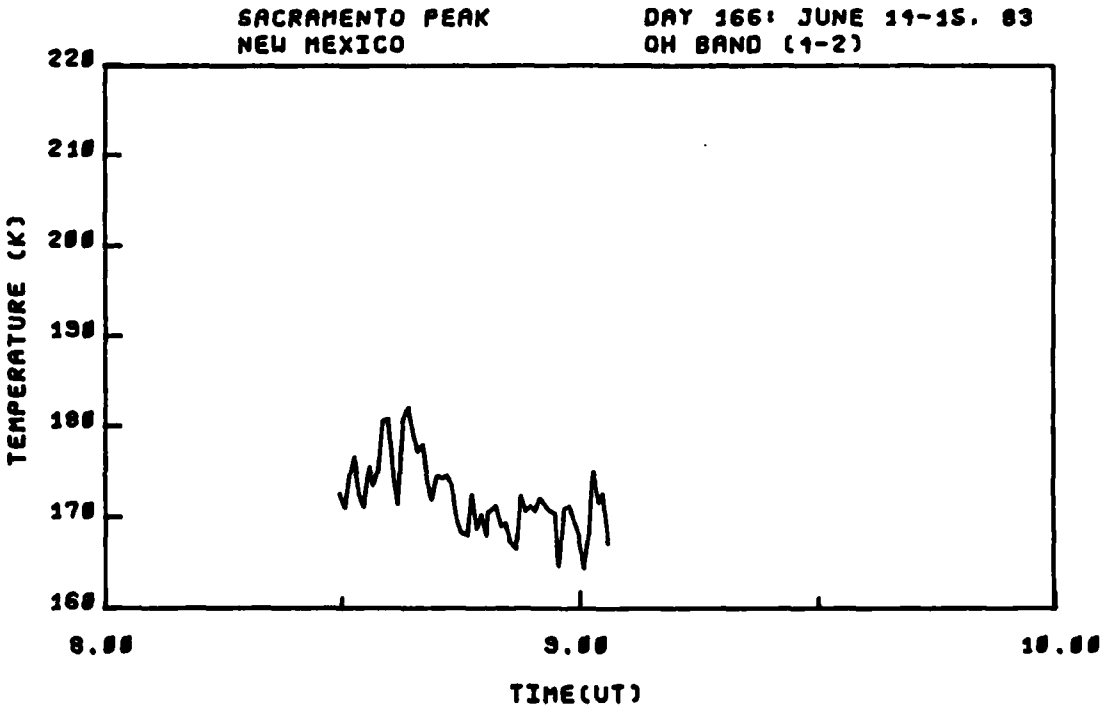

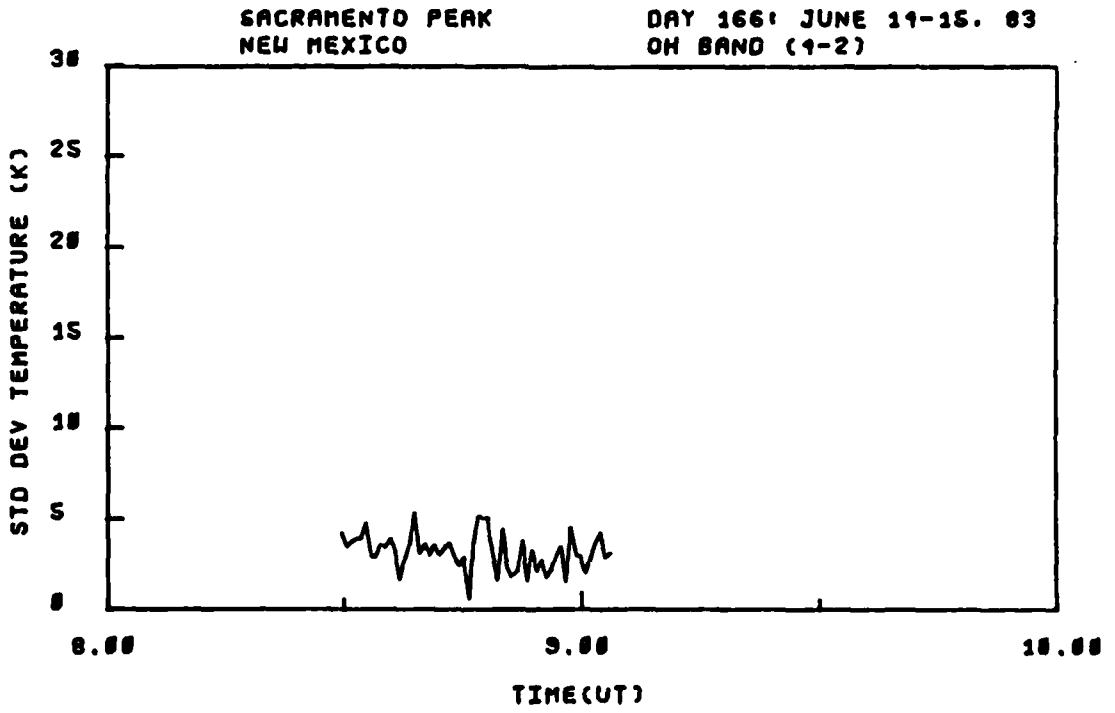

Figure C-38. OH (4,2) band rotational temperature and standard deviation, viewing angle = 15.5° El. 340° Az., day 166, 8:30-9:15 hrs. UT.

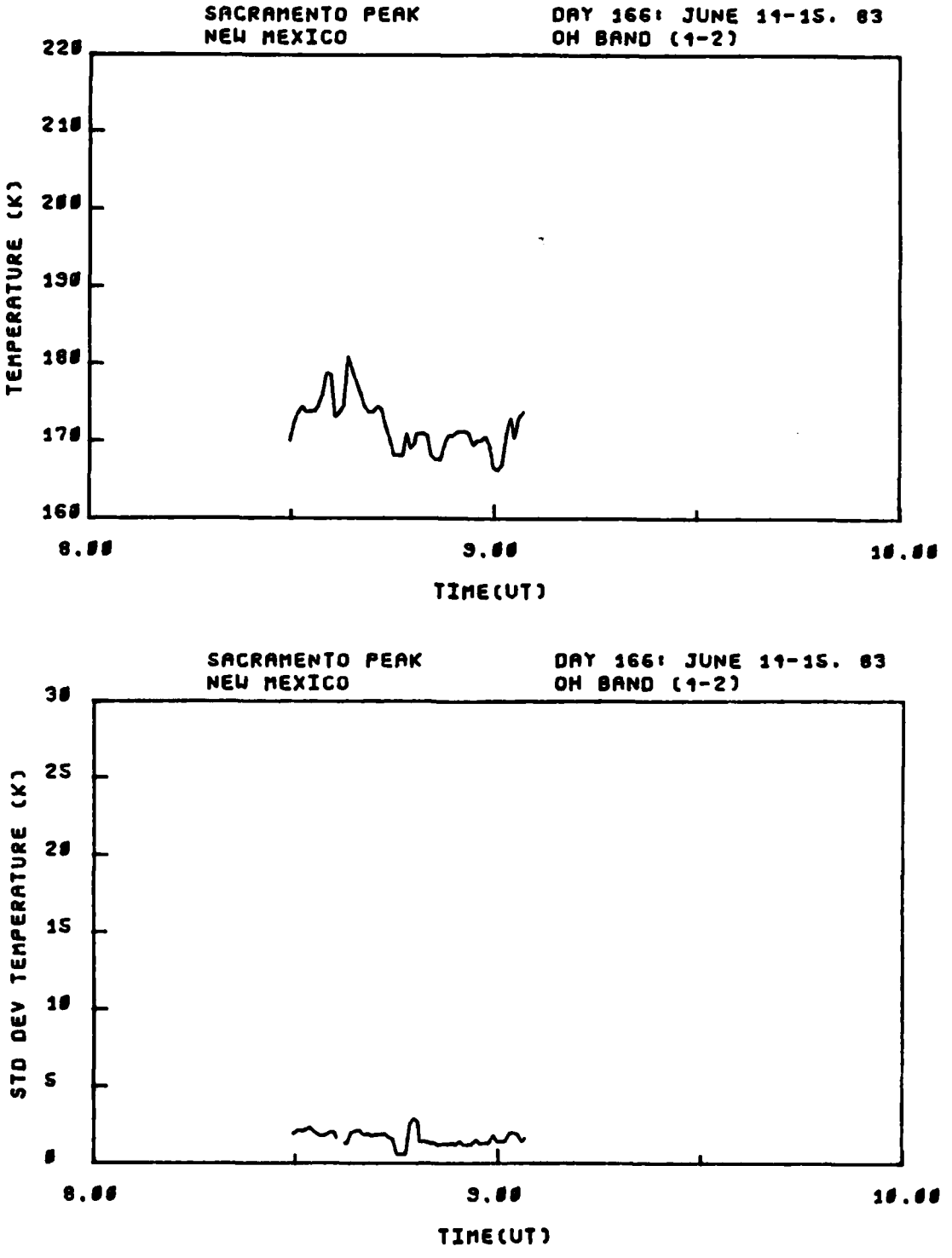

Figure C-39. OH (4,2) band smoothed rotational temperature and standard deviation, viewing angle = 15.5° El. 340° Az., day 166, 8:30-9:15 hrs. UT.

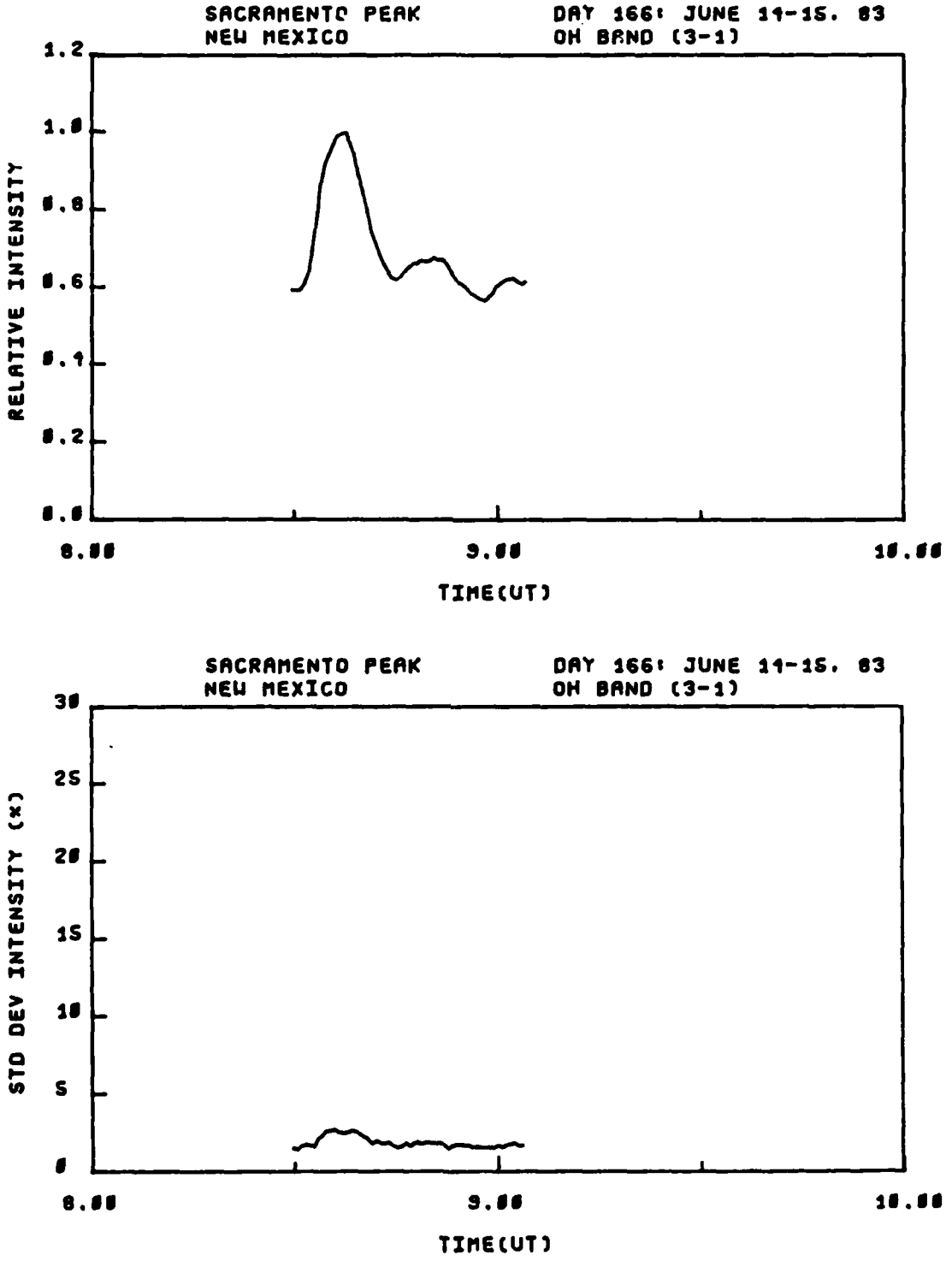

Figure C-40. OH (3,1) band relative intensity and standard deviation, viewing angle = 15.5° El. 340° Az., day 166, 8:30-9:15 hrs. UT.

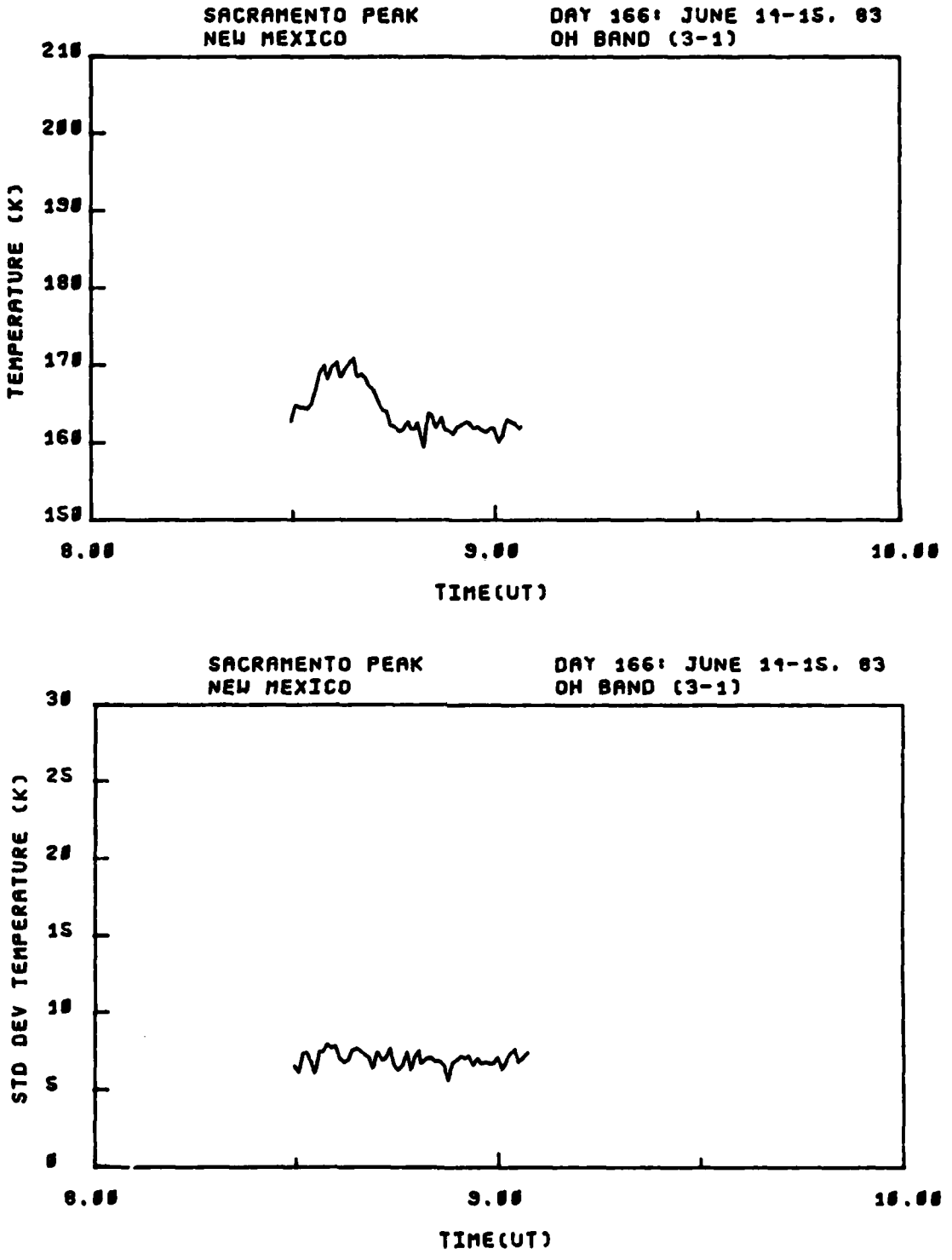

Figure C-41. OH (3,1) band rotational temperature and standard deviation, viewing angle = 15.5° El. 340° Az., day 166, 8:30-9:15 hrs. UT.

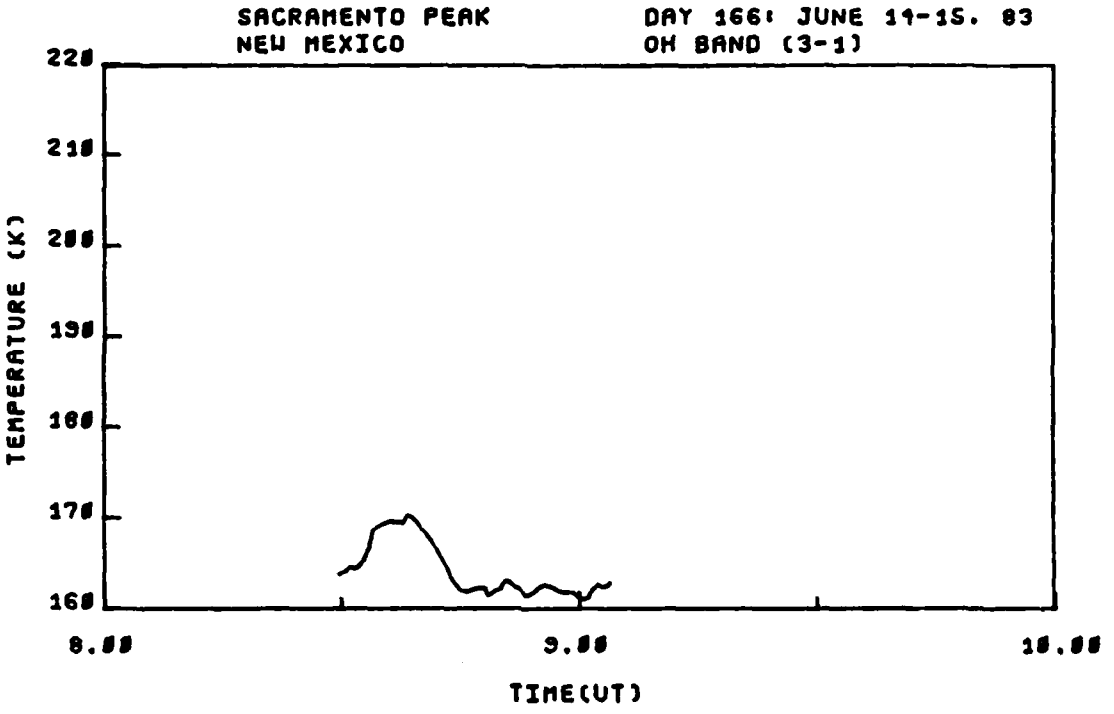

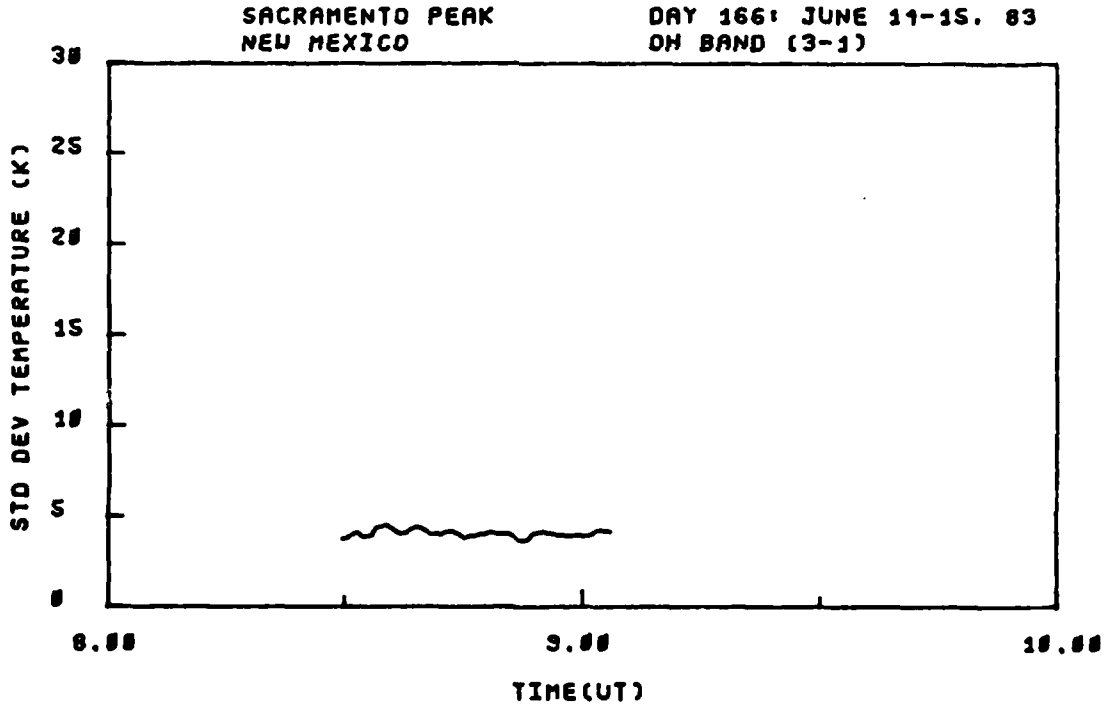

Figure C-42. OH (3,1) band smoothed rotational temperature and standard deviation, viewing angle = 15.5° El. 340° Az., day 166, 8:30-9:15 hrs. UT.

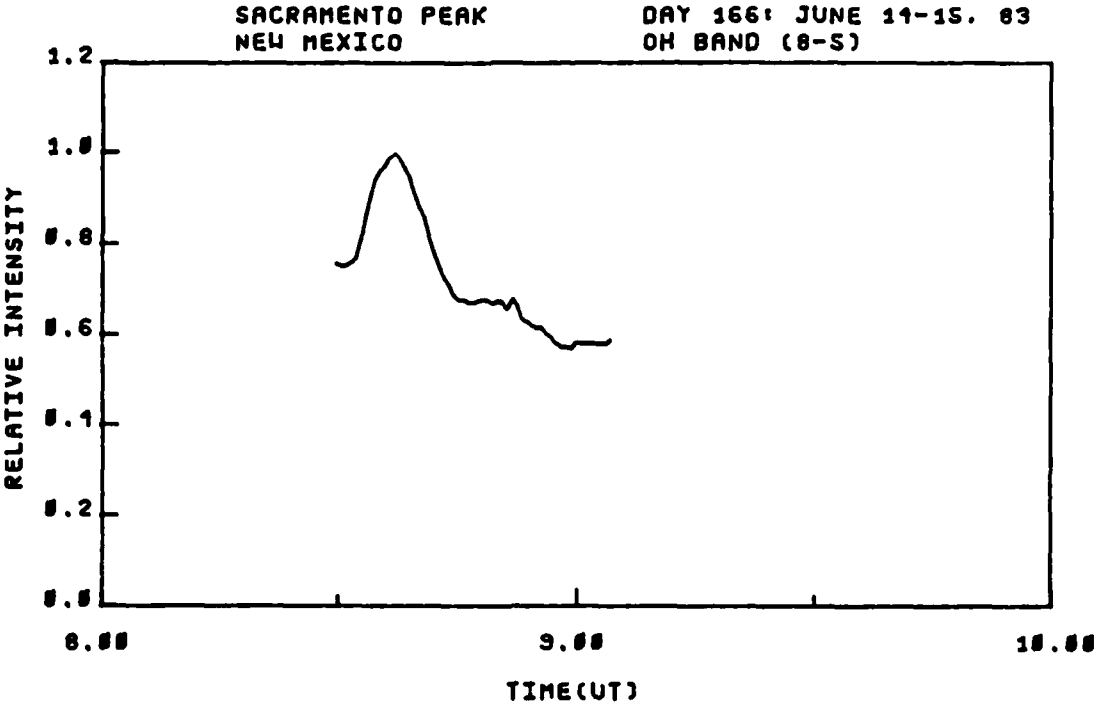

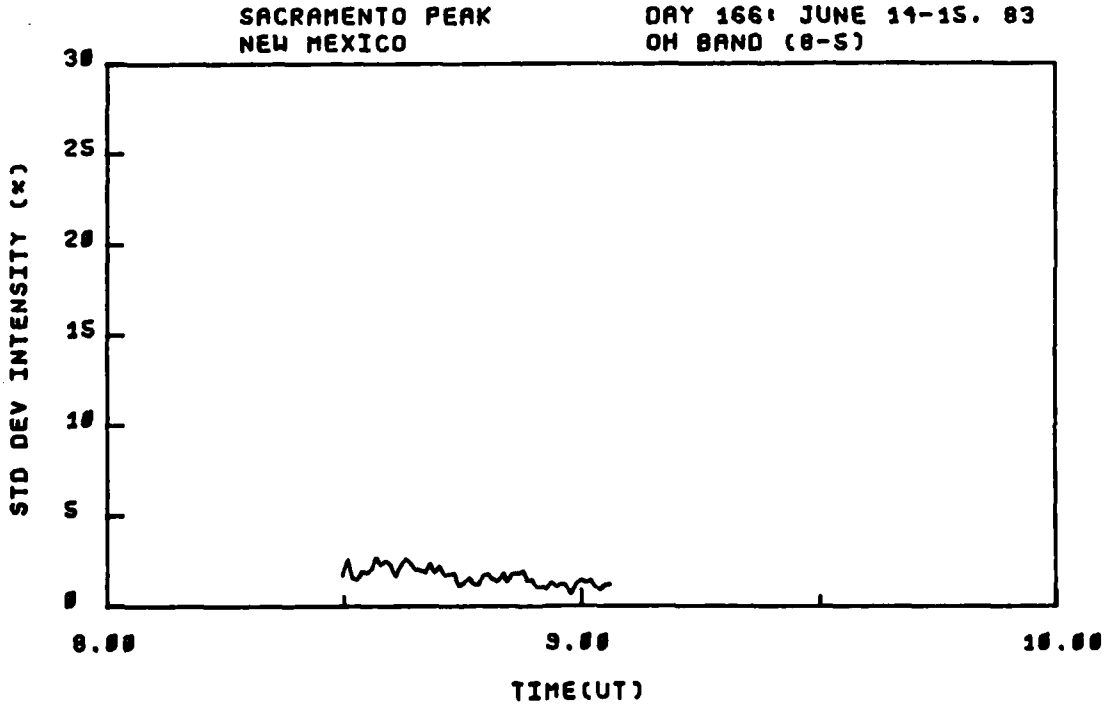

Figure C-43. OH (8,5) band relative intensity and standard deviation, viewing angle = 15.5° El. 340° Az., day 166, 8:30-9:15 hrs. UT.

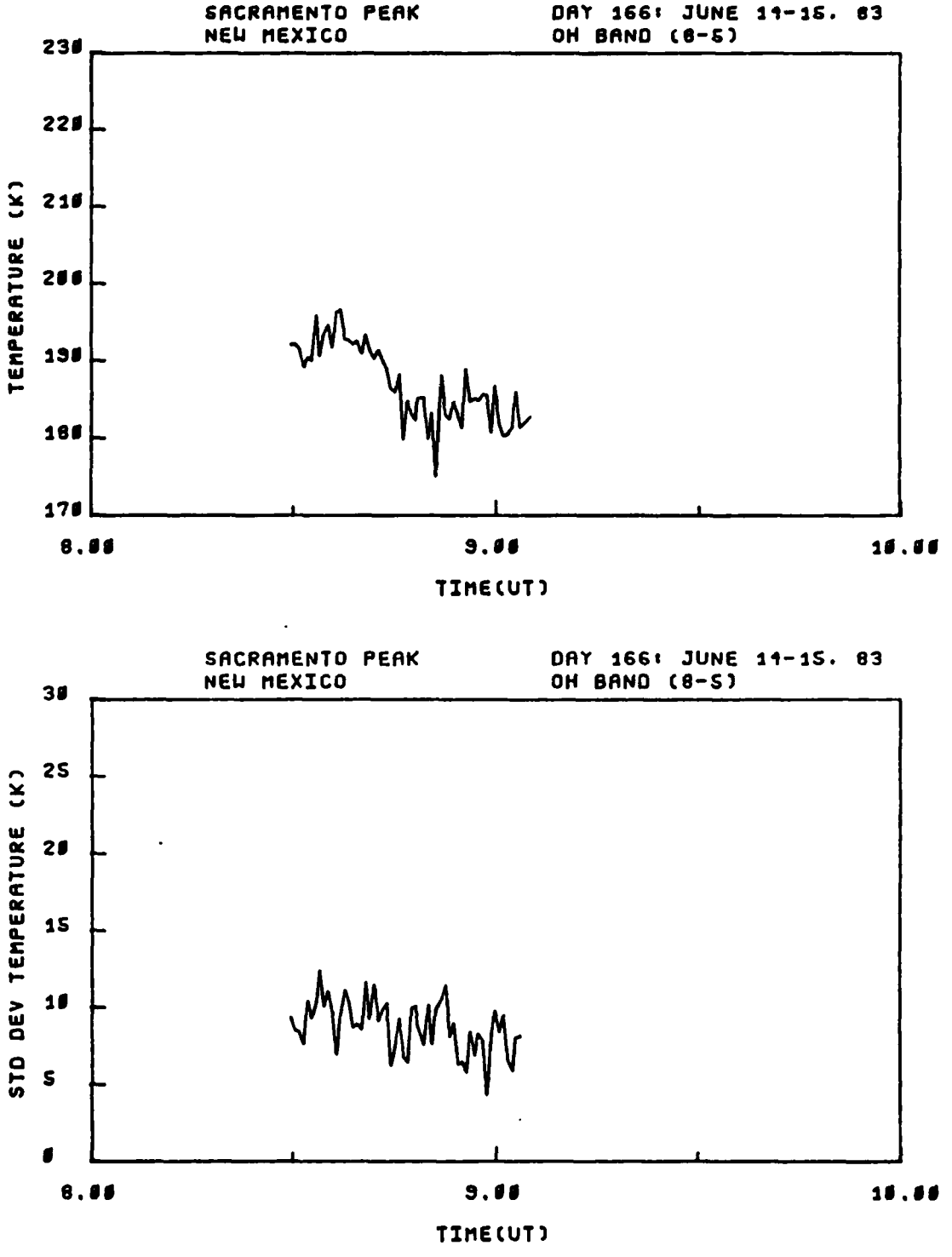

Figure C-44. OH (8,5) band rotational temperature and standard deviation, viewing angle = 15.5° El. 340° Az., day 166, 8:30-9:15 hrs. UT.

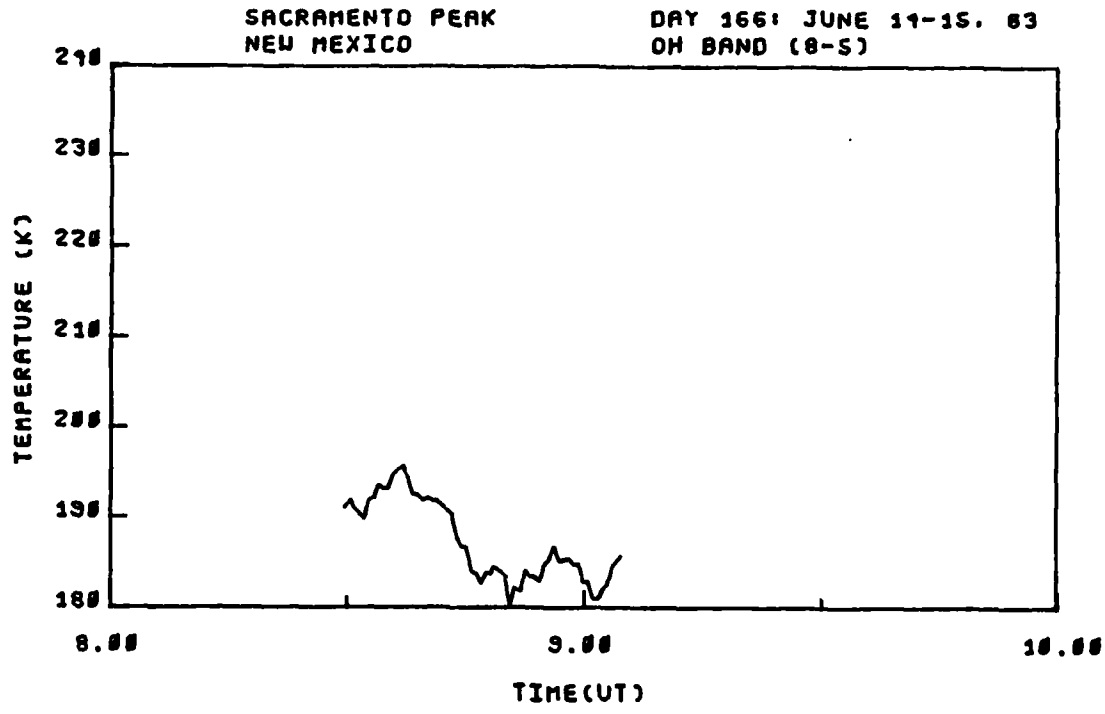

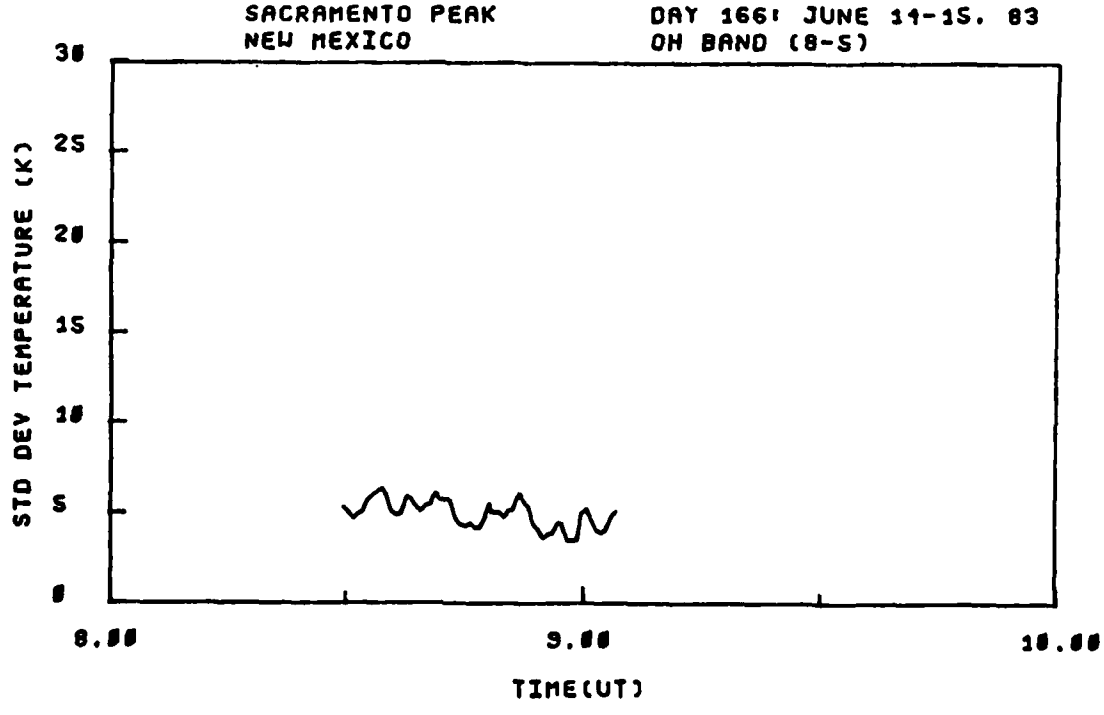

Figure C-45. OH (8,5) band smoothed rotational temperature and standard deviation, viewing angle = 15.5° El. 340° Az., day 166, 8:30-9:15 hrs. UT.

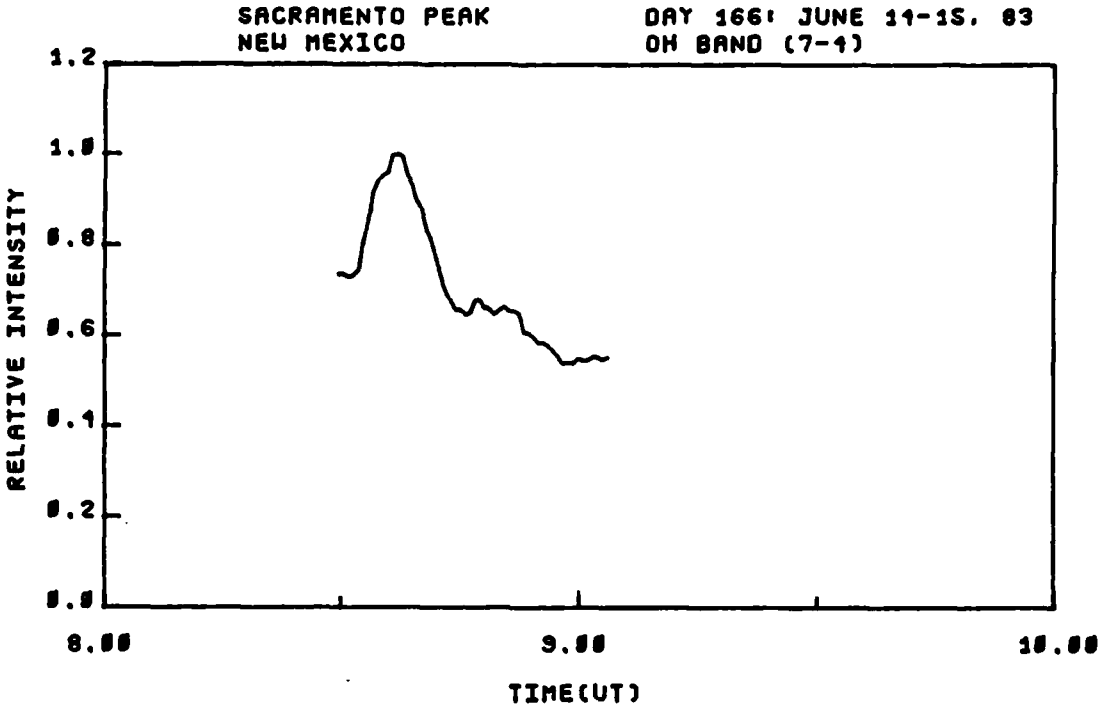

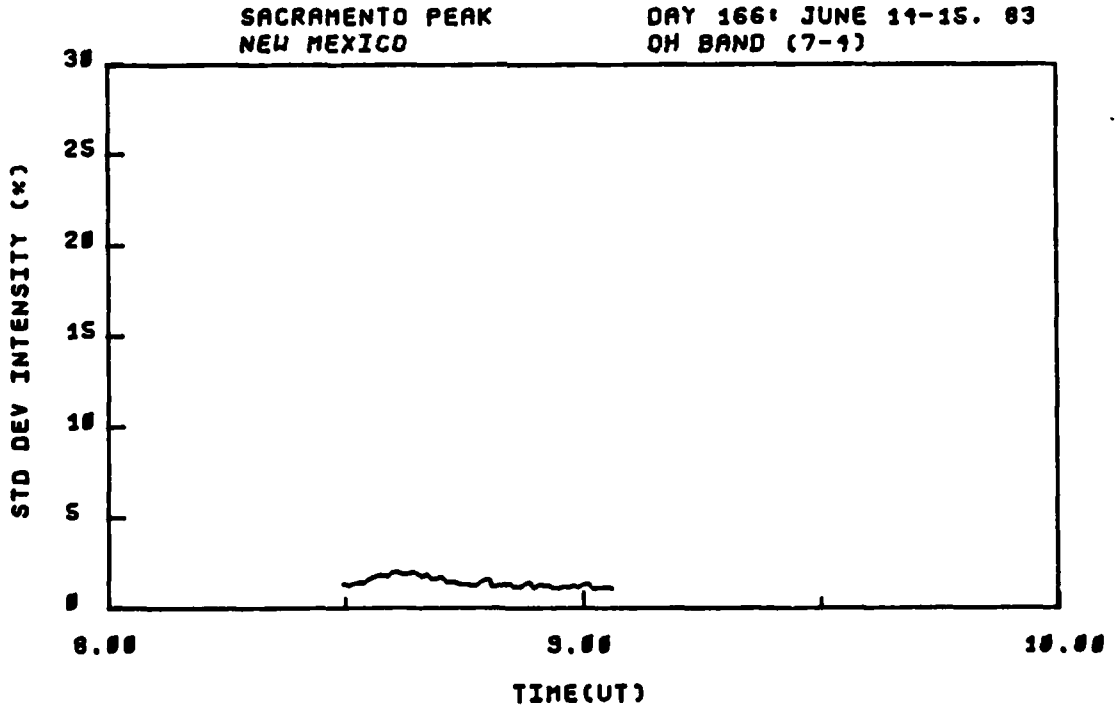

Figure C-46. OH (7,4) band relative intensity and standard deviation, viewing angle = 15.5° El. 340° Az., day 166, 8:30-9:15 hrs. UT.

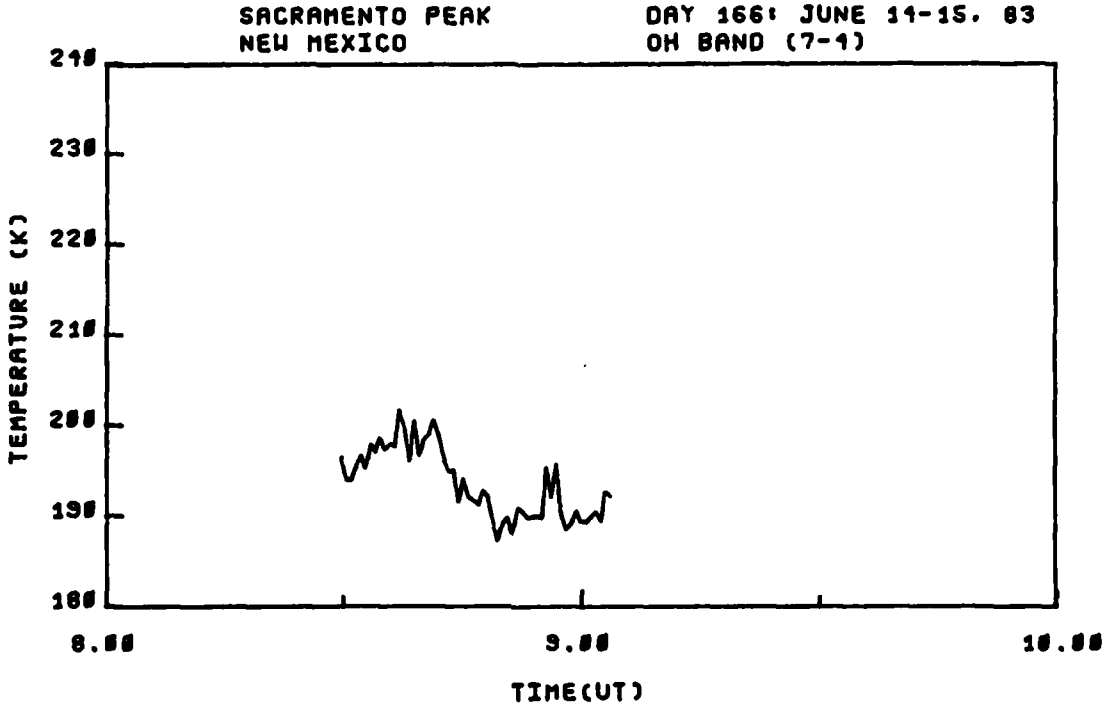

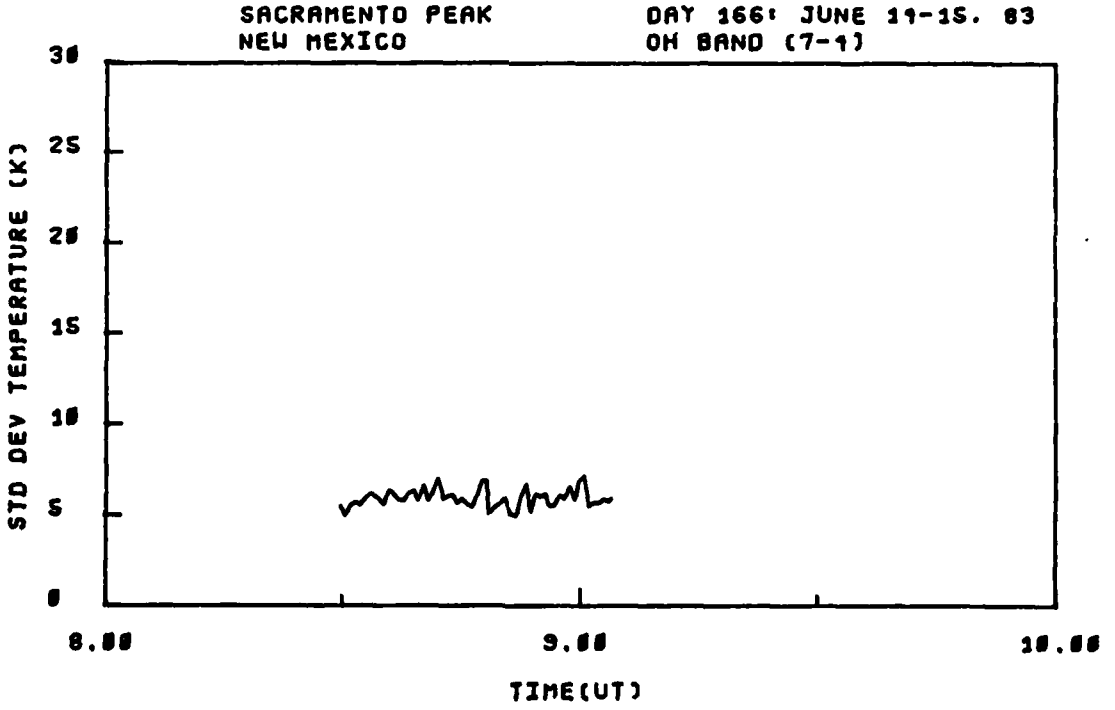

Figure C-47. OH (7,4) band rotational temperature and standard deviation, viewing angle = 15.5° El. 340° Az., day 166, 8:30-9:15 hrs. UT.

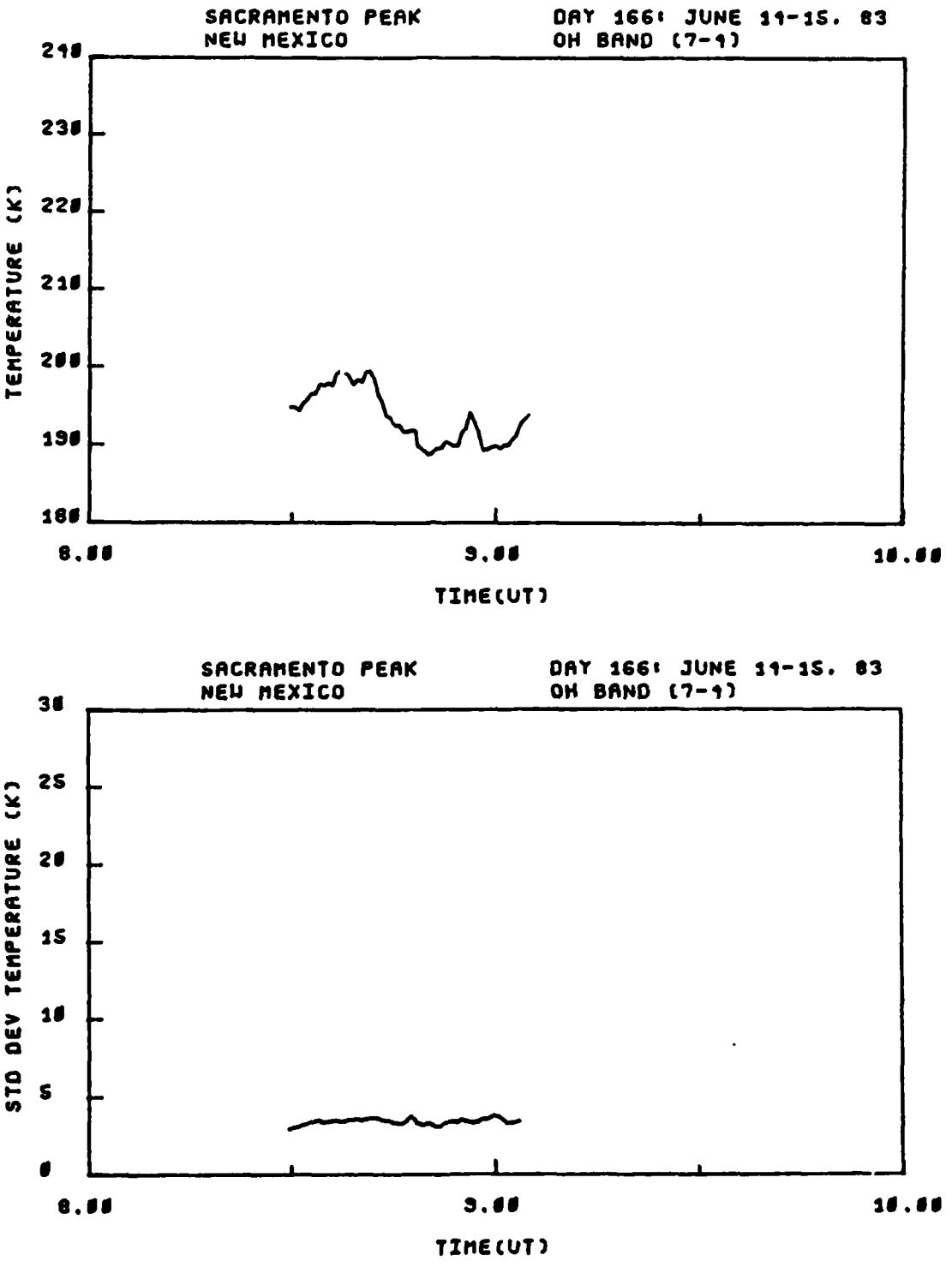

Figure C-48. OH (7,4) band smoothed rotational temperature and standard deviation, viewing angle = 15.5° El. 340° Az., day 166, 8:30-9:15 hrs. UT.

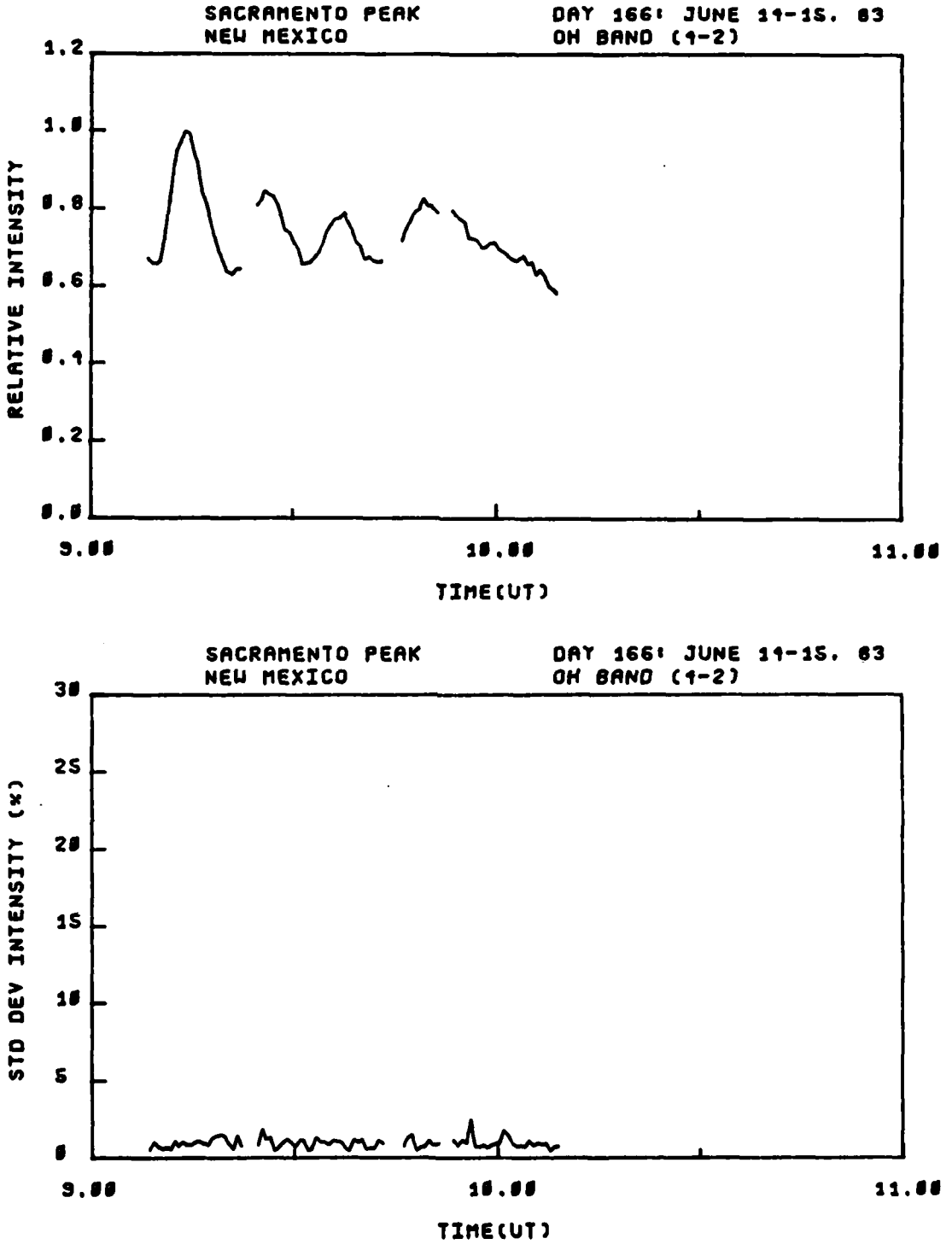

Figure C-49. OH (4,2) band relative intensity and standard deviation, viewing angle = 15.5° El. 309° Az., day 166, 9:15-10:15 hrs. UT.

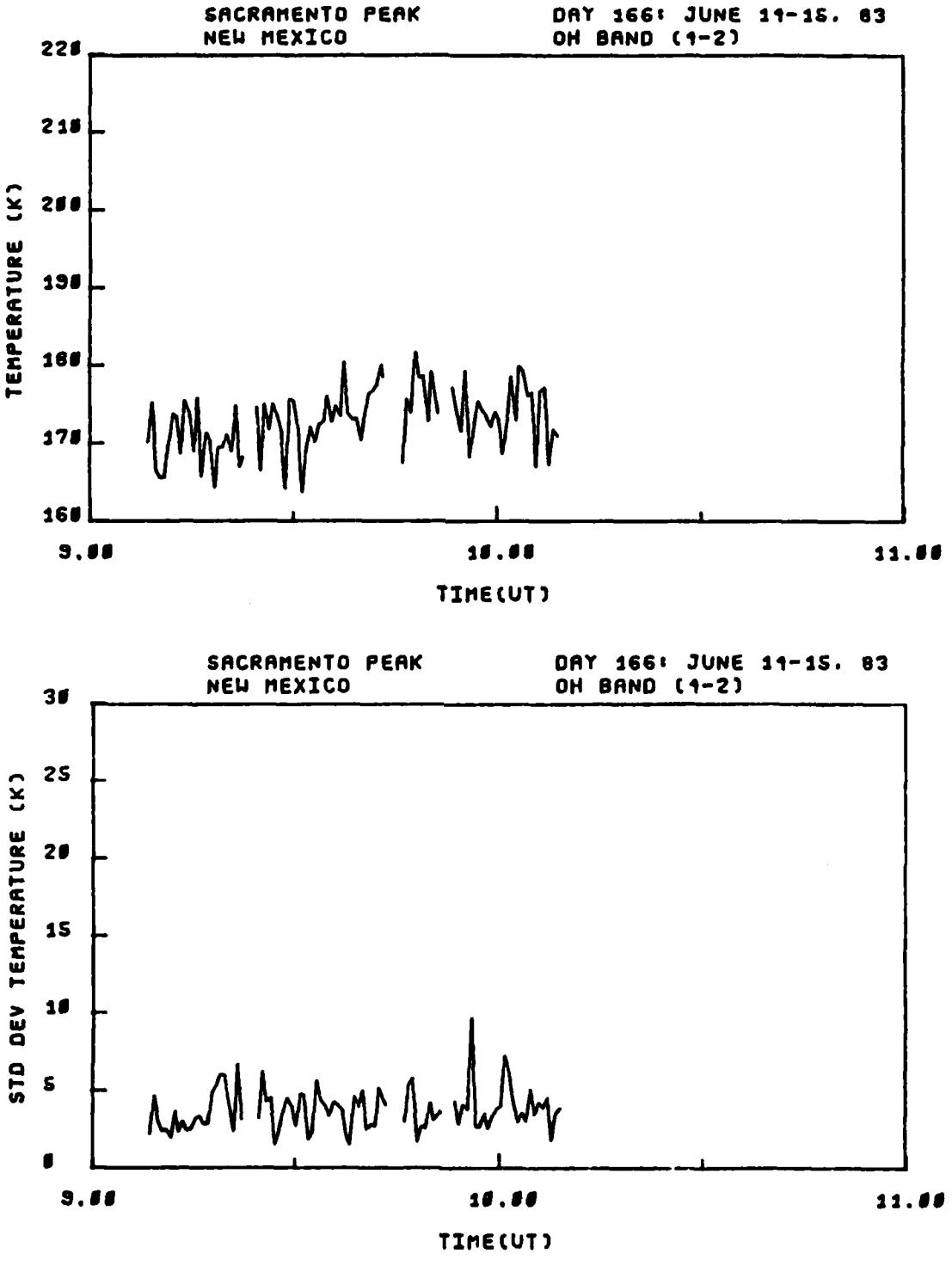

Figure C-50. OH (4,2) band rotational temperature and standard deviation, viewing angle = 15.5° El. 309° Az., day 166, 9:15-10:15 hrs. UT.

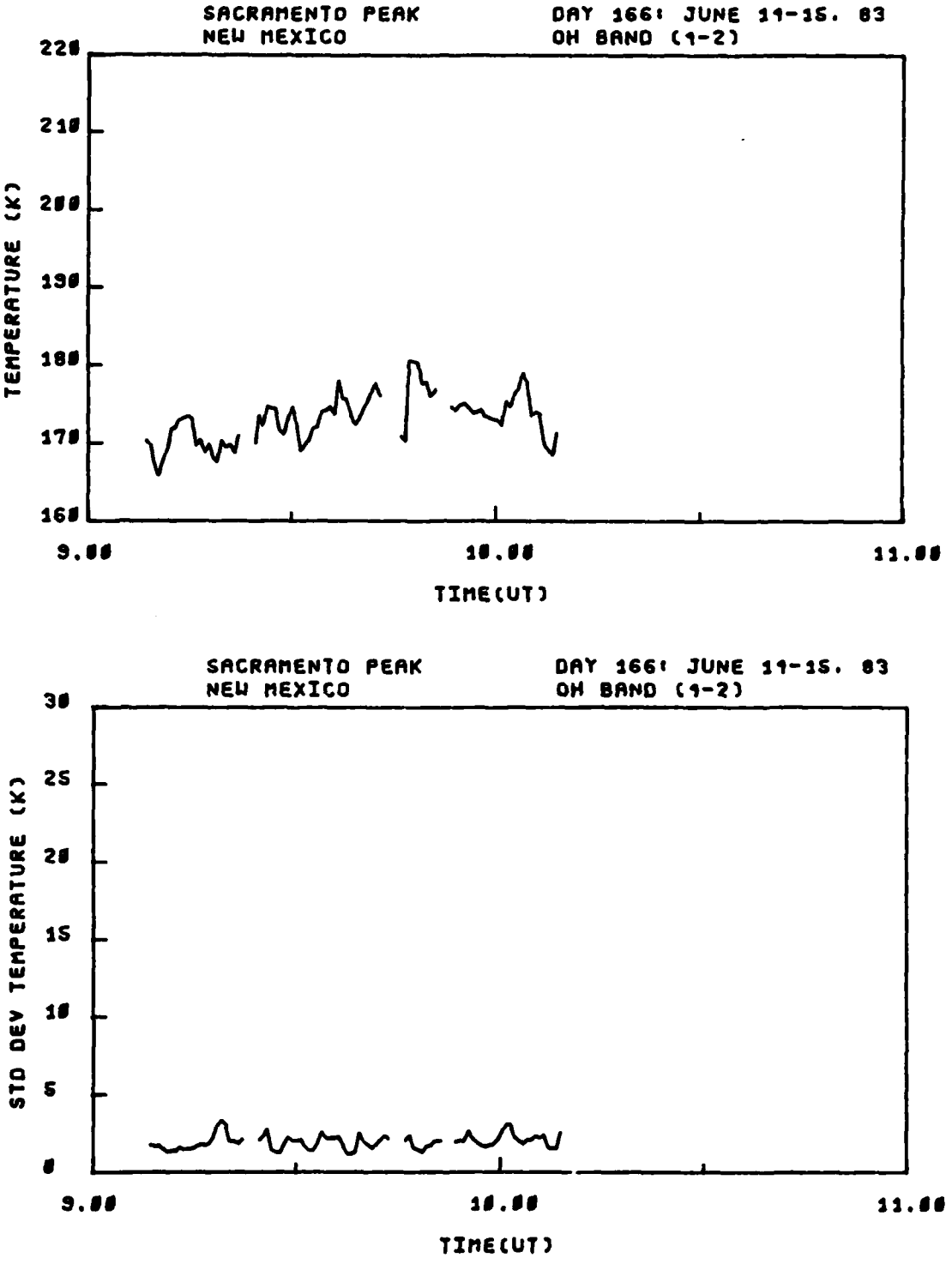

Figure C-51. OH (4,2) band smoothed rotational temperature and standard deviation, viewing angle = 15.5° El. 309° Az., day 166, 9:15-10:15 hrs. UT.

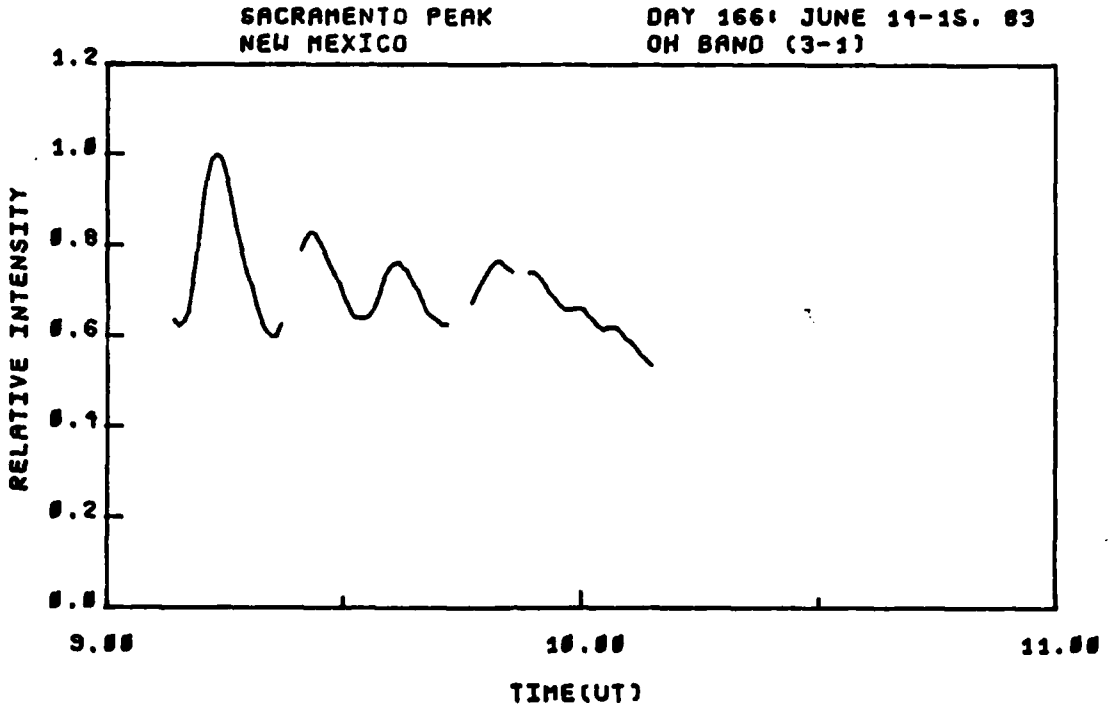

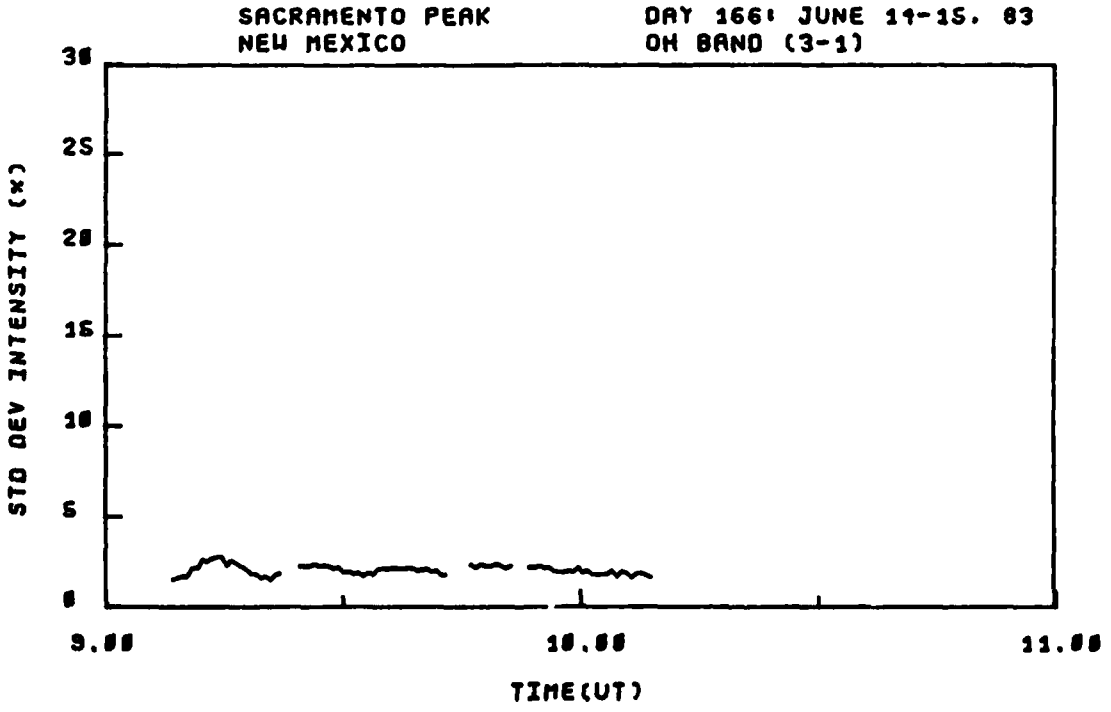

Figure C-52. OH (3,1) band relative intensity and standard deviation, viewing angle = 15.5° El. 309° Az., day 166, 9:15-10:15 hrs. UT.

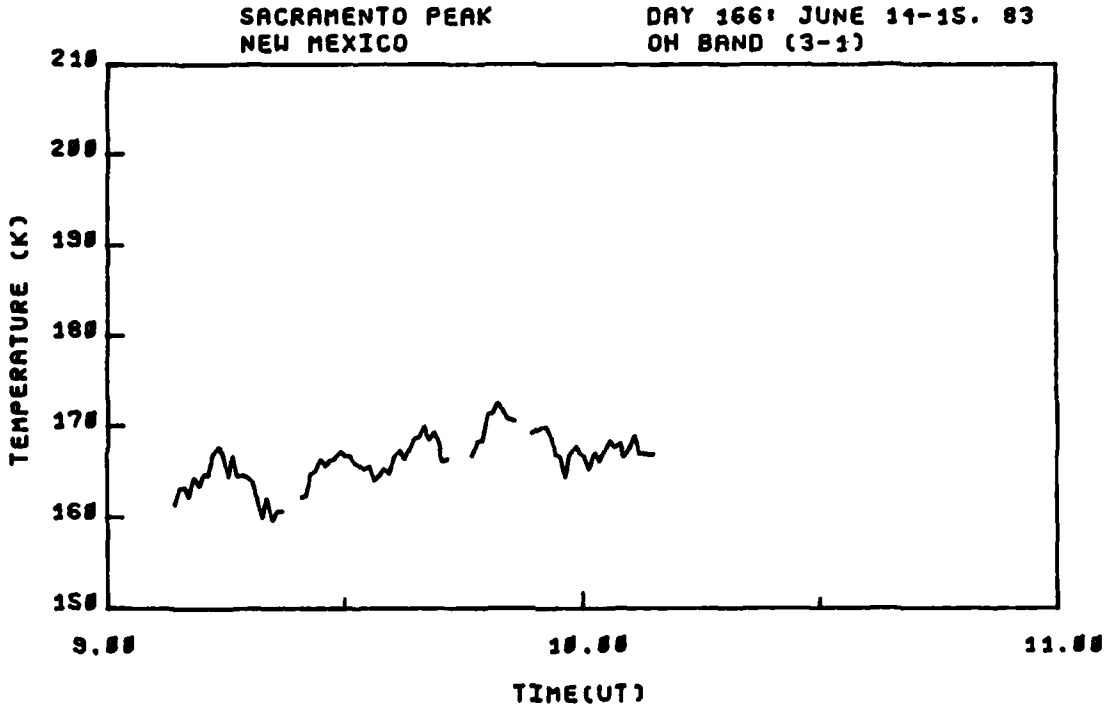

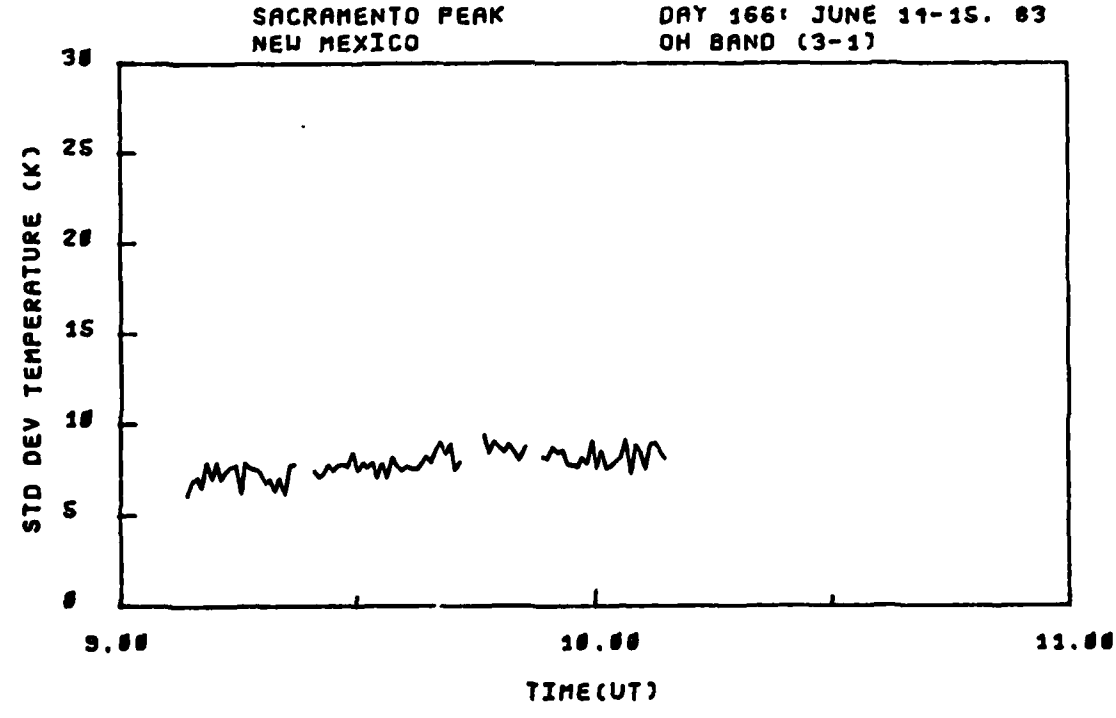

Figure C-53. OH (3,1) band rotational temperature and standard deviation, viewing angle = 15.5° El. 309° Az., day 166, 9:15-10:15 hrs. UT.

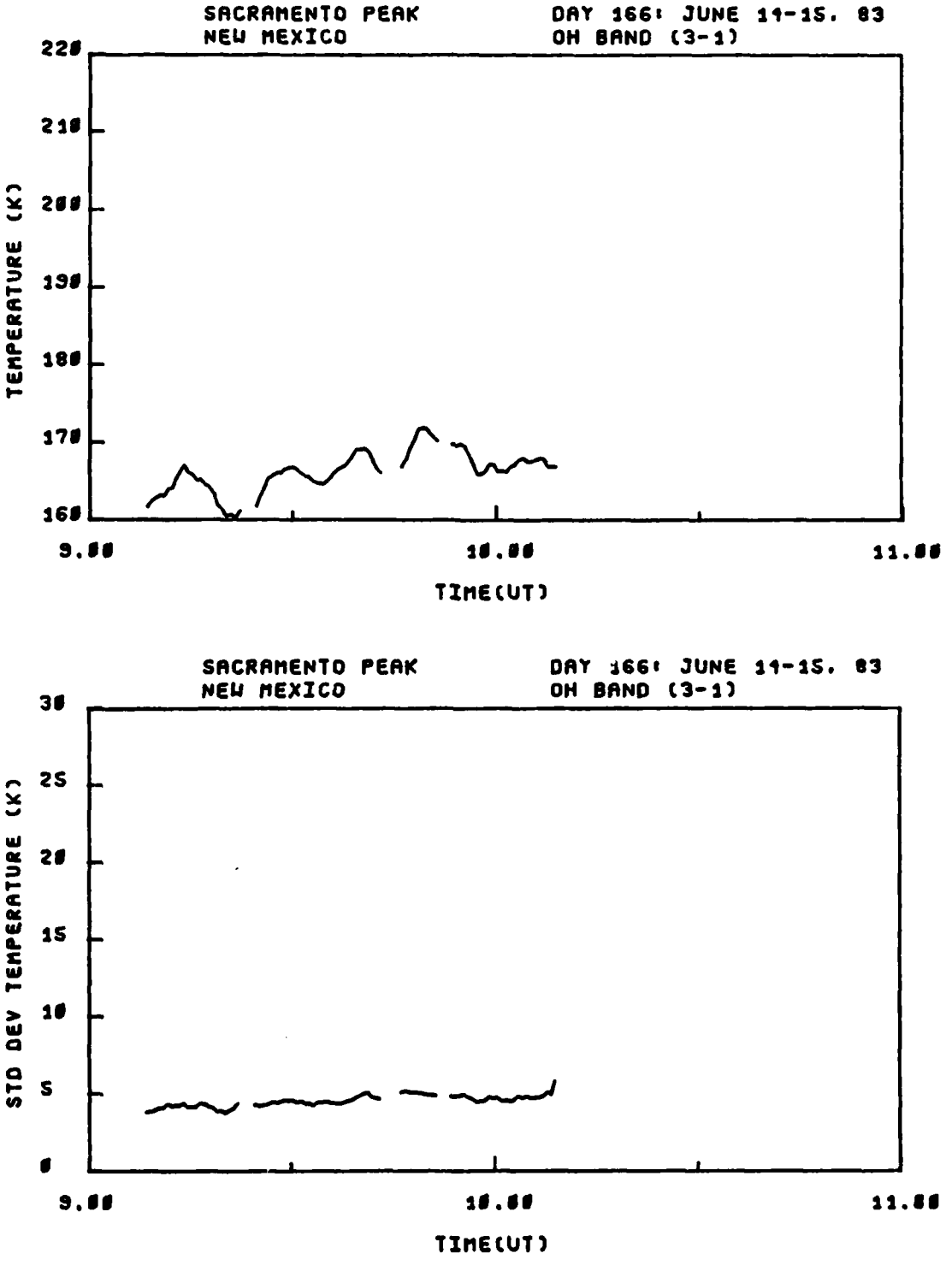

Figure C-54. OH (3,1) band smoothed rotational temperature and standard deviation, viewing angle = 15.5° El. 309° Az., day 166, 9:15-10:15 hrs. UT.

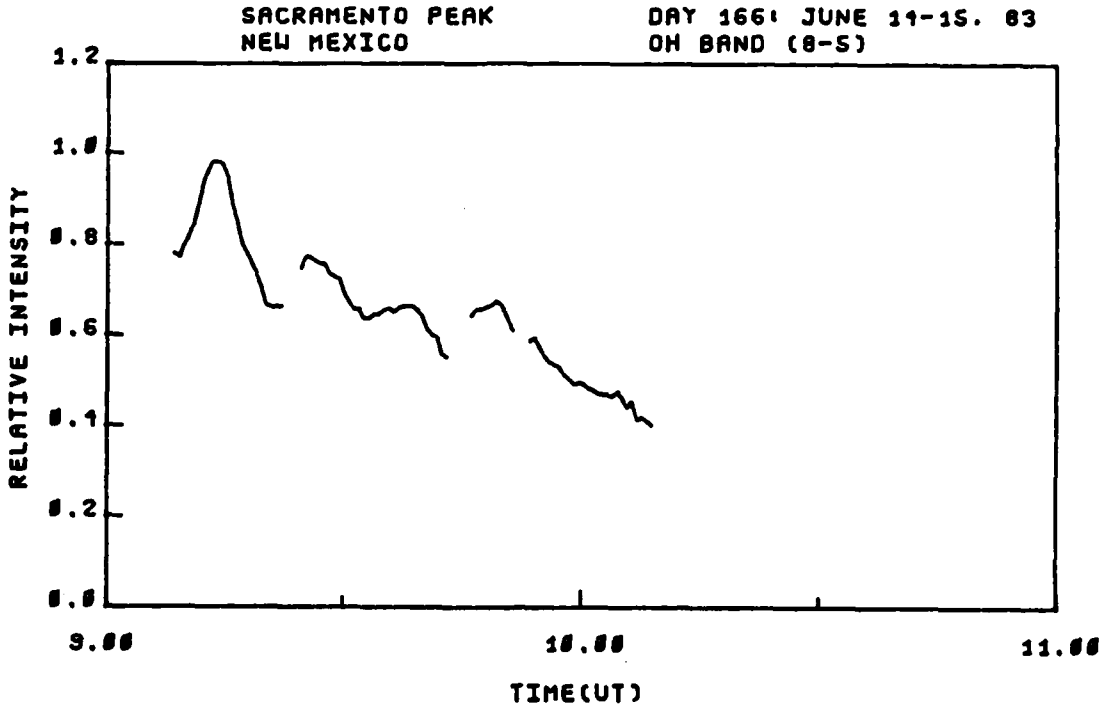

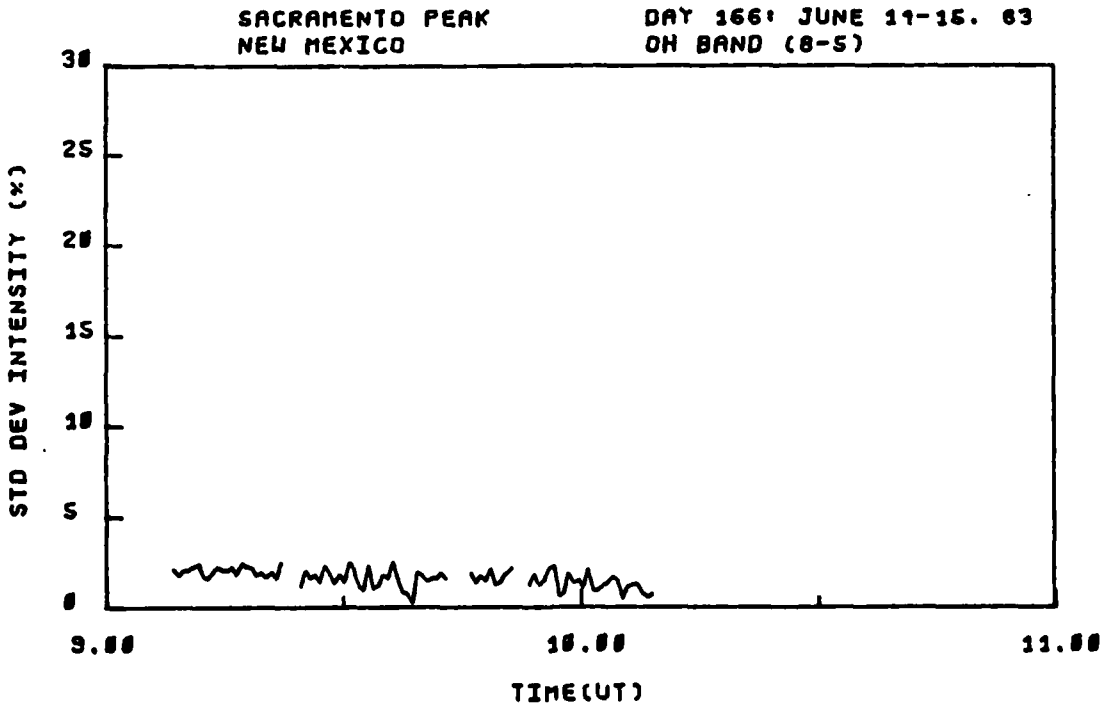

Figure C-55. OH (8,5) band relative intensity and standard deviation, viewing angle = 15.5° El. 309° Az., day 166, 9:15-10:15 hrs. UT.

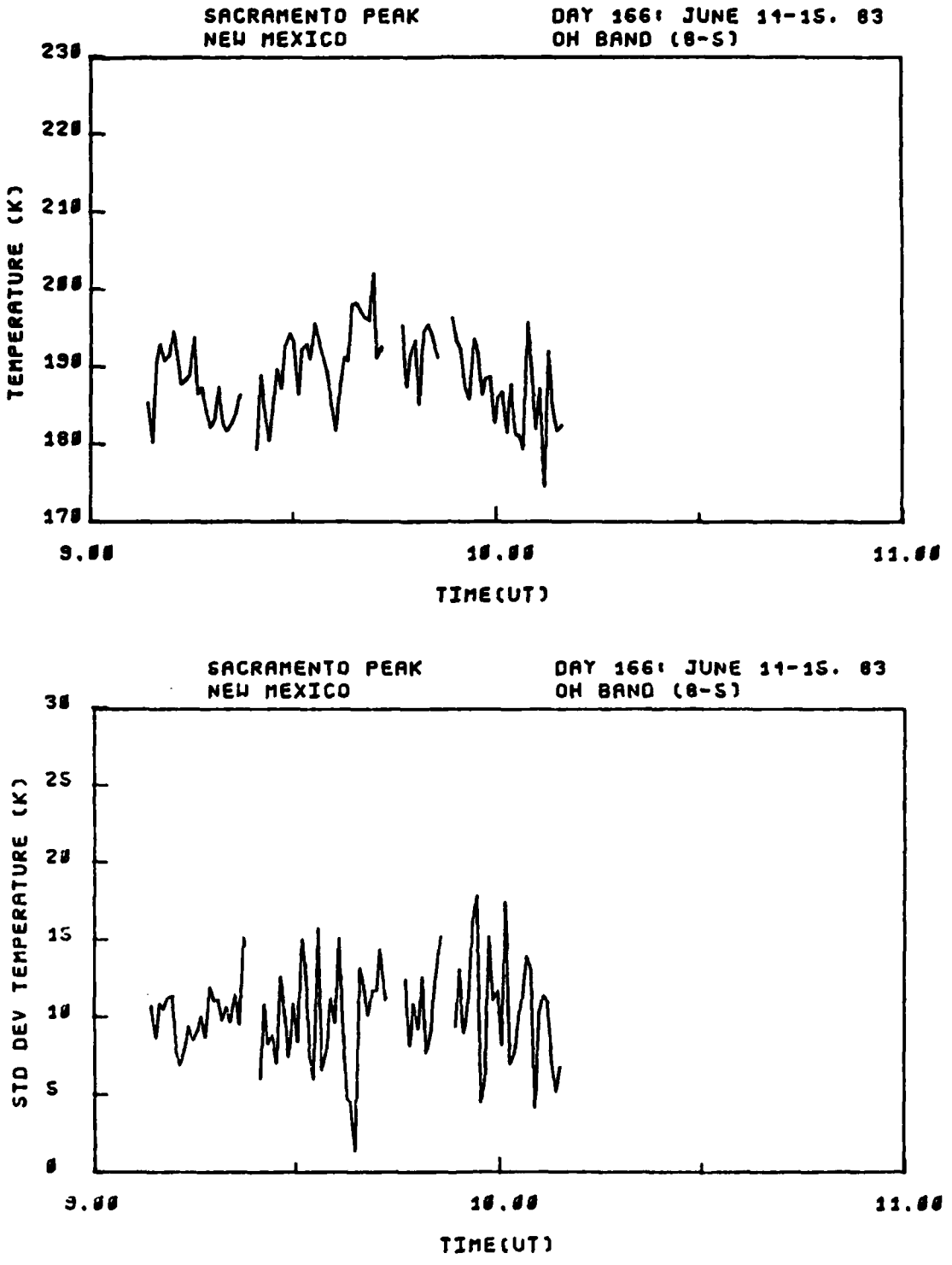

Figure C-56. OH (8,5) band rotational temperature and standard deviation, viewing angle = 15.5° El. 309° Az., day 166, 9:15-10:15 hrs. UT.

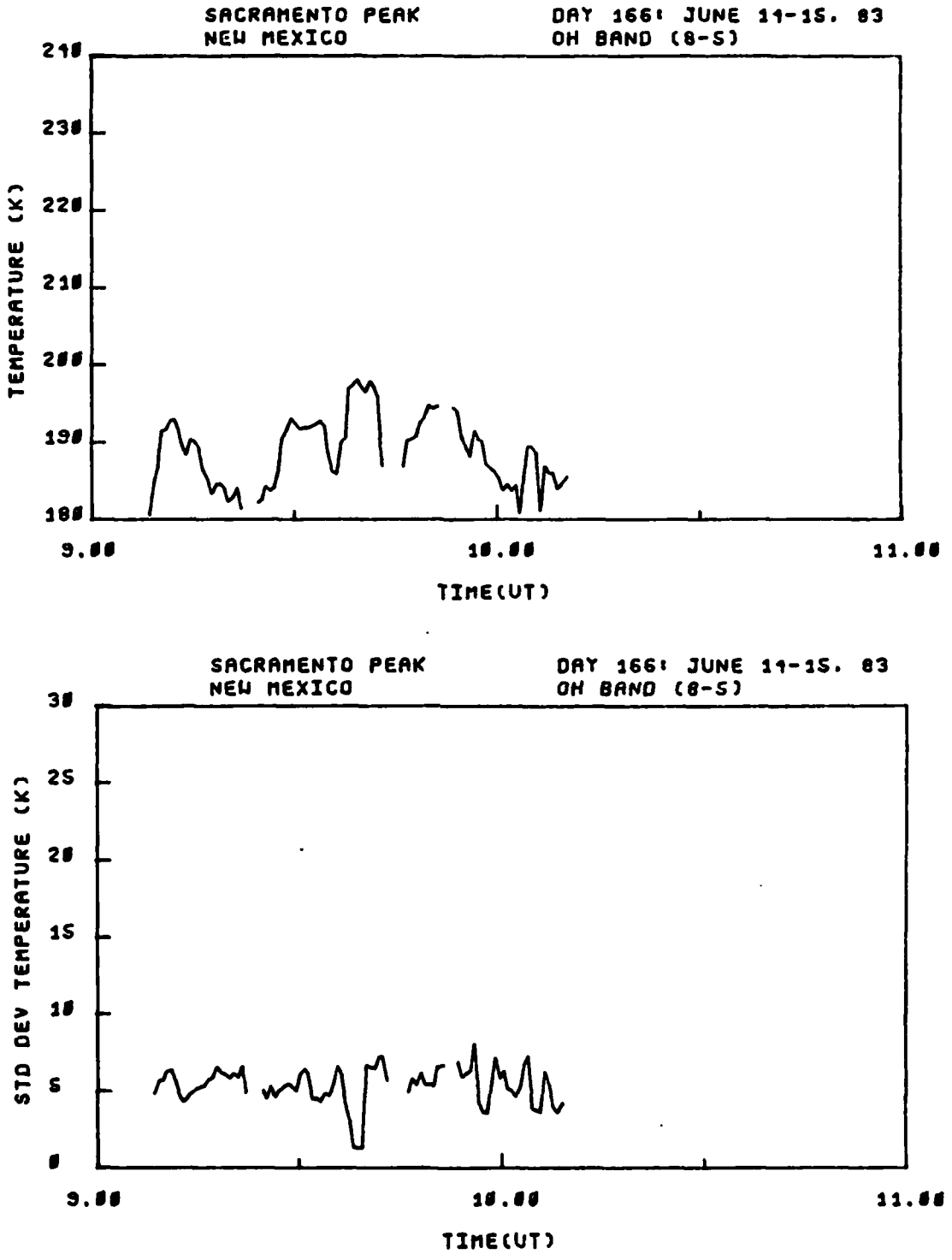

Figure C-57. OH (8,5) band smoothed rotational temperature and standard deviation, viewing angle = 15.5° El. 309° Az., day 166, 9:15-10:15 hrs. UT.

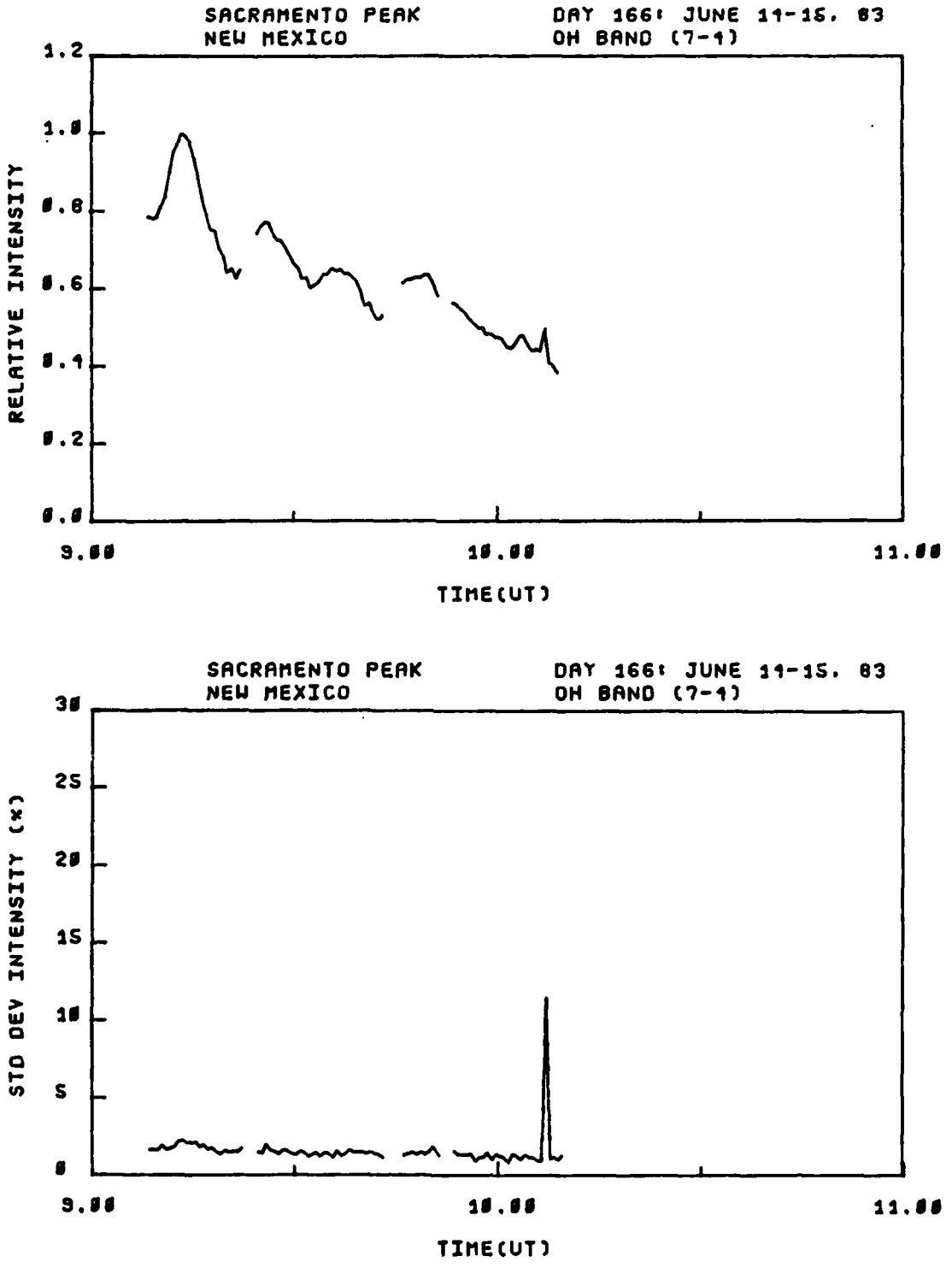

Figure C-58. OH (7,4) band relative intensity and standard deviation, viewing angle = 15.5° El. 309° Az., day 166, 9:15-10:15 hrs. UT.

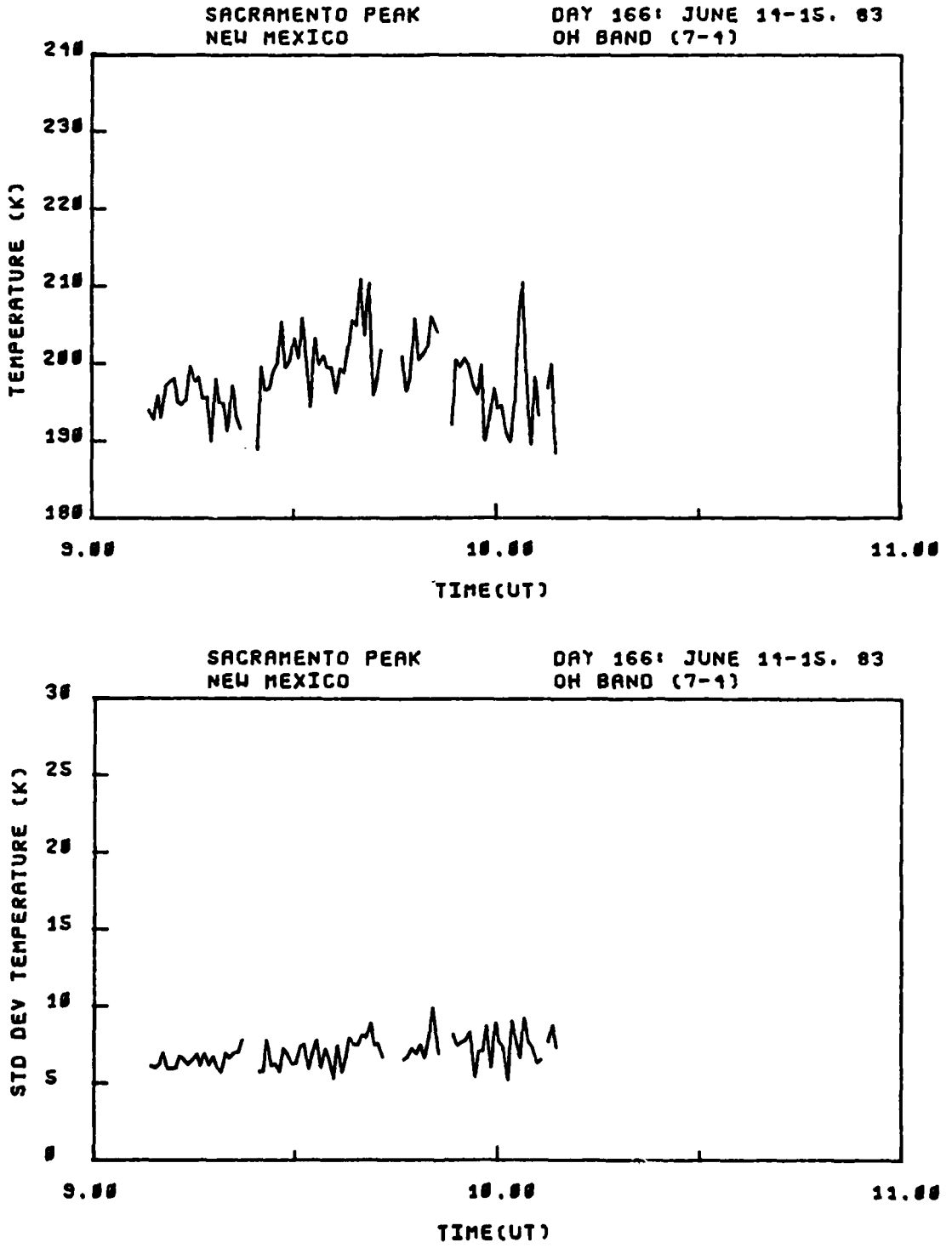

Figure C-59. OH (7,4) band rotational temperature and standard deviation, viewing angle = 15.5° El. 309° Az., day 166, 9:15-10:15 hrs. UT.

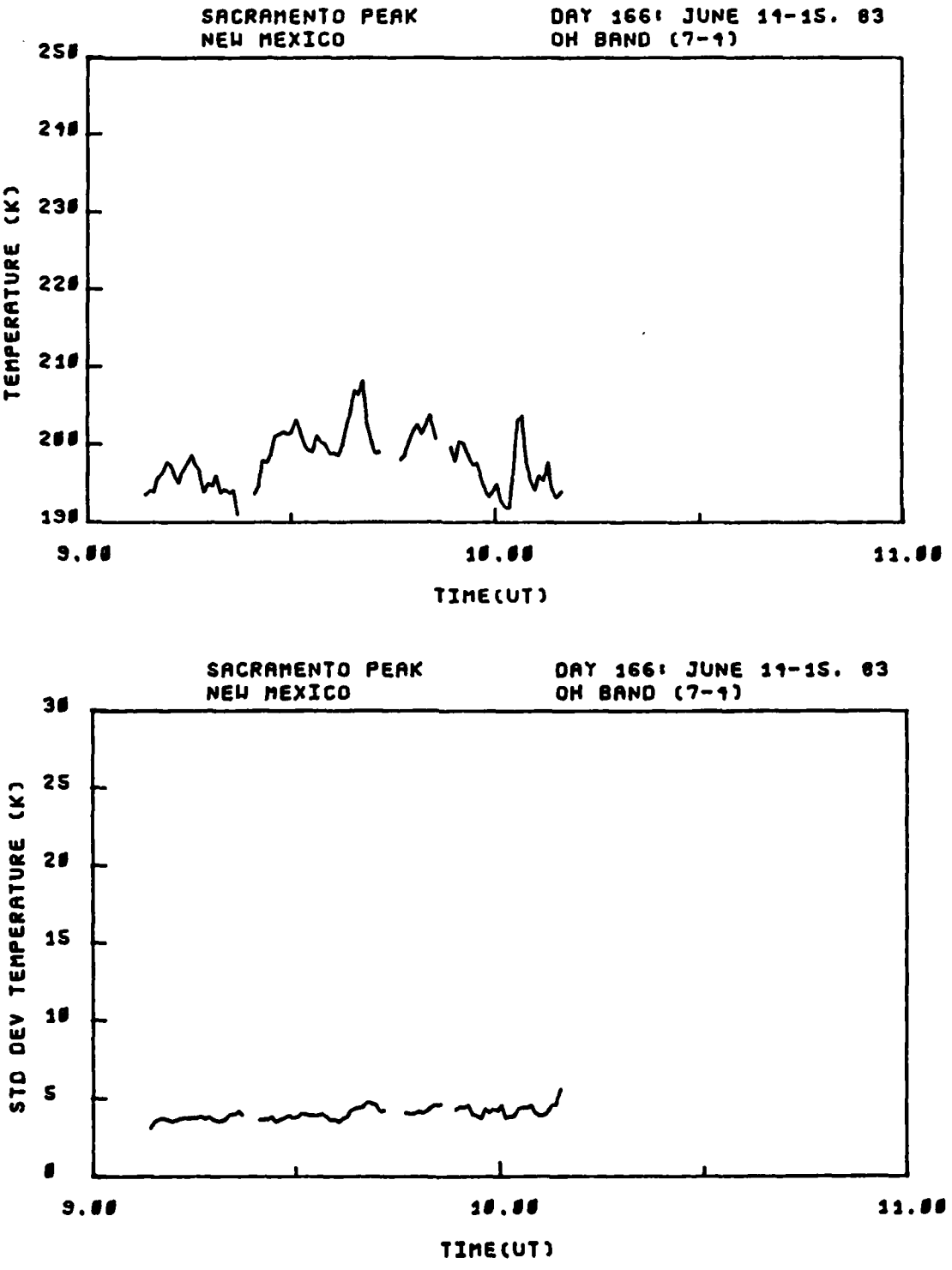

Figure C-60. OH (7,4) band smoothed rotational temperature and standard deviation, viewing angle = 15.5° El. 309° Az., day 166, 9:15-10:15 hrs. UT.

Appendix D

Computer Programs

```
C       FORTRAN IV PROGRAM

      C       FORTRAN IV PROGRAM
      C
      C       FILE NAME = BLTZMD
      C
      C       WRITTEN BY PARRIS NEAL
      C       UTAH STATE UNIVERSITY   JUNE 26,1984
      C
      C       PROGRAM TO CALCULATE THE ROTATIONAL TEMPERATURES
      C       USING OH SPECTRAL DATA
      C
      C       DATA FOR INSTRUMENT RESPONSE AND MOLECULAR CONSTANTS
      C       ARE GENERATED BY PROGRAMS "BBAMP & BBCT & DTAIPT"
      C
      C       DATA FOR OH SPECTRAL LINE STRENGTHS
      C       ARE GENERATED BY PROGRAM "LINAMP"
      C
      C       SUBROUTINES USED ARE:
      C               GNSCL - SCALES LINE STRENGTH DATA FOR FFT & POST AMP GAI
      C               MDLNM -  CALCULATES NORMALIZING FACTOR FOR BOLTZMAN MODEL
      C               BLDB  -  BUILDS ARRAY 'B' FOR LEAST SQUARE FITTING ROUTI
      C               BLDA  -  BUILDS ARRAY 'A' FOR LEAST SQUARE FITTING ROUTI
      C               ASCALE-  SCALES VECTORS IN ARRAY 'A' FOR UNIT LENGTH
      C               HFTI  -  LEAST SQUARE FITTING ROUTINE
      C               H12   -  USED BY HFTI
      C               DIFF  -  USED BY HFTI
      C               NFIT  -  ARRAY SHOWING WHICH LINES USED TO FIT MODEL
      C               NOISE -  CALCULATES STANDARD DEVIATION OF INTENSITY & TE
      C
            DIMENSION RLRS(60),XLSTR(60),SCL(2),H(2),G(2),
           1  RNORM(2),DI(14),B(14),A(14,2),RI(14),IHDTA(20),FIT(14)
      C
            DOUBLE PRECISION WAVN(60),F(60),C(60),EB(14),CB(14),SM,
           1  ANM,DF
      C
            INTEGER IP(2)
      C
      C***  REMIND OF I/O FILE UNIT ASSIGNMENTS
      C
            DO 15 I=1,15
            WRITE(4,10)
      10    FORMAT('     ')
      15    CONTINUE
            WRITE(4,20)
      20    FORMAT(' INPUT INSTRUMENT RESPOSE DATA   UNIT 5 ?')
            WRITE(4,30)
      30    FORMAT(' INPUT FFT LINE AMPLITUDE DATA   UNIT 6 ?')
            WRITE(4,40)
      40    FORMAT(' OUTPUT TEMPERATURE FILE         UNIT 7 ?')
            DO 50 I=1,10
            WRITE(4,10)
```

```
C       FORTRAN IV PROGRAM
 51   50      CONTINUE
 52   C
 53   C***    READ IN TOTAL NUMBER OF LINES FROM INST RES FILE
 54   C
 55           READ(5,100)ITL
 56   100     FORMAT(I6)
 57   C
 58   C***    READ IN MOLECULAR CONSTANTS AND RELATIVE RESPOSE
 59   C
 60           DO 110 I=1,ITL
 61           READ(5,120)WAVN(I),RLRS(I),F(I),C(I)
 62   120     FORMAT(B15.6,E15.6,B12.6,D15.8)
 63   110     CONTINUE
 64   C
 65   C***    READ IN TOTAL NUMBER OF FRAMES FROM LINE AMP FILE
 66   C
 67           READ(6,100)IFMS
 68           WRITE(7,205)IFMS
 69   205     FORMAT(I4)
 70   C
 71   C***    BEGIN TO PROCESS EACH FRAME OF DATA IN TURN
 72   C
 73           DO 9000 IF=1,IFMS
 74   C
 75   C***    READ IN HEADER INFO
 76   C
 77           DO 200 JF=1,10
 78           READ(6,100)IHDTA(JF)
 79   200     CONTINUE
 80   C
 81   C***    READ IN LINE AMPLITUDES
 82   C
 83           DO 210 JF=1,ITL
 84           READ(6,220)SN,XLSTR(JF)
 85   220     FORMAT(F10.2,E15.6)
 86   210     CONTINUE
 87   C
 88           WRITE(4,60)IHDTA(1),IHDTA(2)
 89   60      FORMAT(' FRAME ',I3,'-',I3,' HAS BEEN READ')
 90   C
 91   C***    SCALE LINE AMPLITUDE DATA FOR FFT & POST AMP GAINS
 92   C
 93           IFFT=IHDTA(8)
 94           IGN=IHDTA(10)
 95           CALL GNSCL(IFFT,IGN,ITL,XLSTR)
 96   C
 97   C***    SET UP INITIAL VALUES FOR PROCESS
 98   C
 99           MDA=14
100           MDB=14
```

```
C       FORTRAN IV PROGRAM

101           HCK=1.438833
102           TAU=0.5
103   C
104   C***    WRITE FRAME TIME TO DISK FILE
105   C
106           WRITE(7,225)IHDTA(2),IHDTA(4),IHDTA(5),IHDTA(6),IHDTA(7)
107   225     FORMAT(5I4)
108   C
109   C***    SET UP FOR 4-2 BAND
110   C
111           IBND=2
112           DF=F(5)
113           IBGN=1
114           IEND=12
115   C
116   C***    FILL ARRAY 'FIT' TO INDICATE WHICH DATA POINTS TO USE IN FIT
117   C
118           MQ=6
119           DO 230 IT=1,14
120           FIT(IT)=0.0
121   230     CONTINUE
122           FIT(1)=1.0
123           FIT(3)=1.0
124           FIT(5)=1.0
125           FIT(2)=1.0
126           FIT(4)=1.0
127           FIT(6)=1.0
128   C
129   C***    NUMBER OF DATA POINTS IN FIT = "MQ"
130   C
131           GO TO 5000
132   C
133   C***    SET UP FOR 3-1 BAND
134   C
135   2000    IBND=3
136           DF=F(17)
137           IBGN=13
138           IEND=24
139           GOTO 5000
140   C
141   C       3-5 BAND
142   C
143   3000    IBND=4
144           DF=F(31)
145           IBGN=25
146           IEND=38
147           MQ=4
148           FIT(1)=0.0
149           FIT(2)=0.0
150           FIT(3)=0.0
```

```
C       FORTRAN IV PROGRAM

151           FIT(4)=0.0
152           FIT(7)=1.0
153           FIT(8)=1.0
154           GOTO 5000
155   C
156   C       7-4 BAND
157   C
158   4000    IBND=5
159           DF=(45)
160           IBGN=39
161           IEND=52
162           MQ=12
163           FIT(1)=1.0
164           FIT(2)=1.0
165           FIT(3)=1.0
166           FIT(4)=1.0
167           FIT(10)=1.0
168           FIT(11)=1.0
169           FIT(13)=1.0
170           FIT(14)=1.0
171           GOTO 5000
172   C
173   9000    CONTINUE
174           GO TO 10000
175   C*************************************************************
176   C       TEMPERATURE CALCULATION
177   C
178   5000    TO=190.0
179           BO=HCK/TO
180           M=IEND-IBGN+1
181           N=2
182           NB=1
183           ANM=0.0
184           AO=0.0
185           KRANK=0
186   C
187   C***    FILL ARRAYS WITH BAND DATA
188   C
189           KJ=1
190           DO 300 JQ=IBGN,IEND
191           EB(KJ)=F(JQ)-DF
192           CB(KJ)=C(JQ)
193           RI(KJ)=RLRS(JQ)
194           DI(KJ)=XLSTR(JQ)
195           KJ=KJ+1
196   300     CONTINUE
197   C
198   C***    CALCULATE ARRAYS 'A' AND 'B' FOR LEAST SQUARE FIT TO FIND
199   C***    INITIAL BAND INTENSITY 'AO'
200   C
```

```
C       FORTRAN IV PROGRAM

201           CALL MDLNM(EB,CB,MDA,M,ANM,BO)
202           CALL BLDB(DI,MDA,M,AO,ANM,EB,CB,RI,BO,B)
203           CALL NFIT(B,MDA,M,FIT,2)
204           CALL BLDA(A,MDA,M,AO,RI,EB,CB,ANM,BO)
205           CALL NFIT(A,MDA,M,FIT,2)
206           CALL ASCALE(A,MDA,M,N,SCL)
207   C
208           N=1
209           CALL HFTI(A,MDA,M,N,B,MDB,NB,TAU,KRANK,RNORM,H,G,IP)
210           AO=B(1)/SCL(1)
211           BO=HCK/TO
212           N=2
213   C
214   C***    BEGIN ITERATION TO SOLVE FOR TEMPERATURE AND INTENSITY
215   C
216           DO 350 ILOP=1,50
217           CALL MDLNM(EB,CB,MDA,M,ANM,BO)
218           CALL BLDB(DI,MDA,M,AO,ANM,EB,CB,RI,BO,B)
219           CALL NFIT(B,MDA,M,FIT,1)
220           CALL BLDA(A,MDA,M,AO,RI,EB,CB,ANM,BO)
221           CALL NFIT(A,MDA,M,FIT,2)
222   C
223           CALL ASCALE(A,MDA,M,N,SCL)
224   C
225           CALL HFTI(A,MDA,M,N,B,MDB,NB,TAU,KRANK,RNORM,H,G,IP)
226   C
227   C***    TEST FOR CONVERGENCE OF TEMPERATURE
228   C
229           A1=B(1)/SCL(1)+AO
230           B1=B(2)/SCL(2)+BO
231           TEMPO=HCK/BO
232           TEMP1=HCK/B1
233           AO=A1
234           BO=B1
235   C
236           IF(ABS(TEMPO-TEMP1).LE.0.5) GO TO 370
237   350     CONTINUE
238   370     CONTINUE
239   C
240           IF(KRANK.EQ.MQ) GOTO 993
241           CALL NOISE(A,MDA,M,N,RNORM,KRANK,MQ,SCL,HCK,BO,SDA,SDT)
242   C
243   C***    WRITE OUT DATA TO FILE  UNIT 7
244   C
245   993     WRITE(7,995)ILOP,AO,SDA,TEMP1,SDT
246   995     FORMAT(I4,4E15.6)
247           IF(IBND.EQ.2)GOTO 2000
248           IF(IBND.EQ.3)GOTO 3000
249           IF(IBND.EQ.4)GOTO 4000
250           IF(IBND.EQ.5)GOTO 9000
```

```
C       FORTRAN IV PROGRAM

      10000   END
```

```
C       FORTRAN IV SUBROUTINE
```

```
      C       FORTRAN IV SUBROUTINE
      C
      C       FILE NAME = GNSCL
      C
      C       WRITTEN BY PARRIS NEAL
      C       UTAH STATE UNIVERSITY   JUNE 26,1984
      C
      C       SUBROUTINE SCALES DATA FOR FFT GAIN AND POST AMP GAIN
      C
            SUBROUTINE GNSCL(IFFT,IGN,ITL,XLSTR)
      C
            DIMENSION XLSTR(60)
      C
      C       SCALE FOR FFT GAIN
      C
            SL=0.0
            IF(IFFT.EQ.9) SL=1.0
            IF(IFFT.EQ.3) SL=0.5
            IF(IFFT.EQ.7) SL=0.25
            IF(IFFT.EQ.10)SL=2.0
            DO 100 I=1,ITL
            XLSTR(I)=XLSTR(I)*SL
      100   CONTINUE
      C
      C       SCALE FOR POST AMP GAIN
      C
            SL=0.0
            IF(IGN.EQ.5) SL=4.0
            IF(IGN.EQ.10)SL=2.0
            IF(IGN.EQ.20)SL=1.0
            IF(IGN.EQ.50)SL=0.4
            IF(IGN.EQ.100)SL=0.2
            DO 200 I=1,ITL
            XLSTR(I)=XLSTR(I)*SL
      200   CONTINUE
      C
            RETURN
            END
```

```
C       FORTRAN IV SUBROUTINE

C       FORTRAN IV SUBROUTINE
C
C       FILE NAME = MDLNM
C
C       WRITTEN BY PARRIS NEAL
C       UTAH STATE UNIVERSITY   JUNE 26.1984
C
C       SUBROUTINE CALCULATES THE NORMALIZING FACTOR FOR THE BOLTZMAN
C       TEMPERATURE MODEL
C
        SUBROUTINE MDLNM(EB,CB.MDA.M,ANM,BO)
C
        DOUBLE PRECISION EB(MDA),CB(MDA).ANM.DEXP
        ANM=0.0
        DO 100 I=1,M
        ANM=ANM+(CB(I)*DEXP(-EB(I)*BO))
100     CONTINUE
        RETURN
        END
```

```
C       FORTRAN IV SUBROUTINE

  1  C       FORTRAN IV SUBROUTINE
  2  C
  3  C       FILE NAME = BLDB
  4  C
  5  C       WRITTEN BY PARRIS NEAL
  6  C       UTAH STATE UNIVERSITY   JUNE 26,1984
  7  C
  8  C       SUBROUTINE BUILDS THE ARRAY "B" FOR BOLTZMAN MODEL
  9  C       LEAST SQUARE FITTING ROUTINE
 10  C
 11          SUBROUTINE BLDB(DI,MDA,M,AO,ANM,EB,CB,RI,BO,B)
 12  C
 13          DIMENSION RI(MDA),DI(MDA),B(MDA)
 14          DOUBLE PRECISION EB(MDA),CB(MDA),DEXP
 15  C
 16          DO 100 I=1,M
 17          XMOD=(AO*RI(I)*CB(I)*(DEXP(-EB(I)*BO)))/ANM
 18          B(I)=DI(I)-XMOD
 19  100     CONTINUE
 20          RETURN
 21          END
 22
```

```
C       FORTRAN IV SUBROUTINE

  1  C       FORTRAN IV SUBROUTINE
  2  C
  3  C       FILE NAME = BLDA
  4  C
  5  C       WRITTEN BY PARRIS NEAL
  6  C       UTAH STATE UNIVERSITY   JUNE 26,1984
  7  C
  8  C       SUBROUTINE BUILDS ARRAY "A" FOR BOLTZMAN MODEL
  9  C       DATA IS USED AS PART OF THE INFO FOR LEAST SQUARE DATA FITTING
 10  C
 11          SUBROUTINE BLDA(A,MDA,M,AO,RI,EB,CB,ANM,BO)
 12  C
 13          DIMENSION A(MDA,2),RI(MDA)
 14          DOUBLE PRECISION EB(MDA),CB(MDA),SM,DEXP
 15  C
 16          SM=0.0
 17          DO 100 I=1,M
 18          SM=SM+(CB(I)*EB(I)*(DEXP(-EB(I)*BO)))
 19  100     CONTINUE
 20  C
 21          ANM2=ANM*ANM
 22          DO 200 I=1,M
 23          TM=RI(I)*CB(I)*EXP(-EB(I)*BO)
 24          A(I,1)=TM/ANM
 25          T1=(AO*TM)/ANM2
 26          T2=SM-(EB(I)*ANM)
 27          A(I,2)=T1*T2
 28  200     CONTINUE
 29  C
 30          RETURN
 31          END
 32
```

```
C       FORTRAN IV SUBROUTINE

  1  C       FORTRAN IV SUBROUTINE
  2  C
  3  C       FILE NAME = ASCALE
  4  C
  5  C       WRITTEN BY PARRIS NEAL
  6  C       UTAH STATE UNIVERSITY  JUNE 26,1984
  7  C
  8  C       SUBROUTINE NORMALIZES THE VECTORS IN THE ARRAY "A"
  9  C       THE SCALING FACTOR IS RETURNED IN ARRAY SCL(I)
 10  C
 11          SUBROUTINE ASCALE(A,MDA,M,N,SCL)
 12  C
 13          DIMENSION A(MDA,N),SCL(N)
 14  C
 15          DOUBLE PRECISION SM,DSQRT
 16  C
 17          DO 100 I=1,N
 18          SM=0.0
 19          DO 110 J=1,M
 20          SM=SM+(A(J,I)*A(J,I))
 21  110     CONTINUE
 22          SCL(I)=DSQRT(SM)
 23  100     CONTINUE
 24  C
 25  C       SCALE ARRAY A BY THE SCALE FACTORS SCL(N)
 26  C
 27          DO 200 I=1,N
 28          DO 210 J=1,M
 29          IF(SCL(I).LT.1.0E-10) GO TO 205
 30          A(J,I)=A(J,I)/SCL(I)
 31          GO TO 210
 32  205     A(J,I)=0.0
 33  210     CONTINUE
 34  200     CONTINUE
 35          RETURN
 36          END
 37
```

```
C       FORTAN IV PROGRAM

      C       FORTAN IV PROGRAM
      C
      C       FILE NAME = HFTI
      C
              SUBROUTINE HFTI (A,MDA,M,N,B,MDB,NB,TAU,KRANK,RNORM,H,G,IP)
      C
      C       C.L.LAWSON AND R.J.HANSON, JET PROPULSION LABORATORY, 1973 JUN 12
      C       TO APPEAR IN 'SOLVING LEAST SQUARES PROBLEMS', PRENTICE-HALL, 197
      C           SOLVE LEAST SQUARES PROBLEM USING ALGORITHM, HFTI
      C
              DIMENSION A(MDA,N),B(MDB,NB),H(N),G(N),RNORM(NB)
              INTEGER IP(N)
              DOUBLE PRECISION SM,DZERO,DBLE
              SZERO=0.
              DZERO=0.DO
              FACTOR=0.001
      C
              K=0
              LDIAG=MIN0(M,N)
              IF (LDIAG.LE.0) GO TO 270
                  DO 80 J=1,LDIAG
                  IF (J.EQ.1) GO TO 20
      C
      C       UPDATE SQUARED COLUMN LENGTHS AND FIND LMAX
      C
                  LMAX=J
                      DO 10 L=J,N
                      H(L)=H(L)-A(J-1,L)**2
                      IF (H(L).GT.H(LMAX)) LMAX=L
          10          CONTINUE
                  IF(DIFF(HMAX+FACTOR*H(LMAX),HMAX)) 20,20,50
      C
      C        COMPUTE SQUARED COLUMN LENGTHS AND FIND LMAX
      C
          20      LMAX=J
                      DO 40 L=J,N
                      H(L)=0.
                          DO 30 I=J,M
          30              H(L)=H(L)+A(I,L)**2
                      IF (H(L).GT.H(LMAX)) LMAX=L
          40          CONTINUE
                  HMAX=H(LMAX)
      C
      C        LMAX HAS BEEN DETERMINED
      C
      C        DO COLUMN INTERCHANGES IF NEEDED
      C
          50      CONTINUE
                  IP(J)=LMAX
                  IF (IP(J).EQ.J) GO TO 70
```

```
C       FORTAN IV PROGRAM

 51                    DO 60 I=1,M
 52                    TMP=A(I,J)
 53                    A(I,J)=A(I,LMAX)
 54     60             A(I,LMAX)=TMP
 55                  H(LMAX)=H(J)
 56  C
 57  C           COMPUTE THE J-TH TANSFORMATION AND APPLY IT TO A AND B.
 58  C
 59     70           CALL H12 (1,J,J+1,M,A(1,J),1,H(J),A(1,J+1),1,MDA,N-J)
 60     80           CALL H12 (2,J,J+1,M,A(1,J),1,H(J),B,1,MDB,NB)
 61  C
 62  C           DETERMINE THE PSEUDORANK, K, USING THE TOLERANCE, TAU.
 63  C
 64                  DO 90 J=1,LDIAG
 65                  IF (ABS(A(J,J)).LE.TAU) GO TO 100
 66     90           CONTINUE
 67                  K=LDIAG
 68                  GO TO 110
 69    100           K=J-1
 70    110           KP1=K+1
 71  C
 72  C           COMPUTE THE NORMS OF THE RESIDUAL VECTORS.
 73  C
 74                  IF (NB.LE.0) GO TO 140
 75                      DO 130 JB=1,NB
 76                      TMP=SZERO
 77                      IF (KP1.GT.M) GO TO 130
 78                          DO 120 I=KP1,M
 79    120                       TMP=TMP+B(I,JB)**2
 80    130                   RNORM(JB)=SQRT(TMP)
 81    140           CONTINUE
 82  C                                          SPECIAL FOR PSEUDORANK = 0
 83                  IF (K.GT.0) GO TO 160
 84                  IF (NB.LE.0) GO TO 270
 85                      DO 150 JB=1,NB
 86                          DO 150 I=1,N
 87    150                       B(I,JB)=SZERO
 88                  GO TO 270
 89  C
 90  C           IF THE PSEUDORANK IS LESS THAN N COMPUTE HOUSEHOLDER
 91  C           DECOMPOSITION OF FIRST K ROWS
 92  C
 93    160           IF (K.EQ.N) GO TO 180
 94                      DO 170 II=1,K
 95                      I=KP1-II
 96    170               CALL H12 (1,I,KP1,N,A(I,1),MDA,G(I),A,MDA,1,I-1)
 97    180           CONTINUE
 98  C
 99  C
100                  IF (NB.LE.0) GO TO 270
```

```
C       FORTAN IV PROGRAM

101                 DO 260 JB=1.NB
102   C
103   C           SOLVE THE K BY K TRIANGULAR SYSTEM
104   C
105                       DO 210 L=1,K
106                       SM=DZERO
107                        I=KP1-L
108                       IF (I.EQ.K) GO TO 200
109                       IP1=I+1
110                            DO 190 J=IP1,K
111     190                    SM=SM+A(I,J)*DBLE(B(J,JB))
112     200               SM1=SM
113     210               B(I.JB)=(B(I,JB)-SM1)/A(I.I)
114   C
115   C           COMPLETE COMPUTATION OF SOLUTION VECTOR
116   C
117                   IF (K.EQ.N) GO TO 240
118                       DO 220 J=KP1,N
119     220               B(J,JB)=SZERO
120                       DO 230 I=1.K
121     230               CALL H12 (2,I,KP1,N,A(I,1).MDA.G(I),B(1.JB).1,MDB.1)
122   C
123   C           RE-ORDER THE SOLUTION VECTOR TO COMPENSATE FOR THE
124   C           COLUMN INTERCHANGES.
125   C
126     240               DO 250 JJ=1,LDIAG
127                       J=LDIAG+1-JJ
128                       IF (IP(J).EQ.J) GO TO 250
129                       L=IP(J)
130                       TMP=B(L.JB)
131                       B(L.JB)=B(J.JB)
132                       B(J.JB)=TMP
133     250               CONTINUE
134     260           CONTINUE
135   C
136   C           THE SOLUTION VECTORS. X. ARE NOW
137   C           IN THE FIRST N ROWS OF THE ARRAY B(.).
138   C
139     270       KRANK=K
140               RETURN
141               END
142
```

```
C       FORTRAN IV PROGRAM

  1  C       FORTRAN IV PROGRAM
  2  C
  3  C       FILE NAME = H12
  4  C
  5  C       SUBROUTINE H12 (MODE,LPIVOT,L1,M,U,IUE,UP,C,ICE,ICV,NCV)
  6  C       C.L.LAWSON AND R.J.HANSON, JET PROPULSION LABORATORY, 1973 JUN 1
  7  C       TO APPEAR IN 'SOLVING LEAST SQUARES PROBLEMS', PRENTICE-HALL, 197
  8  C
  9  C       CONSTRUCTION AND/OR APPLICATION OF A SINGELE
 10  C       HOUSEHOLDER TRANSFORMATION..  Q= I + U*(U**T)/B
 11  C
 12  C       MODE    =1 OR 2 TO SELECT ALGORITHM H1 OR H2
 13  C       LPIVOT IS THE INDEX OF THE PIVOT ELEMENT.
 14  C       L1, M   IF L1 .LE. M THE TRANSFORMATION WILL BE CONSTRUCTED TO
 15  C               ZERO ELEMENTS INDEXED FROM L1 THROUGH M.  IF L1 .GT. M
 16  C               THE SUBROUTINE DOES AN INDENTITY TRANSFORMATION.
 17  C       U(),IUE,UP      ON ENTRY TO H1 U() CONTAINS THE PIVOT VECTOR.
 18  C                       IUE IS THE STORAGE INCREMENT BETWEEN ELEMENTS.
 19  C                                       ON EXIT FROM H1 U() AND UP
 20  C                       CONTAIN QUANTITIES DEFINING THE VECTOR U OF THE
 21  C                       HOUSEHOLDER TRANSFORMATION.  ON ENTRY TO H2 U()
 22  C                       AND UP SHOULD CONTAIN QUANTITIES PREVIOUELY COMPUTE
 23  C                       BY H1.  THESE WILL NOT BE MODFIED BY H2.
 24  C       C()     ON ENTRY TO H1 OR H2 C() CONTAINS A MATRIX WHICH WILL BE
 25  C               REGARDED AS A SET OF VECTORS TO WHICH THE HOUSEHOLDER
 26  C               TRANSFORMATION IS TO BE APPLIED.  ON EXIT C() CONTAINS TH
 27  C               SET OF TRANSFORMED VECTORS.
 28  C       ICE     STORAGE INCREMENT BETWEEN ELEMENTS OF VECTORS IN C()
 29  C       ICV     STORAGE INCREMENT BETWEEN VECTORS IN C().
 30  C       NCV     NUMBER OF VECTORS IN C() TO BE TRANSFORMED.  IF NCV .LE.
 31  C               NO OPERATIONS WILL BE DONE ON C().
 32  C
 33          SUBROUTINE H12 (MODE,LPIVOT,L1,M,U,IUE,UP,C,ICE,ICV,NCV)
 34          DIMENSION U(IUE,M),C(1)
 35          DOUBLE PRECISION SM,B,DBLE
 36          ONE=1.
 37  C
 38          IF (0.GE.LPIVOT.OR.LPIVOT.GE.L1.OR.L1.GT.M) RETURN
 39          CL=ABS(U(1,LPIVOT))
 40          IF (MODE.EQ.2) GO TO 60
 41  C                   ****** CONSTRUCT THE TRANSFORMATION ******
 42          DO 10 J=L1,M
 43  10      CL=AMAX1(ABS(U(1,J)),CL)
 44          IF (CL) 130,130,20
 45  20      CLINV=ONE/CL
 46          SM=(DBLE(U(1,LPIVOT))*CLINV)**2
 47          DO 30 J=L1,M
 48  30      SM=SM+(DBLE(U(1,J))*CLINV)**2
 49  C                           CONVERT DBLE. PREC. SM TO SNGL. PREC. SM1
 50          SM1=SM
```

```
C       FORTRAN IV PROGRAM

 51             CL=CL*SQRT(SM1)
 52             IF (U(1,LPIVOT)) 50,50,40
 53  40         CL=-CL
 54  50         UP=U(1,LPIVOT)-CL
 55             U(1,LPIVOT)=CL
 56             GO TO 70
 57  C                ****** APPLY THE TRANSFORMATION I+U*(U**T)/B TO C ******
 58  C
 59  60         IF (CL) 130,130,70
 60  70         IF (NCV.LE.0) RETURN
 61             B=DBLE(UP)*U(1,LPIVOT)
 62  C                           B MUST BE NONPOSITIVE HERE.  IF B=0., RETURN
 63  C
 64             IF (B) 80,130,130
 65  80         B=ONE/B
 66             I2=1-ICV+ICE*(LPIVOT-1)
 67             INCR=ICE*(L1-LPIVOT)
 68             DO 120 J=1,NCV
 69             I2=I2+ICV
 70             I3=I2+INCR
 71             I4=I3
 72             SM=C(I2)*DBLE(UP)
 73             DO 90 I=L1,M
 74             SM=SM+C(I3)*DBLE(U(1,I))
 75             I3=I3+ICE
 76  90         CONTINUE
 77             IF (SM) 100,120,100
 78  100        SM=SM*B
 79             C(I2)=C(I2)+SM*DBLE(UP)
 80             DO 110 I=L1,M
 81             C(I4)=C(I4)+SM*DBLE(U(1,I))
 82             I4=I4+ICE
 83  110        CONTINUE
 84  120        CONTINUE
 85  130        RETURN
 86             END
 87
```

```
C       FORTRAN IV FUNCTION
```

```
      C       FORTRAN IV FUNCTION
      C
      C       FILE NAME = DIFF
      C
              FUNCTION DIFF(X,Y)
      C
      C       C.L. LANSON AND R.J. HANSON, JET PROPULSION LABRATORY, 7 JUN 1973
      C       TO APPEAR IN 'SOLVING LEAST SQUARES PROBLEMS', PRENTICE-HALL 1974
      C
              DIFF=X-Y
              RETURN
              END
```

```
C       FORTRAN IV SUBROUTINE

  1  C       FORTRAN IV SUBROUTINE
  2  C
  3  C       FILE NAME = NFIT
  4  C
  5  C       WRITTEN BY PARRIS NEAL
  6  C       UTAH STATE UNIVERSITY  JUNE 29,1984
  7  C
  8  C       SUBROUTINE TAKES ARRAY 'A' AND MULTPLIES EACH ROW BY
  9  C       THE CORRESPONDING VALUE IN ARRAY 'NFIT'
 10  C
 11          SUBROUTINE NFIT(A,MDA,M,FIT,N)
 12  C
 13          DIMENSION A(MDA,N),FIT(MDA)
 14  C
 15          DO 100 I=1,N
 16          DO 110 J=1,M
 17          A(J,I)=FIT(J)*A(J,I)
 18  110     CONTINUE
 19  100     CONTINUE
 20          RETURN
 21          END
 22
```

```
C       FORTRAN IV SUBROUTINE
```

```
      C       FORTRAN IV SUBROUTINE
      C
      C       FILE NAME = NOISE
      C
      C       WRITTEN BY PARRIS NEAL
      C       UTAH STATE UNIVERSITY   JUNE 29, 1984
      C
      C       SUBROUTINE TAKES RESIDUE FROM LEAST SQUARE FITTING ROUTINE
      C       'HFTI' AND CALCULATES THE STANDARD DEVIATION OF THE
      C       BAND INTENSITY "A" AND THE TEMPERATURE "T"
      C
              SUBROUTINE NOISE(A,MDA,M,N,RNORM,KRANK,MQ,SCL,HCK,BO,SDA,SDT)
      C
              DIMENSION A(MDA,N),SCL(N)
      C
              VARN=(RNORM**2)/(MQ-KRANK)
              VNA=(((A(2,2)**2)*(A(1,2)**2))/((A(1,1)*A(2,2))**2))*VARN
              SDA=(SQRT(VNA))/SCL(1)
              SDB=(SQRT(VARN/(A(2,2)**2)))/SCL(2)
              SDT=(SDB*HCK)/(BO**2)
              RETURN
              END
```

```
C       FORTRAN IV PROGRAM

  1  C       FORTRAN IV PROGRAM
  2  C
  3  C       FILE NAME = LINAMP
  4  C
  5  C       WRITTEN BY PARRIS NEAL
  6  C       UTAH STATE UNIVERSITY   MAY 23,1984
  7  C
  8  C       THIS PROGRAM READS FFT FILES FROM TAPE
  9  C       DATA IS CONVERTED TO FORTRAN IV FORMAT
 10  C       HEADER INFO IS READ
 11  C               TAPE NUMBER
 12  C               DATA FRAME NUMBER
 13  C               FFT EXPONENT
 14  C               A/D GAIN
 15  C               DATE (YEAR,DAY.HOUR,MIN,SEC)
 16  C       FFT IS READ, PHASE CORRECTED, AND LINE AMPLITUDES FOUND
 17  C               THE SAMPLE NUMBER WHERE THE LINE IS EXPECTED TO BE
 18  C               IS READ FROM A DISK FILE AND A SEARCH IS USED TO FIND
 19  C               THE ACTUAL PEAK VALUE USING A HAMMING APODIZATION ROUTIN
 20  C
 21  C       SUBROUTINES USED ARE
 22  C               TAPE.TAPE8          - TAPE DRIVE UTILITIES
 23  C               SPCONV              - CONVERT 12 BIT TO FORTRAN IV 36 BIT
 24  C               FFTRK,RK05C         - DISK DRIVE UTILITIES
 25  C               PHASEC              - PHASE CORRECTION ROUTINE
 26  C               APODI               - HAMMING APODIZATION/INTERPOLATION
 27  C               DTIME               - CONVERTS HEADER INFO TO DATE/TIME
 28  C               LINIT               - INPUTS FRAME NUMBERS TO BE PROCESSED
 29  C               SEARCH              - SEARCHES FOR PEAK AMPLITUDE OF LINES
 30  C               REALPT              - LOADS MEMORY WITH REAL PART OF FFT
 31  C
 32          COMMON/RK05C/BUFO,BUFFER(2047),HBUFO,HBUFF(2047),XRING(1024),
 33        1 YRING(1024),IDATA
 34          DIMENSION IPASS(5),INFRAM(30),IHDTA(10),IGAIN(15),IPOS(60)
 35          DOUBLE PRECISION WAVN(60)
 36  C
 37  C****   READ IN INITIAL VALUES
 38  C
 39          ITFMS=0
 40          NGRPS=0
 41          CALL LINIT(NGRPS,INFRAM,IGAIN,ITFMS)
 42  C
 43  C       WRITE TO OUTPUT FILE TOTAL # OF FRAMES PROCESSED
 44  C
 45          WRITE(6,606)ITFMS
 46  C
 47  C****   WINDOW WIDTHS FOR (# SAMPLES) PHASE CORRECTION ROUTINE
 48  C
 49          IPASS(1)=3
 50          IPASS(2)=5
```

```
C       FORTRAN IV PROGRAM

      IPASS(3)=0
      IPASS(4)=17
      IPASS(5)=65
      NSZ=12
      NPASS=5
      IDATA=1
C
C****   INITIALIZE FFT INPUT TAPE DRIVE
C
      WRITE(4,160)
160   FORMAT('    ')
      WRITE(4,200)
200   FORMAT(' INPUT TAPE DRIVE NUMBER ',$)
      READ(4,110)IDRV
110   FORMAT(I4)
      IF (IDRV.EQ.1)IDRV=2
      IOPR=4
      CALL TAPE(IDRV,2,BUFO,0)
C
C****   READING IN LINE POSITIONS
C
      WRITE(4,160)
      WRITE(4,162)
162   FORMAT(' READING IN LINE POSITIONS')
      READ(5,606)ITL
      DO 170 I=1,ITL
      READ(5,607)IPOS(I),WAVN(I)
607   FORMAT(I6,B15.6)
170   CONTINUE
C
C****   SPACE AHEAD TO FIRST TAPE HEADER
C
      CALL TAPE(IDRV,4,BUFO,2)
C
C****   SPACE TO RECORD SPECIFIED BY INFRAM(1)
C
      ICOUNT=INFRAM(1)-1
      IF(ICOUNT.EQ.0) GO TO 210
      ICOUNT=ICOUNT*2
      CALL TAPE(IDRV,4,BUFO,ICOUNT)
210   CONTINUE
C
C****   START READING DATA
C
      JZ=1
      DO 2000 IJ=1,NGRPS
      DO 1000 IFM=INFRAM(JZ),INFRAM(JZ+1)
C
C*************************************************
C
```

```
C       FORTRAN IV PROGRAM
C       READING HEADER INFO
C
C               XRING(30)=TAPE #
C               XRING(24)=DATA FRAME #
C               XRING(14)=FFT EXPONENT
C               XRING(5) =A/D GAIN
C               XRING(6-)=DATE/TIME
C
C*******************************************************
C
        CALL TAPE(IDRV,7,XRING,256)
        CALL SPCONV(XRING,XRING,256)
        IHDTA(1)=XRING(30)
        IHDTA(2)=XRING(24)
        IHDTA(8)=XRING(14)
        IHDTA(9)=XRING(5)
        IHDTA(10)=IGAIN(IJ)
        CALL DTIME(XRING(6),YEAR,DAY,HOUR,MIN,SEC)
        IHDTA(3)=YEAR
        IHDTA(4)=DAY
        IHDTA(5)=HOUR
        IHDTA(6)=MIN
        IHDTA(7)=SEC
        WRITE(3,525)IHDTA(1),IHDTA(2)
525     FORMAT(' ACTUALLY READ TAPE # ',I6,'    FRAME # ',I6)
C
C****   READING IN FFT RECORDS 5,6 WHICH CONTAIN ALL LINES FOR
C       4-2,5-1,8-5,7-4 OH BANDS
C
        WRITE(4,160)
        WRITE(4,520)IFM
520     FORMAT(" READING IN TRANSFORM ",I4,"  FROM TAPE")
C
C****   SPACE TO RECORD 5
C
        CALL TAPE(IDRV,5,BUF0,4)
C
C****   READ RECORD 5
C
        CALL TAPE(IDRV,7,BUF0,2048)
        CALL SPCONV(BUF0,BUF0,2048)
        ICYLD=0
        IERR=0
        CALL FFTRK(IDATA,ICYLD,1,BUF0,IERR)
C
C****   READ RECORD 6
C
        CALL TAPE(IDRV,7,BUF0,2048)
C
        CALL SPCONV(BUF0,BUF0,2048)
```

```
C       FORTRAN IV PROGRAM

151           ICYLD=1
152           CALL FFTRK(IDATA,ICYLD,1,BUFO,IERR)
153   C
154   C****   READY TO PHASE CORRECT DATA
155   C
156           WRITE(4,160)
157           WRITE(4,540)IFM
158   540     FORMAT(" PHASE CORRECTING FFT FRAME # ",I4)
159           CALL PHASEC(NSZ,NPASS,IPASS)
160           WRITE(4,550)
161   550     FORMAT(" PHASE CORRECTION COMPLETE")
162   C
163   C****   WRITE OUT HEADER DATA TO LINE AMPLITUDE FILE
164   C
165           DO 605 IQ=1,10
166           WRITE(6,606)IHDTA(IQ)
167   606     FORMAT(I6)
168   605     CONTINUE
169   C
170   C****   READ PHASE CORRECTED DATA IN FOR LINE AMPLITUDE SEARCH
171   C
172           CALL REALPT
173   C
174   C****   READ IN HAMMING TABLE VALUES INTO COMMON AREA 'BUFFER'
175   C
176           READ(7)BUFO.BUFFER
177           REWIND 7
178   C
179   C****   START TO FIND LINE POSITIONS AND AMPLITUDES
180   C
181           WRITE(4,850)IFM
182   850     FORMAT(' SEARCHING FRAME # ',I4)
183           DO 900 IT=1,ITL
184           IPST=IPOS(IT)
185           XOFS=0.0
186           VLFS=0.0
187           CALL SEARCH(IPST,XOFS,VLFS)
188   C
189   C****   WRITE SAMPLE NUMBER AND AMPLITUDE TO DISK
190   C
191           WRITE(6,785)XOFS,VLFS
192   785     FORMAT(F10.2,E15.6)
193   900     CONTINUE
194   C
195   C****   SPACE TO NEXT HEADER
196   C
197           CALL TAPE(IDRV,4,BUFO,2)
198   C
199   1000    CONTINUE
200   C
```

```
C        FORTRAN IV PROGRAM

201   C****    SPACE TO NEXT GROUP
202   C
203            IF(IJ.EQ.NGRPS) GO TO 2000
204            JZ=JZ+2
205            ICOUNT=((INFRAM(JZ)-INFRAM(JZ-1))-1)*2
206            CALL TAPE(IDRV,4,BUFO,ICOUNT)
207   C
208   2000     CONTINUE
209   C
210   C****    REWIND TAPE
211   C
212            CALL TAPE(IDRV,2,BUFO,0)
213   C
214            END
215
```

```
C       FORTRAN IV PHASE CORRECTION SUBROUTINE

C       FORTRAN IV PHASE CORRECTION SUBROUTINE
C
C       FON BROWN
C       EE DATA FACILITY
C       LOGAN, UTAH  84322
C
C       THIS SUBROUTINE TAKES A FFT FILE FROM A DISK DRIVE AND
C          PERFORMS A PHASE CORRECTION BY MEANS OF SUCESSIVE
C          AVERAGING AND PHASOR MULTIPLICATION.
C       A MAXIMUM OF FIVE PASSES ARE ALLOWED FOR THE AVERAGING.
C          EACH PASS AVERAGES A GIVEN NUMBER OF DATA POINTS. IT
C          IS IMPOTRANT THAT THE TOTAL NUMBER OF POINTS AVERAGED
C          (ON ONE SIDE OF THE POINT OF INTEREST) OF ALL PASSES
C          DOES NOT EXCEED 1023. IF SO, THE SUBROUTINE WILL RETURN
C          WITHOUT PERFORMING THE CORRECTION.
C
C       CALLING LIST: PHASEC(N,NPASS,IPASS)
C         WHERE:N IS THE LOG BASE 2 OF THE NUMBER OF DATA POINTS
C               NPASS IS THE NUMBER OF PASSES AND CANNOT EXCEED FIVE
C               IPASS IS AN ARRAY OF THE NUMBER OF DATA POINTS TO BE
C                  AVERAGED ON THE NTH PASS. THE SUMATION FROM 1 TO
C                  NPASS OF 2*IPASS(N)+1 CANNOT EXCEED 1024. IF SO, THE
C                  ROUTINE WILL RETURN WITHOUT OPPERATION.
C       NOT NOTED IN THE CALLING LIST, BUT EQUALLY IMPORTANT, IS A COMMON
C          BLOCK NAMED RK05C WITH AT LEAST 6144 FREE LOCATIONS WITH THE
C          6145TH LOCATION INDICATING THE DISK DRIVE TO BE USED.
C
C       REVISION HISTORY:
C             ORIGINAL VERSION                FON BROWN       2 JUL 82
C
      SUBROUTINE PHASEC(N,NPASS,IPAS)
      COMMON/RK05C/BUF0,BUFFER(2048),HBUF(2047),XRING(1024),
     1 YRING(1024),IDATA
      DIMENSION IPAS(1)
      DOUBLE PRECISION XDOUB1,XDOUB2,XDOUB3,XDOUB4,XDOUB5
     1 YDOUB1,YDOUB2,YDOUB3,YDOUB4,YDOUB5
C
C     SET NUMBER OF RECORDS IN FFT
      NREC=N-10
      IF(NREC.LE.0)RETURN
      NREC=2**NREC
C
      NPAS=NPASS
      IF(NPAS.LT.1)NPAS=1
      IF(NPAS.GT.5)NPAS=5
      JEND=NREC/2
      JEND=(1+JEND*2-NREC)*2048
22    FORMAT(X,8F8.2)
C
C     JEND POINTS TO THE LAST POINT IF ON THE LAST RECORD.
```

```
C       FORTRAN IV PHASE CORRECTION SUBROUTINE
 51  C
 52          ASSIGN 800 TO NEXT1
 53          ASSIGN 300 TO NEXT2
 54          ASSIGN 800 TO NEXT3
 55          ASSIGN 800 TO NEXT4
 56          IDIF=0
 57          ISO=1
 58          GOTO (50,40,30,20,10),NPAS
 59  10      NITT5=IPAS(5)
 60          IDIF=IDIF+NITT5
 61          IS5=ISO
 62          I5=ISO
 63          IP5=ISO+NITT5+1
 64          ISO=IP5+NITT5
 65          XDOUB5=0.0D0
 66          YDOUB5=0.0D0
 67          ASSIGN 500 TO NEXT4
 68  20      NITT4=IPAS(4)
 69          IDIF=IDIF+NITT4
 70          IS4=ISO
 71          I4=ISO
 72          IP4=ISO+NITT4+1
 73          ISO=IP4+NITT4
 74          XDOUB4=0.0D0
 75          YDOUB4=0.0D0
 76          ASSIGN 400 TO NEXT3
 77  30      NITT3=IPAS(3)
 78          IDIF=IDIF+NITT3
 79          IS3=ISO
 80          I3=ISO
 81          IP3=ISO+NITT3+1
 82          ISO=IP3+NITT3
 83          XDOUB3=0.0D0
 84          YDOUB3=0.0D0
 85          ASSIGN 300 TO NEXT2
 86  40      NITT2=IPAS(2)
 87          IDIF=IDIF+NITT2
 88          IS2=ISO
 89          I2=ISO
 90          IP2=ISO+NITT2+1
 91          ISO=IP2+NITT2
 92          XDOUB2=0.0D0
 93          YDOUB2=0.0D0
 94          ASSIGN 200 TO NEXT1
 95  50      NITT1=IPAS(1)
 96          IDIF=IDIF+NITT1
 97          IS1=ISO
 98          I1=ISO
 99          IP1=ISO+NITT1+1
100          ISO=IP1+NITT1
```

```
C       FORTRAN IV PHASE CORRECTION SUBROUTINE

101           XDOUB1=0.0D0
102           YDOUB1=0.0D0
103           IF(ISO.GT.1024)RETURN
104   C
105   C       IS1 THRU IS5 ARE POINTERS TO THE FIRST LOCATION OF THEIR
106   C          RESPECTIVE RING BUFFERS. ISO IS USED AS A LIMIT ONLY.
107   C       I1 THRU I5 ARE POINTERS THAT WRAP AROUND IN THEIR BUFFERS
108   C       A PATH HAS BEEN ESTABLISHED USING ASSIGNED GOTO STATEMENTS,
109   C          THEREBY RETAINING GENERALITY WHILE INCREASING SPEED.
110   C
111           IBUF=0
112   C
113   C       IBUF IS THE SUBSCRIPT OF BUFFER SUCH THAT HBUF(IBUF)
114   C       IS THE FIRST LOCATION TO BE LOADED TO OR STORED FROM THE BUFFER.
115   C
116           IPTR=2048
117           JPTR=IPTR-2*IDIF
118   C
119   C       DATA ALWAYS COMES OUT OF THE BUFFER AT IPTR AND IS STORED AT JPTR
120   C          WHICH IS ALWAYS OFFSET FROM IPTR BY THE DIFFERENCE IDIF.
121   C
122           KNT=0
123           DO 60 I=1,ISO-1
124           XRING(I)=0.
125           YRING(I)=0.
126   60      CONTINUE
127           DO 70 I=1024,2047
128           BUFFER(I)=0.
129   70      CONTINUE
130   C
131           IERR=0
132   80      CALL FFTRK(IDATA,KNT,0,HBUF(IBUF),IERR)
133           DO 85 I=IBUF+2050,IBUF+4094,4
134           BUFFER(I)=-BUFFER(I)
135           BUFFER(I+1)=-BUFFER(I+1)
136   85      CONTINUE
137   90      KNT=KNT+1
138           IBUF=-2048-IBUF
139   100     X=BUFFER(IPTR)
140           Y=BUFFER(IPTR+1)
141           XDOUB1=XDOUB1+X-XRING(I1)
142           YDOUB1=YDOUB1+Y-YRING(I1)
143           XRING(I1)=X
144           YRING(I1)=Y
145           X=XDOUB1
146           Y=YDOUB1
147           XMAG=SQRT(X*X+Y*Y)
148           IF(XMAG.NE.0.0)GOTO 150
149           X=1.0
150           XMAG=X
```

```
C       FORTRAN IV PHASE CORRECTION SUBROUTINE

150     XX=X/XMAG
        YY=Y/XMAG
        XO=XRING(IP1)
        YO=YRING(IP1)
        X=XX*XO+YY*YO
        Y=XX*YO-YY*XO
        IP1=IP1+1
        IF(IP1.GE.ISO)IP1=IS1
        I1=I1+1
        IF(I1.GE.ISO)I1=IS1
        GOTO NEXT1
200     XDOUB2=XDOUB2+X-XRING(I2)
        YDOUB2=YDOUB2+Y-YRING(I2)
        XRING(I2)=X
        YRING(I2)=Y
        X=XDOUB2
        Y=YDOUB2
        XMAG=SQRT(X*X+Y*Y)
        IF(XMAG.NE.0.0)GOTO 250
        X=1.0
        XMAG=X
250     XX=X/XMAG
        YY=Y/XMAG
        XO=XRING(IP2)
        YO=YRING(IP2)
        X=XX*XO+YY*YO
        Y=XX*YO-YY*XO
        IP2=IP2+1
        IF(IP2.GE.IS1)IP2=IS2
        I2=I2+1
        IF(I2.GE.IS1)I2=IS2
        GOTO NEXT2
300     XDOUB3=XDOUB3+X-XRING(I3)
        YDOUB3=YDOUB3+Y-YRING(I3)
        XRING(I3)=X
        YRING(I3)=Y
        X=XDOUB3
        Y=YDOUB3
        XMAG=SQRT(X*X+Y*Y)
        IF(XMAG.NE.0.0)GOTO 350
        X=1.0
        XMAG=X
350     XX=X/XMAG
        YY=Y/XMAG
        XO=XRING(IP3)
        YO=YRING(IP3)
        X=XX*XO+YY*YO
        Y=XX*YO-YY*XO
        IP3=IP3+1
        IF(IP3.GE.IS2)IP3=IS3
```

```
C       FORTRAN IV PHASE CORRECTION SUBROUTINE

201             I3=I3+1
202             IF(I3.GE.IS2)I3=IS3
203             GOTO NEXT3
204   400       XDOUB4=XDOUB4+X-XRING(I4)
205             YDOUB4=YDOUB4+Y-YRING(I4)
206             XRING(I4)=X
207             YRING(I4)=Y
208             X=XDOUB4
209             Y=YDOUB4
210             XMAG=SQRT(X*X+Y*Y)
211             IF(XMAG.NE.0.0)GOTO 450
212             X=1.0
213             XMAG=X
214   450       XX=X/XMAG
215             YY=Y/XMAG
216             XO=XRING(IP4)
217             YO=YRING(IP4)
218             X=XX*XO+YY*YO
219             Y=XX*YO-YY*XO
220             IP4=IP4+1
221             IF(IP4.GE.IS3)IP4=IS4
222             I4=I4+1
223             IF(I4.GE.IS3)I4=IS4
224             GOTO NEXT4
225   500       XDOUB5=XDOUB5+X-XRING(I5)
226             YDOUB5=YDOUB5+Y-YRING(I5)
227             XRING(I5)=X
228             YRING(I5)=Y
229             X=XDOUB5
230             Y=YDOUB5
231             XMAG=SQRT(X*X+Y*Y)
232             IF(XMAG.NE.0.0)GOTO 550
233             X=1.0
234             XMAG=X
235   550       XX=X/XMAG
236             YY=Y/XMAG
237             XO=XRING(IP5)
238             YO=YRING(IP5)
239             X=XX*XO+YY*YO
240             Y=XX*YO-YY*XO
241             IP5=IP5+1
242             IF(IP5.GE.IS4)IP5=IS5
243             I5=I5+1
244             IF(I5.GE.IS4)I5=IS5
245   C
246   C         AT THIS POINT, THE SUMS OF ALL THE PASSES ARE IN X AND Y
247   C            AND THESE POINTS CORRISPOND TO WHAT IS IN THE BUFFER
248   C            AT JPTR.
249   C
250   800       BUFFER(JPTR)=X
```

```
C       FORTRAN IV PHASE CORRECTION SUBROUTINE

251           BUFFER(JPTR+1)=Y
252           IPTR=IPTR+2
253           IF(IPTR.GT.4095)IPTR=0
254           JPTR=JPTR+2
255           IF(JPTR.GT.4095)JPTR=0
256           IF(IPTR.NE.0.AND.IPTR.NE.2048.AND.(JPTR.NE.JEND.OR.
257          1  KNT.LE.NREC))GOTO100
258           IF(KNT.LE.1)GOTO 820
259   C
260           CALL FFTRK(IDATA,KNT-2,1,HBUF(IBUF),IERR)
261   820     IF(KNT.LT.NREC)GOTO 80
262           IF(KNT.GT.NREC)RETURN
263           DO 840 I=IPTR,IPTR+1023
264           BUFFER(I)=0.
265   840     CONTINUE
266           GOTO 90
267           END
268
```

```
C       FORTRAN IV TIME CODE DECODE SUBROUTINE

  1  C       FORTRAN IV TIME CODE DECODE SUBROUTINE
  2  C
  3  C       FILE NAME IS 'DTIME'
  4  C
  5  C       GENE WARE
  6  C       UTAH STATE UNIVERSITY
  7  C       LOGAN UTAH 84322
  8  C       JULY 2, 1979
  9  C
 10  C       DTIME DECODES TIME FROM 4 WORDS READ FROM
 11  C       TIME CODE. ARRAY N CONTAINS THIS DATA IN
 12  C       ORDER OF READ.
 13  C
 14  C       SUBROUTINE DTIME(N,YEAR,DAY,HOUR,MIN,SEC)
 15  C               INPUT:  "N" IS THE ARRAY OF WORDS TO BE
 16  C                       DECODED. N SHOULD BE DIMENSIONED
 17  C                       AT LEAST 4. N(1) SHOULD BE THE FIRST
 18  C                       VALUE READ FROM THE TIME CODE.
 19  C               OUTPUT: "YEAR" IS THE YEAR
 20  C                       "DAY"  IS THE NUMBER OF DAYS
 21  C                       "HOUR" IS THE NUMBER OF HOURS
 22  C                       "MIN"  IS THE NUMBER OF MINUTES
 23  C                       "SEC"  IS THE NUMBER OF SECONDS. SEC IS NOT
 24  C                              TO BE AN INTEGER.
 25  C
 26  C***    REVISION HISTORY
 27  C
 28  C        2 JUL 1979     GENE A. WARE    INITIAL VERSION.
 29  C
 30          SUBROUTINE DTIME(N,YEAR,DAY,HOUR,MIN,SEC)
 31          DIMENSION N(4)
 32  C
 33  C***    INITIALIZE
 34  C
 35          N1=N(1)
 36          N2=N(2)
 37          N3=N(3)
 38          N4=N(4)
 39          IF(N1.LT.0)N1=N1+4096
 40          IF(N2.LT.0)N2=N2+4096
 41          IF(N3.LT.0)N3=N3+4096
 42          IF(N4.LT.0)N4=N4+4096
 43  C
 44  C***    SECONDS CALCULATION
 45  C
 46          I1=N1/16
 47          I2=I1/16
 48          I3=N2/16
 49          I4=I3/8
 50          SEC=10*(I3-8*I4)+(N2-16*I3)+.1*I2+.01*(I1-16*I2)+
```

```
C       FORTRAN IV PROGRAM

 800    WRITE(4,130)
 130    FORMAT('  ')
        WRITE(4,140)WAVN(I)
 140    FORMAT(' WAVENUMBER = ',B12.6)
        WRITE(4,130)
        WRITE(4,150)
 150    FORMAT(' TERM VALUE FOR THIS WAVENUMBER = ',$)
        READ(4,160)F(I)
 160    FORMAT(B12.6)
        WRITE(4,170)
 170    FORMAT(' LINE STRENGTH FOR THIS WAVENUMBER = ',$)
        READ(4,180)C(I)
 180    FORMAT(D15.8)
        WRITE(4,130)
        WRITE(4,190)
 190    FORMAT(' IS THIS CORRECT ? (0=N,1=Y) ',$)
        READ(4,100)IANS
        IF(IANS.EQ.0) GO TO 800
 200    CONTINUE
        GO TO 750
 C
 C      GET TERM VALUES FROM OLD DATA FILE
 C
 700    READ(6,100)ITQ
        DO 710 I=1,ITQ
        READ(6,310)X,Y,F(I),C(I)
 710    CONTINUE
 C
 C      WRITE OUT COMPLETE FILE
 C
 750    WRITE(7,100)ITL
        DO 300 I=1,ITL
        WRITE(7,310)WAVN(I),RLRSP(I),F(I),C(I)
 310    FORMAT(B15.6,E15.6,B12.6,D15.8)
 300    CONTINUE
        END
```

```
C       FORTRAN IV PROGRAM

C       FORTRAN IV PROGRAM
C
C       FILE NAME =   LINPOS
C
C       THIS PROGRAM READS FFT TAPE CONVERTS THE 12 BIT DATA
C       INTO 36 BIT FORTRAN IV DATA FORMAT
C       THE DATA IS THEN PHASE CORRECTED
C       INTERACTIVLY YOU ARE ASKED FOR EXPECTED POSITIONS OF
C       LINES IN THE SPECTRA.  POSITIONS IDENTIFIED BY SAMPLE NUMBERS
C       BEGINNING AT '0' THROUGH '2095'
C       THESE SAMPLE NUMBERS CORRESPOND THE SAMPLE NUMBERS OF THE FULL
C       TRANSFORM (REC 5&6) OF 4096-6144 WHERE THE 4-2,3-1,8-5,7-4
C       OH BAND LINES RESIDE
C
C       THE PROGRAM THEN PRESENTS ON SCREEN THE AMPLITUDE OF
C       DATA POINTS (+&- 10) AROUND SPECIFIED POINT .
C       YOU THEN SELECT THE ACTUAL PEAK SAMPLE NUMBER FOR WRITING TO
C       A DISK FILE AS A BEGINNING SEARCH POINT FOR PROGRAM "LINAMP"
C
C
C       WRITTEN BY PARRIS NEAL
C       UTAH STATE UNIVERSITY MAY 25, 1984
C
C       SUBROUTINES USED ARE
C               FFTFIL. TAPE, TAPE8, TERR
C               SPCONV
C               RKFIL, FFTRK, RK05C
C               PHASEC
C               APODI
C
      COMMON/RK05C/BUFO.BUFFER(2048).HBUFF(2047).ARING(1024).
     1 'RING(1024).IDATA
      DIMENSION IPASS(5)
      DOUBLE PRECISION WAVN
C
C****
C
      WRITE(4.160)
160   FORMAT('  ')
      WRITE(4.160)
      WRITE(4.160)
      WRITE(4.170)
170   FORMAT(' DID YOU REMEMBER TO SET UP DISK FILE UNIT 5,6 FOR I/O ?')
C
C       WINDOW WIDTHS IN "BINS" FOR PHASE CORRECTION ROUTINE
C
      IPASS(1)=3
      IPASS(2)=5
      IPASS(3)=9
      IPASS(4)=17
```

```
C       FORTRAN IV PROGRAM

 51           IPASS(5)=65
 52  C
 53  C        INPUT DRIVE NUMBER AND INITIALIZE TAPE DRIVE
 54  C
 55           WRITE(4,500)
 56  500      FORMAT("1 INPUT TAPE DRIVE NUMBER ",$)
 57           READ(4,510)IDRV
 58  510      FORMAT(I4)
 59           IF(IDRV.EQ.1)IDRV=2
 60           INIT=0
 61           IREC=1
 62           IOPR=4
 63           CALL FFTFIL(INIT,IDRV,IREC,IOPR,XRING(1),BUF0)
 64  C
 65  C        DETERMINE WHAT RECORD IS TO BE READ
 66  C
 67           WRITE(4,520)
 68  520      FORMAT(" INPUT FFT FRAME NUMBER TO BE PROCESSED  ",$)
 69           READ(4,510)IFILE
 70  C
 71  C        READ IN HEADER FOR FRAME NUMBER "IFILE"
 72  C
 73  C        FILL IN LATER
 74  C
 75  C
 76  C        READ IN RECORDS 5 AND 6 FROM FRAME "IFILE"
 77  C        WRITE THESE TWO RECORDS TO DISK AND PHASE CORRECT THEM
 78  C
 79           MODE=1
 80           IREC=5
 81           CALL FFTFIL(IFILE,MODE,IREC,IOPR,XRING(1),BUF0)
 82  C
 83  C        CONVERT RECORD 5 TO 36 BIT FORMAT
 84  C
 85           WRITE(4,600)
 86  600      FORMAT(" STARTING TO CONVERT TO 36 BIT")
 87           CALL SPCONV(BUF0,BUF0,2048)
 88  C
 89  C        TRANSFER RECORD TO DISK DRIVE
 90  C
 91           WRITE(4,610)
 92  610      FORMAT(" TRANSFERING TO DISK")
 93           IDATA=1
 94           ICYLD=0
 95           IER=0
 96           CALL FFTRK(IDATA,ICYLD,1,BUF0,IER)
 97  C
 98  C        REPEAT FOR RECORD NUMBER 6
 99  C
100           IREC=6
```

```
C       FORTRAN IV PROGRAM

101           CALL FFTFIL(IFILE,MODE,IREC,IOPR,XRING,BUFO)
102           CALL SPCONV(BUFO,BUFO,2048)
103           ICYLD=1
104           CALL FFTRK(IDATA,ICYLD,1,BUFO,IER)
105     C
106     C     DATA IS NOW ON DISK
107     C     CALL PHASE CORRECTION PROGRAM TO ELIMINATE PHASE SHIFT IN DATA
108     C
109     C     4K DATA POINTS TO PHASE CORRECT THEREFORE N=12
110     C     FIVE PASSES OVER DATA THEREFORE NPASS =5
111     C
112           N=12
113           NPASS=5
114           WRITE(4,620)
115     620   FORMAT(" BEGINNING PHASE CORRECTION")
116           CALL PHASEC(N,NPASS,IPASS)
117     C
118     C     PHASE CORRECTION COMPLETE
119     C
120           WRITE(4,630)
121     630   FORMAT(" PHASE CORRECTION COMPLETE")
122     C
123     C****   ASSEMBLING REAL PART IN ARRAY HBUFF(I)
124     C
125           CALL FFTRK(IDATA,0,0,BUFO,IER)
126           NJ=0
127           DO 700 IJ=0,1023
128           HBUFF(IJ)=BUFFER(NJ)
129           NJ=NJ+2
130     700   CONTINUE
131           CALL FFTRK(IDATA,1,0,BUFO,IER)
132           NJ=0
133           DO 710 IJ=1024,2047
134           HBUFF(IJ)=BUFFER(NJ)
135           NJ=NJ+2
136     710   CONTINUE
137     C
138     C     BRING IN HAMMING TABLE VALUES
139     C
140           READ(6)BUFO,BUFFER
141     C
142     C
143     C****   READING IN EXPECTED PEAK SAMPLE NUMBERS
144     C
145           WRITE(4,160)
146           WRITE(4,750)
147     750   FORMAT(' TOTAL NUMBER OF LINES YOU ARE LOOKING FOR = ',$)
148           READ(4,510)ITL
149     C
150     C****   WRITE TO SEARCH FILE TOTAL NUMBER OF LINES
```

```
C       FORTRAN IV PROGRAM

151   C
152           WRITE(5,790)ITL
153   C
154           DO 1000 IC=1,ITL
155           WRITE(4,160)
156           WRITE(4,514)
157   514     FORMAT(' INPUT WAVENUMBER IN CM-1 FOR LINE ',$)
158           READ(4,516)WAVN
159   755     WRITE(4,760)IC
160   760     FORMAT(' INPUT SAMPLE NUMBER OF',I4,' LINE  = ',$)
161           READ(4,510)ISN
162   516     FORMAT(B15.6)
163           WRITE(4,160)
164   C
165   C****   OUTPUT TO SCREEN POINTS AROUND EXPECTED SAMPLE NUMBER
166   C
167           DO 900 IN=ISN-10,ISN+10
168           CALL APODI(IN,VL)
169           WRITE(4,770)IN,VL
170   770     FORMAT(' ',I6,'  ',E15.6)
171   900     CONTINUE
172   C
173   C****   READ ACTUAL PEAK SAMPLE NUMBER FROM SCREEN AND INPUT TO DISK FILE
174   C
175           WRITE(4,160)
176           WRITE(4,780)
177   780     FORMAT(' INPUT PEAK SAMPLE NUMBER ',$)
178           READ(4,790)IRSN
179   790     FORMAT(I6)
180   C
181   C       IS IT CORRECT?
182   C
183           WRITE(4,793)
184   793     FORMAT(' WAS THIS CORRECT (0=N,1=Y) ',$)
185           READ(4,790)KC
186           IF(KC.EQ.0) GO TO 755
187   C
188           WRITE(5,796)IRSN,WAVN
189   796     FORMAT(I6,B15.6)
190   1000    CONTINUE
191   C
192   C****   REWIND TAPE
193   C
194           CALL FFTFIL(0,IDRV,1,IOPR,XRING,BUF0)
195   C
196           END
197
```

```
C       FORTRAN IV PROGRAM

  1  C       FORTRAN IV PROGRAM
  2  C
  3  C       FILE NAME = HAMTBL
  4  C
  5  C       WRITTEN BY PARRIS NEAL
  6  C       UTAH STATE UNIVERSITY  MAY 22,1984
  7  C
  8  C       PROGRAM TO COMPUTE THE VALUE OF THE HAMMING APODIZING
  9  C       FUNCTION, WHICH IS NORMALIZED FOR UNIT AREA.
 10  C       VALUES COMUPTED FOR POSITIVE OFFSET ONLY.
 11  C       ARRAY OF VALUES ARE COMPUTED FOR 0.01 SAMPLE NUMBER
 12  C       RESOULTION.  STORED IN AN FILE CALLED HAMVL ON DISK
 13  C
 14          COMMON BUFO,BUFFER(2047)
 15  C
 16          DO 15 I=0,2047
 17          BUFFER(I)=0.0
 18  15      CONTINUE
 19          DEL=0.0
 20          BUFFER(0)=0.53836
 21          PI=3.14159
 22          DO 10 I=1,500
 23          DEL=DEL+0.01
 24          FSTM=0.53836*((SIN(PI*DEL))/(PI*DEL))
 25          SCTM=(SIN(PI*(DEL-1.0)))/(PI*(DEL-1.0))
 26          TDTM=(SIN(PI*(DEL+1.0)))/(PI*(DEL+1.0))
 27          BUFFER(I)=FSTM+(0.46164/2.0)*(SCTM+TDTM)
 28  10      CONTINUE
 29  C
 30  C       WRITE OUT TABLE
 31  C
 32          WRITE(5)BUFO,BUFFER
 33          END
 34
```

```
C       FORTRAN IV SUBROUTINE

  1  C       FORTRAN IV SUBROUTINE
  2  C
  3  C       FILE NAME = AVGT
  4  C
  5  C       WRITTEN BY PARRIS NEAL
  6  C       UTAH STATE UNIVERSITY  JULY 18,1984
  7  C
  8  C       PART OF "TPAVG"  THIS IS THE 3 POINT RUNNING AVERAGING WINDOW
  9  C       TO AVERGE TEMPS WEIGHTED BY THEIR STANDARD DEVIATION
 10  C
 11          SUBROUTINE AVGT
 12  C
 13          COMMON IH1(5),IH2(5),IH3(5),IL1(4),IL2(4),IL3(4),AO1(4),AO2(4),
 14         1  AO3(4),SA1(4),SA2(4),SA3(4),TP1(4),TP2(4),TP3(4),ST1(4),ST2(4),
 15         1  ST3(4),TAVG(4),SAVG(4)
 16  C
 17          DO 100 I=1,4
 18          TN=(TP1(I)/(ST1(I)**2))+(TP2(I)/(ST2(I)**2))+(TP3(I)/(ST3(I)**2))
 19          TD=(1.0/(ST1(I)**2))+(1.0/(ST2(I)**2))+(1.0/(ST3(I)**2))
 20          TAVG(I)=TN/TD
 21          SAVG(I)=1.0/(SQRT(TD))
 22  100     CONTINUE
 23  C
 24          RETURN
 25          END
 26
```

```
C       FORTRAN SUBROUTINE

  1  C       FORTRAN SUBROUTINE
  2  C
  3  C       FILE NAME = RFRAM
  4  C
  5  C       WRITTEN BY PARRIS NEAL
  6  C       UTAH STATE UNIVERSITY  JULY 18,1984
  7  C
  8  C       PART OF "TPAVG"  READS FRAME OF TEMPERATURE DATA
  9  C
 10          SUBROUTINE RFRAM(IH,IL,AO,SA,TP,ST)
 11  C
 12          DIMENSION IH(5),IL(4),AO(4),SA(4),TP(4),ST(4)
 13  C
 14          READ(5,100)IH(1),IH(2),IH(3),IH(4),IH(5)
 15  100     FORMAT(5I4)
 16  C
 17          DO 200 I=1,4
 18          READ(5,150)IL(I),AO(I),SA(I),TP(I),ST(I)
 19  200     CONTINUE
 20  150     FORMAT(I4,4E15.6)
 21  C
 22          RETURN
 23          END
 24
```

```
C       FORTRAN IV SUBROUTINE

  1  C       FORTRAN IV SUBROUTINE
  2  C
  3  C       FILE NAME = WFRAM
  4  C
  5  C       WRITTEN BY PARRIS NEAL
  6  C       UTAH STATE UNIVERSITY   JULY 18,1984
  7  C
  8  C       PART OF "TPAVG"  WRITES A FRAME OF AVERAGED TEMP DATA
  9  C
 10          SUBROUTINE WFRAM(IH,IL,AO,SA,TP,ST)
 11  C
 12          DIMENSION IH(5),IL(4),AO(4),SA(4),TP(4),ST(4)
 13  C
 14          WRITE(6,100)IH(1),IH(2),IH(3),IH(4),IH(5)
 15  100     FORMAT(5I4)
 16  C
 17          DO 200 I=1,4
 18          WRITE(6,150)IL(I),AO(I),SA(I),TP(I),ST(I)
 19  200     CONTINUE
 20  150     FORMAT(I4,4E15.6)
 21  C
 22          RETURN
 23          END
 24
```

```
C       FORTRAN IV SUBROUTINE

  1  C       FORTRAN IV SUBROUTINE
  2  C
  3  C       FILE NAME = MOVE
  4  C
  5  C       WRITTEN BY PARRIS NEAL
  6  C       UTAH STATE UNIVERSITY  JULY 18,1984
  7  C
  8  C       PART OF "TPAVG"  MOVES TEMP FRAMS 3 AND 2 TO 2 AND 1
  9  C
 10          SUBROUTINE MOVE
 11  C
 12          COMMON IH1(5),IH2(5),IH3(5),IL1(4),IL2(4),IL3(4),AO1(4),AO2(4),
 13         1  AO3(4),SA1(4),SA2(4),SA3(4),TP1(4),TP2(4),TP3(4),ST1(4),ST2(4),
 14         1  ST3(4),TAVG(4),SAVG(4)
 15  C
 16          DO 100 I=1,5
 17          IH1(I)=IH2(I)
 18          IH2(I)=IH3(I)
 19  100     CONTINUE
 20  C
 21          DO 200 I=1,4
 22          AO1(I)=AO2(I)
 23          AO2(I)=AO3(I)
 24          SA1(I)=SA2(I)
 25          SA2(I)=SA3(I)
 26          TP1(I)=TP2(I)
 27          TP2(I)=TP3(I)
 28          ST1(I)=ST2(I)
 29          ST2(I)=ST3(I)
 30  200     CONTINUE
 31  C
 32          RETURN
 33          END
 34
```

```
C       FORTRAN IV PROGRAM

  1  C       FORTRAN IV PROGRAM
  2  C
  3  C       FILE NAME = RMBDBK
  4  C
  5  C       PROGRAM REMOVES BAD FRAMES OF LINE STRENGTH DATA FROM A FILE
  6  C
  7          DIMENSION IBAD(10),IHDTA(10).SN(52),XLSTR(52)
  8  C
  9          WRITE(4,50)
 10  50      FORMAT(' OLD FILE   UNIT 5')
 11          WRITE(4,60)
 12  60      FORMAT(' NEW FILE   UNIT 6')
 13          WRITE(4.100)
 14  100     FORMAT(' INPUT # FRAMES TO DELETE  ',$)
 15          READ(4.110)IDL
 16  110     FORMAT(I6)
 17          READ(5.110)IFMS
 18          ITF=IFMS
 19          IFMS=IFMS-IDL
 20          WRITE(6,110)IFMS
 21  C
 22  C       INPUT BAD FRAME NUMBERS
 23  C
 24          DO 200 I=1.IDL
 25          WRITE(4.210)
 26  210     FORMAT(' FRAME # TO DELETE = ?',$)
 27          READ(4.110)IBAD(I)
 28  200     CONTINUE
 29  C
 30  C       SET UP READ AND WRITE OF FRAMES
 31  C
 32          IQ=1
 33          DO 1000 IC=1.ITF
 34          DO 300 I=1,10
 35          READ(5.110)IHDTA(I)
 36  300     CONTINUE
 37          DO 350 J=1.52
 38          READ(5,330)SN(J),XLSTR(J)
 39  330     FORMAT\F10.2.E15.6)
 40  350     CONTINUE
 41  C
 42  C       TEST FOR NEGATIVE VALUES
 43  C
 44          DO 370 IT=13.52
 45          IF(XLSTR(IT).LT.0.0)GOTO 395
 46  370     CONTINUE
 47          GOTO 390
 48  395     WRITE(3.380)IHDTA(2)
 49  390     CONTINUE
 50  380     FORMAT(' FRAME ',I4,' HAS NEG VALUE')
```

```
C       FORTRAN IV PROGRAM

 51  C
 52  C         TEST FOR BAD FRAME
 53  C
 54            IF(IBAD(IQ).EQ.IHDTA(2))GOTO 2000
 55            DO 400 I=1,10
 56            WRITE(6,110)IHDTA(I)
 57  400       CONTINUE
 58            DO 500 J=1,52
 59            WRITE(6,330)SN(J),XLSTR(J)
 60  500       CONTINUE
 61            GO TO 1000
 62  2000      IQ=IQ+1
 63  1000      CONTINUE
 64            END
 65
```

```
/FORTRAN IV SINGLE PRECISION CONVERSION

  1  /FORTRAN IV SINGLE PRECISION CONVERSION
  2  /
  3  /FILE NAME IS 'SPCONV.RA'
  4  /
  5  /GENE A. WARE
  6  /ELECTRO-DYNAMICS LABORATORIES
  7  /UTAH STATE UNIVERSITY
  8  /LOGAN, UTAH  84322
  9  /31 DECEMBER 1977
 10  /
 11  /THIS SUBROUTINE CONVERTS 12 BIT SINGLE PRECISION
 12  /INTEGERS (AS LOADED FROM MAG TAPE, FOR INSTANCE)
 13  /INTO FORTRAN IV INTEGERS.  IT ASSUMES THAT THE
 14  /ARRAY OF INTO WHICH THE VALUES WERE LOADED IS
 15  /DIMENSIONED AT LEAST N/3 (ROUNDED UP) WHERE
 16  /N IS THE NUMBER OF 12 BIT DATA WORDS TO BE
 17  /CONVERTED.  THE OUTPUT ARRAY MUST BE DIMENSIONED
 18  /AT LEAST N.  THE INPUT AND OUTPUT ARRAYS MAY BE
 19  /THE SAME ARRAY.
 20  /
 21  /CALLING SEQUENCE
 22  /
 23  /CALL SPCONV(IXIN,IXOUT,N)
 24  /        IXIN = INPUT DATA ARRAY
 25  /        IXOUT = OUTPUT DATA ARRAY
 26  /        N = NUMBER OF 12 BIT DATA WORDS
 27  /
 28           SECT    SPCONV
 29           JA      #ST
 30  #XR.     ORG     .+10
 31           TEXT    +SPCONV+
 32  #RET.    SETX    #XR
 33           SETB    #BASE
 34           JA      .+3
 35  #BASE.   ORG     .+6
 36  IXIN.    ORG     .+3
 37  IXOUT.   ORG     .+3
 38  N.       ORG     .+3
 39  IXI.     ORG     .+3
 40  IXO.     ORG     .+3
 41           ORG     #BASE+30
 42           FNOP
 43           JA      #RET
 44           FNOP
 45  #GOBAK,  0:0
 46  #ARGS.   ORG     .+3
 47  I.       ORG     .+0003
 48  IT1.     ORG     .+0001
 49  IT2.     ORG     .+0001
 50  IT3.     ORG     .+0001
```

```
/FORTRAN IV SINGLE PRECISION CONVERSION

 51  J.       ORG      .+0003
 52  #TMP.    ORG      .+0011
 53  #LIT.    0000
 54           0000
 55           0000
 56           0001
 57           2000
 58           0000
 59           0002
 60           3000
 61           0000
 62           0003
 63           3000
 64           0000
 65           #LBL=.
 66           ORG      #LBL
 67  #RTN.    BASE     #BASE
 68           JA       #GOBAK
 69  #ST.     STARTD
 70           0210
 71           FSTA     #GOBAK,0
 72           0200
 73           SETX     #XR
 74           SETB     #BASE
 75           LDX      0,1
 76           FSTA     #BASE
 77           FSTA     #ARGS
 78           FLDAZ    #BASE,1+
 79           FSTA     IXIN
 80           FLDAZ    #BASE,1+
 81           FSTA     IXOUT
 82           FLDAZ    #BASE,1+
 83           FSTA     N
 84  /
 85  /INITIALIZE
 86  /
 87           STARTF
 88           FLDAZ    N
 89           FSTA     I
 90           FLDA     #LIT+0006
 91           FMULZ    N
 92           FSTA     J
 93  /
 94  /MAIN LOOP
 95  /
 96  #10,     FLDA     I
 97           FSUB     #LIT+0006
 98           FSTA     I
 99           ALN      0
100           STARTD
```

```
/FORTRAN IV SINGLE PRECISION CONVERSION

101             FADD    IXIN
102             FSTA    IXI
103             STARTF
104             FLDAZ   IXI
105             FSTA    IT1
106             FLDA    J
107             FSUB    #LIT+0006
108             FSTA    J
109             JLT     #20
110     /
111     /FIRST WORD
112     /
113             ALN     0
114             STARTD
115             FADD    IXOUT
116             FSTA    IX0
117             STARTF
118             SETX    IT3
119             XTA     0
120             SETX    #XR
121             FSTAZ   IX0
122             FLDA    J
123             FSUB    #LIT+0006
124             FSTA    J
125             JLT     #20
126     /
127     /SECOND WORD
128     /
129             ALN     0
130             STARTD
131             FADD    IXOUT
132             FSTA    IX0
133             STARTF
134             SETX    IT2
135             XTA     0
136             SETX    #XR
137             FSTAZ   IX0
138             FLDA    J
139             FSUB    #LIT+0006
140             FSTA    J
141             JLT     #20
142     /
143     /THIRD WORD
144     /
145             ALN     0
146             STARTD
147             FADD    IXOUT
148             FSTA    IX0
149             STARTF
150             SETX    IT1
```

```
/FORTRAN IV SINGLE PRECISION CONVERSION

151             XTA     0
152             SETX    #XR
153             FSTA%   IX0
154             JA      #10
155   /
156   /DONE--RETURN
157   /
158   #20,      JA      #RTN
159
```

```
C       XEBEC 9000 FORTRAN IV TAPE SUBROUTINE

C       XEBEC 9000 FORTRAN IV TAPE SUBROUTINE
C
C       FILE NAME IS 'TAPE'
C
C       GENE A. WARE
C       ELECTRICAL ENGINEERING DEPARTMENT
C       UTAH STATE UNIVERSITY
C       LOGAN, UTAH  84322
C       17 JULY 1979
C
C       CALLING SEQUENCE
C
C       CALL TAPE(UNIT,COMAND,BUFFER,COUNT)
C                  UNIT = TAPE UNIT TO BE USED
C                                 0 = PHYSICAL UNIT 0 IN 9T MODE
C                                 1 = PHYSICAL UNIT 0 IN 7T MODE
C                                 2 = PHYSICAL UNIT 1 IN 9T MODE
C                                 3 = PHYSICAL UNIT 1 IN 7T MODE
C                        COMAND = TAPE COMMAND
C                                 0 = NO OPERATION
C                                 1 = NO OPERATION
C                                 2 = REWIND
C                                 3 = SET OFFLINE
C                                 4 = SPACE FORWARD N FILES
C                                 5 = SPACE FORWARD N RECORDS
C                                 6 = READ FORWARD 1 RECORD
C                                 7 = READ FORWARD 1 RECORD
C                                 8 = SPACE REVERSE N FILES
C                                 9 = SPACE REVERSE N RECORDS
C                                10 = SPACE REVERSE N RECORDS (EDIT)
C                                11 = READ REVERSE
C                                12 = WRITE FILE MARK
C                                13 = ERASE 3 INCH GAP
C                                14 = WRITE RECORD (EDIT)
C                                15 = WRITE RECORD
C                        BUFFER = BUFFER ARRAY FOR DATA
C                         COUNT = WORD/RECORD COUNT.  NOTE--FOR READ
C                                 AND WRITE COMMANDS, THIS IS THE 12
C                                 BIT WORD COUNT.
C
C       REVISION HISTORY
C
C       17 JUL 1979     GENE A. WARE     INITIAL VERSION
C       14 AUG 1982     GENE A. WARE     CHANGED CALL TO TAPE8(-1,...
C                                        TO HOLD IN MODULE UNTIL DONE
C
C
C       SUBROUTINE TAPE(UNIT,COMAND,BUFFER,COUNT)
C
C***    GET THE ARGUMENTS IN LOCAL VARIABLES
```

```
C       XEBEC 9000 FORTRAN IV TAPE SUBROUTINE

 51  C
 52          IUNIT=UNIT
 53          ICOM=COMAND
 54          JCOM=ICOM/2
 55          KOUNT=COUNT+0.5
 56          I=1
 57  C
 58  C***    DO IT
 59  C
 60  10      CONTINUE
 61          CALL TAPE8(1,IUNIT ICOM,BUFFER,KOUNT)
 62  C
 63  C***    CHECK FOR READ/WRITE OPERATIONS
 64  C
 65          IF((JCOM.EQ.3).OR.(JCOM.EQ.7))GO TO 20
 66          GO TO 30
 67  C
 68  C***    CHECK FOR ERRORS (READ/WRITE ONLY)
 69  C
 70  20      CONTINUE
 71          CALL TAPE8(-1,KREG,KCOM,KBUF,KCNT)
 72          IMTN=(KREG/256)-(KREG/512)*2
 73          IF(IMTN.NE.0)GO TO 20
 74          KREG=KREG/4096
 75          KREG=(KREG/64)+(KREG/8-(KREG/16)*2)
 76          IF(KREG.EQ.0.OR.1.GT.9)GO TO 30
 77  C
 78  C***    BACKSPACE AND TRY AGAIN UP TO 10 TIMES
 79  C
 80          CALL TAPE8(1,IUNIT,9,BUFFER,1)
 81          I=I+1
 82          GO TO 10
 83  C
 84  C***    DONE
 85  C
 86  30      CONTINUE
 87          RETURN
 88          END
 89
```

```
C       FORTRAN IV PROGRAM

  1  C       FORTRAN IV PROGRAM
  2  C
  3  C       FILE NAME = TPAVG
  4  C
  5  C       WRITTEN BY PARRIS NEAL
  6  C       UTAH STATE UNIVERSITY  JULY 18,1984
  7  C
  8  C       PROGRAM READS TEMPERATURE FILES PRODUCED BY "BLTIMD"
  9  C       AND AVERAGES THEM OVER A 3 POINT WINDOW WEIGHTED BY
 10  C       EACH TEMP'S STD DEV
 11  C
 12          COMMON IH1(5),IH2(5),IH3(5),IL1(4),IL2(4),IL3(4),AO1(4),AO2(4),
 13         1  AO3(4),SA1(4),SA2(4),SA3(4),TP1(4),TP2(4),TP3(4),ST1(4),ST2(4),
 14         1  ST3(4),TAVG(4),SAVG(4)
 15  C
 16          READ(5,100)INFMS
 17  100     FORMAT(I4)
 18          WRITE(6,100)INFMS
 19  C
 20          CALL RFRAM(IH1,IL1,AO1,SA1,TP1,ST1)
 21          CALL RFRAM(IH2,IL2,AO2,SA2,TP2,ST2)
 22  C
 23  C
 24          DO 200 I=1,4
 25          TN=(TP1(I)/(ST1(I)**2))+(TP2(I)/(ST2(I)**2))
 26          TD=(1.0/(ST1(I)**2))+(1.0/(ST2(I)**2))
 27          TAVG(I)=TN/TD
 28          SAVG(I)=1.0/(SQRT(TD))
 29  200     CONTINUE
 30  C
 31          CALL WFRAM(IH1,IL1,AO1,SA1,TAVG,SAVG)
 32  C
 33  500     CONTINUE
 34          CALL CHKEOF(E)
 35          READ(5,120)IH3(1),IH3(2),IH3(3),IH3(4),IH3(5)
 36          IF(E.NE.0) GOTO 600
 37  120     FORMAT(5I4)
 38          DO 130 IJ=1,4
 39          READ(5,140)IL3(IJ),AO3(IJ),SA3(IJ),TP3(IJ),ST3(IJ)
 40  130     CONTINUE
 41  140     FORMAT(I4,4E15.6)
 42  C
 43          CALL AVGT
 44  C
 45          CALL WFRAM(IH2,IL2,AO2,SA2,TAVG,SAVG)
 46          CALL MOVE
 47  C
 48          GOTO 500
 49  600     CONTINUE
 50  C
```

```
C       FORTRAN IV PROGRAM

 51             DO 300 I=1,4
 52             TN=(TP1(I)/(ST1(I)**2))+(TP2(I)/(ST2(I)**2))
 53             TD=(1.0/(ST1(I)**2))+(1.0/(ST2(I)**2))
 54             TAVG(I)=TN/TD
 55             SAVG(I)=1.0/(SQRT(TD))
 56  300        CONTINUE
 57  C
 58             CALL WFRAM(IH2,IL2,AO2,SA2.TAVG,SAVG)
 59  C
 60             END
 61
```

/FORTRAN IV FFT RK05 MODULE

```
 1  /FOR.RAN IV FFT RK05 MODULE
 2  /
 3  /GZ.Z A. W!2Z
 4  /E.Z#42)#!. E.').ZZ2).' DZ0'24-Z.4
 5  /U4!( S4!4Z U.)6Z23)49
 6  /L/'!., U4!(  84322
 7  /30 J5.Z 1982
 8  /
 9  /CALLING SEQUENCE
10  /
11  /        CALL FFTRK(UNIT,CYLDR.RDWT,X,ERROR)
12  /
13  /                UNIT = PHYSICAL DISK UNIT NUMBER (0-3)
14  /                CYLDR = CYLINDER TO BE TRANSFERED (0-202)
15  /                RDWT = READ/WRITE SELECT (0 = READ, 1 = WRITE)
16  /                X = BUFFER USED (2048 F4 WORDS)
17  /                ERROR = RK05 STATUS REGISTER
18  /
19  /
20  /REVISION HISTORY
21  /
22  /30 J5.Z 1982   GZ.Z A. W!2Z    I.)4)!, 6Z23)/.
23  /
24  /
25  /DEFINITIONS
26  /
27  DSKP=   6741    /DISK SKIP ON FLAG
28  DCLR=   6742    /DISK CLEAR
29  DLAG=   6743    /LOAD ADDRESS AND GO
30  DLCA=   6744    /LOAD CURRENT ADDRESS
31  DRST=   6745    /READ STATUS
32  DLDC=   6746    /LOAD COMMAND
33  BSW=    7002    /BYTE SWAP
34  /
35  /FFTRK ENTRY
36  /
37          BASE 0
38          SECT FFTRK
39          SETX COM        /SET BASE ADDRESS
40          STARTD          /GET UNIT NUMBER
41          FLDAZ 0,1
42          FSTA 3
43          STARTF
44          FLDAZ 3
45          ALN 0
46          STARTD
47          FSTA UNIT
48          FLDAZ 0,2       /GET CYLINDER NUMBER
49          FSTA 3
50          STARTF
```

```
/FORTRAN IV FFT RK05 MODULE

          FLDAZ 3
          ALN 0
          STARTD
          FSTA CYLDR
          FLDAZ 0.3          /GET READ/WRITE
          FSTA 3
          STARTF
          FLDAZ 3
          ALN 0
          STARTD
          FSTA RKWT
          FLDAZ 0.4          /GET BUFFER ADDRESS
          FSTA 3
          FSTA BUFM
          STARTF
          TRAP4 RK05S        /GO TO 8-MODE SUBROUTINE
          STARTD             /RETURN STATUS REGISTER
          FLDAZ 0.5
          FSTA 3
          STARTF
          FLDA ERROR
          FNORM
          FSTAZ 3
          FLDA 30
          JAC                /RETURN
/
/8-MODE RK05 MODULE
/
          COMMZ RK05M
          ORG .+200
/
/RK05 CONTROL SUBROUTINE
/
RK05S.    0
/
/INITIAL SETUP
/
          CLL CLA IAC        /DO A POWER CLEAR
          DCLR
          CLA IAC RTR        /MAKE LO PART OF READ ALL/WRITE ALL
          TAD RDWT           /GET WRITE BIT
          AND K4001          /MAKE SURE ITS OK
          CLL RTR            /AND MOVE IT INTO POSITION
          DCA COM            /IN THE COMMAND WORD
          TAD CYLN           /NOW GET THE CYLINDER NUMBER
          AND K377           /RESTRICT IT TO 8 BITS
          CLL RAL            /AND PUT IT IN THE PROPER POSITION
          RTL
          RTL
          DCA CYLN           /FOR THE DISK ADDRESS REGISTER (LO)
```

```
/FORTRAN IV FFT RK05 MODULE

101             TAD UNUM            /NOW GET THE UNIT NUMBER
102             AND K3              /UNITS 0-3 ONLY
103             SNA                 /TO NOT ALLOW UNIT 0
104             JMP RKRET           /TO PROTECT OPERATING SYSTEM
105             RAL                 /PUT IT TOGETHER WITH HI CYLINDER BIT
106             TAD COM             /THEN INCLUDE IT
107             DCA COM             /IN THE DISK COMMAND
108             TAD M30             /SET THE BLOCK COUNT
109             DCA BLKCNT          /TO 24C10J BLOCKS (6144 WORDS)
110             DCA ERREG           /RESET THE ERROR WORD
111             IOF                 /SORRY, NO INTERRUPTS ALLOWED
112     /
113     /MAIN DATA TRANSFER LOOP
114     /
115     RLOOP.  DCLR                /CLEAR STATUS
116             TAD BUFL            /GET LO ORDER BUFFER ADDRESS
117             DLCA                /AND LOAD INTO CURRENT ADDRESS
118             TAD BUFH            /GET HI ORDER BUFFER ADDRESS
119             AND K7              /LIMIT TO FIELDS 0-7
120             CLL RAL             /THEN SHIFT IT
121             RTL
122             TAD COM             /AND PUT IN COMMAND WORD
123             DLDC                /LOAD THE COMMAND REGISTER
124             TAD CYLN            /GET THE CURRENT CYLINDER NUMBER
125             DLAG                /LOAD IT AND GO
126             ISZ CYLN            /UPDATE CYLINDER WHILE WAITING
127             CLL CLA             /MUST CLEAR LINK ANYWAY
128             TAD BUFL            /GET LO ORDER BUFFER ADDRESS
129             TAD K400            /AND BUMP IT BY TWO MEMORY PAGES
130             DCA BUFL
131             RAL                 /NOW GET THE OVERFLOW
132             TAD BUFH            /AND ADD IT
133             DCA BUFH            /TO THE HI ORDER BUFFER ADDRESS
134     RWAIT,  DSKP                /IS THE DISK DONE?
135             JMP CNTLC           /CHECK OUT CONTROL C WHILE WAITING
136             DRST                /DONE--GET THE STATUS REGISTER
137             AND K3777           /REMOVE COMPLETION FLAG
138             SZA                 /ANY ERRORS?
139             JMP RERR            /YES--GO CHECK THEM OUT
140             ISZ BLKCNT          /HAVE WE TRANSFERED ALL THE BLOCKS?
141             JMP RLOOP           /NO--DO ANOTHER
142     RWAIT1, DRST                /WAIT FOR THE COMPLETION FLAG
143             SMA CLA
144             JMP RWAIT1
145             ISZ DELAY
146             JMP .-1
147     RKRET.  CDF CIF 0
148             ION                 /TURN THE INTERRUPTS BACK ON
149             JMP% RK05S          /ALL DONE
150     DELAY,  0
```

```
/FORTRAN IV FFT RK05 MODULE

151  /
152  / ERROR CHECK
153  /
154  RERR.   DCA ERREG       / SAVE THE STATUS
155          TAD ERREG       /DO WE NEED
156          AND K403        /TO RECALIBRATE?
157          SNA CLA
158          JMP RKRET       /NO--STOP TRANSFER AND RETURN
159          DCLR            /START THE RECALIBRATE--CLEAR DRIVE
160          STL RTL         /AC = 2
161          DCLR            /RECALIBRATE
162          DSKP            /WAIT
163          JMP .-1         /UNTIL DONE
164          DCLR            /CHEAR STATUS REGISTER
165          DRST            /WAIT FOR STATUS
166          SZA CLA
167          JMP .-2         /STILL DOING RECALIBRATE
168          JMP RKRET       /NOW STOP TRANSFER AND RETURN
169  /
170  /CONTROL C CHECK
171  /
172  CNTLC,  KRS             /READ KEYBOARD STATIC
173          AND K177        /REMOVE PARITY BIT
174          TAD M3          /IS IT A ^C?
175          SNA CLA
176          KSF             /IT IS A ^C -- IS THE FLAG UP?
177          JMP RWAIT       /NO -- KEEP ON TRUCKING
178          JMP RKRET       /A ^C -- LET FRTS TAKE CARE OF IT
179  /
180  /PARAMETERS
181  /
182  COM.    0
183  ONE.    1
184  TWO.    2
185  THRE.   3
186  FOUR.   4
187  FIVE.   5
188  UNIT.   0
189  UNUM.   0
190  CYLDR.  0
191  CYLN.   0
192  RKWT.   0
193  RDWT.   0
194  BUFH.   0
195  BUFL.   0
196  ERROR.  27
197          0
198  ERREG.  0
199  BLKCNT. 0
200  COMS.   3210
```

```
/FORTRAN IV FFT RK05 MODULE

201   /
202   /CONSTANTS
203   /
204   K3,       3
205   K7,       7
206   K177,     177
207   K377,     377
208   K400,     400
209   K403,     403
210   K3777,    3777
211   K4001,    4001
212   M3,       -3
213   M30,      -30
214   /
215   /SETUP THE ARRAY SPACE
216   /
217             ORG .+400
218             FIELD1 RK05C
219             ORG .+3
220
```

```
/XEBEC 9000 FORTRAN IV 8-MODE SUBROUTINES

/XEBEC 9000 FORTRAN IV 8-MODE SUBROUTINES
/
/FILE NAME IS 'TAPE8.RA'
/
/GENE A. WARE
/ELECTRICAL ENGINEERING DEPARTMENT
/UTAH STATE UNIVERSITY
/LOGAN, UTAH  84322
/12 JULY 1979
/
/CALLING SEQUENCE
/
/       CALL TAPE8(1,IUNT,ICOM,IBUF,ICNT)
/                  1 = TAPE OPERATION MODE
/              IUNT = TAPE UNIT NUMBER
/              ICOM = TAPE COMMAND
/              IBUF = TAPE BUFFER NAME
/              ICNT = WORD/RECORD COUNT
/
/       CALL TAPE8(0,IUNT,IFMT,PRDN,RTFG)
/                  0 = TAPE PARAMETER SET MODE
/              IUNT = TAPE UNIT NUMBER
/              IFMT = TAPE UNIT FORMAT
/              PRDN = TAPE UNIT PARITY-DENSITY
/              RTFG = TAPE UNIT READ THRESHOLD-FAST GAP
/
/       CALL TAPE8(-1,IREG,TCOM,JBUF,JCNT)
/                 -1 = TAPE REGISTER READ MODE
/              IREG = TAPE UNIT ERROR REGISTER-OPERATING STATUS
/              TCOM = TAPE COMMAND WORD
/              JBUF = TAPE BUFFER ADDRESS
/              JCNT = RESIDUAL WORD/RECORD COUNT
/
/IUNT   TAPE UNIT VALUES
/       0 = PHYSICAL UNIT 0 IN 9T MODE
/       1 = PHYSICAL UNIT 0 IN 7T MODE
/       2 = PHYSICAL UNIT 1 IN 9T MODE
/       3 = PHYSICAL UNIT 1 IN 7T MODE
/
/ICOM   TAPE COMMAND VALUES
/        0 = NO OPERATION
/        1 = NO OPERATION
/        2 = REWIND
/        3 = SET OFFLINE
/        4 = SPACE FORWARD N FILES
/        5 = SPACE FORWARD N RECORDS
/        6 = READ FORWARD 1 RECORD
/        7 = READ FORWARD 1 RECORD
/        8 = SPACE REVERSE N FILES
/        9 = SPACE REVERSE N RECORDS
```

```
/XEBEC 9000 FORTRAN IV 8-MODE SUBROUTINES

/         10 = SPACE REVERSE N RECORDS (EDIT)
/         11 = READ REVERSE
/         12 = WRITE FILE MARK
/         13 = ERASE 3 INCH GAP
/         14 = WRITE RECORD (EDIT)
/         15 = WRITE RECORD
/
/IFMT     TAPE FORMAT MODE CONTROL
/         0 = UNPACKED DATA FORMAT
/         1 = TEST DATA FORMAT
/         2 = PACKED FORMAT A
/         3 = PACKED FORMAT B
/
/PRDN     TAPE PARITY-DENSITY CONTROL
/         0 = EVEN PARITY-LOW DENSITY(NRZI)
/         1 = EVEN PARITY-HIGH DENSITY (PE)
/         2 = ODD PARITY-LOW DENSITY (NRZI)
/         3 = ODD PARITY-HIGH DENSITY (PE)
/
/RTFG     TAPE READ THRESHOLD-FAST GAP CONTROL
/         0 = NORMAL THRESHOLD-NO FAST GAP
/         1 = NORMAL THRESHOLD-FAST GAP SET
/         2 = LOW THRESHOLD-NO FAST GAP
/         3 = LOW THRESHOLD-FAST GAP SET
/
/IREG     TAPE REGISTERS--LOW ORDER 12 BITS CONTAIN THE OPERATING
/         REGISTER.  THE HIGH ORDER 12 BITS CONTAIN THE ERROR
/         REGISTER.
/
/TCOM     TAPE COMMAND REGISTER CONTAINED IN LOW ORDER 12 BITS.
/
/IOT INSTRUCTION DEFINITIONS
/
SKNB=     6354      /SKIP ON CONTROLLER NOT BUSY
LDMA=     6335      /LOAD MEMORY ADDRESS
LDMF=     6333      /LOAD MEMORY FIELD
LHWC=     6311      /LOAD HI WORD COUNT
LDWC=     6327      /LOAD LO WORD COUNT
LDCM=     6325      /LOAD COMMAND REGISTER AND GO
RDWC=     6347      /READ RESIDUAL WORD COUNT
RHWC=     6312      /READ HI RESIDUAL WORD COUNT
RDST=     6343      /READ STATUS REGISTER
RDES=     6345      /READ ERROR REGISTER
DSIN=     6351      /DISABE TAPE INTERRUPT
BSW=      7002      /BYTE SWAP
/
/
/REVISION HISTORY
/
/12 JUL 1979      GENE A. WARE      INITIAL VERSION
```

```
/XEBEC 9000 FORTRAN IV 8-MODE SUBROUTINES

101   /
102   /
103   /TAPE8 ENTRY (FPP INTERFACE)
104   /
105             BASE 0
106             SECT TAPE8
107             SETX MODE
108             STARTD              /GET MODE VALUE
109             FLDAI 0,1
110             FSTA 3
111             STARTF
112             FLDAI 3
113             ATX 0               /STORE MODE VALUE
114             JLT M1              /GO TO MODE = -1 SECTION
115             STARTD              /GET REMAINDER OF ARGUMENTS
116             FLDAI 0,2           /GET WORD 2
117             FSTA 3
118             STARTF
119             FLDAI 3
120             ALN 0
121             STARTD
122             FSTA WD2H
123             FLDAI 0,3           /GET WORD 3
124             FSTA 3
125             STARTF
126             FLDAI 3
127             ALN 0
128             STARTD
129             FSTA WD3H
130             FLDAI 0,5           /GET WORD 5
131             FSTA 3
132             STARTF
133             FLDAI 3
134             ALN 0
135             STARTD
136             FSTA WD5H
137             FLDAI 0,4           /GET WORD 4 ADDRESS
138             FSTA 3
139             STARTF
140             XTA 0               /GET MODE AGAIN
141             JEQ MZ              /GO TO MODE = 0 SECTION
142   /
143   /TAPE CONTROL SECTION (MODE = 1)
144   /
145             STARTD
146             FLDA 3
147             FSTA JBUFH
148             STARTF
149             TRAP4 PDPT
150             FLDA 30
```

```
/XEBEC 9000 FORTRAN IV 8-MODE SUBROUTINES

151             JAC
152     /
153     /TAPE PARAMETER INITIALIZATION SECTION (MODE = 0)
154     /
155     MZ.     FLDAZ 3         /GET WORD 4 VALUE (JBUF)
156             ALN 0
157             STARTD
158             FSTA WD4H
159             STARTF
160             TRAP4 PDPZ      /GO TO ZERO 8-MODE SECTION
161             FLDA 30
162             JAC
163     /
164     /TAPE REGISTER READ SECTION (MODE = -1)
165     /
166     M1.     TRAP4 PDPM1     /GO TO 8-MODE SECTION TO READ REGISTERS
167             STARTD
168             FLDAZ 0,2       /RETURN WORD 2 (IREG)
169             FSTA 3
170             STARTF
171             FLDA WD2
172             FNORM
173             FSTAZ 3
174             STARTD
175             FLDAZ 0,3       /RETURN WORD 3 (TCOM)
176             FSTA 3
177             STARTF
178             FLDA WD3
179             FNORM
180             FSTAZ 3
181             STARTD
182             FLDAZ 0,4       /RETURN WORD 4 (JBUF)
183             FSTA 3
184             STARTF
185             FLDA JBUF
186             FNORM
187             FSTAZ 3
188             STARTD
189             FLDAZ 0,5       /RETURN WORD 5 (JCNT)
190             FSTA 3
191             STARTF
192             FLDA WD5
193             FNORM
194             FSTAZ 3
195             FLDA 30
196             JAC
197     /
198     /8-MODE TAPE CONTROL SECTION
199     /
200             COMMZ RK05M
```

```
/XEBEC 9000 FORTRAN IV 8-MODE SUBROUTINES

201             ORG .+400
202     /
203     /8-MODE TAPE CONTROL (MODE = 1)
204     /
205     PDPT,   0
206             CLA
207             TAD WD2L        /GET THIS UNIT NOP COMMAND POINTER
208             AND K3
209             TAD TNOP+1
210             DCA TNOP
211             TAD WD2L        /GET THIS UNIT LAST COMMAND POINTER
212             AND K3
213             TAD TCOM+1
214             DCA TCOM
215             IOF             /NO INTERRUPTS
216             SKNB            /ISSUE NOP COMMAND WHEN CONTROLLER READY
217             JMP .-1
218             TADZ TNOP
219             LDCM
220             CLA
221             RDST            /WAIT UNTIL THIS UNIT IS ON LINE, READY
222             AND K7000       /AND NOT REWINDING
223             TAD M6000
224             SZA CLA
225             JMP .-4
226             TAD JBUFL       /LOAD LO BUFFER ADDRESS
227             LDMA
228             CLA
229             TAD JBUFH       /LOAD HI BUFFER ADDRESS
230             AND K17
231             LDMF
232             CLA
233             TAD WD5H        /LOAD HI WORD COUNT
234             AND K17
235             LHWC
236             CLA
237             TAD WD5L        /LOAD LO WORD COUNT
238             LDWC
239             CLA
240             TAD WD3L        /FORM COMMAND WORD
241             AND K17
242             BSW
243             CLL RTL
244             TADZ TNOP
245             LDCM            /LOAD COMMAND WORD AND GO
246             DCAZ TCOM       /SAVE COMMAND WORD
247             SKNB
248             JMP .-1
249             CIF CDF 0
250             ION             /TURN THE INTERRUPTS BACK ON
```

```
/KEBEC 9000 FORTRAN IV 8-MODE SUBROUTINES

251             JMPZ PDPT       /DONE
252     /
253     /8-MODE PARAMETER INITIALIZATION (MODE = 0)
254     /
255     PDPI,   0
256             CLA
257             TAD WD2L        /CALCULATE TAPE NOP ADDRESS
258             AND K3
259             TAD TNOP+1
260             DCA TNOP
261             TAD WD3L        /MASK FORMAT WORD
262             AND K3
263             DCA WD3H
264             TAD WD4L        /MASK PARITY-DENSITY WORD
265             AND K3
266             DCA WD4H
267             TAD WD5L        /MASK THRESHOLD-GAP WORD
268             AND K3
269             DCA WD5H
270             TAD WD3L        /BUILD NOP COMMAND
271             CLL RTL
272             TAD WD4H
273             RTL
274             TAD WD5H
275             RTL
276             TAD WD2L
277             DCAZ TNOP       /STORE NOP COMMAND
278             CIF CDF 0
279             JMPZ PDPI       /DONE
280     /
281     /8-MODE REGISTER SECTION (MODE = -1)
282     /
283     PDPM1.  0
284             IOF             /TURN OFF INTERRUPTS
285             SKNB            /WAIT UNTIL CONTROLLER NOT BUSY
286             JMP .-1
287             RDWC            /GET LO RESIDUAL WORD COUNT
288             DCA WD5L
289             RHWC            /GET HI RESIDUAL WORD COUNT
290             AND K17
291             DCA WD5H
292             TADZ TCOM       /GET LAST UNIT TAPE COMMAND
293             DCA WD3L
294             DCA WD3H
295             RDST            /GET STATUS REGISTER
296             DCA WD2L
297             RDES            /GET ERROR REGISTER
298             DCA WD2H
299             CIF CDF 0
300             ION             /TURN ON INTERRUPTS
```

```
/XEBEC 9000 FORTRAN IV 2-MODE SUBROUTINES

301             JMPZ PDPM1      /DONE
302   /
303   /PARAMETERS
304   /
305   MODE,     0
306   ONE.      1
307   TWO,      2
308   THRE.     3
309   FOUR,     4
310   FIVE.     5
311   WD2,      27              /IUNT/IUNT/IREG
312   WD2H,     0
313   WD2L.     0
314   WD3.      27              /ICOM/IFMT/TCOM
315   WD3H.     0
316   WD3L,     0
317   WD4.      27              /IBUF/PRDN/JBUF
318   WD4H,     0
319   WD4L.     0
320   WD5.      27              /ICNT/RTFG/JCNT
321   WD5H,     0
322   WD5L.     0
323   JBUF,     27
324   JBUFH,    0
325   JBUFL,    0
326   TNOP,     ADDR TNOPO      /NOP INSTRUCTION POINTER
327   TNOPO,    240             /244 => FAST GAP
328   TNOP1,    241
329   TNOP2,    242
330   TNOP3,    243
331   TCOM,     ADDR TCOMO
332   TCOMO,    0
333   TCOM1,    0
334   TCOM2,    0
335   TCOM3,    0
336   K3.       3
337   K17.      17
338   K7000,    7000
339   M6000.    -6000
340
```

VITA

Parris C. Neal

Candidate for the Degree of

Doctor of Philosophy

Dissertation: High Resolution Measurements of OH Infrared Airglow Structure.

Major Field: Electrical Engineering

Biographical Information:

Personal Data: Born at Tremonton, Utah, October 15, 1948, son of Chester P. and Ruth May Neal; married Dorothy Bott September 18, 1970; children--Allan Kirk, Farah, Amber, Derek Chester, Tyler Parris.

Education: Attended elementary school in Portage, Utah, graduated from Bear River High School in 1966, received a Bachelor of Science degree in Electrical Engineering from Utah State University, Logan, Utah, 1973; received a Master of Science degree in Electrical Engineering from Utah State University, 1975; completed requirements for Doctor of Philosophy with a major in Electrical Engineering at Utah State University, 1985.

Professional Experience: 1970-73, Electronics technician designing rocket-borne atmospheric instrumentation, Space Sciences Laboratory, Utah State University, Logan, Utah; 1973, Commissioned a 2nd Lt. USAF; 1973-74, Research Assistant performing data analysis on atmospheric measurements, Space Sciences Laboratory, Utah State University; 1974-77, Program Test Engineer managing the test of US Air Force traffic control and landing systems, USAF Electronics Systems Division, Hanscom AFB, Mass.; 1977-79, Space Systems Research Scientist testing infrared detector systems for NASA's IRAS satellite, NASA Ames Research Center, Sunnyvale, CA.; 1979-1981, Instructor of Electrical Engineering at US Air Force Academy, Colorado Springs, CO.; 1981-84, PhD student at Utah State University; 1984-85, Associate Professor of Electrical Engineering at US Air Force Academy, Colorado Springs, CO.

Publications:

Lum, H., D. Wong, P. Neal, and E. Long. 1979. On-Board Data Processing for the IRAS Telescope System. Progress in Astronautics and Aeronautics 67:265-267.

Baker, D.J., P.C. Neal, C.R. Harris, and W.R. Pendleton, Jr. 1983. High Throughput Compensated Interferometer for Spatial and Temporal Infrared Airglow Measurements. Poster presentation at International Fourier Spectroscopy Conference, Durham, England. Sept.

Taylor, M.J., P. Rothwell, W.R. Pendleton, Jr., D.J. Baker, P.C. Neal, and R. Armstrong. 1983. OH Airglow Structure, Results from Co-Ordinated Imaging and Temperature Observations. Paper presented at the Annual Meeting on Atmospheric Studies by Optical Methods, Lindau, W. Germany.

Pendleton, W.R. Jr., D.J. Baker, P.C. Neal, P. Rothwell, and M.J. Taylor. 1984. Coordinated Video and Time-Resolved Interferometric Measurements of OH Meinel Airglow Structures During the Bright Night of June 14-15, 1983. Transactions, American Geophysical Union 65(16):249.

END
FILMED
4-86
DTIC